Assessment of Existing Slender Masonry Walls beyond the Scope of the EN 1996 Norm

Numerically Based Analytical Solution to determine the Capacity under combined Vertical and Lateral Loading

Efstathios Peponis

TUDelft Delft University of Technology

Pieters BOUWTECHNIEK
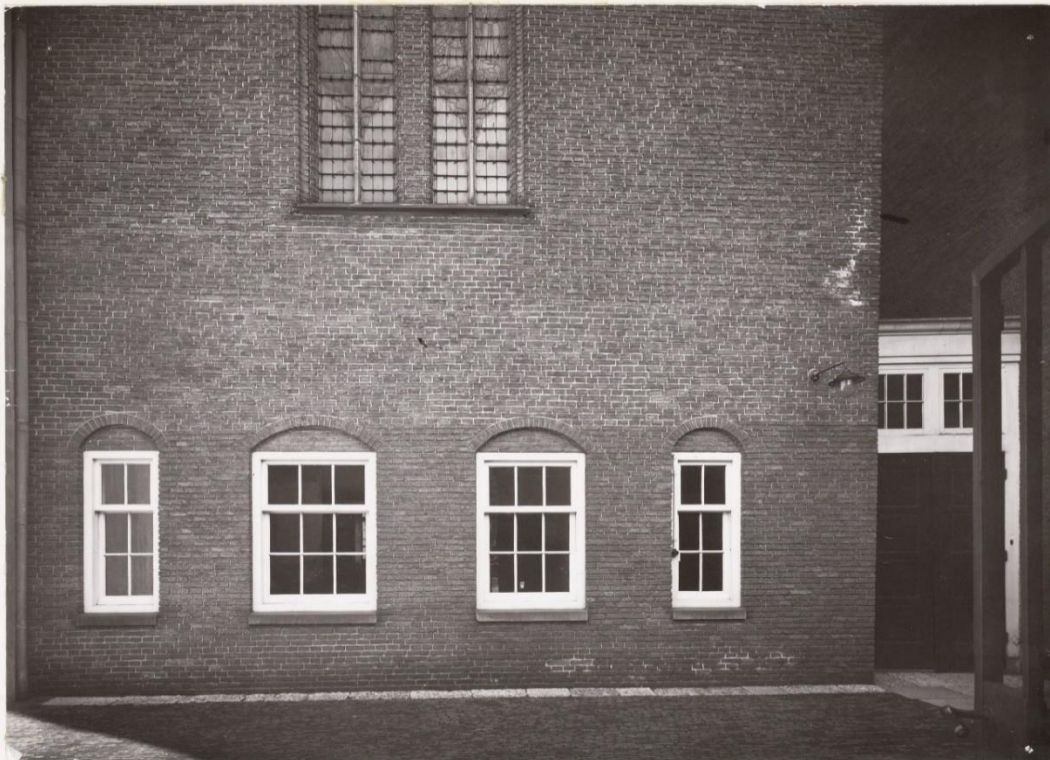
(This page is intentionally left blank)

Assessment of Existing Slender Masonry Walls beyond the Scope of the EN 1996 Norm

Numerically Based Analytical Solution to determine the Capacity under combined Vertical and Lateral Loading

Master Thesis (Final Report)

by

Efstathios Peponis

to obtain the Master of Science degree in
Civil Engineering

Student Number:	4740211
E-mail:	stathispeponis@gmail.com

Project Duration	March 14, 2019 – December 20, 2019
Date of Report:	20/12/2019

Thesis Committee:	Prof.dr.ir. J.G. Rots	TU Delft, Chairman
	Ir. S. Pasterkamp	TU Delft – Pieters Bouwtechniek
	Dr. R. Esposito	TU Delft
	Dr. O. Copuroglu	TU Delft

Source image front page: *https://beeldbank.amsterdam.nl/*

TUDelft Delft University of Technology

Pieters BOUWTECHNIEK

(This page is intentionally left blank)

Acknowledgements

This graduation project is the last chapter of my master's studies in Building Engineering at the Delft University of Technology. During my studies, I had a particular interest in the topic of the assessment of the structural capacity, aiming at the reuse of existing buildings. Various social, cultural, economic and environmental benefits result from maintaining and reusing existing buildings. Masonry structures have a dominant position in the building stock worldwide. Therefore, I researched an appropriate method for estimating the capacity of existing slender masonry walls. I worked on this subject for, almost, nine months. I gained valuable knowledge on the structural response of slender walls, the mechanical properties of masonry and the use of tools for finite element modelling and analysis. There are several people that I would like to thank, before continuing writing about the procedure and the outcome of my graduation work. Their guidance or support were really important for me.

First of all, I would like to express my gratitude to the members of my graduation committee. Sander Pasterkamp initiated the topic of the thesis, monitored the research and shared his knowledge with me. His interest in the work and the outcome was inspirational for me. Additionally, the expertise that Rita Esposito has in masonry structures and her experience with numerical modelling were crucial to carrying out of the research. Jan Rots is the chairman of the committee and provided guidance through the graduation work. His insightful advice defined the research process. Furthermore, the comments that Oguzhan Copuroglu made on the execution of the thesis were truly constructive.

I, also, want to thank Pieters Bouwtechniek for offering me a position, to work on my graduation project, in the office in Amsterdam. During my internship, I had the chance to join the inspection of an existing building. The masonry structure of the building was relevant to the structures, that I studied. Hence, I could obtain useful information about slender existing masonry walls. In addition, I am grateful to Pieters' people. Although I was working on my own project and I have a basic knowledge of the Dutch language, they made me feel an actual part of the team.

Researchers and professionals, outside TU Delft and Pieters Bouwtechniek, contributed to the study. I would like to thank Simon Wijte for the discussion we had about the structural behavior of existing masonry walls. He, also, provided me with information, about the recommendations in the Dutch national Annex, to the EN 1996 norm, as well as about the design principles in the withdrawn Dutch norm NEN 6790. I want to express my gratitude to Arturo Schultz and Tammam Bakeer, for explaining the derivation and the use of their formulas, that estimate the vertical resistance of masonry walls. In addition, Arturo Schultz provided a more recent paper, that he published on the topic, as a reference for my thesis. Finally, I am grateful to the DIANA FEA support team, and specifically Kesio Palacio, for the prompt and insightful answers to my questions, with respect to the use of the software.

Last but not least, I would like to express my deep gratitude to my family and friends. Either they were nearby or several kilometers away, their understanding and support motivated me to continue working. Especially, in bad times during this nine-month journey.

I hope that you enjoy reading!

Stathis Peponis

Delft, December 2019

(This page is intentionally left blank)

Contents

List of Figures

List of Tables

1 Summary

Problem Statement

In the last decade, maintenance and adaptive reuse, of the existing building stock, have gained ground in the construction sector. For the adaptive reuse of a building, it is required to analyze, meticulously, the existing structure. Unreinforced masonry structures are indicative of the Dutch built environment. The European Standard EN 1996 is, currently, the national standard, used by the members of CEN, for the design of new masonry structures and the assessment of the structural capacity of existing ones. Masonry walls of high slenderness (i.e. 100 mm thickness), often, comprise the structure of existing buildings, in the Netherlands. Values of slenderness ratio, approximately equal to 30, are quite common. However, the EN 1996 norm specifies a maximum slenderness ratio of 27, for masonry walls, mainly subjected to vertical loading.

The calculation of the vertical resistance, of a slender URM wall in an existing building, was an input for the thesis. The consultancy firm "STRACKEE BV Bouwadviesbureau" carried out the adaptive structural reuse of the building and provided the calculation. The building is a characteristic Dutch masonry construction, that dates back to the late 19th – early 20th century. The vertical resistance was calculated according to the EN 1996 norm and the withdrawn Dutch norm NEN 6790. The NEN 6790 norm had been in use in the Netherlands, until the EN 1996 norm became the respective national standard. The value of the vertical resistance, calculated according to the EN 1996 norm, was approximately half of the value, calculated according to the NEN 6790 norm. It should be mentioned that, the NEN 6790 norm was developed on the basis of the Dutch building practice, with respect to masonry buildings, and takes into account cases of walls, with values of slenderness ratio up to 30.

Considering the specified maximum slenderness ratio and the comparison, with the withdrawn Dutch norm NEN 6790, it seemed uncertain whether the EN 1996 norm is applicable to existing slender URM walls. The main research question formed, because of this concern:

What is an Appropriate Verification Method for Existing Slender Masonry Walls in One-way Bending?

An alternative formula was sought, so that the vertical resistance of existing slender URM walls, subjected to combined vertical and lateral loading, is estimated precisely. This way the capacity will not be underestimated and relevant techniques will be adopted for strengthening slender URM walls, when the latter is, actually, required.

Literature Research

Initially, literature research was conducted, with respect to the adaptive structural reuse, in the field of building engineering. As it was mentioned, the adaptive reuse entails the assessment of the structural capacity of existing buildings. The research revealed information, relevant to the definition of the practice, the appropriate structural design process, possible advantages and disadvantages as well as the opportunities and risks, from altering the use of an existing building.

The assessment of existing slender masonry walls is the topic of the thesis. Therefore, common characteristics of the structural system, in existing masonry buildings, were studied. Additionally, the definition of slenderness was sought. Available literature suggests criteria for distinguishing slender from squat walls. The type of failure is a criterion. Slender walls, usually, fail because of buckling. On the other hand, in squat walls excessive stresses on the material, normally, cause the failure.

Case Study

For the review of the EN 1996 norm and the development of an alternative formula, that estimates the vertical resistance of existing slender masonry walls, an appropriate case study was defined. The case study is one of the slenderest interior URM walls, that form the structure of a relevant existing building block in Amsterdam. STRACKEE BV Bouwadviesbureau provided the technical drawings of the building block, as a source for the thesis. Information about the building practice was obtained from the technical drawings. The interior URM walls are main elements of the load-bearing structure. Brickwork with lime mortar comprise the assembly of the walls. Additionally, the walls are subjected to vertical loads and out-of-plane lateral loads. The slenderness ratio of the case study of URM wall is, approximately, equal to 27. The wall is simply supported along the top and bottom edges and is not stiffened on the vertical edges. This is the only scenario, with respect to the support conditions of the walls, that is taken into consideration, in the thesis.

It is known that the building block was constructed during the late 19th – early 20th century. Indicative, for the construction period, properties of brickwork, with lime mortar, were found in relevant literature as well as in the Dutch practice guideline NPR 9998:2018. As a result, a dataset with the mechanical properties of masonry was created. Namely, the characteristic compressive strength and the short-term secant modulus of elasticity.

Review of Current Analytical Solutions for the Vertical Resistance of Masonry Walls

Alternative methods for the calculation of the vertical resistance of URM walls, have, already, been proposed, in order to deal with the conservative estimation of the capacity, when the provisions, in the EN 1996 norm, are applied. The vertical resistance of the case study of URM wall, was estimated according to the formulas, in the norms EN 1996 and NEN 6790, as well as applying the alternative methods. The respective results were compared for the review of the analytical solutions. More specifically, a comparative sensitivity analysis was performed. The variable factors for the sensitivity analysis were the short-term secant modulus of elasticity and the characteristic compressive strength of masonry. It was inferred, that the formula, for the calculation of the vertical resistance, in the EN 1996 norm, describes a rather paradoxical behavior of masonry walls. Particularly, when the short-term secant modulus of elasticity remained constant and the characteristic compressive strength increased, the vertical resistance decreased. This is shown in Fig. 1.
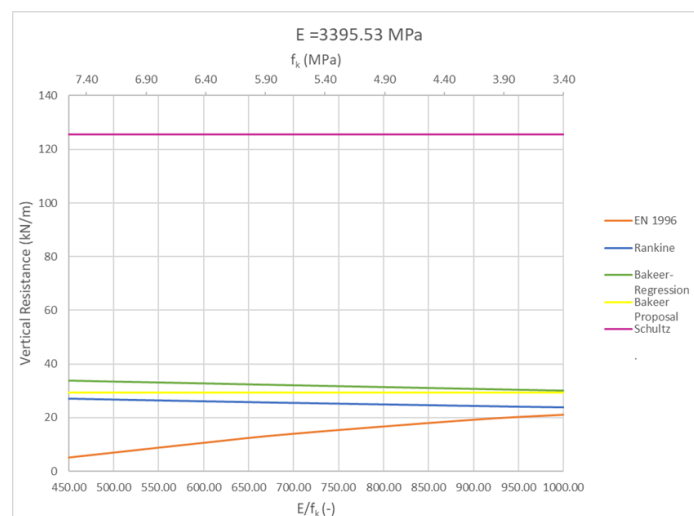
Fig. 1 Variation in the Vertical Resistance when the Compressive Strength Changes and the Modulus of Elasticity is Constant

Numerical Analysis & Proposed Analytical Solution

Reference values for the vertical resistance, of existing slender masonry walls, were necessary to develop an appropriate formula. Therefore, the response of slender URM walls, subjected to combined vertical and lateral loading, was estimated according to the results of FE analysis. A macro-model of the wall was created. The case study of URM wall was the reference for the geometry of the FE model. Information about the mechanical properties of the case study were not available. Therefore, the properties of masonry, that are prescribed in the NPR 9998-2018 norm, were the input for the initial material model. Specifically, the characteristics of clay brick masonry with mortar, for general use, constructed before 1945. The scope of the non-linear FE analysis was to determine the value of the vertical resistance of the wall, when it is subjected to different values of wind load, including the case when the wind load is zero. Initially, the vertical load, for which the wall fails, when zero wind load is applied on it, was calculated (orange dot in the graph in Fig. 4). The sequence of loading and the evolution of the non-linear analysis are shown in Fig. 2. Following, for different values of the vertical load, the value of the wind load, that leads the wall to failure, was specified every time. The sequence of loading and a representative curve, of the evolution of each non-linear analysis, are shown in Fig. 3. The grey dots in the graph, in Fig. 4, are the combinations of vertical load – wind load, that lead the wall to failure.

Models of slender URM walls, with different geometrical and material properties, were analyzed. Particularly, a parametric study was carried out, to define the influence of geometrical and material characteristics on the vertical resistance of existing slender URM walls. Namely, the slenderness ratio, the eccentricity, at the top and bottom edges, as well as the characteristic compressive strength, the short-term secant modulus of elasticity and the tensile strength. Curves with the combinations of vertical load – wind load, that lead the wall to failure, equivalent to the one in the graph in Fig. 4, were created for every case of analyzed URM wall.

The FE analysis results revealed an interaction, between vertical load and wind load, that led the studied URM walls to failure. According to this interaction, a formula was developed, for the estimation of the vertical resistance of existing slender URM walls, subjected to combined vertical and lateral loading. The proposed formula is described in Equation 1. The vertical resistance is a function of various parameters. Namely, the slenderness ratio of the wall, the short-term secant modulus of elasticity and the characteristic compressive strength of masonry as well as the eccentricity, at the top and the bottom of the wall, and the eccentricity, caused by the maximum first-order bending moment, due to the wind load. The influence of each parameter, on the vertical resistance, was defined according to the FE analysis results. Appropriate expressions introduce the parameters in the proposed formula. The contribution of the tensile strength of masonry is not included in the formula. It was verified that the actual vertical resistance, of slender URM walls, when the tensile strength of masonry is halved, is larger than the respective value, which is estimated from the proposed formula. Therefore, the proposed formula, for the estimation of the vertical resistance, can bring the structural assessment of slender URM walls, in existing buildings, to the safe side. The proposed formula was verified by comparing its results with the respective results, from the FE analysis. An indicative comparison is shown in Fig. 5.

The results, from the proposed formula, were compared with the respective results, from the formula, in the EN 1996 norm. The graph, in Fig. 6, juxtaposes the respective curves of the aforementioned formulas, by way of illustration. Taking into account that, the results from the proposed formula are comparable to the respective FE analysis results, it was inferred, that the EN 1996 norm underestimates the vertical resistance of the analyzed slender URM walls. Especially for large values of wind load, the formula in the EN 1996 norm results in values of vertical resistance, which are, approximately, equal to zero.
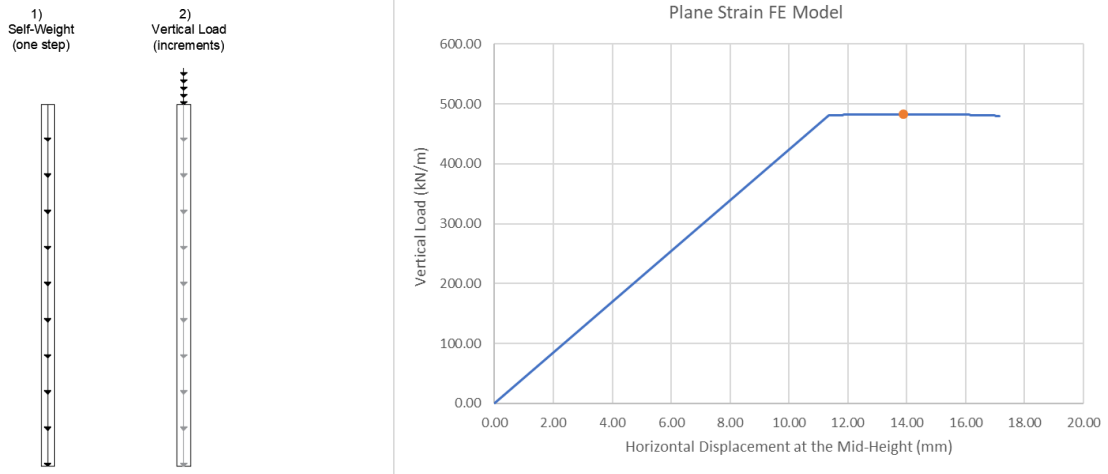
Fig. 2 Sequence of Loading and Evolution of the Non-linear FE Analysis for the definition of the Vertical Load, for which the wall Fails, when Zero Wind Load is applied on it
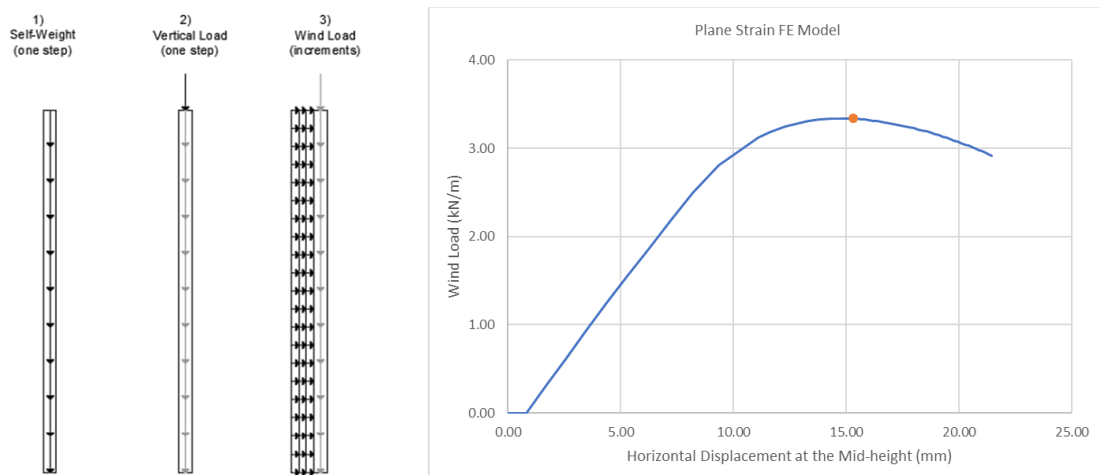
Fig. 3 Sequence of Loading and Evolution of the Non-linear FE Analysis for the definition of the Wind Load, for which the wall Fails, when certain Vertical Load is applied on it
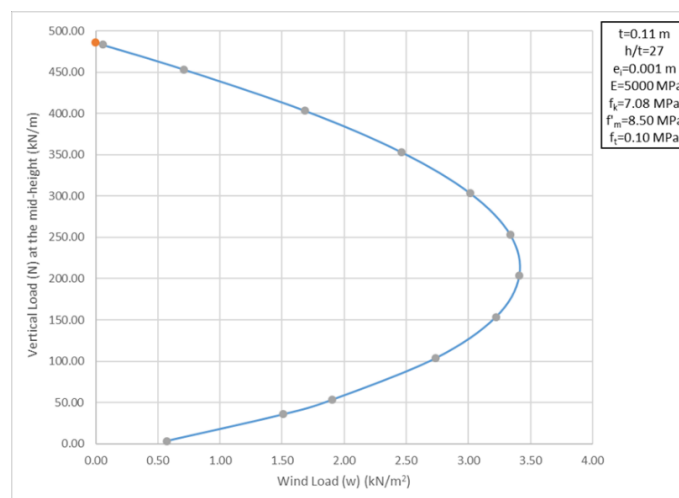
Fig. 4 Combinations of Vertical Load and Wind Load that lead the Case Study of URM wall to failure

Equation 1 Proposed Formula for the Estimation of the Design Value of the Vertical Resistance of slender URM walls, subjected to Combined Vertical and Lateral Loading

$$N_{Rd} = \frac{1.49}{\gamma_M} E^{0.60} f_k{}^{0.40} \left(\frac{t_{ef}}{h_{ef}}\right)^{1.46} t \left(1 - 2\frac{e_{mk}}{t}\right)^{2.40} \left(0.41 + 0.59 \sqrt{1 - 18.20 \left(\frac{h_{ef}}{t_{ef}}\right)^{0.38} \left(\frac{f_k}{E}\right)^{0.23} \frac{\frac{e_{wd}}{t}}{1 - 2.10\frac{e_{mk}}{t}}}\right),$$

where:

γ_M: partial factor for material

E: the short-term secant modulus of elasticity

f_k: the characteristic compressive strength

t_{ef}:   the effective thickness of the wall

h_{ef}:   the effective height of the wall

t: the thickness of the wall

e_{mk}:   the eccentricity at the mid-height of the wall (Equation 2)

e_{wd}:   the eccentricity at the mid-height of the wall, caused by the design value of the maximum first-order bending moment on the wall, because of the wind load (Equation 4)

Equation 2 Eccentricity at the mid-height of the wall

$$e_{mk} = e_i + e_k,$$ where:

e_i: the eccentricity at the top or bottom of the wall

e_k: the eccentricity due to creep (Equation 3)

Equation 3 Proposed expression for calculating the eccentricity due to creep at the mid-height of the wall

$$e_k = 0.002\, \varphi_\infty \frac{h_{ef}}{t_{ef}} \sqrt{t_{ef}\, e_i},$$ where:

φ_∞:   the final creep coefficient

Equation 4 Eccentricity at the mid-height of the URM wall, caused by the design value of the maximum first-order bending moment on the wall, because of the wind load (effects of creep are considered in the eccentricity at the mid-height (e_{mk}))

$$e_{wd} = \frac{M_{wd}}{\frac{1.49}{\gamma_M} E^{0.60} f_k{}^{0.40} \left(\frac{t_{ef}}{h_{ef}}\right)^{1.46} t \left(1 - 2\frac{e_{mk}}{t}\right)^{2.40}},$$ where:

M_{wd}:   the design value of the bending moment at the mid-height of the wall because of the wind load (Equation 5)

Equation 5 Design value of the Maximum First-Order Bending Moment on the wall because of the Wind Load

$$M_{wd} = \frac{w_d\, h^2}{8},$$ where:

w_d: the design value of the wind load

h: the clear storey height
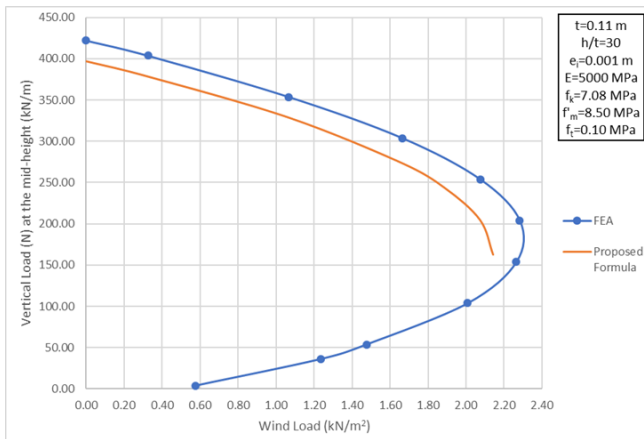
Fig. 5 Verification of the Proposed Formula
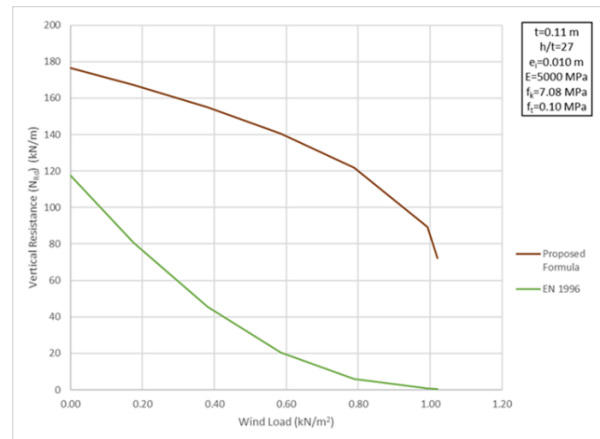
Fig. 6 Comparison Between the results from the proposed formula and the formula of the EN 1996 norm

Limitations of the Study & Recommendations for Further Research

The proposed formula for the estimation of the design value of the vertical resistance, of existing slender URM walls, subjected to combined vertical and lateral loading, is applicable to one case of support conditions. Particularly, to walls, that are simply supported along the top and bottom edges. Additionally, the formula was derived from and verified with the results, from FE analysis of URM walls, with certain geometric and material properties. The range of values of slenderness ratio (h/t) was between 27 and 39. The formula is applicable to URM walls with a minimum value of eccentricity, at the top and the bottom, equal to 0.001 m, and a maximum value of eccentricity, equal to 0.029 m. Furthermore, the characteristic compressive strength and the short-term secant modulus of elasticity, of the analyzed URM walls, ranged from 5.00 MPa to 7.08 MPa and from 5000 MPa to 7083 MPa, respectively.

The comparison between the FE analysis results and the results, from relevant experimental testing of existing slender URM walls, is recommended. This way, the validity of the formula can be assessed. The influence of the characteristic compressive strength and the short-term secant modulus of elasticity of masonry, on the vertical resistance, was introduced with appropriate expressions in the proposed formula. These expressions were derived from the review of the FE analysis results. The impact of the material properties, on the vertical resistance, was assessed from the analysis of URM walls, with two different values of slenderness ratio. Particularly, the values 27 and 30. It will be interesting to review, whether the material properties affect the vertical resistance of existing URM walls, with higher values of slenderness ratio, in a different way. Last but not least, proceeding with the FE analysis of URM walls, with smaller values of slenderness ratio, is recommended. The proposed formula is applicable to URM walls, with values of slenderness ratio from 27 to 39. The FE analysis results showed that the studied URM walls behaved as slender, under every possible combination of applied vertical load and wind load. The walls failed because of buckling, before the stresses on masonry reach the compressive strength. Analyzing URM walls, with smaller values of slenderness ratio, can reveal the lower limit of the ratio, for which the proposed formula is valid. Moreover, an appropriate condition can be specified, for characterizing URM walls, in existing masonry buildings, as squat or slender.

TUDelft
Delft
University of
Technology

Pieters
BOUWTECHNIEK

2 Introduction

2.1 Adaptive Structural Reuse of Existing Buildings

The orientation of the building construction sector has been altered in the last decade. It is noticed that the immense construction of new buildings, that has occurred ever since the end of World War II, is being replaced by the maintenance and adaptive reuse of the existing building stock. In the Netherlands, this phenomenon can be attributed to two main factors. The first relates to the increasing number of church buildings, not being used anymore. Except for church buildings, more and more office and store spaces remain unoccupied, since they cannot meet current respective requirements. [1] The vacancy rate for office spaces in the Netherlands was 15% in 2013. This percentage exceeds the normal vacancy level (3-8%). [2] Existing vacant buildings form an unprofitable factor for the market. Therefore, refurbishment or a possible change in use seem to be necessary. [1]

Analyzing, meticulously, the existing structure is substantial for the adaptive reuse of a building. [1] Unreinforced masonry structures are indicative of the Dutch built environment. [3] The European Standard EN 1996 [4], consisting of a number of parts, is currently the national standard, used by the members of CEN, for the design of masonry structures. The EN 1990 norm, accordingly, functions as the basis for the structural design and can be applied in cases of assessment of the structural capacity of existing structures. Additionally, the standards NEN 8700:2011 and NPR 9998:2018 can be used in the Netherlands for reconstruction purposes, as supporting to the EN 1990 and EN 1996 norms. The NEN 8700:2011 norm suggests appropriate load combinations, that should be taken into account in cases of assessing existing structures. The NPR 9998:2018 norm provides guidelines for the appraisal of the structural safety of buildings, subjected to earthquake loads. Material properties, which are derived from testing samples, extracted from existing buildings, are, also, included in the standard.

2.2 The EN 1996 norm and Existing Masonry Structures

The acquired knowledge in different European countries, where masonry structures have traditionally been constructed, is compiled in the EN 1996 norm. However, to derive a standard, that is generally applied, in the members of CEN, the various approaches towards building in masonry were compromised. [5] The slenderness ratio of masonry walls is one case, where the provisions, in the EN 1996 norm, do not cover a characteristic Dutch building practice. Masonry walls of high slenderness (i.e. 100 mm thickness), often, comprise the structure of existing buildings in the Netherlands. [6] Considering an average storey height of 3,00 m in buildings, constructed before 1920, a slenderness ratio equal to 30 is derived. The latter value does not conform to the requirement for a maximum slenderness ratio equal to 27, for masonry walls mainly subjected to vertical loading, that is specified in the standard. Effects of slenderness influence the verification of unreinforced masonry walls according to the EN 1996 norm. It is uncertain, therefore, if the calculation procedure, suggested in the relevant fields of the standard, is appropriate for the estimation of the vertical resistance of slender walls.

The consultancy firm "STRACKEE BV Bouwadviesbureau" performed a calculation of the vertical resistance, of a URM wall in an existing building, as part of a reconstruction project. The building is a characteristic Dutch masonry construction, that dates back to the late 19th – early 20th century. The assessed wall was subjected to vertical loads. Only the eccentricity due to construction imperfections was taken into account. The slenderness ratio of the wall is equal to 28. For the same design compressive strength of the masonry, two values were calculated for the vertical resistance of the wall. The first value was derived according to the suggested procedure in the EN 1996 norm. The

second value was calculated from the formula that is specified in the Dutch norm NEN 6790. This norm provides basic requirements and calculation methods for masonry structures and had been in use in the Netherlands, until the EN 1996 norm became the respective national standard. Comparing the two values of the vertical resistance of the masonry wall, it was noticed that the one, calculated according to the EN 1996 norm, was approximately half of the value, calculated according to the NEN 6790 norm. This was a comparison between the values of vertical resistance of the same masonry wall, as derived from two different standards. None of these values can be considered as a reference. However, the difference between them, specifically 26 kN/m, according to the EN 1996 norm, and 53 kN/m, according to the NEN 6790 norm, is noticeable. Account should be, also, taken of the fact that the NEN 6790 norm was developed on the basis of the Dutch building practice, with respect to masonry buildings, and considers cases of walls with values of slenderness ratio up to 30.

Concern arises about the applicability of the provisions, in the EN 1996 norm, in cases of existing slender URM walls. The value of the resistance, that is derived according to the suggested formula, might be too conservative in these cases. Hence, it becomes more possible that an existing slender URM wall would fail to meet the structural capacity criteria, specified in the EN 1996 norm, and, therefore, require strengthening. It is a fact that rehabilitation projects need twenty percent more manual labor, compared to constructing new buildings. [7] In cases where the structural capacity of slender URM walls is assessed conservatively, money is wasted. Particularly, the money spent for the rehabilitation work as well as the cost for the owner(s) of the real estate, because of the additional time, that the building remains vacant, during the rehabilitation project. An alternative formula could be applied to estimate more precisely the resistance of existing slender URM walls and, consequently, indicate if strengthening is, actually, required.

2.3   Research Approach

Since the topic of the master thesis refers to existing buildings, a slender URM wall, that is part of an actual building structure, will be the case study (section 8.1). As it is mentioned in the introduction, an adaptive structural reuse project from "STRACKEE BV Bouwadviesbureau" is an input for realizing the knowledge gap. STRACKEE BV Bouwadviesbureau is an engineering firm and provided the technical drawings of a relevant existing building block in Amsterdam, as a source for the thesis. Fig. 10 shows the typical load-bearing structure of historical masonry buildings in Amsterdam. Information about the building practice can be, also, acquired from the technical drawings (Fig. 11, Fig. 12) and the reconstruction project. The interior walls as well as the exterior side walls are the main elements of the load-bearing structure. These URM walls consist of brickwork with lime mortar. They are restrained on every floor level by timber floors. The floors are supported on timber beams, which run through the URM walls. The façade walls complement the building structure. In some cases, they were constructed in a later stage since the initial construction. Brickwork was, also, used in that case. The façade walls are connected to the main load-bearing walls. This way, sufficient bracing of the structure is achieved and, therefore, stability and resistance to horizontal loads.

The research will focus on the slenderest interior URM walls. (Fig. 17). Second order effects, that could be caused by the sway of the structure, will not be taken into account. Each wall is subjected to vertical loads (self-weight and the loads that are transferred from the floors). The timber beams run through the URM walls and, therefore, the loads from the floors to the walls are applied in the center of the wall section. Additionally, it is considered that the connections between the timber beams and the URM walls are not moment resisting. Hence, zero bending moments result at the top and the bottom of the walls at the floor levels. Only at the foundation level, moments can develop on the masonry walls. External wind loads are not applied on interior walls. However, the internal pressure on the

walls, because of the air leakage inside the building and the presence of openings (doors, windows), can cause a substantial surface loading on the interior walls. [8] According to the aforementioned remarks and assumptions, the interior URM walls are subjected to combined vertical and lateral loading (Fig. 21). Only out-of-plane lateral loads will be considered. Thus, defining and validating an appropriate method for the verification of slender existing URM walls, under combined vertical and lateral loading, forms the major objective of the research. Particularly, it is intended to derive an appropriate formula for the calculation of the vertical resistance of slender URM walls. Slenderness effects as well as the eccentricity, resulting from horizontal loads, influence the values of the resistance. In-plane shear resistance is not considered relevant, when out-of-plane lateral loads are applied on the wall. One scenario, with respect to the support conditions of the URM wall, will be taken into consideration. The wall is supported along its bottom and top edges. Since the connections between the timber beams and the URM walls are not moment resisting, the supports are hinged (Fig. 20).

Information about several interior URM walls can be obtained from the technical drawings (Fig. 11, Fig. 12). The dimensions of the wall and the cross section (Fig. 19) as well as the loads, that are transferred from the floors (Fig. 21), are required. The interest lies on the slenderest interior URM walls. These walls have a thickness of *0.11 m*. Details about the properties of masonry are not provided. As it was mentioned in section 2.1, the Dutch practice guideline NPR 9998:2018 includes average values for the properties of different types of masonry, used in existing buildings in the Netherlands. For the properties of brickwork, the year of construction is a criterion for categorization. Additionally, relevant research can reveal the possible properties of the clay bricks and the lime mortar, that were used in the project, considering the time it was constructed. A range of strength values for the clay bricks and the lime mortar will be defined (Section 5.2.1). The EN 1996 norm provides an equation for the calculation of the characteristic compressive strength of masonry, when the values of compressive strength of the masonry units and the mortar are known. The design value of the compressive strength of masonry will be, also, calculated according to the suggested procedure in the EN 1996 norm. When the short-term secant modulus of elasticity is not determined after testing, it can be estimated, based on the characteristic compressive strength. The EN 1996 norm as well as relevant literature recommend different relationships between the short-term secant modulus of elasticity and the characteristic compressive strength (Section 5.2.2). As a result, a dataset will be created, with the mechanical properties of masonry (Appendix A). These properties will be indicative of existing masonry buildings in the Netherlands, constructed during the late 19th – early 20th century.

Making use of the dataset with the mechanical properties of masonry, the possible values of vertical resistance, of the case study of URM wall, will be calculated according to the formulas in the EN 1996 and NEN 6790 norms. Literature research will be conducted, with respect to the appropriate estimation of the load-bearing capacity of slender URM walls. In case of proposed alternative solutions, they will be used, accordingly, for determining the value of vertical resistance of the case study of URM wall. The respective results for the vertical resistance, from standards and proposed alternative solutions, will be compared (section 8.2).

FE models of slender URM walls will be created. A macro-modelling approach is considered suitable in this case. The research interest lies on the behavior of the masonry wall, as a structural component. Localized phenomena are of secondary importance. Lourenço [9, p. 304] stated that *"in a macro-modelling strategy - units, mortar and unit-mortar interface are smeared out in a homogeneous continuum"*. Hence, continuum elements will be used for the FE modelling of the slender URM walls. The results from the FE analysis, with respect to the vertical resistance of the URM walls, will form the reference values (Section 9.2). The parameters that influence the response of slender URM walls,

subjected to combined vertical and lateral loading, will be defined. How every parameter affects the vertical resistance of existing slender URM walls, will be specified from the FE analysis results (Section 9.3). Literature, relevant to the load-bearing capacity of slender URM walls, as well as the FE analysis results can guide the derivation of an alternative formula. This formula will estimate the vertical resistance of existing slender URM walls, subjected to combined vertical and lateral loading. The results, from the proposed formula, will be compared with the respective results, from the formula in the EN 1996 norm, since, currently, this is the national standard for the design of masonry structures. Hence, it can be proposed that the proposed formula replaces the formula in the EN 1996 norm, for cases of existing slender walls (Chapter 10).

2.4 Theoretical Framework

The out-of-plane shear deformation of the slender URM walls is disregarded. Hence, the Euler-Bernoulli beam theory is valid in this case. [10] According to Simone [11], this means that 'plane cross-sections remain planar and normal to the beam axis in a beam subjected to bending'.

A masonry wall can be regarded as a continuum element with anisotropic properties. [5] The assembly and the connection of the components of the masonry wall cause the anisotropic behavior. Taking into consideration a plane strength domain and, particularly, the principal stress-strength domain (Fig. 7), a stress vector σ with two components, the two principal stresses σ_1, σ_2, is defined. In the case of brickwork, it is assumed that the principal directions, almost, match the horizontal and vertical directions of the wall plane. [12] Equation 6 and Equation 7 show the stress vector σ and the strain vector ε, respectively.

Equation 6 Stress Vector

$$\sigma = \begin{bmatrix} \sigma_{xx} \\ \sigma_{yy} \end{bmatrix}$$

Equation 7 Strain Vector

$$\varepsilon = \begin{bmatrix} \varepsilon_{xx} \\ \varepsilon_{yy} \end{bmatrix}$$
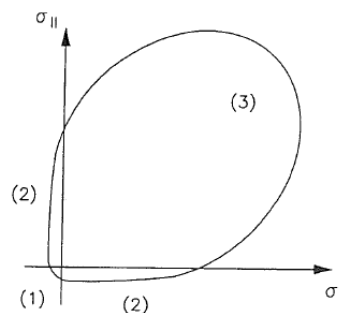
Fig. 7 Scheme of the principal stress plane domain

Since buckling is the major form of failure with respect to slender walls [13], Euler's formula (Equation 8) can be a guide for the definition of the critical load for stability failure:

Equation 8 Euler's Buckling Formula

$$F = \frac{\pi^2 EI}{h_{ef}^2},$$

where:

F: maximum or critical load

E: modulus of elasticity

I: the moment of inertia

h_{ef}*:* the effective height of the masonry wall

2.5 Research Questions

2.5.1 Main Question

What is an Appropriate Verification Method for Existing Slender Masonry Walls in One-way Bending?

2.5.2 Sub-questions

- What is the context of adaptive structural reuse in the field of building engineering?
- What are the characteristics of masonry, as structural system, in existing buildings?
- What is the definition of slenderness with respect to masonry walls?
- Which are the indicative properties of masonry?
- How should masonry walls be verified according to the provisions in the EN 1996 norm?
- What did the Dutch norm NEN 6790 prescribe for the verification of masonry walls, before the establishment of the EN 1996 norm?
- Is research, relevant to the response of slender masonry walls, included in existing literature?
- How can the vertical resistance of existing slender masonry walls, in one-way bending, be calculated, using an alternative method to the established standards?

3 Adaptive Reuse of Existing Building Structures

3.1 Definition and Structural Design Process

The adaptive structural reuse entails the improvement of the existing building, up to the point that it meets modern requirements and is suitable for an alternative use. [14] It does not affect the identity of the existing building, neither does it degrade its cultural significance. The materials and details of the original construction remain unaltered. Thus, the practice is considered, generally, feasible as well as cost-effective. [7]

The adaptive reuse of existing buildings entails a different process of structural design in comparison with the construction of new buildings. In the case of new constructions, it is the definition of the design problem that, commonly, determines the progress from a conceptual to a detailed stage. This design paradigm is characterized as AD (from abstraction to detail). However, the design of an existing structure has, already, been detailed, since the time it was initially constructed. This should be taken into consideration when determining the adaptive reuse design process. [1] Pasterkamp [1] forms the hypothesis that DAD design paradigm is more appropriate in this case. The design process evolves from detail to abstraction to detail.

In the beginning of the adaptive reuse design process, it is crucial that the information of the existing structure is, meticulously, analyzed. Additionally, there is no border between the design and the construction stage. The former should continue evolving along with the latter stage. This way, possible differences between the as-designed and the as-built state of the structure can be taken into account and influence the structural design, for the adaptive reuse project. It is important that these distinctive attributes of the adaptive reuse design are translated into appropriate contract conditions. Furthermore, emphasis must be given to the historic value of the structure during the design and construction procedures. [1]

3.2 Advantages and Disadvantages

The adaptive structural reuse is regarded as a sustainable practice. Existing buildings remain functional for a longer period of time. Hence, the embodied energy of the building is reclaimed over a larger number of years (building life) and the environmental impact is reduced. Adaptive reuse is, also, the alternative to demolition and reconstruction. [14] Comparing adaptive reuse and demolition - reconstruction in the built environment, the former option is generally the most efficient, since there are not any structural safety issues about the existing building. Equivalent results are achieved in both cases, but demolition – reconstruction is more harmful for the environment, considering the material waste. [15] It is a fact that, the sector of Building Construction covers 40 percent of the global annual raw material usage. Approximately 85 percent of the embodied energy in materials corresponds to manufacture and transport. Demolition - reconstruction entail wasting the existing building's embodied energy as well as consuming resources for new materials and assembly. It is important to mention, that the energy requirements for the raw material production, nowadays, and for modern construction techniques are, comparatively, high. Old buildings can be, also, energy efficient. Specifying the orientation of the building, so as to take advantage of the solar energy, as well as designing the floor lay-out and arranging the openings, aiming at effective ventilation and cooling, were popular techniques to decrease the energy consumption in buildings. Despite the environmental benefits, the LEED certificate program does not promote the adaptive reuse of historic buildings. In these cases, the rating is only 2/69. [7]

After the alteration of use, vacant properties are occupied again. This, additionally, leads to the revival of abandoned neighborhoods, diminishing, at the same time, the phenomenon of urban sprawl. [14] Adaptively reused existing buildings become again objects of investment activity. Furthermore, transforming the use of an existing building entails construction work. Hence, new employment prospects appear. Former industrial buildings, located in urban cores, have been abandoned since the beginning of the 20th century, when the focus of the economy shifted from industry to services. These buildings are representative cases of vacant properties and it is highly possible that they are contaminated sites. In general, abandoned buildings can be hazardous for public health and the environment. Leakages can occur inside the buildings as well as they can be sites where waste is illegally disposed. As a result, the chances of fire incidents increase. [7]

On the other hand, rehabilitation projects can be intensive and rather expensive. The improvement of the efficiency of existing buildings, from a sustainability perspective, up to the level that standards specify, nowadays, is not feasible in every case. [14] Furthermore, buildings that date back to the 19th or the beginning of the 20th century, cannot meet current requirements in HVAC systems. The necessary upgrading entails significant cost. [7] Energy saving during building operation is an advantage of a new construction [15] Furthermore, the expected functional life of an existing building is definitely shorter, when compared to a new construction, despite the improvements. The additional maintenance cost should be taken into account when assessing the options of adaptive reuse and demolition-reconstruction. [14] It is possible that contamination is present in vacant residential as well as industrial buildings. Asbestos has been in use in the building industry until the 1980's and is a characteristic source of contamination. Contamination in former industrial buildings is simultaneously a motive and an obstacle for reusing them. Investors become concerned about the risks from the underestimation of the size of the contamination or the inaccurate identification of the contaminants. [7]

3.3   Opportunities and Risks

The building per se can influence the applicability of adaptive reuse. Listed as well as culturally-historically important buildings are suitable for adaptive reuse. [2] Additionally, demolishing and reconstructing buildings is not a preferable option, from a sustainable viewpoint, in cases where the technical condition is adequate. [16] However, demolition and reconstruction are suggested in cases where several buildings need to be subject to transformation and enlargement is required. [15]

Study has been conducted with respect to the potential of converting office buildings to housing. [2] [16] Opportunities as well as risks are addressed. A number of issues have to be taken into consideration before converting office buildings into housing. Namely urban planning, the arrangement of spaces within the building and the required costs for conversion. It is, also, important to assess whether the existing floor lay-out can accommodate an alternative building function. Additionally, the necessary adjustments to the structure, the staircases and the façade should not exceed the estimated profit from the reuse of a building. [2]

Converting office buildings to housing will result in creating more residential spaces and simultaneously will terminate the long-term vacancy period (three or more years) of office spaces. It can be particularly applied to buildings located in city centers. On the other hand, the reuse of office as residential buildings is not suitable in business parks, unless the location has been transformed in advance. Generally, office buildings are designed to withstand higher loads in comparison with residential buildings. Therefore, additional floors can be constructed over the existing structure, in case this is required. However, problems can arise when placing the necessary installations for residential spaces. Especially in cases of structures consisting of prestressed concrete floors, since

penetrating the floors becomes complicated. In addition, the installations can significantly decrease the free floor-height. [2]

4 Existing Masonry Building Structures

4.1 Structural System

Masonry structures do not comprise linear elements, such as columns and beams, but two – or three – dimensional elements. [17] The primary two-dimensional structural elements in existing masonry buildings are walls, floors and the roof. [18]

The load-bearing masonry walls can be categorized with respect to the type of masonry units and the composition of the mortar. Clay as well as natural stone units are common in existing masonry buildings. Clay units can be either solid or perforated. Usually, lime mortars were used. More recently constructed masonry buildings consist of mortar, which is composed of lime and cement. Frequently, different types of masonry walls are combined within the same building. The units are different and, most of the times, the same mortar is used. In cases of subsequent changes or additions to the load-bearing structure, a different type of mortar could have been used, compared to the one in the original masonry construction. [18]

Different types of floors can be found in existing masonry buildings. In some cases, the floors are, also, masonry constructions. Brickwork, supported on steel beams (Fig. 8b), as well as brickwork or natural stone masonry, with single or double curvature (Fig. 8d), can form the floors in existing masonry buildings. Additionally, reinforced concrete slabs (Fig. 8a) and timber floors, supported on timber beams (Fig. 8c), are characteristic flooring types. The roof in existing masonry buildings, usually, consists of timber trusses, purlins and roofing. [18]
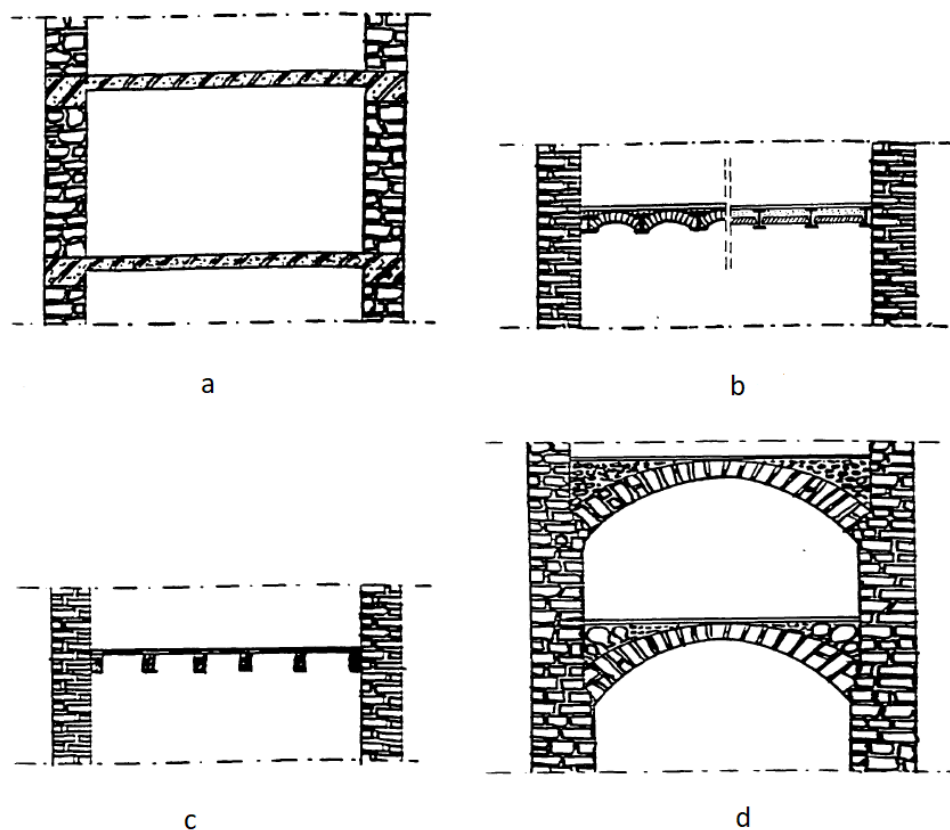
Fig. 8 Flooring Types in Existing Masonry Buildings [18]

4.2 Slenderness of Masonry Walls

Initially, the approach to the issue of slenderness is addressed with respect to standards, for the design of masonry structures. Maximum allowable values of the slenderness ratio are defined for masonry walls. The European Standard EN 1996 is currently the national standard, used by the members of CEN, for the design of masonry structures. The specified maximum value of slenderness ratio, for masonry walls, mainly subjected to vertical loading, is 27. The Dutch norm NEN 6790 provides basic requirements and calculation methods for masonry structures and had been in use in the Netherlands, until the EN 1996 norm became the respective national standard. The tables, for the design of masonry walls or columns, in the NEN 6790 norm, include values of slenderness ratio up to 30.

The criterion for characterizing a masonry wall as slender is the type of failure. There are two different types of failure for masonry walls, under vertical loading. Slender walls usually fail because of buckling. On the other hand, in squat walls excessive stresses on the material, normally, cause the failure. [13] These remarks are obvious in Fig. 9. Johnson suggested that a different formula estimates the load bearing capacity for each type of failure. The formulas have been applicable to steel elements as well as concrete and masonry walls, for small values of eccentricity of loading. Johnson differentiates between the two types of failure, based on the value of the slenderness ratio h/t. For $\frac{h}{t} \leq 28.6$ the wall is considered squat whereas for $\frac{h}{t} > 28.6$ the wall is slender. [19]

The effect of slenderness on the load-bearing capacity of masonry walls is usually combined with the masonry stiffness. [20] The EN 1996 norm as well as other empirical formulas [20], [19] specify a reduction factor Φ at the mid-height, for the verification of masonry walls, mainly subjected to vertical loading. The reduction factor takes into account second-order effects. Slenderness and masonry stiffness are introduced in the Φ factor with the non-dimensional parameter λ, according to Equation 9. The effect of the eccentricity of loading e_i is, also, considered in the Φ factor. Bakeer [19] proposed an alternative formula, for the EN 1996 norm, that calculates the factor Φ at the mid-height of the wall. The formula has two branches. As with Johnson's formulas, the first branch is relevant to the material failure and the second is relevant to the buckling failure. The parameter λ as well as the eccentricity of loading e_i are the criteria to distinguish between the two failure types, according to the expressions in Equation 10.
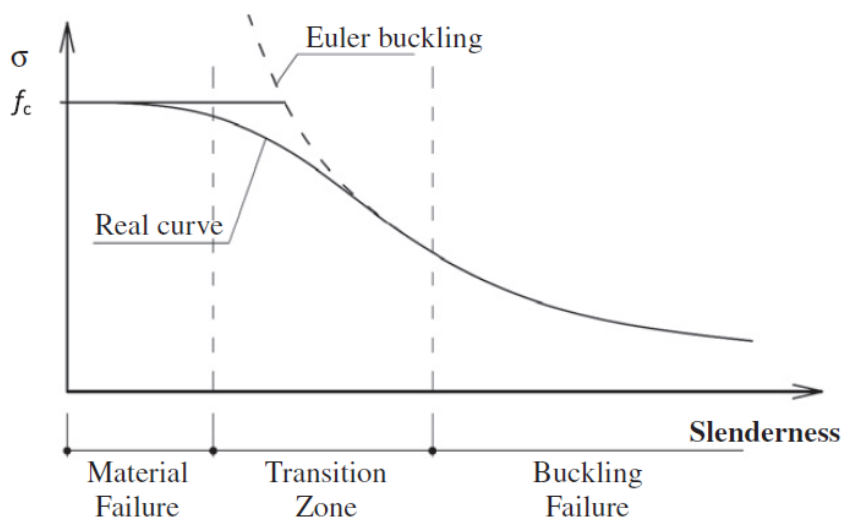
Fig. 9 Relationship Between Compressive Stress and Slenderness Ratio [13]

Equation 9 Non-dimensional Parameter that considers the Slenderness of the Wall and the Masonry Stiffness

$$\lambda = \frac{h}{t} \sqrt{\frac{f_k}{E}}, \text{ where}$$

h: the wall height

t: the wall thickness

f_k: the characteristic compressive strength of masonry

E: the modulus of elasticity

Equation 10 Distinguishing the Failure Types of Masonry Walls [19]

$$Material\ Failure \rightarrow \lambda < 1.26 \left(1 - 2\frac{e_i}{t}\right)$$

$$Buckling\ Failure \rightarrow \lambda \geq 1.26 \left(1 - 2\frac{e_i}{t}\right), \text{ where:}$$

λ: non-dimensional parameter that considers the slenderness and the masonry stiffness

e_i: the eccentricity at the top of the wall

t: the thickness of the wall
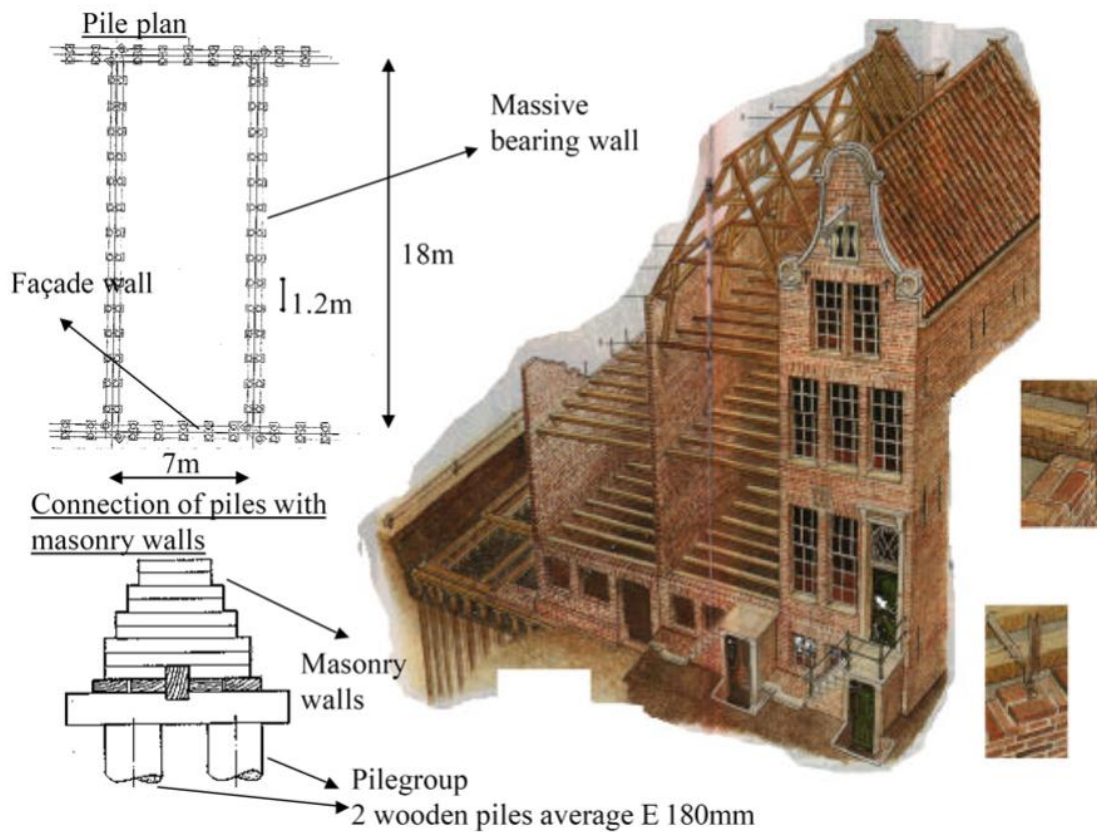
Fig. 10 Typical Historical Masonry Building in Amsterdam [21]

The research will focus on existing masonry buildings, located in the city of Amsterdam. Fig. 10 shows the typical load-bearing structure of historical masonry buildings in the city. The technical drawings of a building block in Amsterdam have been provided, by the company STRACKEE BV Bouwadviesbureau, as a source for this thesis. Information about the building practice are acquired from the technical drawings, which are shown in Fig. 11 and Fig. 12.The interior walls as well as the exterior side walls are the main elements of the load bearing structure. The URM walls consist of brickwork with lime mortar. They are restrained on every floor level by timber floors. The floors are supported on timber beams, which run through the masonry walls. The façade walls complement the building structure. In some cases, they have been constructed in a later stage since the initial construction. Brickwork was, also, used in that case. The façade walls are connected to the main load bearing walls. This way, sufficient bracing of the structure is achieved and, therefore, stability and resistance to horizontal loads.

As it has been mentioned in section 2.3, the slenderest interior URM walls are of interest. They are located on the upper floors of the building block (not on the ground floor). The thickness of the walls is equal to *0.11 m*. Since the timber beams run through the masonry walls, the loads, from the floors to the walls, are applied in the center of the wall section. Additionally, it is considered that the connections, between the timber beams and the URM walls, are not moment resisting. Hence, zero bending moments result at the top and the bottom of the walls, at the floor levels. Only at the foundation level, moments can develop on the masonry walls. Horizontal pressure is applied on the surface of the interior URM walls, because of the air leakage inside the building and the presence of openings (doors, windows). [8] Hence, the interior URM walls are subjected to vertical loading as well as out-of-plane lateral loading.

Fig. 11 Floor Plans - Ground Floor Level
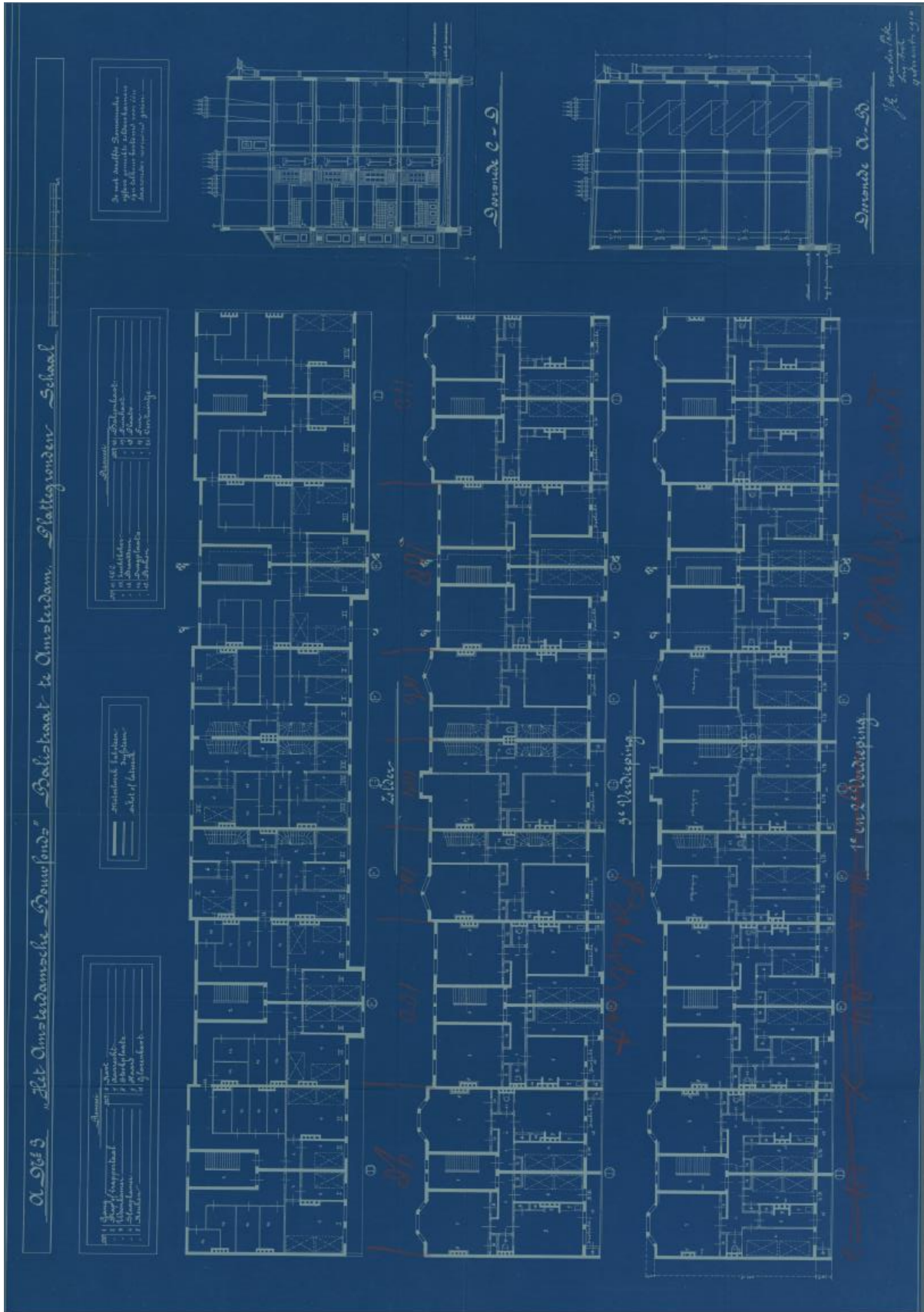
Fig. 12 Floor Plans of Upper Floors & Building Sections

5 Properties of Masonry

5.1 General Information

The research focuses on existing masonry buildings, located in the city of Amsterdam. These buildings date back to the end of the 19th − beginning of the 20th century. A common building practice, then, was the use of clay bricks and lime mortar for the assembly of the masonry. Usually, the bricks are arranged in a staggered pattern and connected with the mortar. [12]

5.1.1 Brickwork

A considerable number of parameters influence the characteristics of brickwork. Namely, the category of masonry units (bricks), the category of mortar, the dimensions of each component and the resulting ratio as well as the assembly on the wall. The thickness of the mortar ranges from 10 to 13 mm. Increasing the thickness of the mortar has a negative effect on the strength of masonry. The decrease in strength can be attributed to creep and shrinkage phenomena. Additionally, mortars are more deformable than bricks and have a lower strength. Therefore, the deformation of mortar creates transversal tensile stresses on the brick, which can lead to cracking. [12]

The assembly and the connection of the components (bricks and mortar) cause the anisotropic behavior of the masonry wall. [12] The values of the Young's modulus and the compressive strength are different, in the direction normal to the bed-joints, compared to the respective values, in the direction normal to the head-joints. When out-of-plane loads are applied on a masonry wall, the crack pattern depends on the failure plane (parallel to the bed- or head-joints) and different tensile resistance corresponds to each crack pattern. Under tensile stresses, masonry fails in a quasi-brittle way and secant unloading/reloading follow. When compressed, masonry is more ductile, softening is linear and unloading is elastic, until the compressive stress reaches a value approximately equal to zero. [22]

5.1.2 Bricks

Bricks consist, mainly, of clay. Clay is mixed with water and sand and, then, the firing of the mixture follows. The burning temperature exceeds 900°C. [23] The average brick height, in the period 14th-19th century, was 55 mm. The network of pores in brick contain water. As evaporation occurs, soluble salts produce crystals. Soluble salt crystallization is a decay mechanism for brick and depends on the porosity of the material as well as the temperature of air, vegetation, bacteria and wind. The quantity of clay and the burning temperature influence the porosity. [12]

The composition, the drying process, the baking temperature as well as the level of decay specify the mechanical properties of bricks. An indicative range for the compressive strength of good quality baked bricks is 15-30 MPa. The tensile strength is, approximately, 5-8% of the compressive strength. The modulus of elasticity is proportional to the compressive strength and can take values from 5000 MPa to 10000 MPa. Poisson's ratio varies between 0.15 and 0.20. [12]

5.1.3 Mortar

A binder, an aggregate and water comprise the mortar. Similar agents, as in the case of brick, lie behind mortar decay. The materials and their proportions in the mortar mixture as well as the mixing procedure define the porosity and, consequently, the durability of mortar.

A historical mortar, that consists of common lime and sand in a proportion 1:3 to 1:5, has a compressive strength of, approximately, 2.5 MPa. The tensile strength is, almost, 5% of the compressive strength. The ageing of mortar influences its strength. [12]

5.2   Mechanical Properties

5.2.1   Compressive Strength

The compressive strength and the failure under compression depend on the angle of application of the compressive load with respect to the bed joints. The compressive strength perpendicular to the bed joints is addressed. The compressive strength of common masonry types, where the compressive strength of the masonry units is higher than the strength of the mortar, is lower than the compressive strength of the masonry units but exceeds the strength of the mortar. [18]

For a brickwork of burnt bricks, the compressive strength can take values within the range 2-11 MPa. [12] The Dutch practice guideline NPR 9998:2018 "Assessment of structural safety of buildings in case of erection, reconstruction and disapproval – Induced Earthquakes – Basis of design, actions and resistances" includes mean values of material properties for different types of masonry. For clay brick masonry with mortar, for general use, constructed before 1945, the proposed value of the mean compressive strength is 8.5 MPa.

Relevant literature reveals information about indicative values of compressive strength for the components of masonry in buildings, that were built in the 19th century or in the beginning of the 20th century. Mean values of the compressive strength of clay bricks and lime mortar were obtained after testing samples, that were taken from existing buildings. Tests were performed separately on clay bricks and lime mortars and not on the masonry as composite. A typical value of 20.8 MPa uniaxial compressive strength characterizes the clay bricks, that were used in buildings in Spain, constructed at the period 18th-19th century. [24] Testing grouts, which were designed, based on lime mortars, and were used in historic buildings in Greece, resulted in 0.69 MPa compressive strength, after 90 days of hardening. [25] Representative values of compressive strength of solid clay bricks and natural hydraulic lime mortar, that form historical masonries, are approximately 25 MPa and 1.9 MPa, respectively. [26] A study on masonry buildings in Riga, constructed during the period 1890-1940, revealed a range of values 5-25 MPa for the compressive strength of clay bricks. [27] Samples of bricks and structural mortars were obtained from buildings in Thessaloniki, that date back to the end of the 19th century. Testing in the laboratory defined the mechanical properties, namely the compressive strength of compact bricks, which ranged from 3.2 to 21 MPa, and the compressive strength of lime mortar with a range 0.5-0.7 MPa. [28]

5.2.2   Modulus of Elasticity

The EN 1996 norm recommends the relationship $E=1000f_k$, when the short-term secant modulus of elasticity is not determined after testing. E is the short-term secant modulus of elasticity and f_k the characteristic compressive strength of the masonry, perpendicular to the bed joints. The recommendation in the Dutch national annex to the EN 1996 norm is different and the relationship becomes $E=700f_k$. ACI-530 (Masonry Standards Joint Committee, 2005) suggests the use of the same relationship ($E=700f_k$). [29] The withdrawn Dutch norm NEN 6790 considers a relationship $E=900f'_{rep}$, where f'_{rep} is the representative value of the compressive strength. [30] The formula for the calculation of f'_{rep}, is given in Equation 29.The recommended, in the Mexican code (Gobierno del Distrito Federal, 2004), relationship, for short-term actions, is $E=350f_k$ and, respectively, $E=600f_k$ for long-term actions.

Results from different experimental tests revealed ranges for the ratio *E/f$_k$* from *600* to *800*, between *120* and *300* or even lower from *40* to *70*. [29]

5.2.3   Tensile Strength

The tensile strength of masonry is significantly lower than the compressive strength. The angle of application of the tensile load, with respect to the bed joints, has a great influence, also, in the case of the tensile strength. [18] There is a significant deviation of the values of the property. [18] In most cases, the tensile strength can be disregarded since it becomes negligible, when microcracks due to shrinkage occur. [12] It is a common practice that codes for the design of masonry structures consider masonry as a non-tension material. The flexural strength of masonry is defined when lateral loads are applied (wind, earthquakes). [18]

The low tensile strength of masonry as well as the non-reliability of the property, because of the deviation of the values, contribute to being neglected in most codes for the design of masonry structures. However, taking into account the tensile strength can have a noticeable impact on the vertical resistance of masonry walls of high slenderness, subjected to eccentric vertical loads. [31] The tensile strength is, almost, 2-5% of the compressive strength perpendicular to the bed joints. [12]

The tensile strength of masonry depends on the tensile strength of the mortar and the bond between the masonry unit and the mortar. [18] As it was aforementioned, the masonry walls in Dutch buildings, that date back to the end of the 19th – beginning of the 20th century, consist of lime mortars. High-lime mortars are workable, adaptable, adherent and water absorbent. Therefore, the space, between the bricks, and even irregularities, on the brick surfaces, are completely filled. Hence, a durable bond, between the brick and the mortar, is created and the extent of bond is, also, significant. Additionally, the procedure of hardening is slow for high-lime mortars. The mortar, because of the elasticity and flexibility, can bear the applied stresses, when the wall moves, and cracking is restricted. Minute cracks in lime-based mortars can be healed and minute voids can be, also, filled. Masonry that consists of mortar, rich in lime, is characterized by rather high values of modulus of elasticity and flexural strength. Furthermore, because the adhesive (bond) strength of high-lime mortars is higher than the cohesive (internal) strength, the most probable position, where a crack can be noticed, is within the mortar and not at the interface, between brick and mortar. [32]

6 Calculation of the Vertical Resistance of Masonry Walls according to current and withdrawn Standards

6.1 The EN 1996 Norm

The European Standard EN 1996, consisting of a number of parts, is currently the national standard, used by the members of CEN, for the design of masonry structures. The proposed formula, for the calculation of the vertical resistance, of a single leaf wall, per unit length, is described by Equation 11.

Equation 11 Design value of vertical resistance according to the EN 1996 norm

$N_{Rd} = \Phi\, t\, f_d$, where:

   N_{Rd}:   the design value of the vertical resistance

   Φ: the capacity reduction factor (Equation 12, Equation 14)

   t: the thickness of the wall

   f_d: the design compressive strength of masonry (Equation 24)

Equation 12 Capacity Reduction Factor at the Top or Bottom of the Wall

$\Phi_i = 1 - 2\dfrac{e_i}{t}$, where:

   e_i: the eccentricity at the top or the bottom of the wall, as appropriate (Equation 13)

   t: the thickness of the wall

Equation 13 Eccentricity at the Top or the Bottom of the Wall

$e_i = \dfrac{M_{id}}{N_{id}} + e_{he} + e_{init} \geq 0.05\, t$, where:

   M_{id}:   the design value of the bending moment at the top or the bottom of the wall, resulting from eccentricity of the floor load at the support

   N_{id}:   the design value of the vertical load at the top or bottom of the wall

   e_{he}:   the eccentricity at the top or bottom of the wall, if any, resulting from horizontal loads (for example wind)

   e_{init}:   the initial eccentricity (Equation 17), a sign that increases the absolute value of e_i

   t: the thickness of the wall

Equation 14 Capacity Reduction Factor at the Mid-height of the Wall

$$\Phi = \left(1 - 2\frac{e_{mk}}{t}\right) * e^{-\frac{u^2}{2}}, \text{ where:}$$

e_{mk}:   the eccentricity at the mid-height of the wall (Equation 15)

t: the thickness of the wall

u: a non-dimensional parameter, that takes into account the slenderness of the wall, the eccentricity of loading and the masonry stiffness (Equation 19)

Equation 15 Eccentricity at the Mid-height of the Wall

$$e_{mk} = e_m + e_k \geq 0.05\,t, \text{ where:}$$

e_m: the eccentricity due to loads (Equation 16)

e_k: the eccentricity due to creep (Equation 18)

t: the thickness of the wall

Equation 16 Eccentricity due to Loads at the Mid-height of the Wall

$$e_m = \frac{M_{md}}{N_{md}} + e_{hm} + e_{init}, \text{ where:}$$

M_{md}:   the design value of the greatest moment, at the mid-height of the wall, resulting from the moments at the top and bottom of the wall, including any load applied eccentrically to the face of the wall (e. g. brackets)

N_{md}:   the design value of the vertical load, at the mid-height of the wall, including any load applied eccentrically to the face of the wall (e. g. brackets)

e_{hm}:   the eccentricity at mid-height, resulting from horizontal loads (for example wind)

e_{init}:   the initial eccentricity (Equation 17), a sign that increases the absolute value of e_m

Equation 17 Initial Eccentricity of the Wall in accordance with the EN 1996 norm

$$e_{init} = \frac{h_{ef}}{450}, \text{ where:}$$

h_{ef}:   the effective height of the wall (equal to the clear storey height, *h*, for walls restrained, at the top and bottom, by timber floors or roofs, spanning from both sides at the same level)

Equation 18 Eccentricity due to creep at the mid-height of the wall

$$e_k = 0.002 \; \varphi_\infty \; \frac{h_{ef}}{t_{ef}} \; \sqrt{t \, e_m}, \text{ where:}$$

φ_∞:   the final creep coefficient

h_{ef}:   the effective height of the wall (equal to the clear storey height, *h*, for walls restrained, at the top and bottom, by timber floors or roofs, spanning from both sides at the same level)

t_{ef}:   the effective thickness of the wall (equal to the actual thickness of the wall, *t*, for single-leaf walls)

t: the thickness of the wall

e_m: the eccentricity due to loads (Equation 16)

Equation 19 Non-dimensional parameter, that takes into account the slenderness of the wall, the eccentricity of loading and the masonry stiffness (definition in the EN 1996 norm)

$$u = \frac{\lambda - 0.063}{0.73 - 1.17 \frac{e_{mk}}{t}}, \text{ where:}$$

λ: a non-dimensional parameter, that takes into account the slenderness of the wall and the masonry stiffness (Equation 20)

e_{mk}:   the eccentricity at the mid-height of the wall (Equation 15)

t: the thickness of the wall

Equation 20 Non-dimensional parameter, that takes into account the slenderness of the wall and the masonry stiffness (definition in the EN 1996 norm)

$$\lambda = \frac{h_{ef}}{t_{ef}} \sqrt{\frac{f_k}{E}}, \text{ where:}$$

h_{ef}:   the effective height of the wall (equal to the clear storey height, *h*, for walls restrained at the top and bottom by timber floors or roofs spanning from both sides at the same level)

t_{ef}:   the effective thickness of the wall (equal to the actual thickness of the wall, *t*, for single-leaf walls)

f_k: the characteristic compressive strength of masonry (Equation 21)

E: the short-term secant modulus of elasticity of masonry (Equation 22, Equation 23)

Equation 21 Characteristic compressive strength of masonry

$$f_k = K \, f_b{}^\alpha \, f_m{}^\beta, \text{ where:}$$

K, α, β: constants

f_b: the normalized mean compressive strength of the units, in the direction of the applied action effect

f_m: the compressive strength of the mortar

Equation 22 Short-term secant modulus of elasticity of masonry - when it is not determined by tests in accordance with EN 1052-1 – (definition in the EN 1996 norm)

$E = 1000\, f_k$, where:

f_k: the characteristic compressive strength of masonry (Equation 21)

Equation 23 Short-term secant modulus of elasticity of masonry when it is not determined by tests in accordance with EN 1052-1 – (definition in the Dutch National Annex to the EN 1996 norm)

$E = 700\, f_k$, where:

f_k: the characteristic compressive strength of masonry (Equation 21)

Equation 24 Design compressive strength of masonry (definition in the EN 1996 norm)

$f_d = \dfrac{f_k}{\gamma_M}$, where:

f_k: the characteristic compressive strength of masonry (Equation 21)

γ_M partial factor for material

The Dutch national Annex to the EN 1996 norm suggests an additional testing, for the verification of masonry walls. In cases of walls, restrained at the top and the bottom and, independently, of the efficiency of the connections to the floors, the effective height should be taken equal to the clear storey height of the wall. A constant value of first-order eccentricity, over the height of the wall, should be considered. The value must be equal to the maximum of *10 mm* or *h_ef/300*. (Equation 25)

Equation 25 Constant Eccentricity over the of Height of the Wall, in accordance with the Dutch National Annex to the EN 1996 norm

$$e_i = e_{mk} = \max \begin{cases} 10 \text{ mm} \\ \dfrac{h_{ef}}{300} \end{cases}, \text{ where:}$$

h_{ef}:   is the effective height of the wall (equal to the clear storey height *h*)

6.2 The NEN 6790 Norm

NEN 6790 is the Dutch norm, for the design and calculation of masonry structures, and had been the respective national standard, until the EN 1996 norm was established. The norm suggests a simplified method for the estimation of the load-bearing capacity of braced walls. The first-order eccentricity may vary linear over the height of the wall. A load capacity factor α, that allows for the effects of first-order eccentricities and slenderness, influences the vertical resistance of the wall. This simplified method considers the geometrically as well as the physically non-linear behavior of the wall. [33] The formula in Equation 26 was used in the Netherlands for the calculation of the vertical resistance of masonry walls.

The modulus of elasticity of masonry is considered equal to *900 f'_rep*. [30] The values for the constants *K, α, β*, in Equation 21 and Equation 29, are specified in tables, in the Dutch national Annex to the EN 1996 norm and the withdrawn NEN 6790 norm, respectively. The two tables are identical.

Equation 26 Design Value of Vertical Resistance according to the NEN 6790 norm

$N'_{u;d} = \alpha\, f'_d\, b\, t$, where:

α: capacity reduction factor, which is derived from graphs, according to the slenderness of the wall λ (Equation 27) and the values of first-order eccentricity e_0, e_1 (Fig. 13)

f'_d: the design compressive strength of masonry (Equation 28)

b: the width of the wall

t: the thickness of the wall

Equation 27 Slenderness (definition in the NEN 6790 norm)

$\lambda = \dfrac{h_{ef}}{t}$, where:

h_{ef}:   the effective height of the wall (equal to the clear storey height, *h*, for walls restrained at the top and bottom by timber floors or roofs spanning from both sides at the same level)

t: the thickness of the wall

Equation 28 Design Compressive Strength of Masonry (definition in the NEN 6790 norm)

$f'_d = \dfrac{f'_{rep}}{\gamma_M}$, where:

f'_{rep}:   the representative value of the compressive strength of masonry (Equation 29)

γ_M: partial factor for material

Equation 29 Representative Value of the Compressive Strength of Masonry

$f'_{rep} = K\, f'_b{}^{\alpha}\, f'_m{}^{\beta}$, where:

K, α, β: constants

f'_b: the normalized mean compressive strength of the units, in the direction of the applied action effect

f'_m: the compressive strength of the mortar
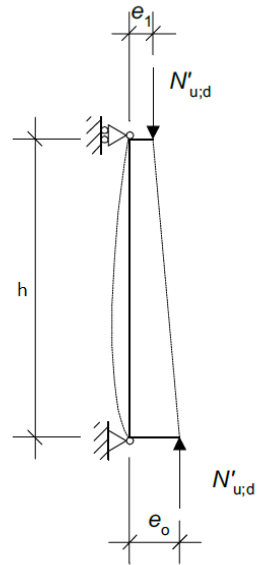
Fig. 13 Values of First-Order Eccentricity over the Height of a Masonry Wall [34]

7 Review of Literature on the Appropriate Estimation of the Load-Bearing Capacity of Slender URM Walls

7.1 Underestimation of the Capacity of Masonry Walls by the Formula in the EN 1996 norm

Journal articles [31], [35] address the conservative estimation of the vertical resistance of masonry walls, when the provisions, in the EN 1996 norm, are applied. These articles include experimental and numerical modelling results, for the behavior of masonry walls, under concentric or eccentric vertical loads. The walls are simply supported along the bottom and top edges. Different values of slenderness ratio and load eccentricity were included in the research. It was noticed that the deviation between the capacity, calculated according to the EN 1996 norm, and the respective result, from the numerical model, increases as the slenderness of the wall increases. [35]

Furthermore, tests on full-scale walls revealed that the relationships between the short-term secant modulus of elasticity and the characteristic compressive strength of masonry, that the EN 1996 norm suggests ($E=1000f_k$ or $E=700f_k$), result in large values of the modulus of elasticity. [31] Another issue that is mentioned, is the influence of the tensile strength to the resistance of masonry walls. This influence becomes significant for higher values of slenderness ratio and load eccentricity. [35]

7.2 Proposed Alternative Methods for the Calculation of the Vertical Resistance of Masonry Walls

7.2.1 Review of Developed Formulas

Sandoval & Roca [20] suggested three different procedures for the estimation of the vertical resistance of brick masonry walls. The procedures focus on the calculation of the capacity reduction factor (Φ), at the mid-height of the wall, which considers the effects of slenderness and eccentricity of loading. This research, also, allows for the estimation of the influence of the tensile strength, on factor (Φ), for relatively large values of load eccentricity. The proposed procedures were validated with experimental results, from masonry walls hinged at both ends (top and bottom).

A critical review of current empirical formulas, for the assessment of the structural capacity of masonry walls, under vertical loads (concentric or eccentric), was the subject of the research work from Bakeer [19]. The reviewed formulas are listed in Table 1. All the expressions estimate the capacity reduction factor (Φ), at the mid-height of the wall. The formula, that the EN 1996 norm prescribes, for the calculation of factor (Φ), as well as the respective formulas, that Sandoval & Roca [20] developed, were, also, evaluated. A reference numerical model of a masonry wall, with hinged supports on the bottom and top edge, was used for the review of the empirical formulas. The modulus of elasticity of masonry remained constant and different ratios of modulus of elasticity to compressive strength (E/f) were taken into account.

The relation between the load-bearing capacity and the compressive strength was the criterion for the comparison between the formulas. The oxymoron, that the load-bearing capacity of the wall decreased while the compressive strength of the masonry increased, was noticed at the results of the formula of Mann, the formula of Kirtschig and the formulas of Sandoval/Roca. This behavior was, mainly, observed for E/f ratios lower than 700. The derivation method of these formulas is common and consists of the assumption of a regression model. The parameters are changed until the solution is equal to the reference value. Particularly, the definition of the capacity reduction factor Φ, in the formula of Kirtschig, which is suggested in the EN 1996 norm, has been derived for a specific E/f_k ratio, equal to 1000. [19]

The other formulas were characterized by, relatively, reliable results. Johnson's Parabola describes accurately the material failure, that has been discussed in section 4.2. However, equations, based on Johnson's parabola, for the material failure, and Angervo's analytical solution, for the buckling failure, have limited applicability, in cases of small eccentricities. U.S. masonry design codes include expressions for the critical axial load capacity, that are related to the Moment Magnifier Method. [19] The formulas, that Schultz [36] proposed, develop the respective ones from U.S. masonry design codes, considering the influence of the lateral load on masonry members. Therefore, the solution proposed by Schultz is addressed, later, in the thesis. The formula of Graubner/Glock introduces the non-linearity of masonry with a parameter c and the ultimate strain ε_c. [19] Without further explanation, about the application of the formula, and taking into account, that in practical cases of assessment of the load-bearing capacity of existing masonry walls ,the ultimate strain of the material is not known, the suitability of the formula is doubted. An underestimation was noticed when the load bearing capacity was calculated according to Rankine method, for both types of failure. Hence, the results are on the safe side.

Table 1 Current Empirical Formulas Reviewed by Bakeer [19]

Johnson's Parabola
Rankine Method
Moment Magnifier Method
Formula of Mann
Formula of Kirtschig (EN 1996 norm)
Formula of Graubner/Glock
Formulas of Sandoval/Roca
Formula of Graubner/Förster

7.2.2 Appropriate Developed Formulas

The review of current empirical formulas [19] is considered for the appropriate choice of the ones that are assessed in this thesis. It has been mentioned that the results from the Rankine method were on the safe side. Equation 30 describes the Rankine method.

Following the review, Bakeer [19] suggested two alternative equations for the calculation of the capacity reduction factor (Φ), at the mid-height of masonry walls, subjected to concentric or eccentric vertical loading. The first expression (Equation 31) attempts to correct the inconsistency, observed in the formulas, that were based on regression models. The formulas of Sandoval/Roca are based on regression models [19]. Sandoval & Roca [20] introduced three proposals for the estimation of the capacity reduction factor (Φ), at the mid-height of masonry walls. The equation for each proposal has the form of Equation 33. Bakeer [19], actually, reviewed the three expressions for Φ_0 and suggested the aforementioned correction (Equation 31) It is considered interesting for the context of the thesis to investigate, how the consideration of the masonry tensile strength will affect the vertical resistance of masonry walls.

A second formula is proposed, for the EN 1996 norm, by Bakeer [19]. For masonry walls under vertical loading the two, already mentioned, types of failure can occur (section 4.2). The first is the material failure and the second is the buckling failure. Different expression of the capacity reduction factor (Φ), at the mid-height of the wall, is derived for each type of failure. The two expressions are described in Equation 39. It is noticed in Equation 40 that, the value of the initial characteristic modulus of elasticity is used for the calculation of the non-dimensional parameter λ'. The modulus of elasticity has a minor influence in the case of the material failure, whereas it is crucial, for the buckling failure,

in which the compressive strength of masonry plays no rule. The buckling failure, probably, happens, when the material is still in the elastic stage and, in most cases, at the beginning of the stress-strain diagram. Therefore, the use of the initial characteristic modulus of elasticity is important for the estimation of the buckling failure. When the initial characteristic modulus of elasticity is not determined by tests, it can be estimated according to Equation 41. Equation 41 makes use of the initial mean modulus of elasticity. An expression for the calculation of the initial mean modulus of elasticity is given in Equation 42. Replacing the value of the initial mean modulus of elasticity, from Equation 42 into Equation 41, it is derived that the initial characteristic modulus of elasticity is equal to the short-term secant modulus of elasticity (Equation 43). [37]

Schultz [36] developed analytical expressions for the calculation of the critical axial load in slender unreinforced masonry compression members. The members are subjected to a combination of eccentric axial load and lateral load. The expression for the critical axial load (Equation 44), was derived, based on the assumption that masonry is a linear and elastic material, which has no tensile strength. When the moment on the masonry member, because of the lateral load, and the load path are known, the vertical resistance of the member can be calculated. A graphic representation of the expression for the critical axial load, in Fig. 15, shows the combinations of P_{ef} and M_w, that lead to instability of the masonry member, according to the load path. The formula in Equation 44 can be applied, on condition that the maximum moment on the member does not exceed the moment capacity. Equation 49 and Equation 50 include the definition of the peak axial load and the moment capacity, respectively. When the moment is larger than the peak moment, the stability limit is exceeded and, therefore, the design of the member must be reconsidered. The critical axial load capacity for masonry members, subjected to eccentric vertical loads, can be expressed as a function of the axial load for the first Euler buckling mode (Equation 51). Therefore, Equation 49 and Equation 50 can be rewritten to Equation 52 and Equation 53, respectively.

The axial load on masonry walls in buildings is caused by the self-weight of the masonry and the permanent and variable loads from the floors. Environmental loads and, specifically, wind loads, which are considered in this master thesis, create bending moments on the walls. Hence, most of the axial load will be present when the wind load produces the bending moments. Therefore, the compression branch, as depicted in Fig. 15, is more appropriate for the studied cases. [38] The critical axial load in the compression branch, when M_w is known, is specified in Equation 54. The accuracy of the expression was determined, comparing the results with the respective ones, obtained from stability tests on slender, simply supported URM walls. [36]

Equation 30 Rankine method for calculation of the capacity reduction factor (Φ), at the mid-height of the wall [19]

$$\Phi = \frac{1-2\frac{e_{mk}}{t}}{1+\frac{12}{\pi^2}\left(\frac{\lambda}{1-2\frac{e_{mk}}{t}}\right)^2}, \text{ where:}$$

e_{mk}:   the eccentricity at the mid-height of the wall (Equation 15)

t: the thickness of the wall

λ: a non-dimensional parameter, that takes into account the slenderness and the masonry stiffness (Equation 20)

Equation 31 Solution by T. Bakeer for calculation of the capacity reduction factor (Φ) at the mid-height of the wall – based on regression models [19]

$$\Phi = \left(1 - 2\frac{e_{mk}}{t}\right)\left[5.1\left(\frac{e_{mk}}{t}\right)^2 - 2.4\frac{e_{mk}}{t} + 1\right]\frac{atan(1.13\ u'^2)}{1.13\ u'^2},\ \text{where:}$$

e_{mk}:   the eccentricity at the mid-height of the wall (Equation 15)

t: the thickness of the wall

u':   a non-dimensional parameter, that takes into account the slenderness of the wall, the eccentricity of loading and the masonry stiffness (Equation 32)

Equation 32 Non-dimensional parameter, that takes into account the slenderness of the wall, the eccentricity of loading and the masonry stiffness (definition by T. Bakeer) [19]

$$u' = \frac{\lambda}{1 - 2\frac{e_{mk}}{t}},\ \text{where:}$$

λ: a non-dimensional parameter, that takes into account the slenderness of the wall and the masonry stiffness (Equation 20)

e_{mk}:   the eccentricity at the mid-height of the wall (Equation 15)

t: the thickness of the wall

Equation 33 Proposal by C. Sandoval, P. Roca for considering the influence of the masonry tensile strength, on the capacity reduction factor (Φ), at the mid-height of the wall [20]

$$\Phi = \Phi_0 + \Delta\Phi_{f_t},\ \text{where:}$$

Φ_0:   the capacity reduction factor considering that the tensile strength of the material is zero (Equation 31)

$\Delta\Phi_{ft}$:   factor that allows for the influence of the tensile strength of masonry (Equation 34)

Equation 34 Factor that allows for the influence of the tensile strength of masonry on the capacity reduction factor (Φ) at the mid-height of the wall [20]

$$\Delta\Phi_{f_t} = f_t\left[\frac{1}{X + Y\Phi_e + Z\sqrt{\Phi_e}}\right],\ \text{where:}$$

f_t: the tensile strength of masonry in N/mm^2

Φ_e: factor that allows for the effect of the load eccentricity (Equation 35)

X, Y, Z: parameters that depend on the load eccentricity (Equation 36,Equation 37,Equation 38)

Equation 35 Factor that allows for the effect of the load eccentricity [20]

$$\Phi_e = \left(1 - 2\,\frac{e_{mk}}{t}\right)^{\frac{3.5\,\lambda^2 + 0.65}{\lambda^2 + 0.65}}, \text{ where:}$$

e_{mk}:   the eccentricity at the mid-height of the wall (Equation 15)

t: the thickness of the wall

λ: a non-dimensional parameter, that takes into account the slenderness of the wall and the masonry stiffness (Equation 20)

Equation 36 Parameter X [20]

$$X = \begin{cases} -144261\,\frac{e_{mk}}{t} + 29306 & for\ 0.1\ t \le e_{mk} \le 0.2\ t \\ -3017.3\,\frac{e_{mk}}{t} + 1057.4 & for\ 0.2\ t \le e_{mk} \le 0.3\ t' \end{cases}$$

Equation 37 Parameter Y [20]

$$Y = \begin{cases} -259620\,\frac{e_{mk}}{t} + 53542 & for\ 0.1\ t \le e_{mk} \le 0.2\ t \\ -9550\,\frac{e_{mk}}{t} + 3528 & for\ 0.2\ t \le e_{mk} \le 0.3\ t' \end{cases}$$

Equation 38 Parameter Z [20]

$$Z = \begin{cases} 387930\,\frac{e_{mk}}{t} - 79273 & for\ 0.1\ t \le e_{mk} \le 0.2\ t \\ 10833\,\frac{e_{mk}}{t} - 3853.6 & for\ 0.2\ t \le e_{mk} \le 0.3\ t' \end{cases}$$

where:

e_{mk}:   the eccentricity at the mid-height of the wall (Equation 15)

t: the thickness of the wall

Note: Equation 34 is valid for the range of eccentricities: $0.1 \le \frac{e_{mk}}{t} \le 0.3$.

Equation 39 Solution by T. Bakeer for calculation of the capacity reduction factor (Φ) at the mid-height of the wall – proposal for the EN 1996 norm [19]

$$\Phi = \begin{cases} 1 - 2\,\frac{e_{mk}}{t} - \dfrac{1}{3.15\left(1 - 2\frac{e_{mk}}{t}\right)}\lambda'^2 & for\ \lambda' < 1.26\left(1 - 2\frac{e_i}{t}\right) \\ 0.79\left(1 - 2\,\frac{e_{mk}}{t}\right)^3 \dfrac{1}{\lambda'^2} & for\ \lambda' \ge 1.26\left(1 - 2\frac{e_i}{t}\right) \end{cases}, \text{ where:}$$

e_{mk}:   the eccentricity at the mid-height of the wall (Equation 15)

t: the thickness of the wall

λ':   a non-dimensional parameter, that takes into account the slenderness and the masonry stiffness (Equation 40)

Equation 40 Non-dimensional parameter, that takes into account the slenderness and the masonry stiffness (definition by T. Bakeer) [37]

$$\lambda' = \frac{h_{ef}}{t_{ef}} \sqrt{\frac{f_k}{E_{0k}}}, \text{ where:}$$

h_{ef}:   is the effective height of the wall (equal to the clear storey height, h, for walls restrained at the top and bottom by timber floors or roofs spanning from both sides at the same level)

t_{ef}:   the effective thickness of the wall (equal to the actual thickness of the wall, t, for single-leaf walls)

f_k: the characteristic compressive strength of masonry in N/mm^2 (Equation 21)

E_{0k}:   the initial characteristic modulus of elasticity of masonry (Equation 43)

Equation 41 Initial Characteristic Modulus of Elasticity [37]

$$E_{0k} = \frac{E_{0mean}}{1.2}, \text{ where:}$$

E_{0mean}:   the initial mean modulus of elasticity (Equation 42)

Equation 42 Initial Mean Modulus of Elasticity [37]

$$E_{0mean} = (1.1 - 1.2)\, E, \text{ where:}$$

E: the short-term secant modulus of elasticity of masonry (Equation 22, Equation 23)

Equation 43 Relationship between the Initial Characteristic Modulus of Elasticity and the short-term Secant Modulus of Elasticity [37]

$$E_{0k} = E, \text{ where:}$$

E: the short-term secant modulus of elasticity of masonry (Equation 22, Equation 23)

Equation 44 Critical Axial Load of Unreinforced Masonry Compression Members, under the combination of Eccentric Vertical Loads and Lateral Loads [36]

$$P_{ef} = P_E \left[1 - 0.577 \left(\frac{e_i + \lambda_m e_f}{r} \right) \right]^3, \text{ where:}$$

P_E: the axial load for the first Euler buckling mode (Equation 45)

e_i: the eccentricity at the top or bottom of the wall

λ_m: a coefficient that takes into account the distribution of the lateral load and the support conditions (Equation 47)

e_f: the eccentricity caused by first-order bending moments from the lateral load (Equation 48)

r: radius of gyration of the net section of the masonry member

Equation 45 Axial Load for the First Euler Buckling Mode [36]

$$P_E = \frac{\pi^2 E_m I_n}{h_{ef}^2}, \text{ where:}$$

E_m: the secant modulus of elasticity of masonry (Equation 46)

I_n: the moment of inertia of the net section of the masonry member

h_{ef}:   the effective height of the masonry wall

Equation 46 Secant Modulus of Elasticity of Masonry – specified by the MSJC in the US [39]

$$E_m = \frac{0.33f_k - 0.05f_k}{\varepsilon_{0.33} - \varepsilon_{0.05}}, \text{ where:}$$

f_k: the characteristic compressive strength of masonry in N/mm^2 (Equation 21)

$\varepsilon_{0.33}$:   the compression strain in masonry at a stress equal to *0.33 f_k*

$\varepsilon_{0.05}$:   the compression strain in masonry at a stress equal to *0.05 f_k*

Equation 47 Coefficient that takes into account the Distribution of the Lateral Load and the Support Conditions [38]

$$\lambda_m = \left(\frac{A_M}{M_{max} h}\right)^{0.3}, \text{ where:}$$

A_M, M_{max}:   depicted in an indicative diagram of first-order bending moments along the height of the masonry member in Fig. 14

h: clear storey height

Equation 48 Eccentricity caused by first-order Bending Moments from the Lateral Load [36]

$$e_f = \frac{M_w}{P_{ef}}, \text{ where:}$$

M_w: the first-order bending moment from the lateral load

P_{ef}:   the critical axial load of unreinforced masonry compression members, under the combination of eccentric vertical loads and lateral loads (Equation 44)

Equation 49 Peak Axial Load of Unreinforced Masonry Compression Members, under the combination of Eccentric Vertical Loads and Lateral Loads [36]

$$P_{cp} = \left(\frac{27}{64}\right) P_E \left(1 - 0.577 \frac{e_i}{r}\right)^3, \text{ where:}$$

P_E: the axial load for the first Euler buckling mode (Equation 45)

e_i: the eccentricity at the top or the bottom of the wall

r: radius of gyration of the net section of the masonry member

Equation 50 Moment Capacity of Unreinforced Masonry Compression Members, under the combination of Eccentric Vertical Loads and Lateral Loads [36]

$$M_{mp} = \frac{0.1828r}{\lambda_m} P_E \left(1 - 0.577 \frac{e_i}{r}\right)^4, \text{ where:}$$

r: radius of gyration of the net section of the masonry member

λ_m: a coefficient that takes into account the distribution of the lateral load and the support conditions (Equation 47)

P_E: the axial load for the first Euler buckling mode (Equation 45)

e_i: the eccentricity at the top or the bottom of the wall

Equation 51 Critical Axial Load Capacity for Masonry Members subjected to Eccentric Vertical Loads [36]

$$P_e = P_E \left(1 - 0.577 \frac{e_i}{r}\right)^3, \text{ where:}$$

P_E: the axial load for the first Euler buckling mode (Equation 45)

e_i: the eccentricity at the top or the bottom of the wall

r: radius of gyration of the net section of the masonry member

Equation 52 Peak Axial Load of Unreinforced Masonry Compression Members, under the combination of Eccentric Vertical Loads and Lateral Loads [36]

$$P_{cp} = \left(\frac{27}{64}\right) P_e, \text{ where;}$$

P_e: the critical axial load capacity for masonry members subjected to eccentric vertical loads (Equation 51)

Equation 53 Moment Capacity of Unreinforced Masonry Compression Members, under the combination of Eccentric Vertical Loads and Lateral Loads [36]

$$M_{mp} = \frac{0.1828r}{\lambda_m} P_e \left(1 - 0.577 \frac{e_i}{r}\right), \text{ where:}$$

r: radius of gyration of the net section of the masonry member

λ_m: a coefficient that takes into account the distribution of the lateral load and the support conditions (Equation 47)

P_e: the critical axial load capacity for masonry members subjected to eccentric vertical loads (Equation 51)

e_i: the eccentricity at the top or the bottom of the wall

Equation 54 Critical Axial Load of Unreinforced Masonry Compression Members, in the Compression Branch under the combination of Eccentric Vertical Loads and Lateral Loads [36]

$$P_{ef1} = 0.422 P_e \left[1 + 1.37 \sqrt{1 - \frac{M_w}{M_{mp}}} \right] = P_e \left[0.422 + 0.578 \sqrt{1 - \frac{5.47 \frac{\lambda_m M_w}{P_e r}}{1 - 0.577 \frac{e_i}{r}}} \right], \text{ where:}$$

P_e: the critical axial load capacity for masonry members subjected to eccentric vertical loads (Equation 51)

M_w: the first-order bending moment from the lateral load

M_{mp}:   the moment capacity of masonry members, under the combination of eccentric vertical loads and lateral loads (Equation 53)

λ_m: a coefficient that takes into account the distribution of the lateral load and the support conditions (Equation 47)

r: radius of gyration of the net section of the masonry member

e_i: the eccentricity at the top or bottom of the wall
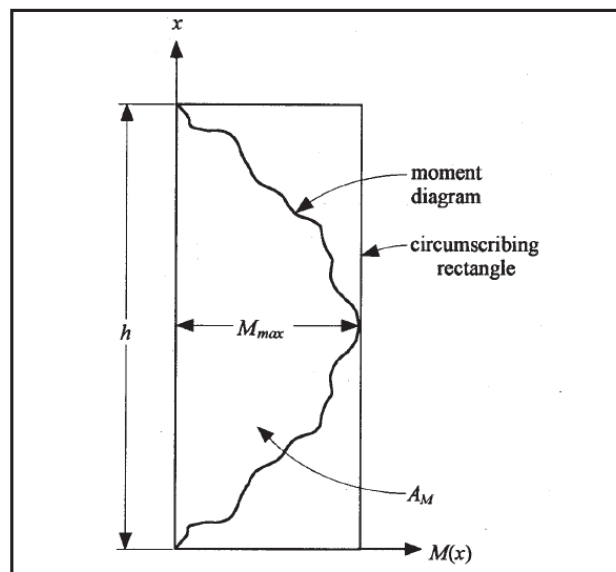
Fig. 14 Definition of A_M and M_{max} on a moment diagram [38]
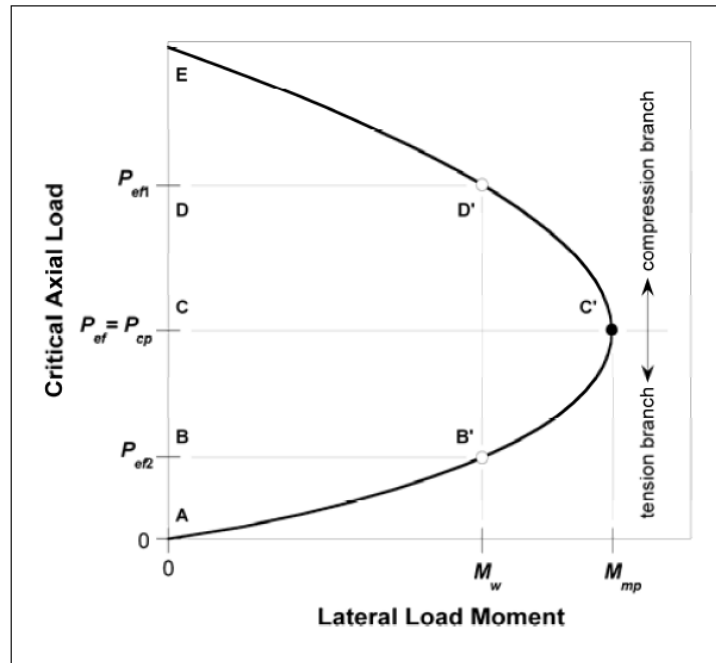
Fig. 15 Stability Failure (P_ef-M_w) Combinations [36]

8 Estimation of the Vertical Resistance of a Slender URM Wall according to Standards and Developed Formulas

8.1 Case Study

An interior URM wall is chosen from the technical drawings of the building block in Amsterdam (Fig. 11, Fig. 12). The wall is located on the first floor of the building. Fig. 16 - Fig. 20 show information, with respect to the geometry and the support conditions of the wall. According to the EN 1996 norm, when a wall is stiffened on one vertical edge and the length of the wall l is $l \geq 15\,t$, where t is the thickness of the wall, the wall should be considered as supported only on the top and bottom edges (Fig. 20).

The wall is subjected to a combination of vertical and lateral loads. The vertical loads result from the self-weight of masonry and the permanent and variable loads on the floors. The lateral load is caused by internal wind pressures. Fig. 21 shows the applied loads on the studied wall. The loads are calculated according to the EN 1991 norm and the Dutch national annexes to it. For the definition of the load combination, that results to the design values of actions, the provisions in the NEN 8700:2011 norm are considered. The applied load combination is described in Equation 55. The resulting design vertical load at the mid-height of the studied wall is *35.71 kN/m*. The design wind load is *0.624 kN/m^2*.

The timber beams, that support the timber floors of the building block, run through the masonry walls. Therefore, the loads from the floors are applied in the center of the wall section. An initial eccentricity is taken into account for the wall, as suggested in the EN 1996 norm (Equation 17). The wind load creates bending moments on the wall, which cause eccentricities. The eccentricity at the mid-height of the wall, because of the wind load is calculated according to Equation 56. Fig. 22 shows the variation of the eccentricity, along the wall height. The eccentricity due to creep is, also, considered at the mid-height of the wall, according to Equation 15 and Equation 18. Equation 15 results in the value of 0.028 m, for the eccentricity at the mid-height of the wall (e_{mk}). The wall is restrained, at the top and the bottom edges, by timber floors. Hence, the effective height is equal to the clear storey height of the wall. The Dutch National Annex to the EN 1996 norm suggests assuming a constant value of first-order eccentricity, over the height of the wall. This value is given in Equation 25 and, for the studied wall, is equal to 0.010 m. The value of eccentricity at the mid-height, calculated from Equation 15, is more unfavorable for the wall, compared to the respective value from Equation 25. Therefore, the value $e_{mk}=0.028\ m$ is considered.
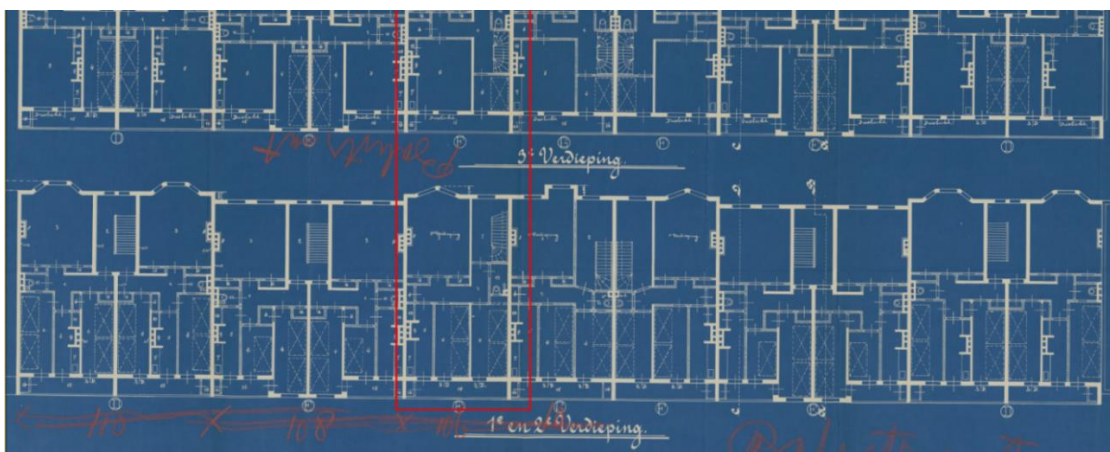
Fig. 16 Floor Plan of the first floor
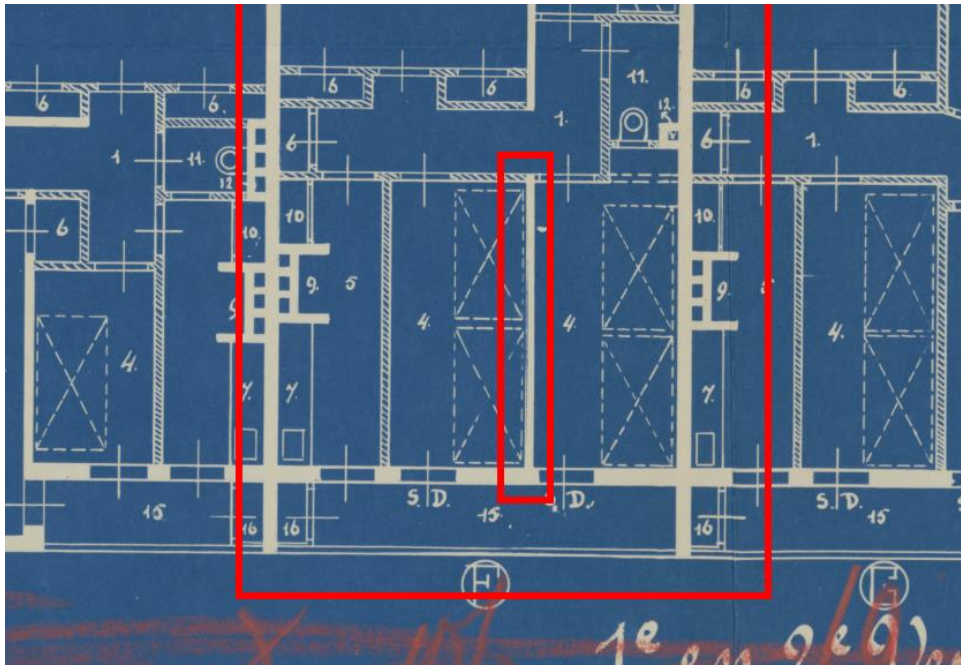
Fig. 17 Wall to be studied
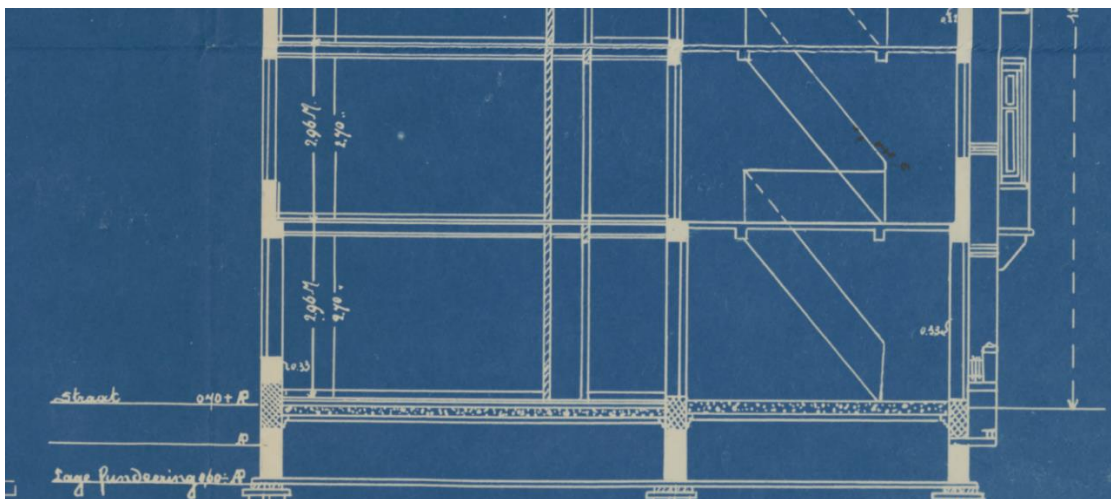
Fig. 18 Floor Heights
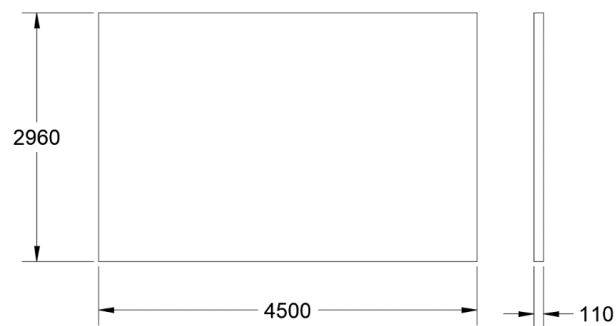
Fig. 19 Dimensions of the wall
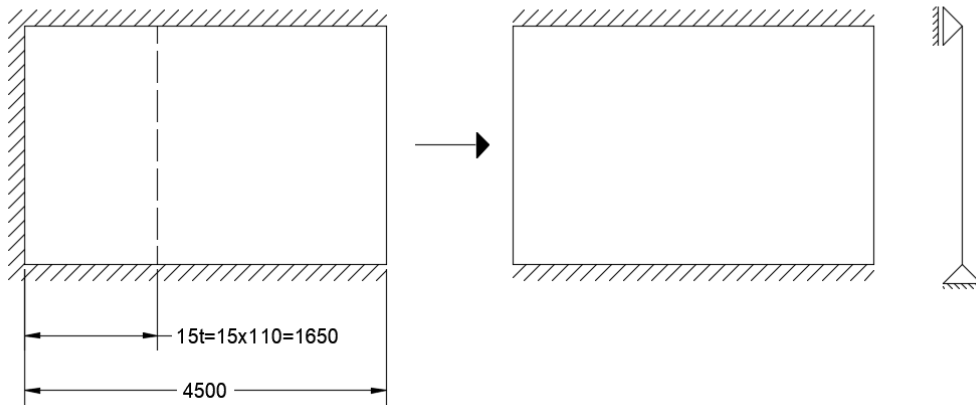
Fig. 20 Support Conditions of the wall
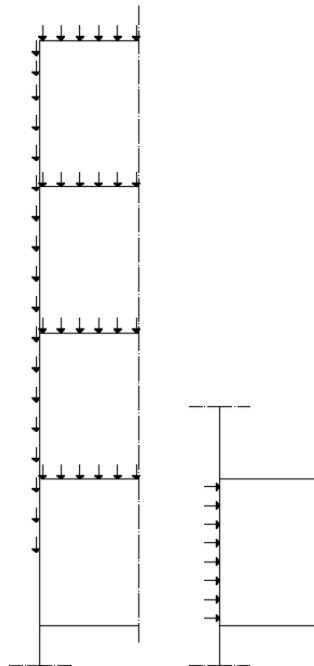
Fig. 21 Applied Loads on the studied wall

Equation 55 Load Combination with the Design Values of Actions [40]

$$1.15 \; x \; permanent \; loads + 1.3 \; x \; wind \; load + 1.3 \; x \; 0.4 \; x \; variable \; floor \; load$$

Equation 56 Eccentricity at the Mid-height of the Wall resulting from the Wind Load

$$e_{hm} = \frac{M_{wd}}{N_d}, \text{ where:}$$

    M_{wd}:   the design value of the moment, at the mid-height of the wall, because of the wind load

    N_{md}:   the design value of the vertical load, at the mid-height of the wall
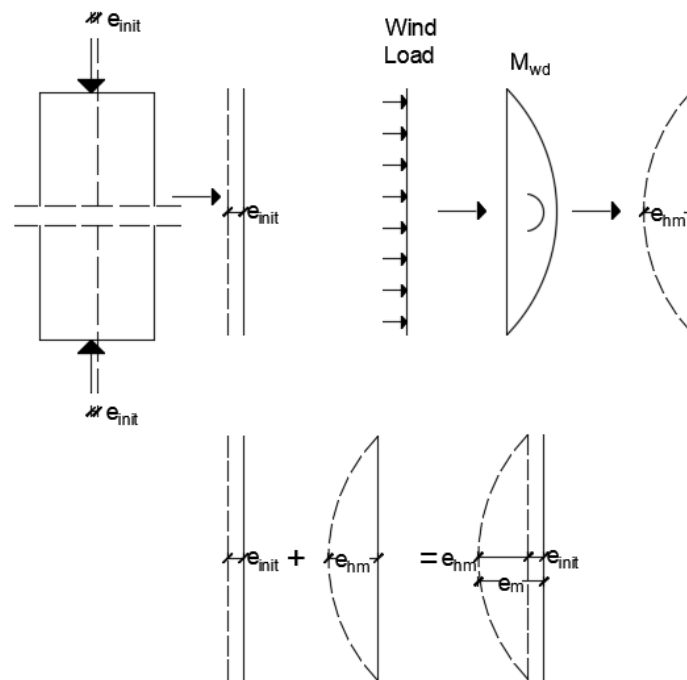
Fig. 22 Eccentricity along the height of the wall

Indicative values of the compressive strength, for the components of masonry walls in buildings, that were built in the late 19th - ealry20[th] century, were mentioned in section 5.2.1. These values are introduced in the formula for the calculation of the characteristic compressive strength of masonry (Equation 21). The constants *K, α, β* are obtained from the Dutch national annex to the EN 1996 norm. Their values are *K = 0.6, α = 0.65, β = 0.25*. The compressive strength for clay brick masonry, with mortar for general use, constructed before 1945, is *8.5 MPa* according to the Dutch practice guideline NPR 9998:2018. This is a mean value. The EN 1052-1 norm provides the relationship in Equation 57, in order to obtain the characteristic value of the compressive strength f_k, from the respective mean value *f*. Hence, the characteristic compressive strength, in this case, is *7.08 MPa*. Different possible values of the ratio E/f_k were discussed in section 5.2.2. In the context of the thesis, the following values are taken into account for the ratio E/f_k: 300, 450, 600, 700, 900, 1000. A table is created, with the possible combinations of values, for the characteristic compressive strength and the short-term secant modulus of elasticity of masonry. The table is in Appendix A. The listed mechanical properties are indicative for existing masonry buildings in the Netherlands, constructed in the late 19th - ealry20[th] century.

$f_k = \frac{f}{1.2}$, where:

    f: the mean compressive strength of masonry

8.2 Comparison Between Standards and Developed Formulas

A comparative sensitivity analysis is performed, with respect to the formulas for the estimation of the vertical resistance of URM walls, subjected to combined vertical and lateral loading. The formulas in the standards EN 1996 and NEN 6790 as well as the developed formulas, that were described in section 7.2.2, are taken into consideration. The table in Appendix B summarizes the expressions of the aforementioned formulas. The variable factors for the sensitivity analysis are the short-term secant modulus of elasticity and the characteristic compressive strength of masonry. The short-term secant modulus of elasticity changes while the characteristic compressive strength remains constant and vice versa. Considering different values of short-term secant modulus of elasticity, for a specific value of characteristic compressive strength, and vice versa is possible, when applying the formula in the EN 1996 norm (Equation 14), Bakeer's formulas (Equation 31, Equation 39) and Rankine method (Equation 30). However, the modulus of elasticity is not included in the calculation method of the vertical resistance for a masonry wall, suggested in the NEN 6790 norm (Equation 26). A specific ratio E/f_k is specified in the norm, that was mentioned in section 6.2. When using the expression of the critical axial load in Equation 54, it is suggested that the modulus of elasticity is calculated according to Equation 46. Equation 46 estimates the secant modulus of elasticity in a similar way as the short-term secant modulus of elasticity is calculated, according to the EN 1052-1 norm. Therefore, it is assumed that Equation 54 can be used for the calculation the critical axial load of walls, for different values of the ratio E/f_k for the masonry.

The eccentricity at the mid-height of the wall (e_{mk}) consists of the initial eccentricity (e_{init}), the eccentricity due to wind load (e_{hm}) and the eccentricity due to creep (e_k). The value of the eccentricity, at the mid-height, is mentioned in section 8.1. This value is used for the calculation of the capacity reduction factor at the mid-height of the wall ($\varPhi$), according to Equation 14, Equation 30, Equation 31 and Equation 39.

    The formula in Equation 54 makes use of two expressions for the eccentricity. Namely, the eccentricity e_i at the top or the bottom of the wall and the expression $\frac{\lambda_m M_w}{P_e r}$, for the eccentricity due to wind load. It is assumed that the eccentricity e_i is equal to the summation of the initial eccentricity e_{init} and the eccentricity due to creep e_k.

    The formula in Equation 26 was derived for linear variation of the first-order eccentricity, over the height of the wall. The user is allowed to specify the eccentricity at the top and the bottom of the wall (Fig. 13). Hence, it is not possible to consider the eccentricity scheme in Fig. 22. The eccentricity, at both ends of the wall, is assumed equal to the eccentricity at the mid-height of the wall (e_{mk}). This way, it is expected that the formula in Equation 26 will give a conservative estimation of the vertical resistance, each time.

The formulas, that make use of the capacity reduction factor at the mid-height of the wall ($\varPhi$), estimate the vertical resistance of the wall based on the design compressive strength. To obtain the design compressive strength from the characteristic compressive strength, a partial material factor (γ_M) equal to 1.70 is taken into consideration. [42] The critical axial load, that is estimated according to Equation

54, is, also, divided by the factor (γ_M). This way, the results, from the different formulas, can be compared on an equal basis.

The graphs in Fig. 23 - Fig. 26 show the variation in the vertical resistance of a slender URM wall, subjected to combined vertical and lateral loading, when the characteristic compressive strength of masonry (f_k) is constant and the short-term secant modulus of elasticity (E) increases. It is obvious that, the increase of the modulus of elasticity does not influence the value of the vertical resistance, which is calculated according to the formula in the NEN 6790 norm. This was expected, since a specific ratio E/f_k is specified in the norm and the modulus of elasticity is not included in the formula in Equation 26. It has, already, been discussed that, the formula in Equation 54 can be applied, on condition that the maximum moment on the member does not exceed the moment capacity. When the moment is larger than the peak moment, the stability limit is exceeded. Given the geometrical properties and the eccentricity e_i, it seems that the slender URM wall, which was described in section 8.1, cannot bear the applied wind load, when the short-term secant modulus of elasticity of masonry is smaller than 1800 MPa, approximately. For larger values of the modulus of elasticity, the formula in Equation 54 estimates, considerably, higher values of the vertical resistance, compared to the respective results, from the remaining formulas.

The influence on the vertical resistance, of a slender URM wall, from decreasing the characteristic compressive strength while the short-term secant modulus of elasticity of masonry remains constant, is shown in the graphs in Fig. 27- Fig. 29. The oxymoron, that the load-bearing capacity of the wall decreases while the compressive strength of the masonry increases, which was noticed by Bakeer [19], is verified in the curves, that represent the results from the formula in the EN 1996 norm. When the short-term secant modulus of elasticity remains constant and the ratio E/f_k decreases (the characteristic compressive strength increases), the vertical resistance decreases. It is noticed that the value of the characteristic compressive strength has no effect on the value of the vertical resistance, that is calculated from the second branch of Equation 39 and from Equation 54. Bakeer [37] stated that, in cases of slender masonry walls, which fail because of buckling, the vertical resistance depends exclusively on the modulus of elasticity.
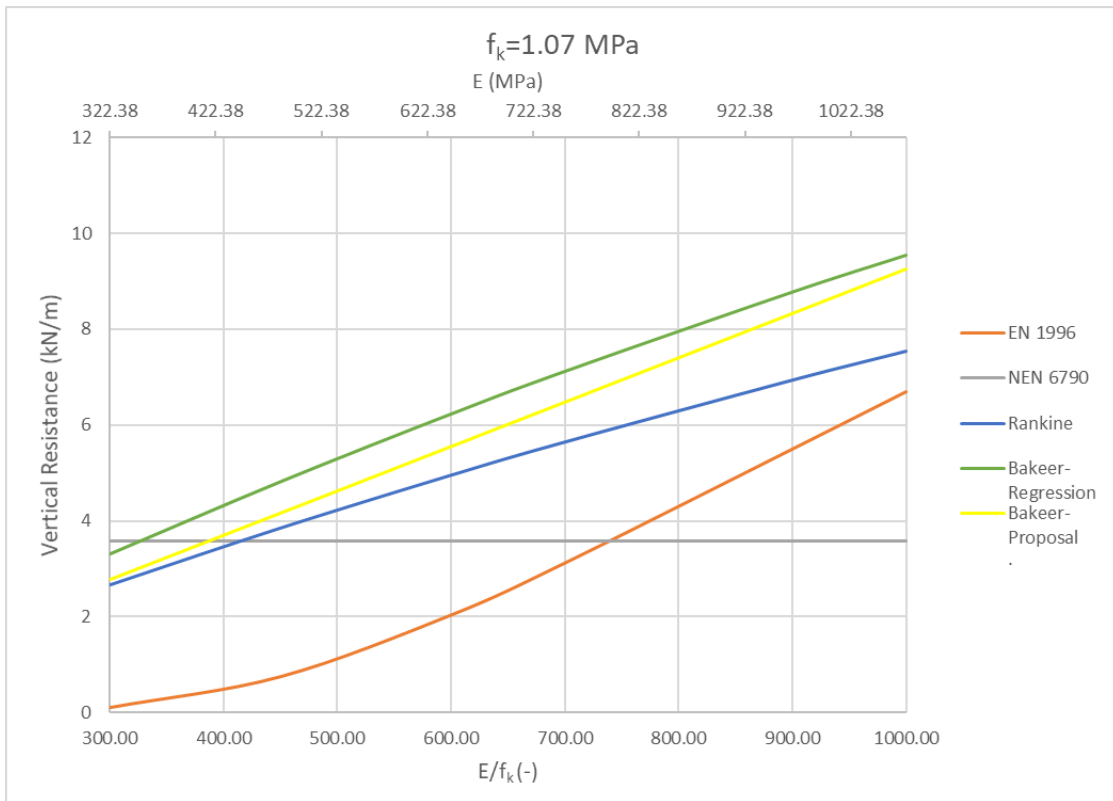
Fig. 23 Variation in the Vertical Resistance of a Slender URM wall when E changes and f_k=1.07 MPa
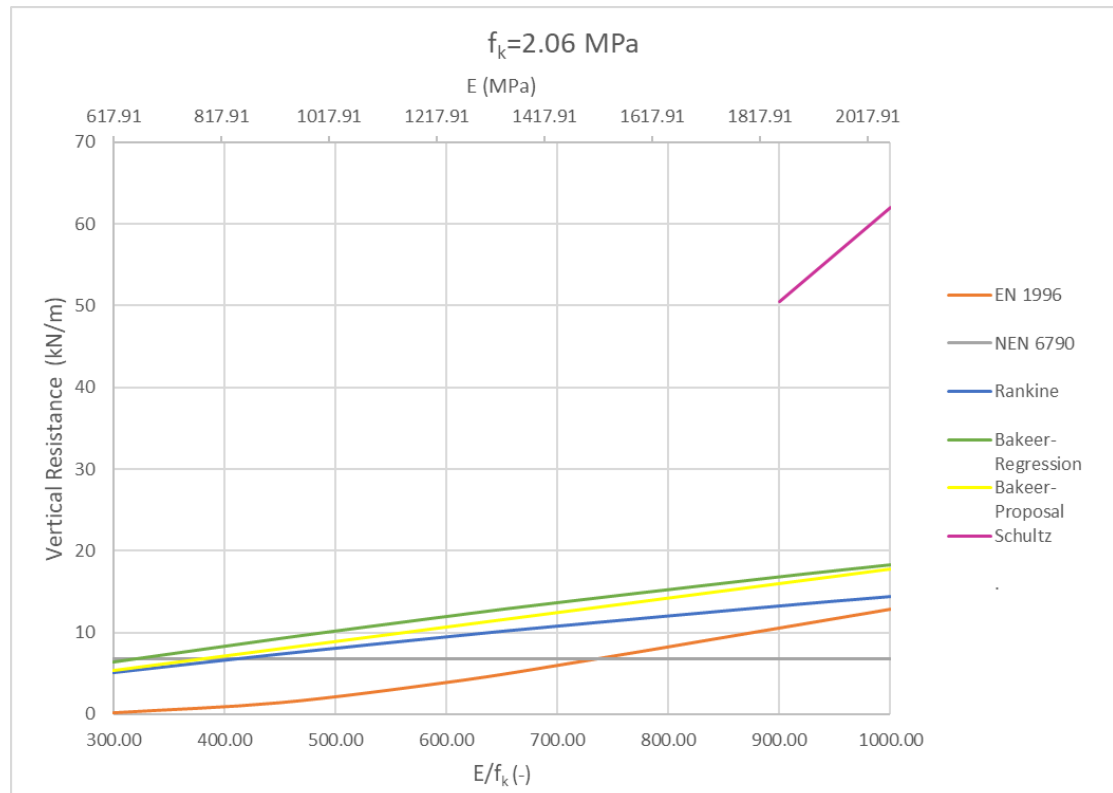
Fig. 24 Variation in the Vertical Resistance of a Slender URM wall when E changes and f_k=2.06 MPa
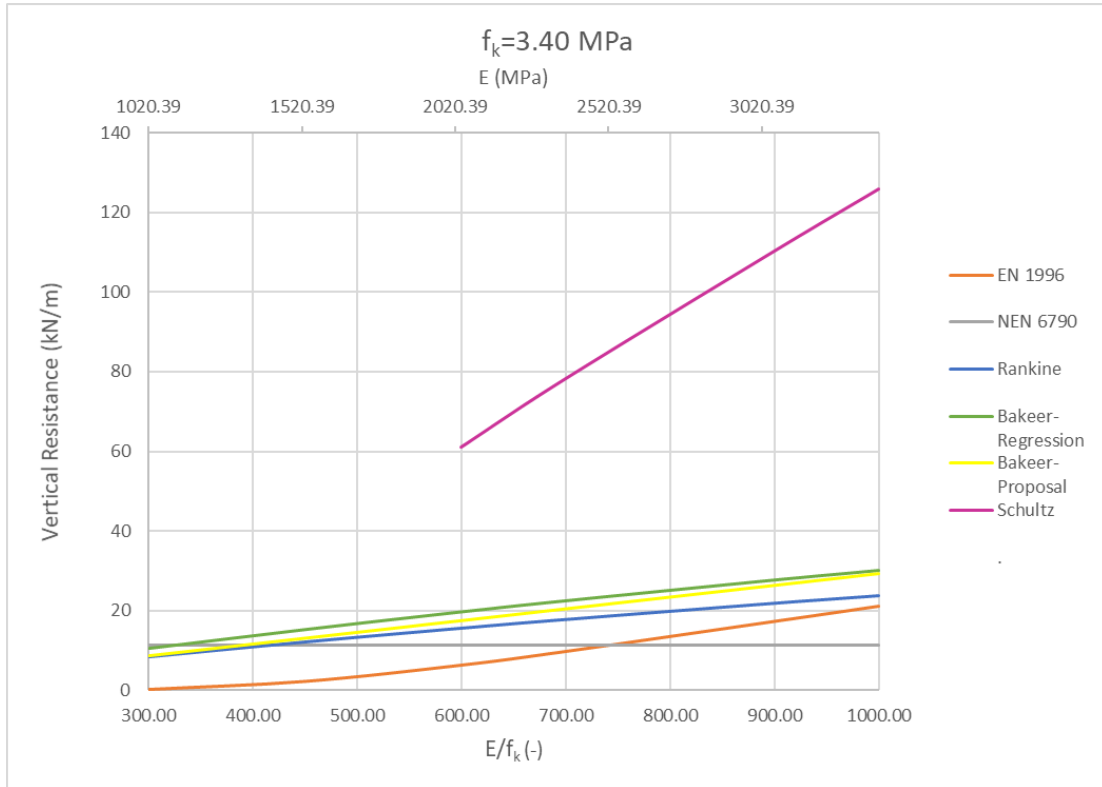
Fig. 25 Variation in the Vertical Resistance of a Slender URM wall when E changes and f_k=3.40 MPa
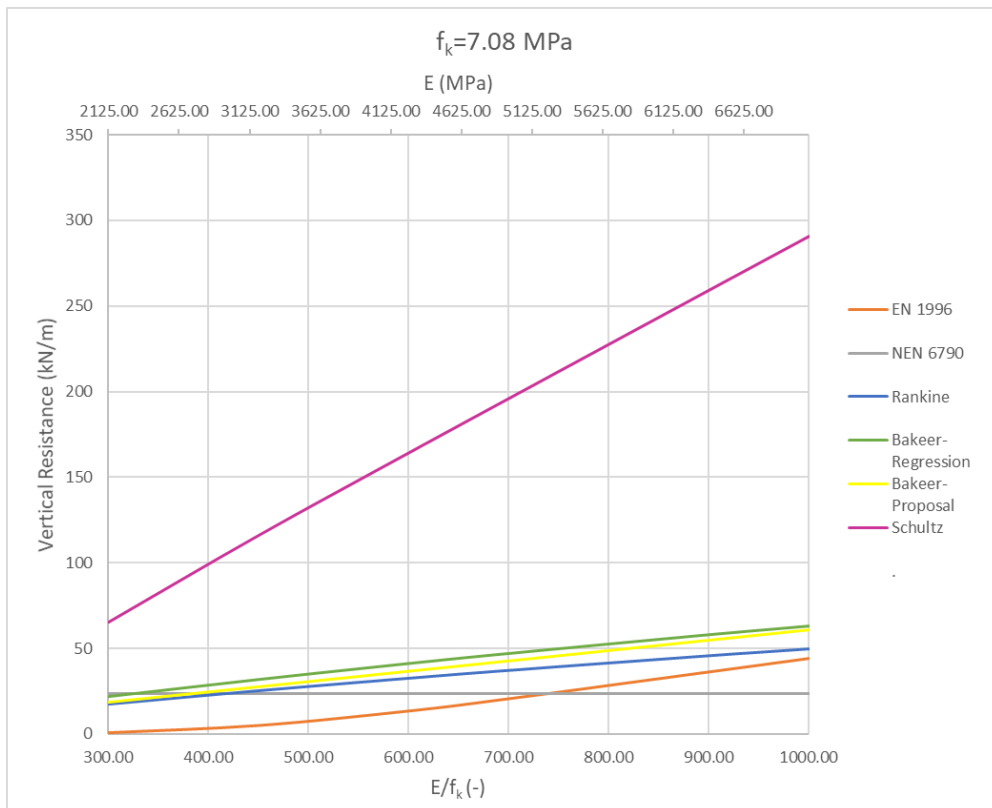
Fig. 26 Variation in the Vertical Resistance of a Slender URM wall when E changes and f_k=7.08 MPa
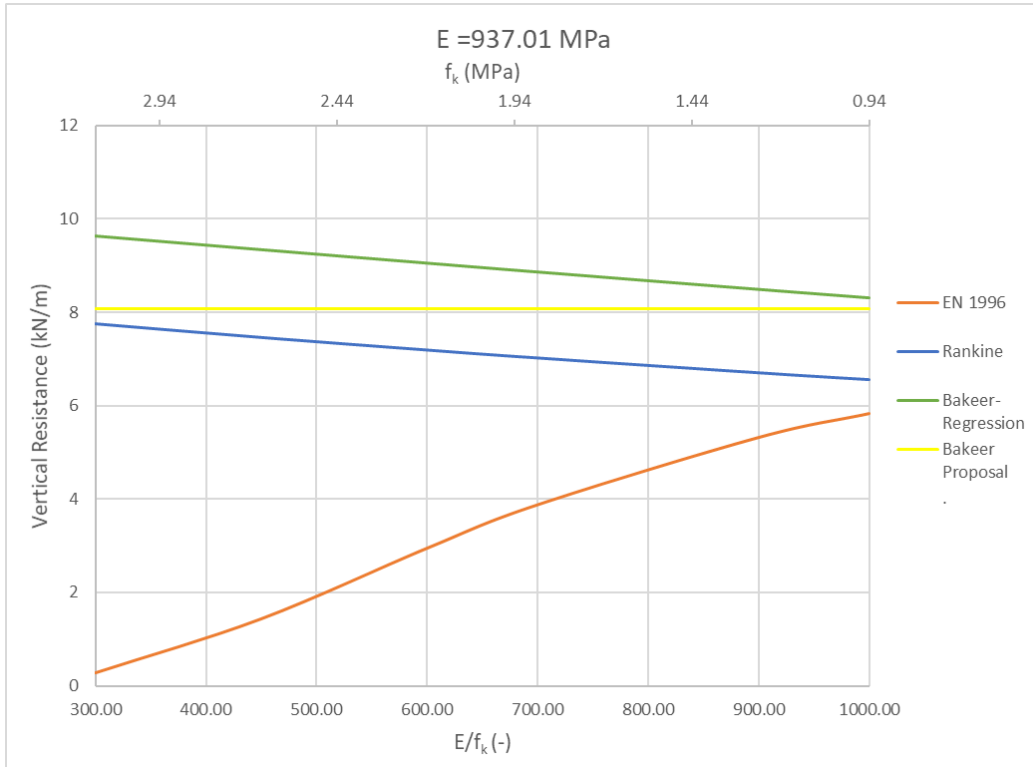
Fig. 27 Variation in the Vertical Resistance of a Slender URM wall when f_k changes and E=937.01 MPa
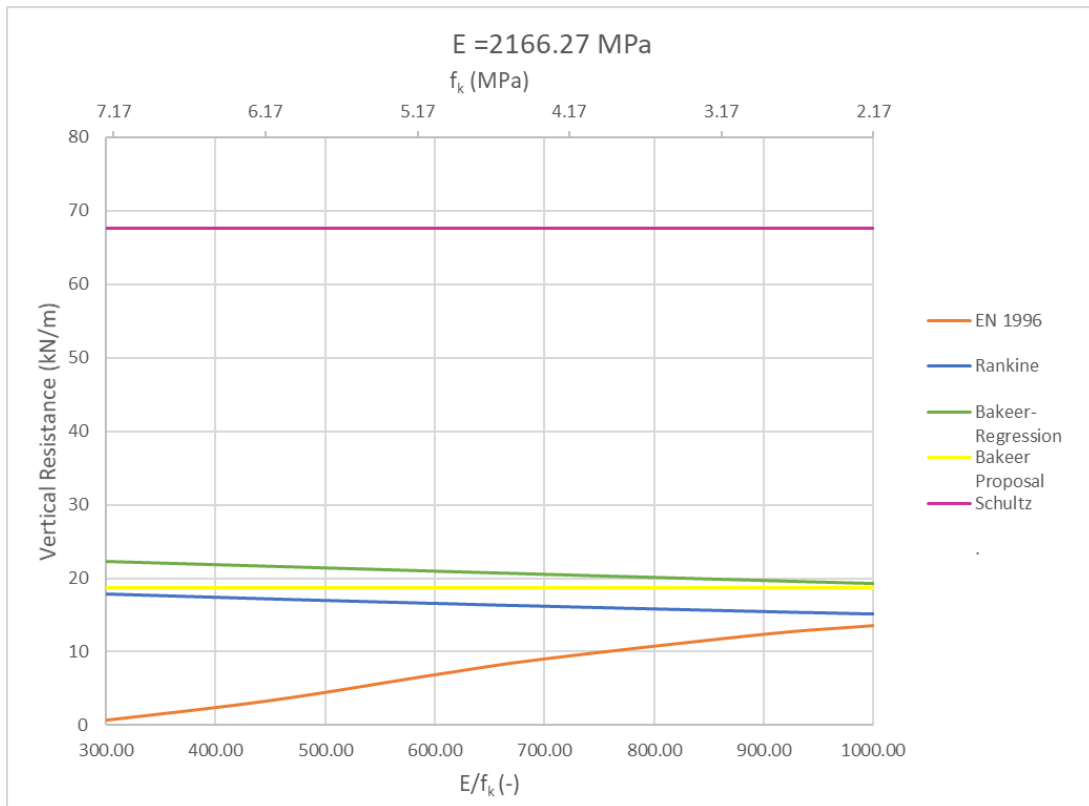
Fig. 28 Variation in the Vertical Resistance of a Slender URM wall when f_k changes and E=2166.27 MPa
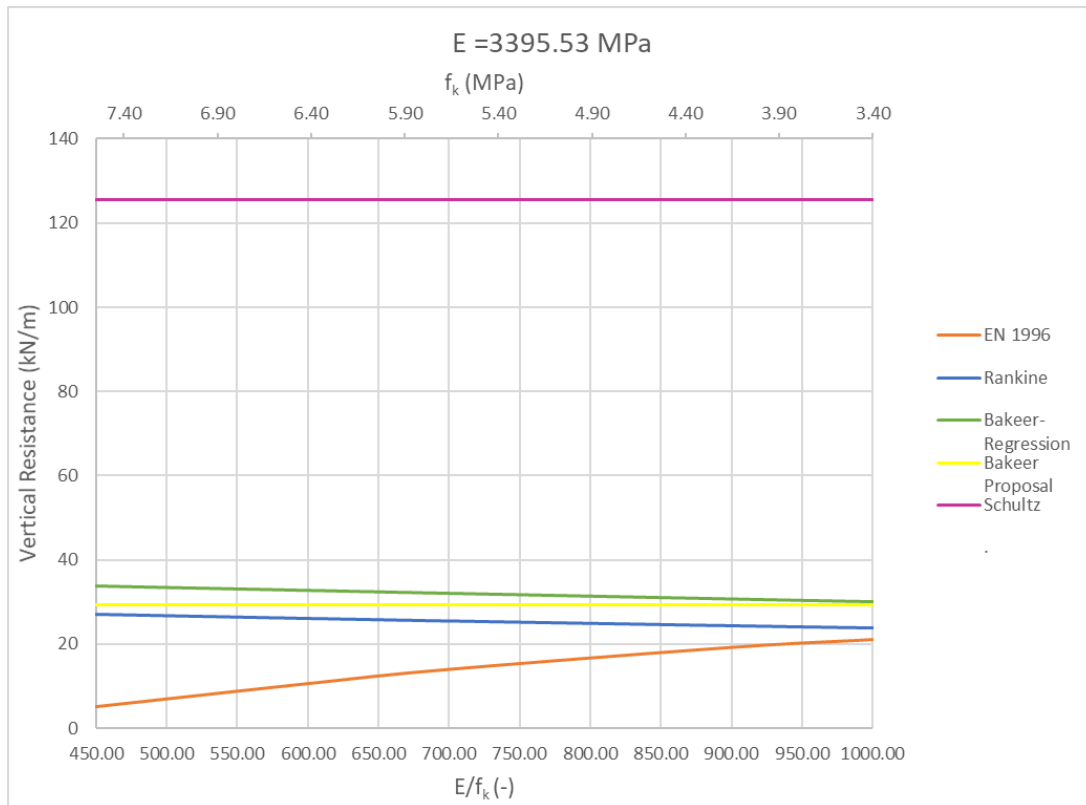
Fig. 29 Variation in the Vertical Resistance of a Slender URM wall when f_k changes and E=3395.53 MPa

8.3   Assessing the influence of the Tensile Strength on the Vertical Resistance

The formula in Equation 31 estimates the capacity reduction factor (Φ), at the mid-height of the wall. This expression neglects the tensile strength of masonry. Replacing the factor (Φ_0), in Equation 33, with the expression for (Φ), from Equation 31, the formula in Equation 58 is derived. The tensile strength is assumed to be 3% of the respective compressive strength. The following graphs (Fig. 30 - Fig. 33) compare the results from Equation 31 and Equation 58. The variable parameters are, again, the short-term secant modulus of elasticity and the characteristic compressive strength of masonry. Each time, one parameter changes and the other remains constant.

The influence of tensile strength on the vertical resistance, of the slender URM wall, increases as the value of the characteristic compressive strength becomes higher. This was expected, since the tensile strength is defined as a fraction of the respective compressive strength of masonry. It is, also, noticed that, the deviation between the values of vertical resistance, from Equation 31 and Equation 58, becomes larger as the value of the short-term secant modulus of elasticity increases.

Equation 58 Capacity Reduction Factor (Φ) at the Mid-height of the Wall considering the Influence of the Masonry Tensile Strength [20], [19]

$$\Phi = \left(1 - 2\frac{e_{mk}}{t}\right)\left[5.1\left(\frac{e_{mk}}{t}\right)^2 - 2.4\,\frac{e_{mk}}{t} + 1\right]\frac{atan\left(1.13\,u'^2\right)}{1.13\,u'^2} + \Delta\Phi_{f_t}, \text{ where:}$$

e_{mk}:   the eccentricity at the mid-height of the wall (Equation 15)

t: the thickness of the wall

u':   a non-dimensional parameter, that takes into account the slenderness, the eccentricity of loading and the masonry stiffness (Equation 32)

$\Delta\Phi_{ft}$:   factor that allows for the influence of the tensile strength of masonry (Equation 34)
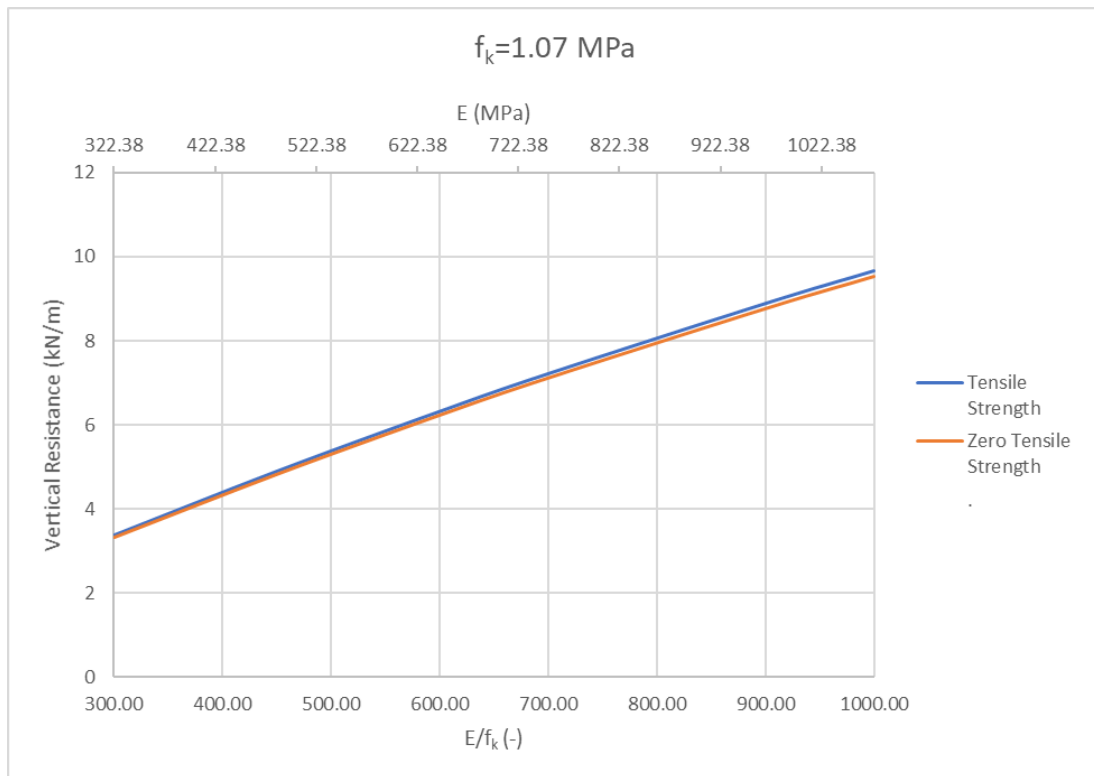
Fig. 30 Comparison between the results from Equation 31 and Equation 58 when E changes and f_k=1.07 MPa
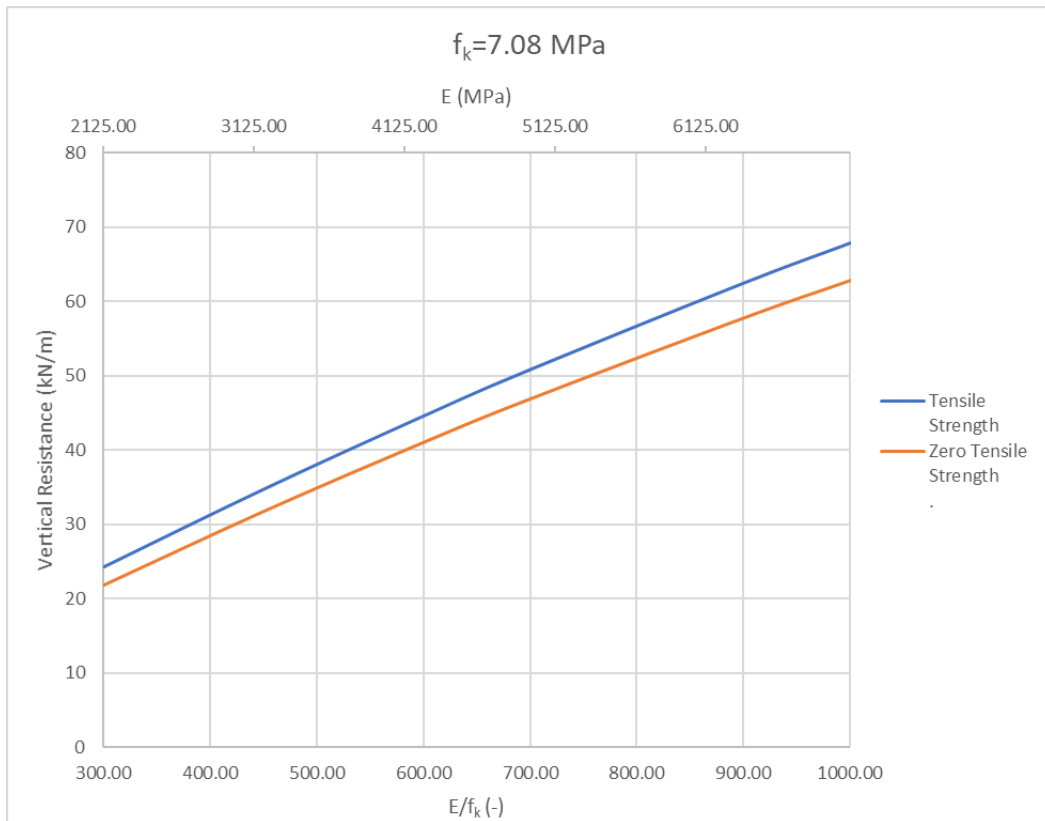
Fig. 31 Comparison between the results from Equation 31 and Equation 58 when E changes and f_k=7.08 MPa
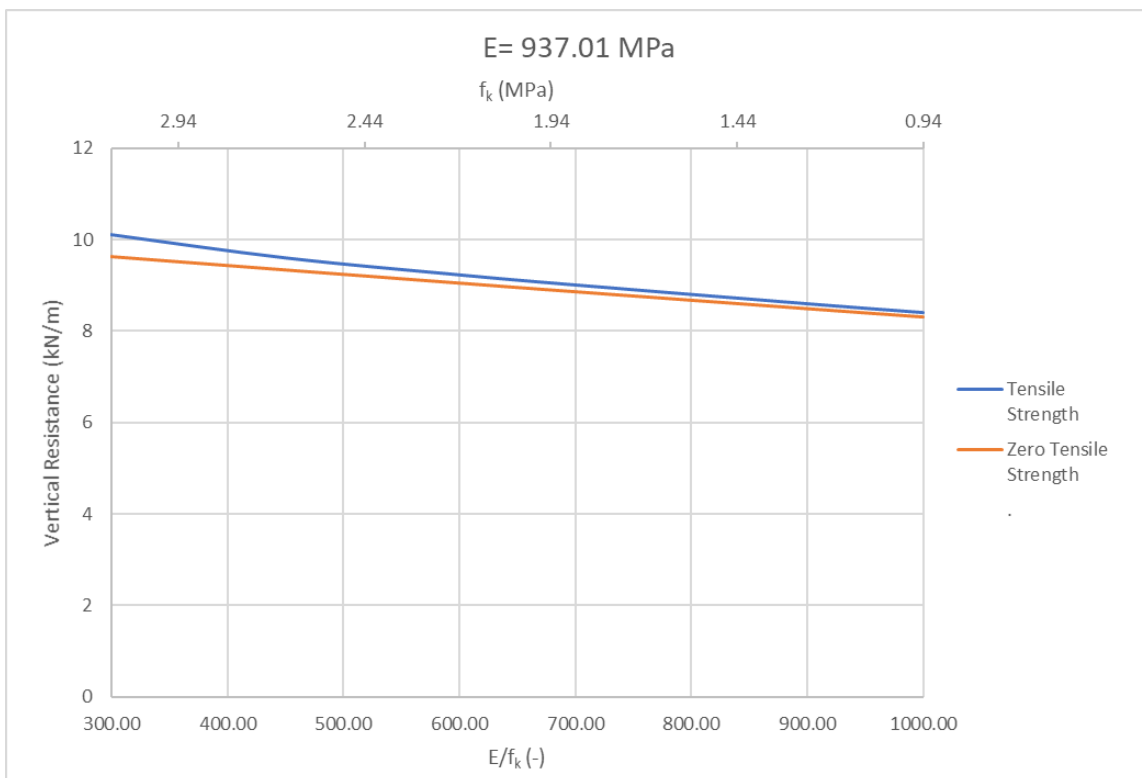
Fig. 32 Comparison between the results from Equation 31 and Equation 58 when f_k changes and E=937.01 MPa
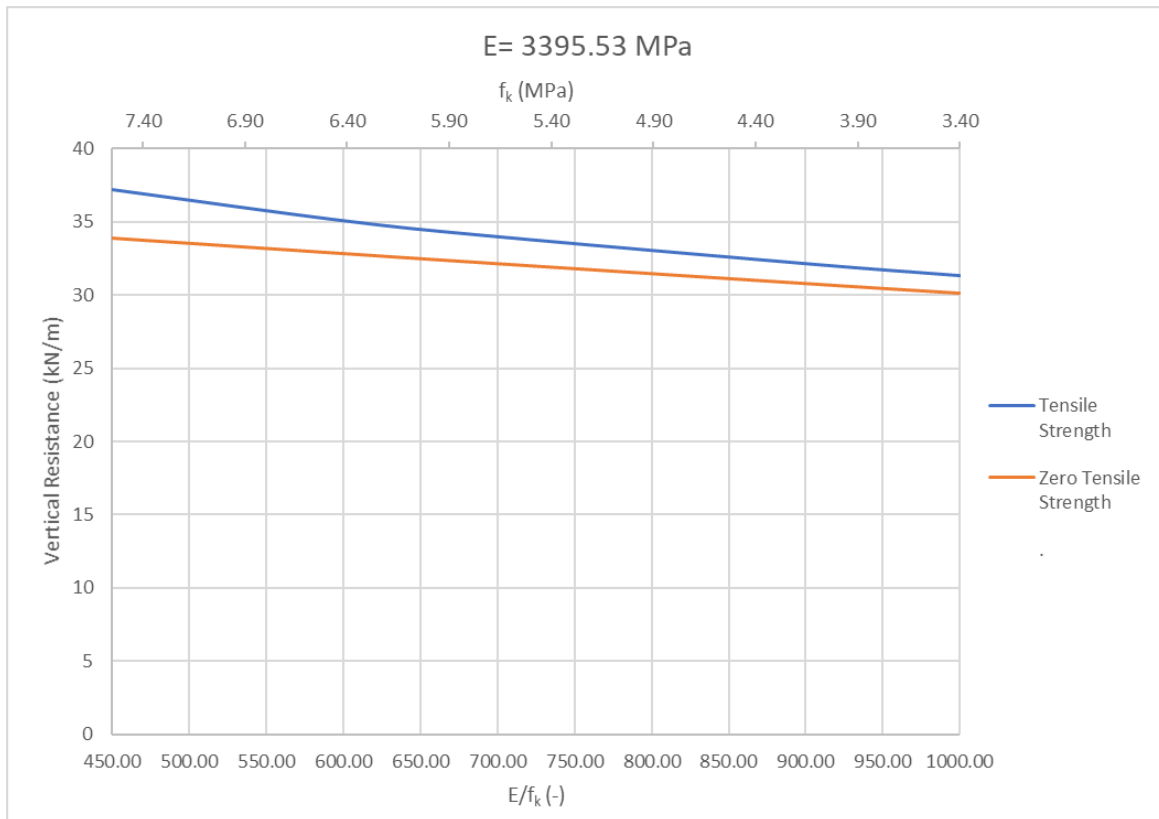
Fig. 33 Comparison between the results from Equation 31 and Equation 58 when f_k changes and E=3395.53 MPa

9 Finite Element Analysis

9.1 Finite Element Model

An appropriate FE model for the case study of URM wall (section 8.1) needs to be created. Non-linear analysis will be performed on the model. The results from the non-linear FE analysis will provide the value of the vertical resistance of the wall, when it is subjected to different values of wind load, including the case when the wind load is zero. Further, FE models of slender URM walls, with different geometrical and material properties will be created and analyzed. Changing one relevant parameter, each time, their influence on the vertical resistance of the wall can be estimated. The parameters, that seem to affect the vertical resistance of URM walls, according to standards, for the design of masonry structures, as well as the mentioned literature, will be assessed. Namely, the slenderness ratio, the eccentricity, the compressive and the tensile strength of masonry as well as the modulus of elasticity.

The research interest lies on the behavior of the masonry wall, as a structural component. Localized phenomena are of secondary importance. Therefore, a macro-modelling approach is considered suitable in this case. Lourenço [9, p. 304] stated that *"in a macro-modelling strategy - units, mortar and unit-mortar interface are smeared out in a homogeneous continuum"*. Hence, continuum elements will be used for the FE modelling of the wall. The finite element software package DIANA will be used for the analysis. A numerical integration is carried out, on the finite elements, and integration points are defined over the area of each element. [43] The smeared concept applies for the formation of cracks on the URM wall, too. Cracking is dispersed over the area of influence of an integration point. [5] Therefore, an appropriate crack bandwidth will be determined for the software. [44]

Three different FE models of the case study of URM wall (section 8.1) are created. The first model consists of curved shell elements (Fig. 34). Since the wall is simply supported on the top and bottom edges, a model of a unit-length segment of the wall is specified. The height and the thickness of the wall are shown in Fig. 19. The stresses, in the direction normal to the plane of curved shell elements, are assumed to be zero ($\sigma_{zz}=0$). [45] The second technique models the URM wall as a beam (Fig. 35). The smallest dimension of the cross-section of the beam is equal to the wall thickness. The other dimension has a unit length. The third model comprises plane strain elements (Fig. 36). In this case, the cross-section of the wall is modelled. This technique seems, also, appropriate, given the support conditions of the wall (Fig. 20). Plane strain elements have a unit thickness t and the strains, in the direction normal to their face, are zero ($\varepsilon_{zz}=0$). [46]

The same material model is assigned to the three aforementioned FE models of the URM wall. Specifically, the Total Strain Crack Model. The modulus of elasticity, the Poisson's ratio as well as the parameters, that define the response of the material under compression, tension and shear, comprise the input for the material model. The tension softening is defined as linear – based on the fracture energy. Furthermore, a parabolic compression curve, again, based on the fracture energy, is considered. The default shear parameters are assigned. [47] The material properties are obtained from the Dutch practice guideline NPR 9998:2018. The properties for clay brick masonry, with mortar for general use, constructed before 1945, are relevant. The values of strength and modulus of elasticity are mean values and are introduced, as such, in the software, for consistency reasons. Table 2 shows the input for the material model. The crack bandwidth is determined according to Rots' element-based method. The size, the shape and the interpolation function, of the used finite element, specify the crack bandwidth h. [48] Hence, the crack band-width will be different in every FE model.

The case study of URM wall is subjected to the self-weight of masonry, the loads from the floors as well as the lateral load, which is caused by internal wind pressures (Fig. 21). The wall is located on the first floor of the building. The self-weight of masonry consists of the weight of the analyzed wall, which has a height equal to the clear storey height, and the total weight of the respective walls on the upper floors. Three load cases are assigned in the FE model. The first includes the self-weight of the analyzed wall. The self-weight of the respective walls, on the upper floors, as well as the loads from the floors are considered in the second load case. The third load case is relevant to the wind load. The self-weight of solid brick masonry with lime mortar is equal to 18kN/m^3. [49] Taking into consideration the load combination, which is described in Equation 55, the design value of the self-weight is 20.7 kN/m^3. A random value of 250 kN is assumed for the second load case. The design value of the wind load is assigned to the third load case. This value is equal to 0.624 kN/m^2.

In every FE model, an eccentricity, equal to 0.001 m, is specified over the height of the wall. The value is small, just to initiate bending moments on the URM wall, because of the eccentric application of the vertical loading. The sign of eccentricity is considered in an appropriate way, so that it increases the value of eccentricity from the wind load. The resulting eccentricity scheme, along the height of the wall, is shown in Fig. 22.

A non-linear analysis is performed for each FE model. The vertical loads (load cases 1,2) are applied in one step. The wind load (load case 3) is applied in small increments until the wall fails. The sequence of loading is shown in Fig. 37. The analysis is force-controlled. The arc-length control is, also, activated for the unrestrained nodes. The displacement of the unrestrained nodes, in the direction of application of the wind load, is taken into account for the arc-length control. The combined effects of force and displacement define the size of the load increments, in arc-length control. [50] The case study of URM wall is considered a slender wall. As it has already been discussed in section 4.2, slender walls fail because of buckling. Hence, both physically and geometrically non-linear effects need to be taken into consideration for the analysis. Initially, it is interesting to compare the results from the non-linear analysis of the three FE models and review the response of the wall, each time. Therefore, it is considered more appropriate to neglect the additional non-linearity, that is caused by the deformation of the geometry of the wall. The following sections describe the properties and the results from the non-linear analysis of the three FE models. One model is chosen, in order to continue with analyzing URM walls, of different geometrical and material properties. The influence on the results of the FE analysis, from introducing geometrically non-linear effects, is, also, assessed.
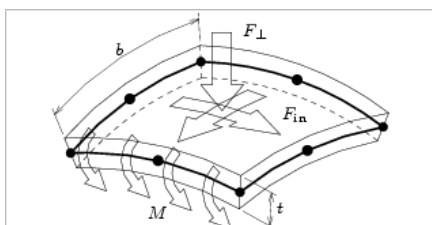
Fig. 34 Curved Shell Element [45]
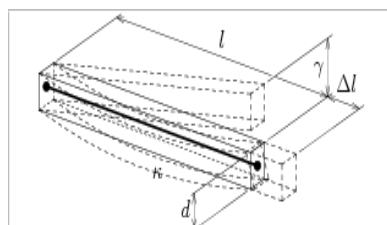
Fig. 35 Beam Element [51]
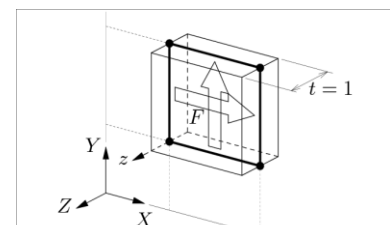
Fig. 36 Plane Strain Element [46]

Table 2 Input for the Material Model of the FE models

	Total Strain Based Crack Model		Source of Information
	Linear Material Properties		
	Young's modulus	5×10^9 N/m^2	NPR 9998:2018
	Poisson's Ratio	0.2	Literature [52]
	Mass Density	0 kg/m^3	
	Total Strain Based Crack Model		
	Crack Orientation	Fixed	
	Tensile Behavior		
	Tensile Curve	Linear-Crack Energy	
	Tensile Strength	100000 N/m^2	
	Mode-I Tensile Fracture Energy	10 N/m	
Material Model	Crack Bandwidth Specification	h [48]	
	Residual Tensile Strength	-	
	Compressive Behavior		
	Compression Curve	Parabolic	
	Compressive Strength	8.5×10^6 N/m^2	NPR 9998:2018
	Compressive Fracture Energy	20000 N/m	NPR 9998:2018
	Residual Compressive Strength	-	
	Reduction due to Lateral Cracking	No reduction	
	Stress Confinement	No increase	
	Shear Behavior		
	Shear Retention Function	Constant	Default by software
	Shear Retention	0.01	Default by software
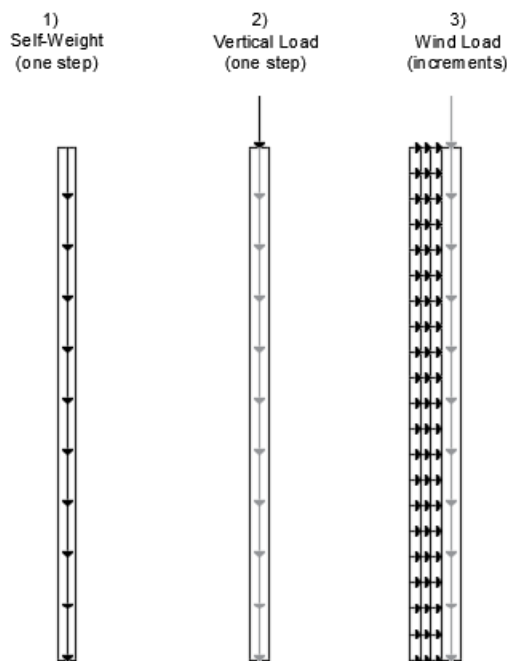
Fig. 37 Sequence of Loading in the Non-linear FE Analysis for the definition of the Wind Load, for which the Wall Fails, under certain Vertical Load

9.1.1 Model with Curved Shell Elements

The first model consists of curved shell elements. Fig. 38 shows the geometry and the support conditions of the FE model. The support conditions are, also, described in Table 3. Table 4 lists the properties of the finite elements. The area of the finite element is 0.01 m². The crack bandwidth h for higher order two-dimensional elements is $h = \sqrt{A}$, where A is the area of the element. [48] The self-weight of the wall (load case 1) is applied as surface load. Therefore, it is assigned to the software, after being multiplied with the thickness of the wall. Fig. 39 and Fig. 40 show the vertical and lateral loading (load cases 2,3), that the wall is subjected to. Defining eccentricity in the geometry of the elements, does not result in a constant bending moment along the height of the wall, as it is expected. Therefore, instead of the eccentricity, the bending moments on the top and the bottom of the wall, that the eccentricity would cause, are assigned as loads in the second load case. The load cases and the magnitude of loads are listed in Table 5. A non-linear analysis of the FE model is performed. Table 6 lists the characteristics of the analysis.

The evolution of the non-linear FE analysis, in terms of load – displacement, is shown in the graph in Fig. 43. The displacement is estimated on the highlighted node in Fig. 41. The graphs, in Fig. 44 and Fig. 45, show the evolution of stresses and strains, in the direction normal to the bed joints, on the most tensioned and compressed side of the wall, respectively. The latter graphs refer to the highlighted finite element in Fig. 42. Stresses and strains are estimated on the integration points. The output curves represent the analysis results. The input curves are drawn, according to the material model (Table 2). [47] The juxtaposition shows that the curves match. The stresses, in the direction normal to the bed joints of the masonry wall, when the maximum wind load is applied (orange dot on the curve in Fig. 43), are shown in Fig. 46 - Fig. 50. Different layers along the thickness of the wall are mentioned. Fig. 51 - Fig. 55 show the respective strains. The width, in the direction normal to the bed joints of the masonry wall, and the depth of the cracks are shown in Fig. 56 and Fig. 57.
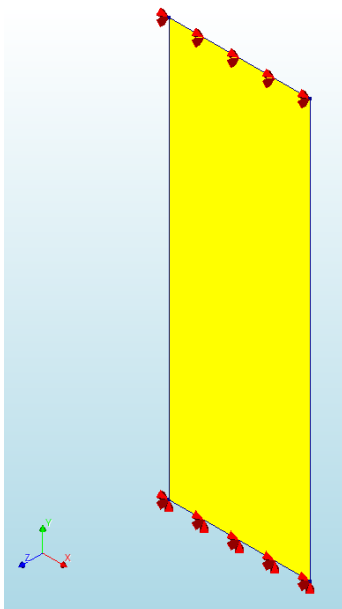
Fig. 38 Model with Curved Shell Elements
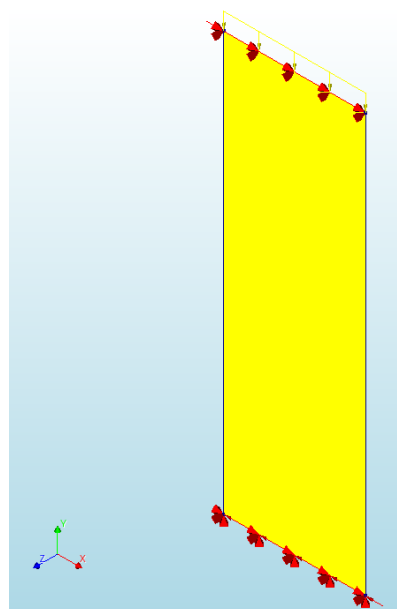
Fig. 39 Vertical Loading on Model with Curved Shell Elements
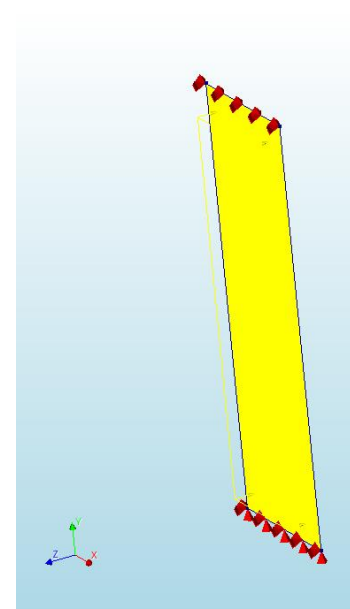
Fig. 40 Wind Load on Model with Curved Shell Elements

Table 3 Support Conditions of the Model with Curved Shell Elements

Supports	Top Edge	Fixed Translations	Tx, Tz
		Fixed Rotations	No fixed rotation
	Bottom Edge	Fixed Translations	Tx, Ty, Tz
		Fixed Rotations	No fixed rotation

Table 4 Properties of the Curved Shell Elements

Element	Class	Regular Curved Shells	
	Geometry	Thickness	0.11 m
		Size of Finite Elements	0.10 x 0.10 m^2
	Data	Type	CQ40S
		DOF	Ux, Uy, Uz, Φx, Φy - 8-noded
		Interpolation Scheme	Quadratic
		Integration Scheme over Element Area	Regular
		Integration Scheme over Element Thickness (number of integration points)	11

Table 5 Loads on the Model with Curved Shell Elements

Loads	*Masonry Weight (Load Case 1)*	
	Surface Force pointing downwards (negative y direction)	2277 N/m^2
	Loads from floors and walls above (Load Case 2)	
	Distributed force on top edge	250000 N/m
	Distributed moment on top and bottom edge (simulate the eccentricity of loading)	250 N
	Wind Load (Load Case 3)	
	Distributed force on the face of the element	624 N/m^2

Table 6 Characteristics of the Non-linear Analysis of the Model with Curved Shell Elements

Analysis	Structural Non-Linear	
	Non-Linear Effects	Physically Non-linear
	Equilibrium Iteration	
	Iterative Method	
	Maximum Number of iterations	200
	Method	Secant (Quasi-Newton)
	Type	BFGS
	First Tangent	Previous Iteration
	Convergence Norm	
	Satisfy all specified norms	Yes
	Displacement	Yes
	Convergence Tolerance	0.01
	No Convergence	Terminate
	Force	Yes
	Convergence Tolerance	0.01
	No Convergence	Terminate
	Load Steps	
	Masonry Weight (Load Case 1)	1
	Load from floors and walls above (Load Case 2)	1
	Wind Load (Load Case 3)	0.5(28)
		0.1(3)
		0.1(100) Arc-length control activated for the unrestrained nodes in the horizontal direction (direction of application of wind load)
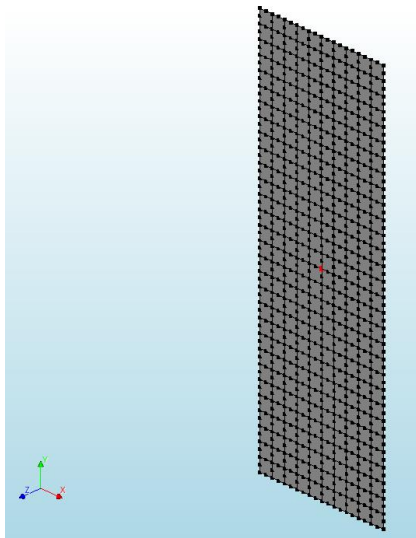
Fig. 41 Node at the Mid-height of the Model with Curved Shell Elements
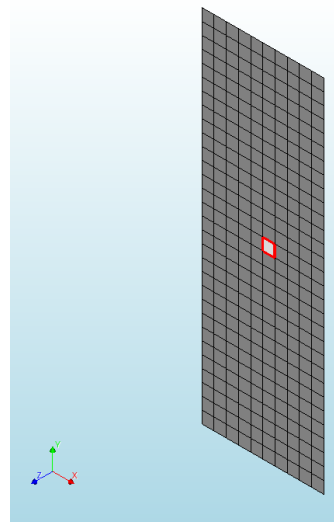
Fig. 42 Element at the Mid-height of the Model with Curved Shell Elements
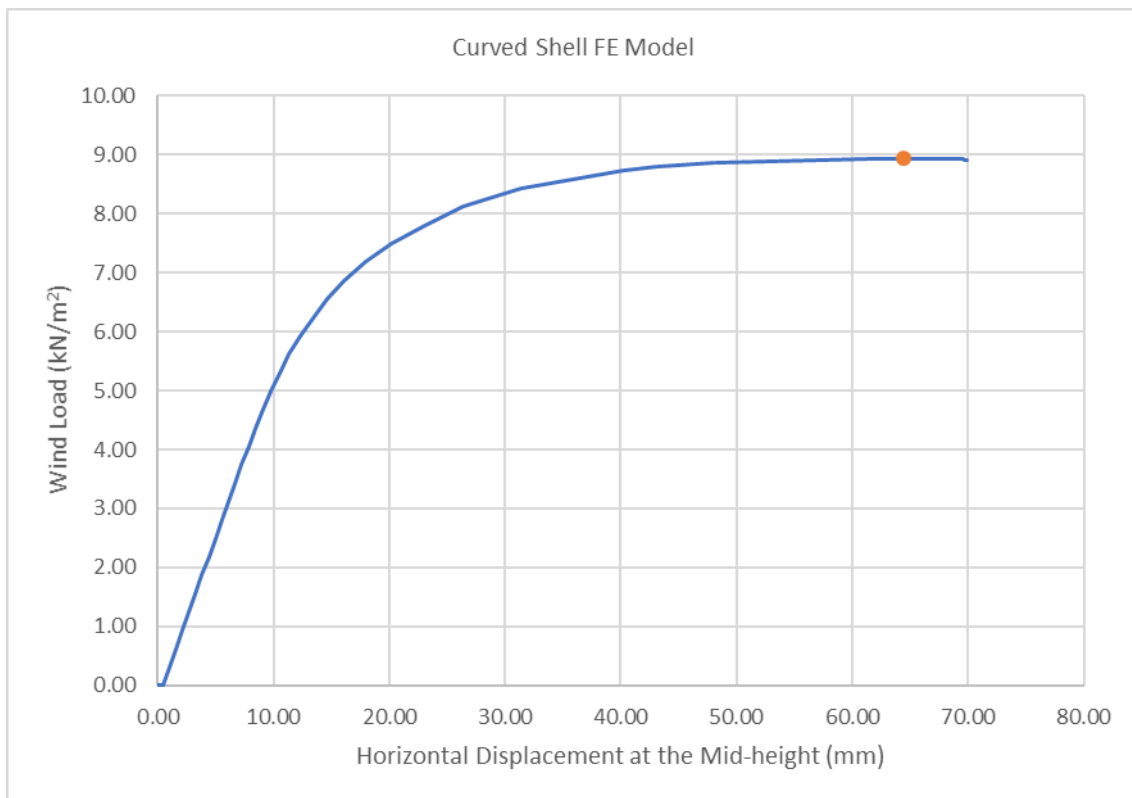
Fig. 43 Load - Displacement Curve for the Model with the Curved Shell Elements
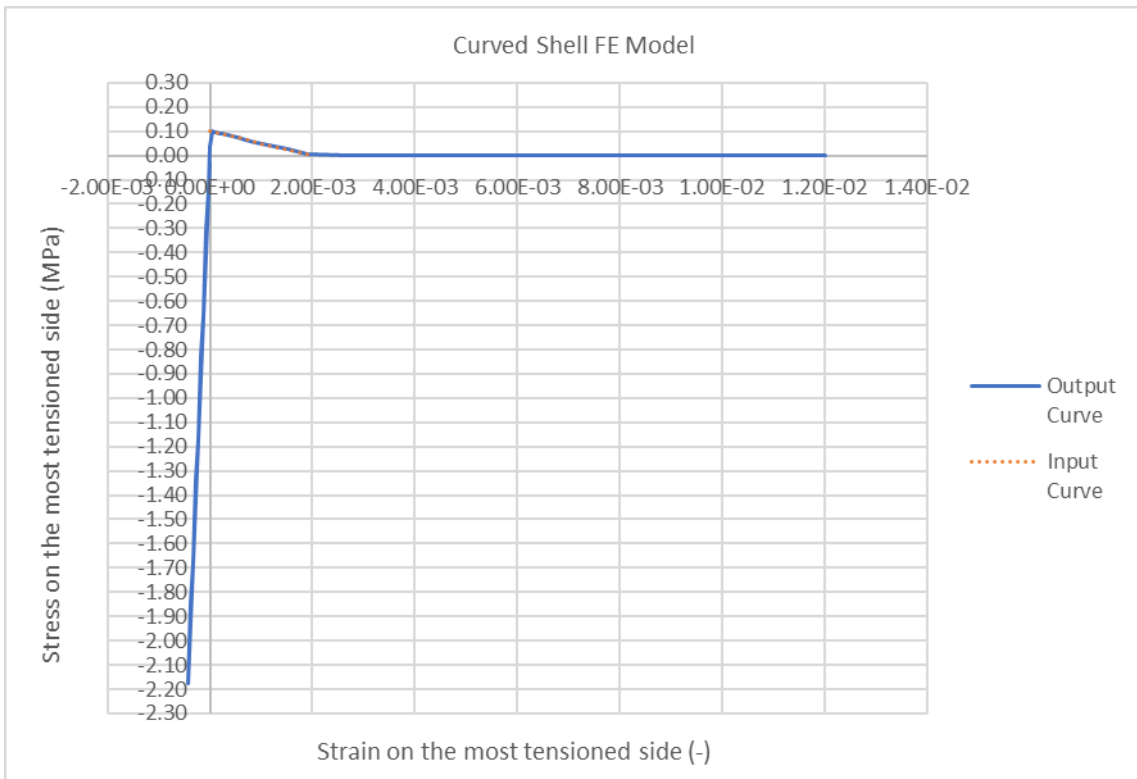
Fig. 44 Stress-Strain Evolution at the most tensioned side of the wall, modelled with Curved Shell Elements
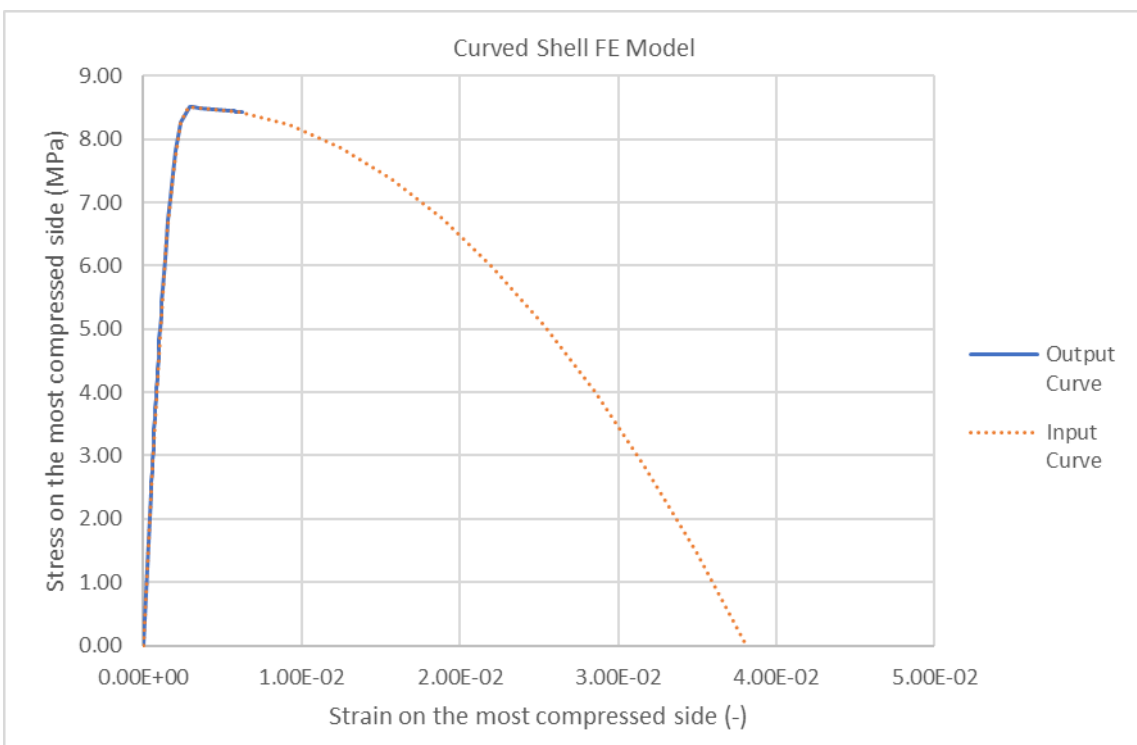
Fig. 45 Stress-Strain Evolution at the most compressed side of the wall, modelled with Curved Shell Elements
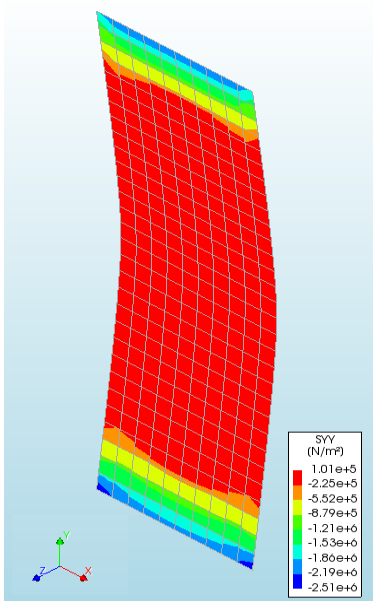
Fig. 46 Stresses on the Most Tensioned Side (layer 1/11) of the Wall modelled with Curved Shell Elements
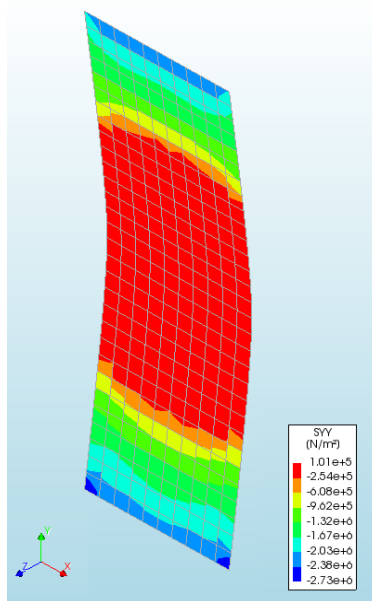
Fig. 47 Stresses on Layer 4/11 along the thickness of the Wall modelled with Curved Shell Elements
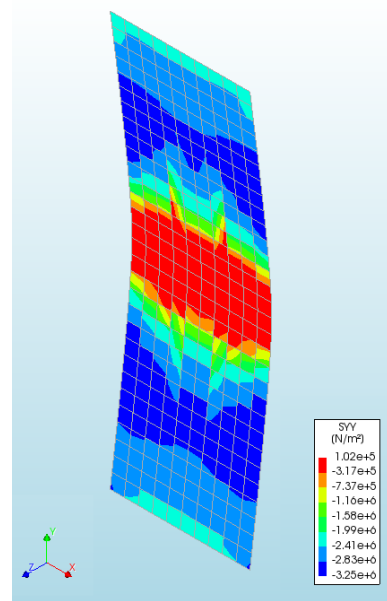
Fig. 48 Stresses on Layer 7/11 along the thickness of the Wall modelled with Curved Shell Elements
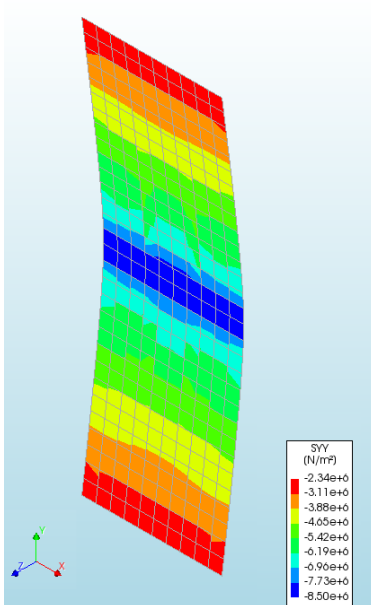
Fig. 49 Stresses on Layer 9/11 along the thickness of the Wall modelled with Curved Shell Elements
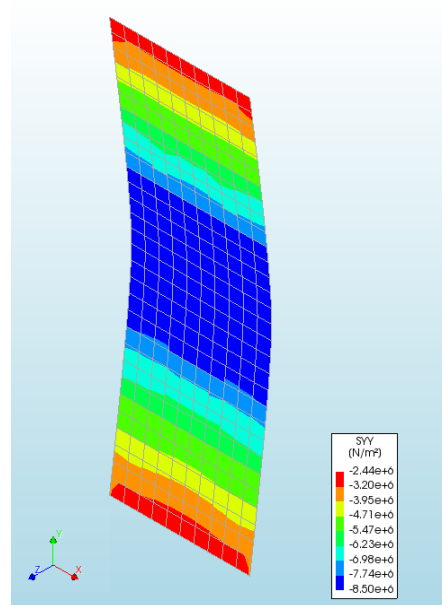
Fig. 50 Stresses on the Most Compressed Side (layer 11/11) of the Wall modelled with Curved Shell Elements
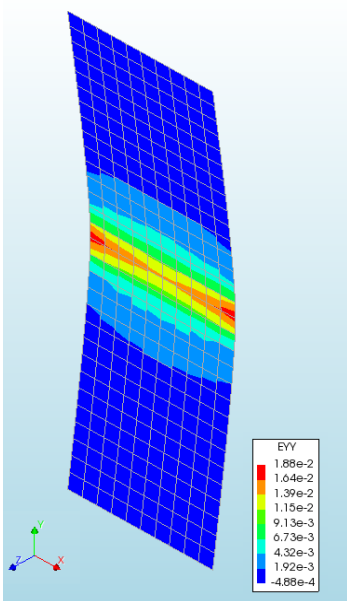
Fig. 51 Strains on the Most Tensioned Side (layer 1/11) of the Wall modelled with Curved Shell Elements
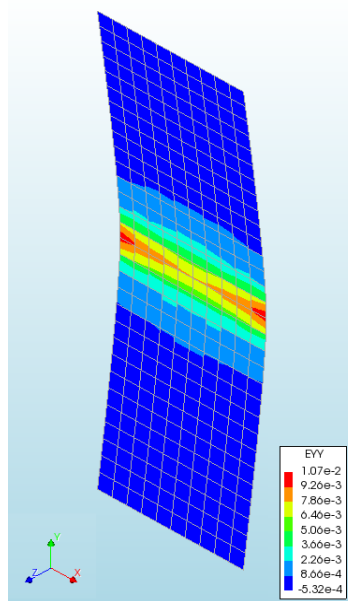
Fig. 52 Strains on Layer 4/11 along the thickness of the Wall modelled with Curved Shell Elements
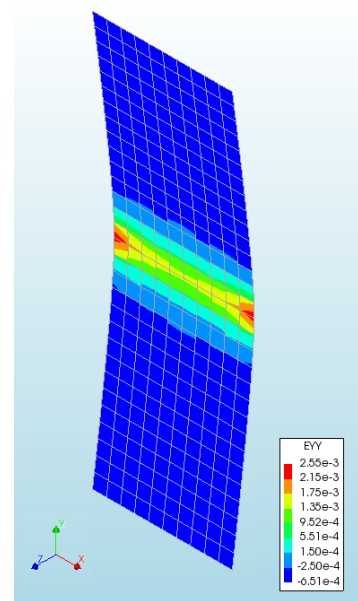
Fig. 53 Strains on Layer 7/11 along the thickness of the Wall modelled with Curved Shell Elements
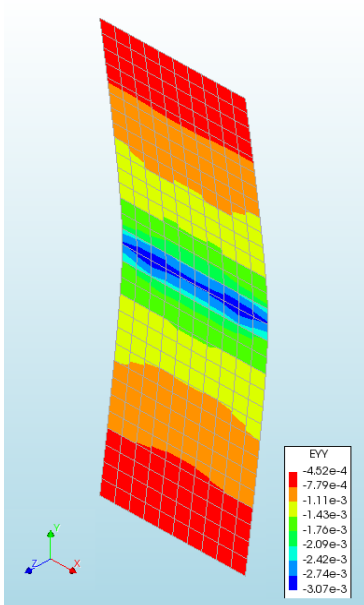
Fig. 54 Strains on Layer 9/11 along the thickness of the Wall modelled with Curved Shell Elements
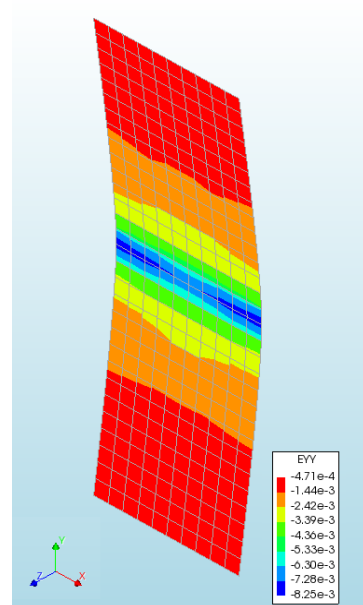
Fig. 55 Strains on the Most Compressed Side (layer 11/11) of the Wall modelled with Curved Shell Elements
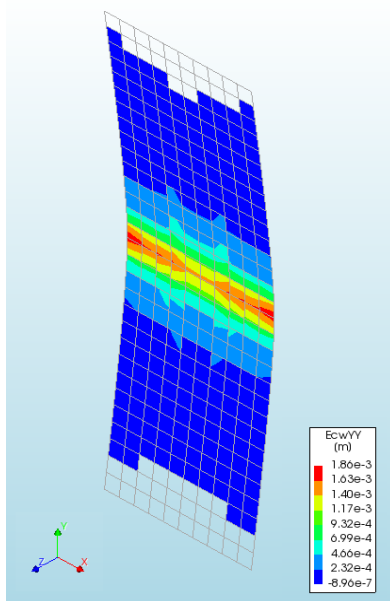
Fig. 56 Crack Widths on the Most Tensioned Side (layer 1/11) of the Wall modelled with Curved Shell Elements
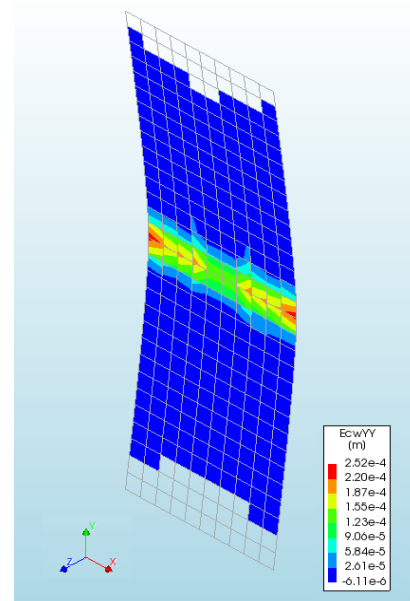
Fig. 57 Crack Widths on Layer 7/11 along the thickness of the Wall modelled with Curved Shell Elements

9.1.2 Model with Beam Elements

The second technique models the URM wall as a beam. Fig. 58 shows the geometry and the support conditions of the FE model. The support conditions are, also, described in Table 7. Table 8 lists the properties of the finite elements. The length of the finite element is 0.1 m. The crack bandwidth *h* for beam elements is equal to the length of the element. [48] The self-weight of the wall (load case 1) is uniformly distributed along the height. Therefore, it is assigned to the software, after being multiplied with the thickness of the wall. Fig. 59 and Fig. 60 show the vertical and lateral loading (load cases 2,3), that the wall is subjected to. The load cases and the magnitude of loads are listed in Table 9. The eccentricity is defined in the geometry of the elements. A non-linear analysis of the FE model is performed. Table 10 lists the characteristics of the analysis.

The evolution of the non-linear FE analysis, in terms of load – displacement, is shown in the graph in Fig. 63. The displacement is estimated on the highlighted node in Fig. 61. The graphs, in Fig. 64 and Fig. 65, show the evolution of stresses and strains, in the direction normal to the bed joints, on the most tensioned and compressed side of the wall, respectively. The latter graphs refer to the highlighted finite element in Fig. 62. Stresses and strains are estimated on the integration points. The output curves represent the analysis results. The input curves are drawn, according to the material model (Table 2). [47] The juxtaposition shows that the curves match. The stresses, in the direction normal to the bed joints of the masonry wall, when the maximum wind load is applied (orange dot on the curve in Fig. 63), are shown in Fig. 66 - Fig. 70. Different layers along the thickness of the wall are mentioned. Fig. 71 - Fig. 75 show the respective strains. The width, in the direction normal to the bed joints of the masonry wall, and the depth of the cracks are shown in Fig. 76 and Fig. 77.

Fig. 58 Model with Beam Elements
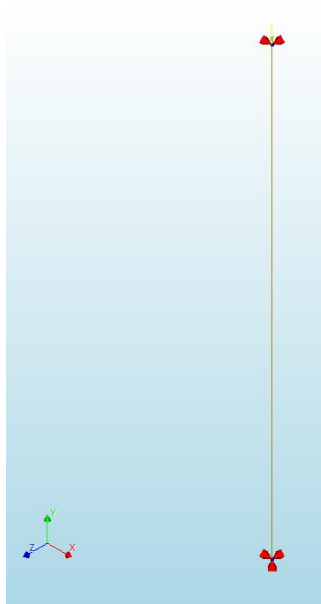
Fig. 59 Vertical Loading on Model with Beam Elements
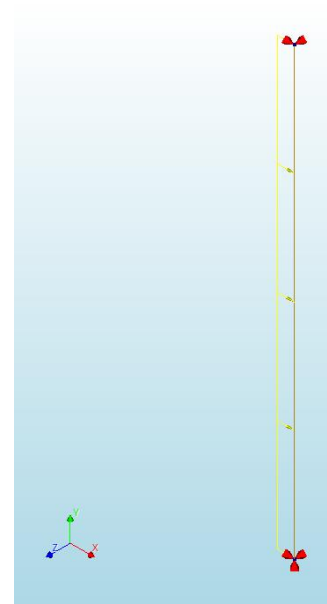
Fig. 60 Wind Load on Model with Beam Elements

Table 7 Support Conditions of the Model with Beam Elements

Supports	Top Edge	Fixed Translations	Tx, Tz
		Fixed Rotations	No fixed rotation
	Bottom Edge	Fixed Translations	Tx,Ty,Tz
		Fixed Rotations	No fixed rotation

Table 8 Properties of the Beam Elements

Element	Class	Class-III Beams 3D	
	Geometry	Shape	Rectangle
		Height of Rectangle	0.11 m
		Width of Rectangle	1.00 m
		Size of Elements	0.10 m
	Data	Type	CL18B
		DOF	Ux, Uy, Uz, Φx, Φy, Φz - 3-noded
		Interpolation Scheme	Quadratic
		Integration Scheme along the axis	2-point Gauss
		Integration Scheme in the area of the cross-section	11 x 11

Table 9 Loads on the Model with Beam Elements

Loads	Masonry Weight (Load Case 1)	
	Distributed force on the line (beam axis), pointing downwards (negative y direction)	2277 N/m
	Loads from floors and walls above (Load Case 2)	
	Point force on top vertex	250000 N
	Wind Load (Load Case 3)	
	Horizontal distributed force on the line (beam axis)	624 N/m

Table 10 Characteristics of the Non-Linear Analysis of the Model with Beam Elements

Analysis	Structural Non-Linear	
	Non-Linear Effects	Physically Non-linear
	Equilibrium Iteration	
	Iterative Method	
	Maximum Number of iterations	200
	Method	Secant (Quasi-Newton)
	Type	BFGS
	First Tangent	Previous Iteration
	Convergence Norm	
	Satisfy all specified norms	Yes
	Displacement	Yes
	Convergence Tolerance	0.01
	No Convergence	Terminate
	Force	Yes
	Convergence Tolerance	0.01
	No Convergence	Terminate
	Load Steps	
	Masonry Weight (Load Case 1)	1
	Load from floors and walls above (Load Case 2)	1
	Wind Load (Load Case 3)	0.5(28)
		0.1(2)
		0.05(250) Arc-length control activated for the unrestrained nodes in the horizontal direction (direction of application of wind load)
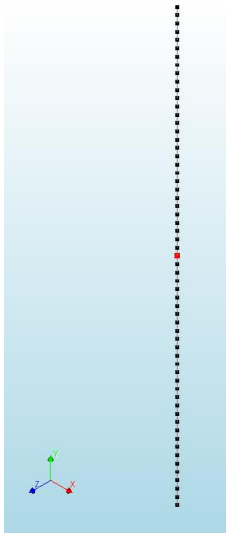
Fig. 61 Node at the Mid-height of the Model with Beam Elements
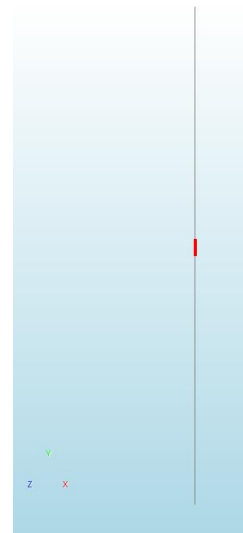
Fig. 62 Element at the Mid-height of the Model with Beam Elements
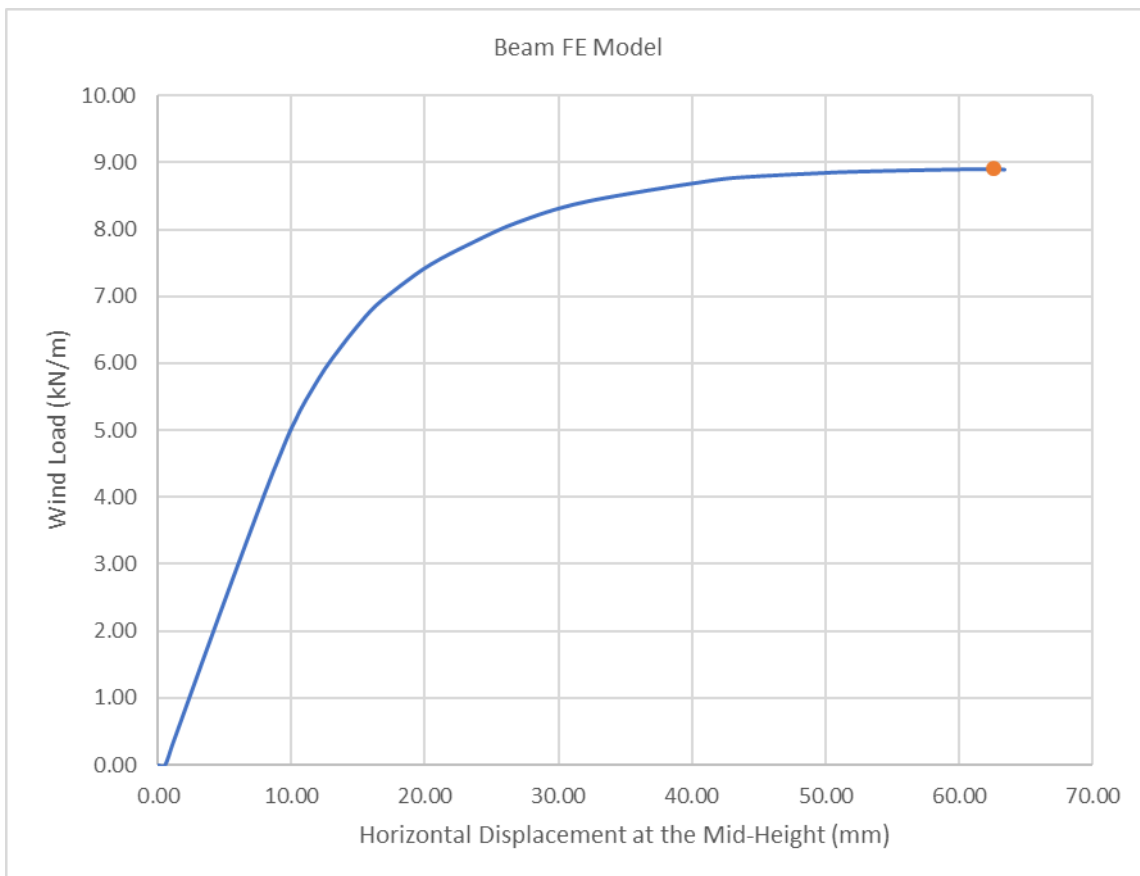
Fig. 63 Load – Displacement Curve for the Model with the Beam Elements
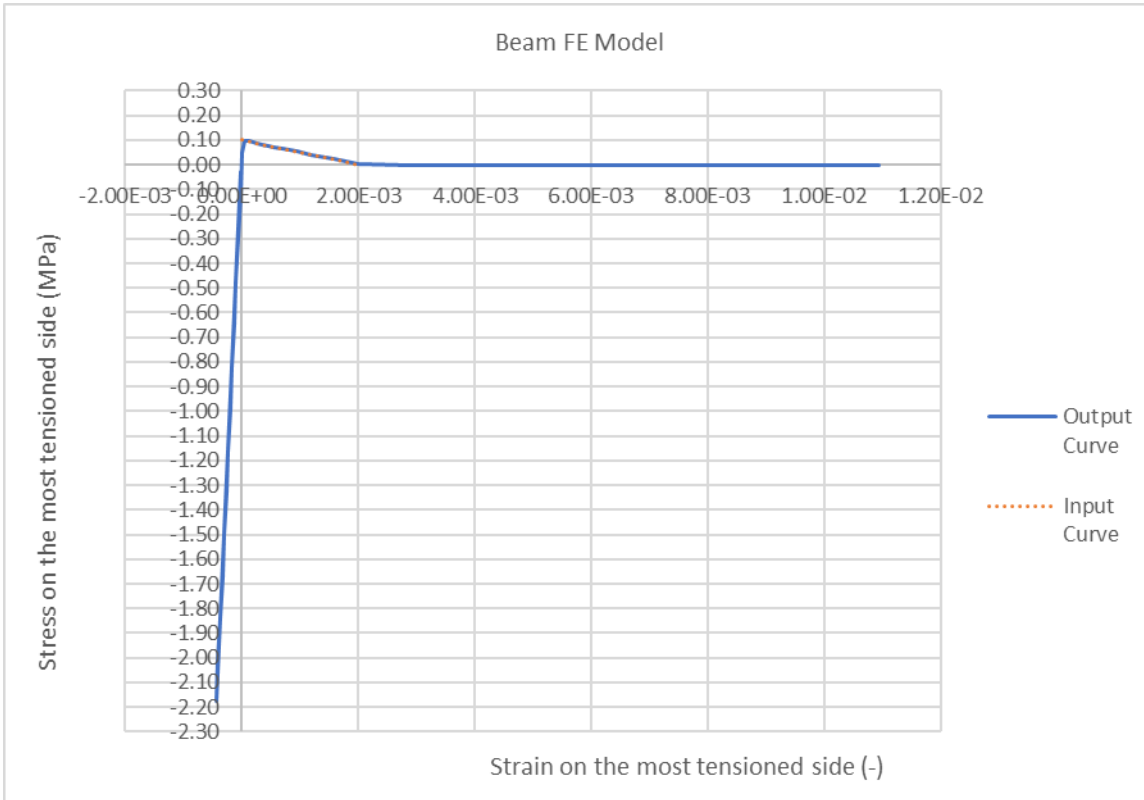
Fig. 64 Stress-Strain Evolution at the most tensioned side of the wall, modelled with Beam Elements
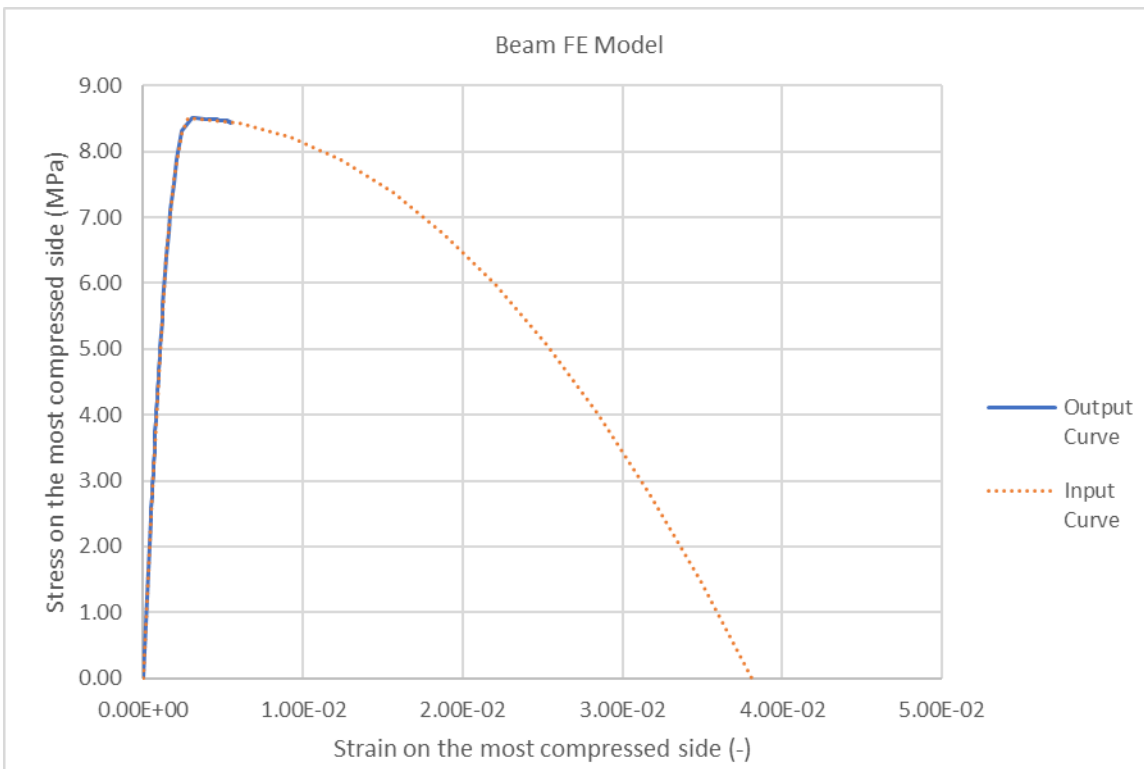
Fig. 65 Stress-Strain Evolution at the most compressed side of the wall, modelled with Beam Elements
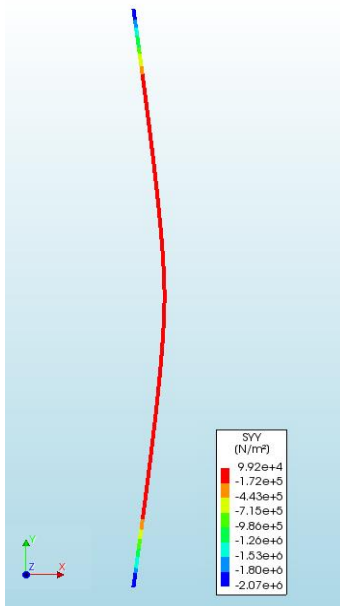
Fig. 66 Stresses on the Most Tensioned Side (layer 1/11) of the Wall modelled with Beam Elements
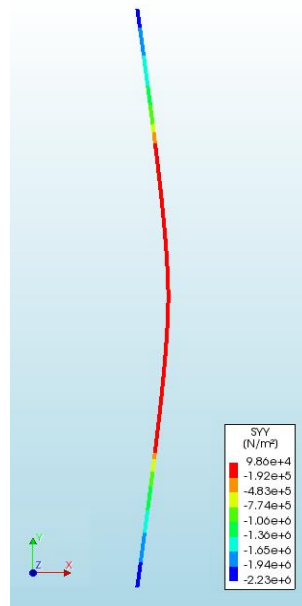
Fig. 67 Stresses on Layer 4/11 along the thickness of the Wall modelled with Beam Elements
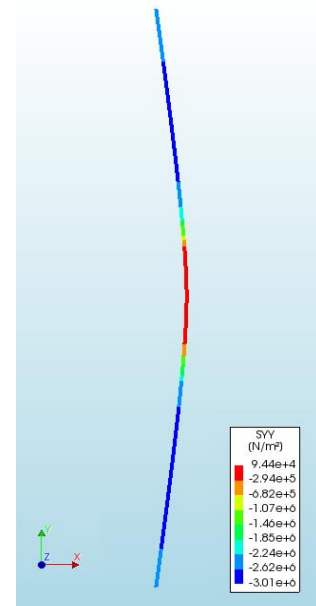
Fig. 68 Stresses on Layer 7/11 along the thickness of the Wall modelled with Beam Elements
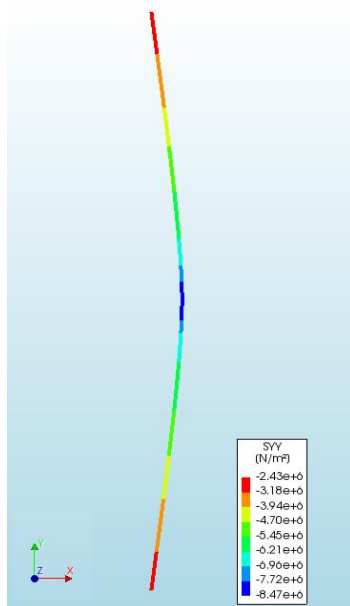
Fig. 69 Stresses on Layer 9/11 along the thickness of the Wall modelled with Beam Elements
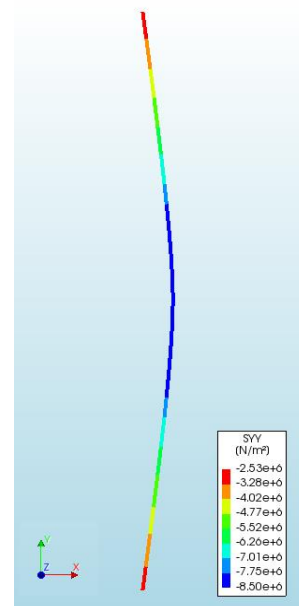
Fig. 70 Stresses on the Most Compressed Side (layer 11/11) of the Wall modelled with Beam Elements
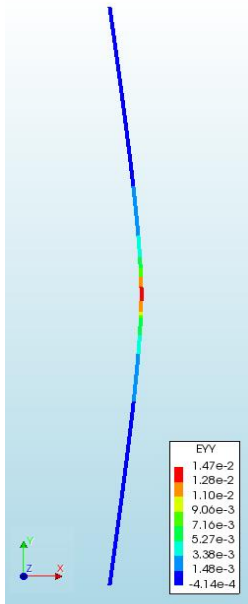
Fig. 71 Strains on the Most Tensioned Side (layer 1/11) of the Wall modelled with Beam Elements
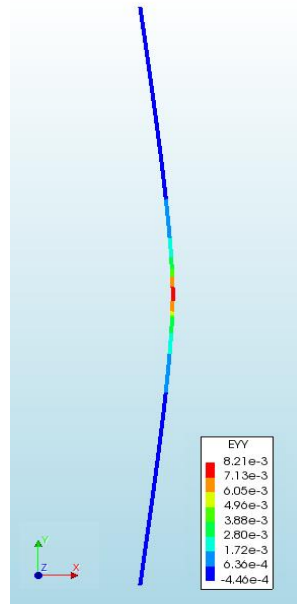
Fig. 72 Strains on Layer 4/11 along the thickness of the Wall modelled with Beam Elements
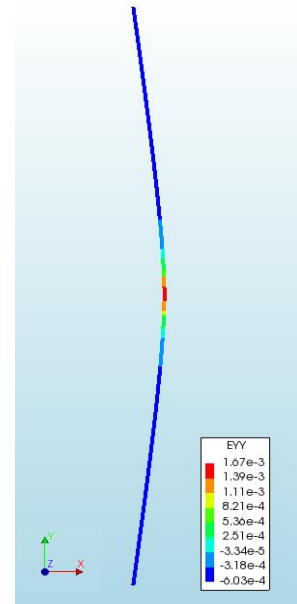
Fig. 73 Strains on Layer 7/11 along the thickness of the Wall modelled with Beam Elements
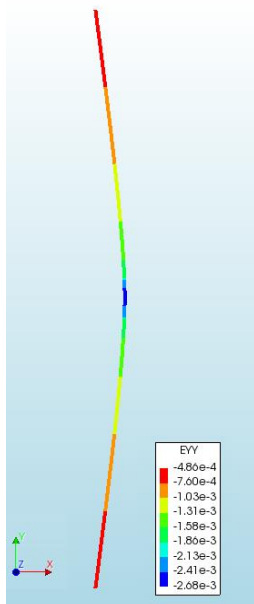
Fig. 74 Strains on Layer 9/11 along the thickness of the Wall modelled with Beam Elements
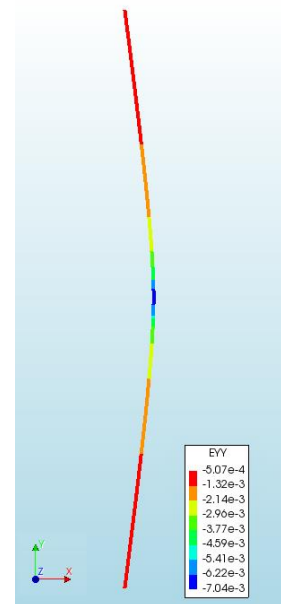
Fig. 75 Strains on the Most Compressed Side (layer 11/11) of the Wall modelled with Beam Elements
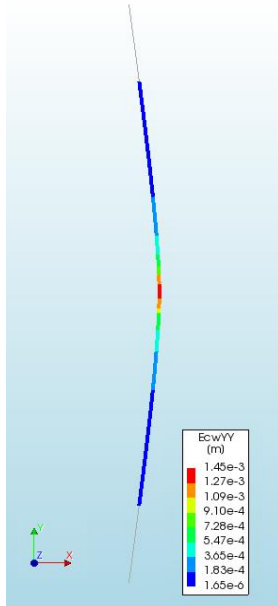
Fig. 76 Crack Widths on the Most Tensioned Side (layer 1/11) of the Wall modelled with Beam Elements
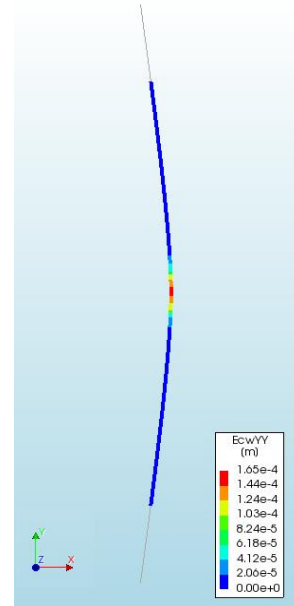
Fig. 77 Crack Widths on Layer 7/11 along the thickness of the Wall modelled with Beam Elements

9.1.3 Model with Plane Strain Elements

The third model comprises plane strain elements. In this case, the cross-section of the wall is modelled. Fig. 78 shows the geometry and the support conditions of the FE model. The support conditions are, also, described in Table 11. Table 12 lists the properties of the plane strain elements. The area of the element is 0.000196 m². The crack bandwidth h for higher order two-dimensional elements is $h = \sqrt{A}$, where A is the area of the element. [48]. The self-weight of the wall (load case 1) is applied as surface load on the model (cross-section of the wall). Fig. 79 and Fig. 80 show the vertical and lateral loading (load cases 2,3), that the wall is subjected to. The vertical load is applied eccentrically on the cross-section. Particularly, the point of application lies 0.001 m away, from the central axis of the cross-section, towards the negative X direction (Fig. 79). The supports, on the top and bottom edge of the wall, are, also, located 0.001 m away, from the central axis of the cross-section, towards the negative X direction. In order to avoid stress concentrations on the points of supports – point of application of vertical load, stiffer steel plates are placed at the top and bottom edges of the wall. The steel plates are modeled with infinite shell elements. Their properties are listed in Table 12. The material model for the steel plates is described in Table 13. The load cases and the magnitude of loads are listed in Table 14. A non-linear analysis of the FE model is performed. Table 15 lists the characteristics of the analysis.

The model with plane strain elements consists of eight finite elements in the x direction (along the thickness of the wall). The integration scheme is 3x3. Hence, eight finite elements with three integration points, each, results in a total of 24 integration points, along the thickness of the wall. The models with curved shell elements and beam elements consist of 11 integration points, along the thickness of the wall. This is the recommended maximum number of integration points, for curved shell elements. It would be preferable for the review, that the different FE models have similar integration schemes, along the thickness of the wall. However, the choice of mesh size and integration scheme, for the model with the plane strain elements, is based on the effort to avoid divergence or non-convergence, at the early steps of the non-linear analysis, before the maximum wind load is

attained and unloading starts. This is, also, the reason why the iterative solution method, that is used for the analysis of every FE model, is the secant (quasi-newton) and not the default regular Newton-Raphson. [50]

The evolution of the non-linear FE analysis, in terms of load – displacement, is shown in the graph in Fig. 84. The displacement is estimated on the highlighted node in Fig. 81. The graphs, in Fig. 85 and Fig. 86, show the evolution of stresses and strains, in the direction normal to the bed joints, on the most tensioned and compressed side of the wall, respectively. The former graph refers to the highlighted finite element, in Fig. 82, and the latter to the highlighted finite element, in Fig. 83. Stresses and strains are estimated on the integration points. The output curves represent the analysis results. The input curves are drawn, according to the material model (Table 2). [47] The juxtaposition shows that the curves match. The stresses on the cross-section of the wall, in the direction normal to the bed joints, when the maximum wind load is applied (orange dot on the curve in Fig. 84), are shown in Fig. 87. Fig. 88 shows the respective strains. The width, in the direction normal to the bed joints of the masonry wall, and the depth of the cracks are shown in Fig. 89.
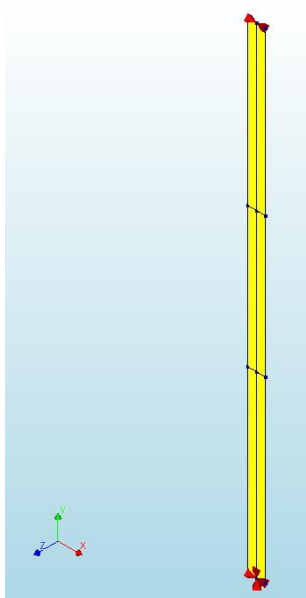
Fig. 78 Model with Plane Strain Elements
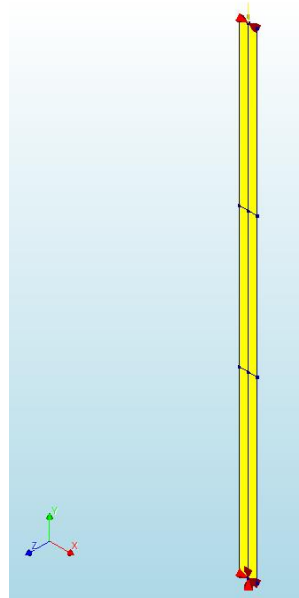
Fig. 79 Vertical Loading on Model with Plane Strain Elements
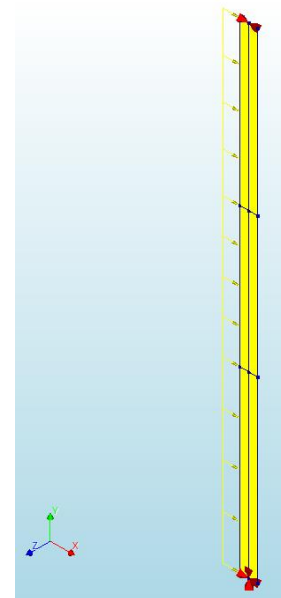
Fig. 80 Wind Load on Model with Plane Strain Elements

Table 11 Support Conditions of the Model with Plane Strain Elements

Supports	*Top Edge*	Fixed Translations	Tx
		Fixed Rotations	No fixed rotation
	Bottom Edge	Fixed Translations	Tx, Ty
		Fixed Rotations	No fixed rotation

Table 12 Properties of the Plain Strain Elements and the Infinite Shells

	Class	Plane Strain Elements	
Element 1	Geometry	Dimensions	0.014 x 0.014 m^2
	Data	Type	CQ16E
		DOF	Ux,Uy - 8-noded
		Interpolation Scheme	Quadratic
		Integration Scheme	3x3 HIGH
Element 2	Class	Infinite Shells	
	Geometry	Thickness	0.1 m
		Shape Definition Type	Flat
		Size of Finite Elements	0.014 m
	Data	Type	CL9PE
		DOF	Ux,Uy, Φz - 3-noded
		Interpolation Scheme	Quadratic
		Integration Scheme	2x2 Gauss

Table 13 Material Model for Steel Plates

	Steel - Linear Elastic Isotropic	
Steel	Linear Material Properties	
	Young's modulus	2x10^{11} N/m^2
	Poisson's Ratio	0.3
	Mass Density	0 kg/m^3

Table 14 Loads on the Model with Plain Strain Elements

	Masonry Weight (Load Case 1)	
Loads	Surface Force pointing downwards (negative y direction)	20700 N/m^2
	Loads from floors and walls above (Load Case 2)	
	Point force on top vertex	250000 N/m
	Wind Load (Load Case 3)	
	Distributed force on the edge of the element	624 N/m

Table 15 Characteristics of the Non-linear analysis of the Model with Plane Strain Elements

Analysis	Structural Non-Linear	
	Non-Linear Effects	Physically Non-linear
	Equilibrium Iteration	
	Iterative Method	
	Maximum Number of iterations	200
	Method	Secant (Quasi-Newton)
	Type	BFGS
	First Tangent	Previous Iteration
	Convergence Norm	
	Satisfy all specified norms	Yes
	Displacement	Yes
	Convergence Tolerance	0.01
	No Convergence	Terminate
	Force	Yes
	Convergence Tolerance	0.01
	No Convergence	Terminate
	Load Steps	
	Masonry Weight (Load Case 1)	1
	Load from floor and masonry above (Load Case 2)	1
	Wind Load (Load Case 3)	0.5(27)
		0.1(5)
		0.5(120) Arc-length control activated for the unrestrained nodes in the horizontal direction (direction of application of wind load)
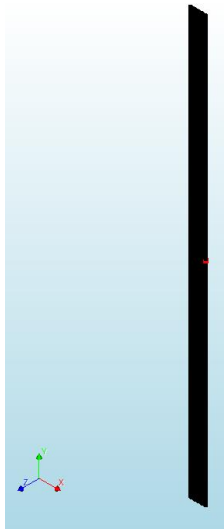
Fig. 81 Node at the mid-height of the Model with Plane Strain Elements
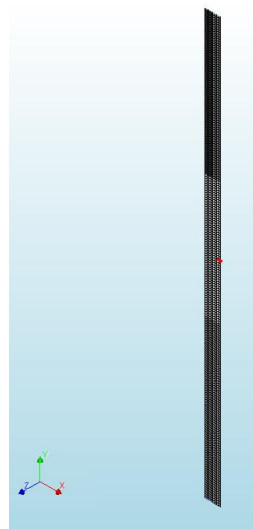
Fig. 82 Element at the mid-height, on the most tensioned side of the Model with the Plane Strain Elements

Fig. 83 Element at the mid-height, on the most compressed side of the Model with the Plane Strain Elements
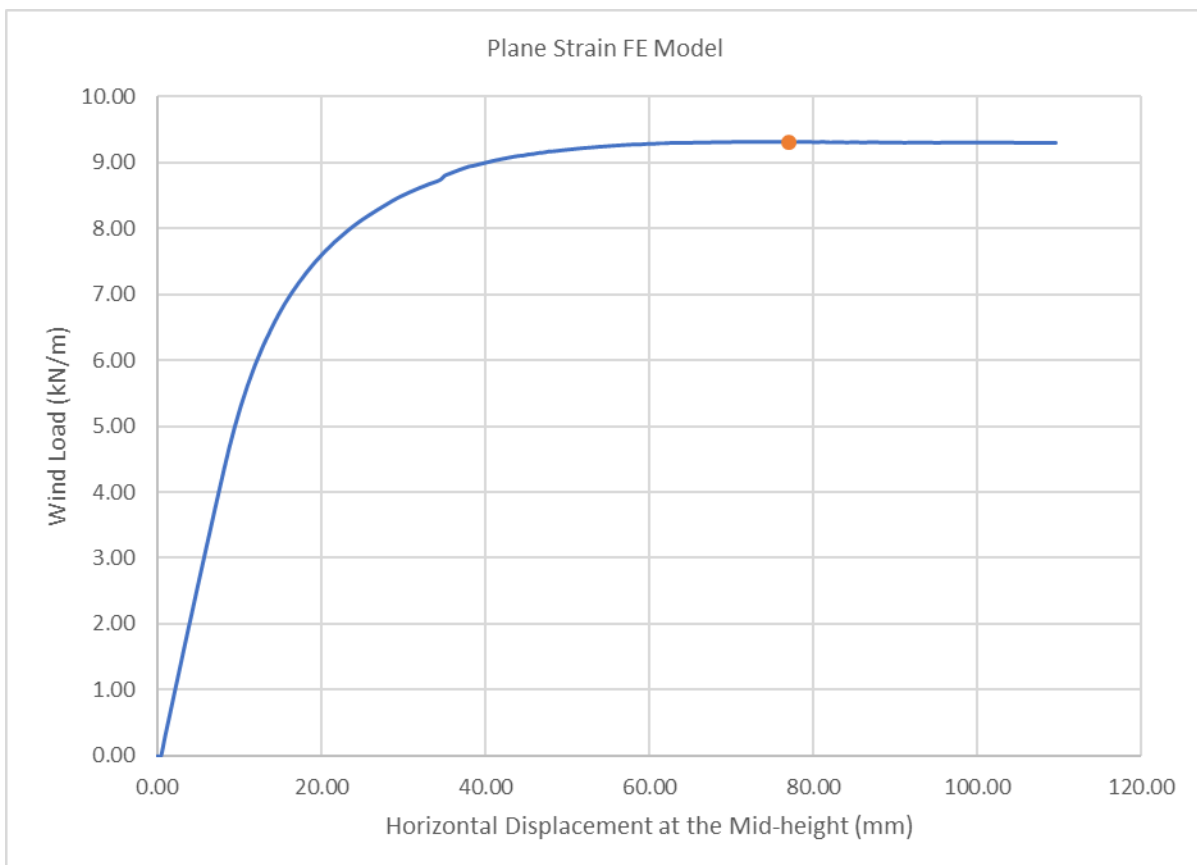
Fig. 84 Load – Displacement Curve for the Model with Plane Strain Elements
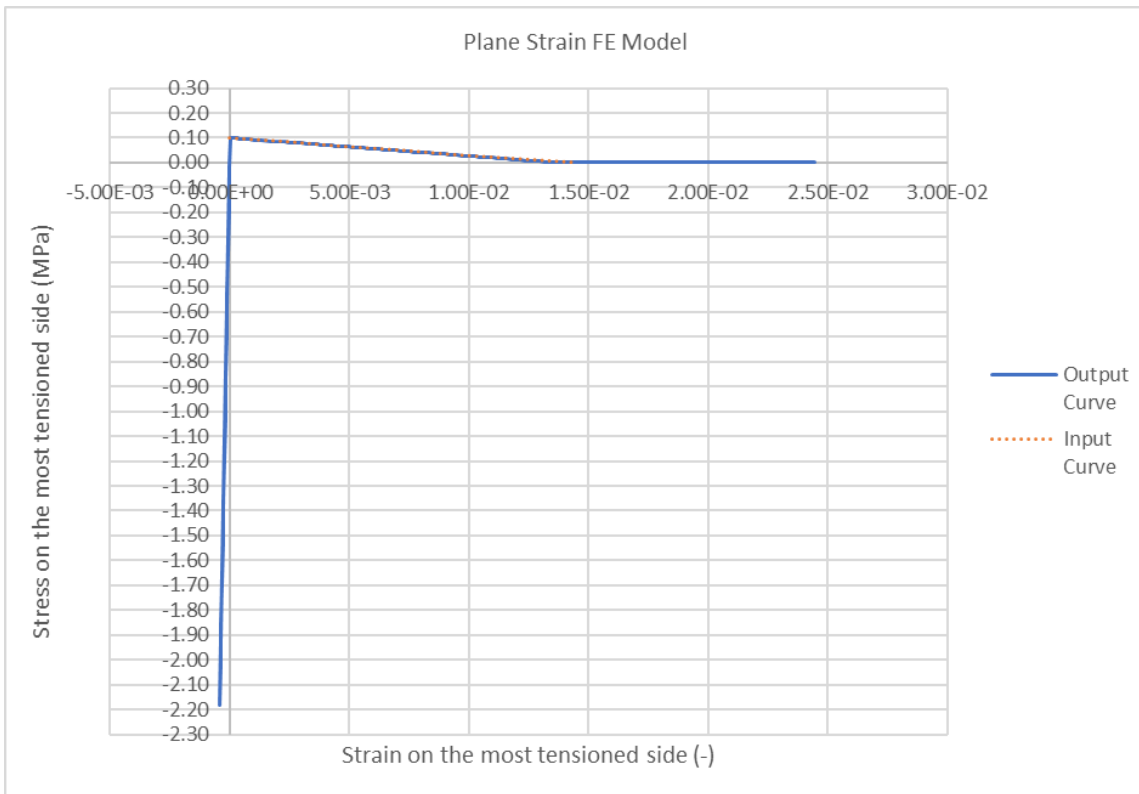
Fig. 85 Stress-Strain Evolution at the most tensioned side of the wall, modelled with Plane Strain Elements
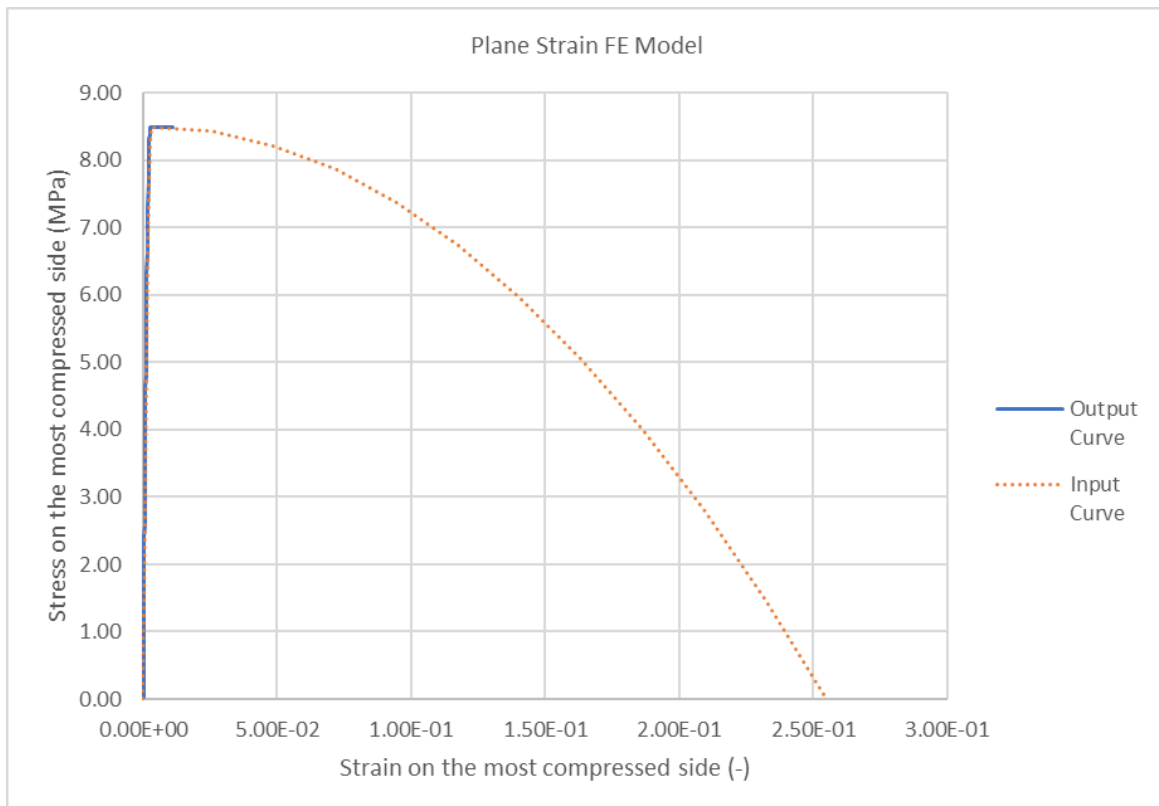
Fig. 86 Stress-Strain Evolution at the most compressed side of the wall, modelled with Plane Strain Elements
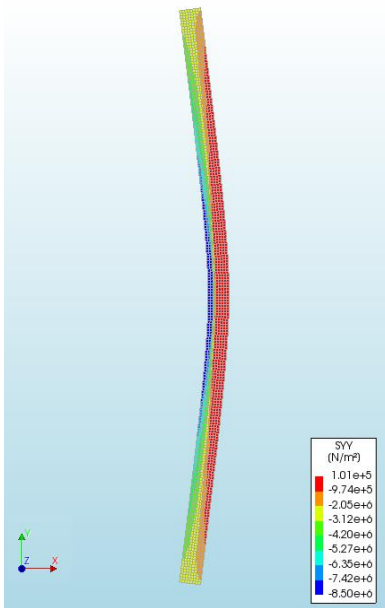
Fig. 87 Stresses on the Wall Modelled with Plane Strain Elements
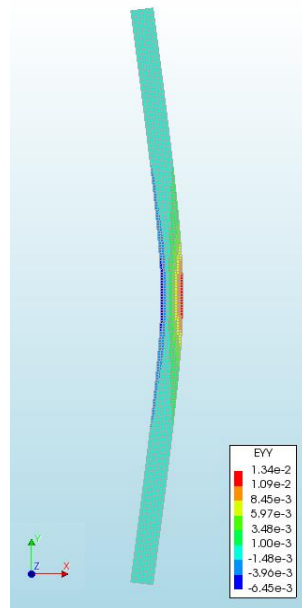
Fig. 88 Strains on the Wall Modelled with Plane Strain Elements
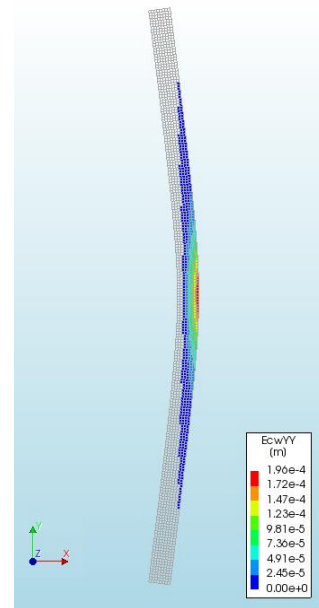
Fig. 89 Crack Widths on the Wall Modelled with Plane Strain Elements

9.1.4   Choice of FE model and Geometrically Non-linear Effects

The results of the analysis of the FE models, that were described in the previous sections, show comparable results, with respect to the load – displacement curves. This is shown in Fig. 90. The load-displacement curve is the criterion for comparing the three models, since the scope of the analysis is the definition of the maximum wind load, that the URM wall can withstand, when it is subjected to a certain vertical load. The wall, that is modelled with the plane strain elements, fails for a higher value of wind load, compared to the other two models. As it has already been mentioned, the models with curved shell elements and beam elements have 11 integration points, along the thickness of the wall. The model with the plane strain elements has 24 integration points, respectively. Therefore, the accuracy of the latter FE model is higher and this might be the cause for the deviation, in the curves in Fig. 90.

One scenario, with respect to the support conditions of slender URM walls, is taken into consideration in the thesis. The walls are simply supported along the top and bottom edges (Fig. 20). Additionally, the walls are subjected to vertical and out-of-plane lateral loading. Therefore, it is expected that, stresses and deformations do not change along the length of the wall. The out-of-plane lateral displacements, along the height of the wall, as well as stresses and strains, on the cross-section, are of interest. The model with plane strain elements provides relevant contour plots, as it can be seen in Fig. 87 and Fig. 88. On the other hand, contour plots of stresses and strains, on one particular layer, along the thickness of the wall, can be obtained from the models with curved shell elements and beam elements (Fig. 46 - Fig. 55 and Fig. 66 - Fig. 75). After, writing down the values of stresses or strains, along the wall thickness, the user can create graphs with the stress or strain distribution. Each graph refers to a specific level of the height of the wall. Eventually, the model with plane strain elements is chosen, in order to continue with analyzing slender URM walls, of different geometrical and material properties.

The model with the plane strain elements was analyzed in section 9.1.3. Only physically non-linear effects were taken into account for the analysis. The case study of URM wall is considered a slender wall and is expected to fail because of buckling. [13] Therefore, geometrically non-linear effects are, also, relevant. A new non-linear analysis is performed on the model with plane strain elements. The sequence of loading remains the same (Fig. 37). This time geometrically non-linear effects are activated, as Table 16 shows. In this case, the option for the first tangent is switched from previous iteration to tangential. This modification allows the non-linear analysis to proceed further to the unloading phase, avoiding divergence or non-convergence, immediately, after the maximum wind load is attained. [50]

The evolution of the non-linear FE analysis, in terms of load – displacement, is shown in the graph in Fig. 91. The displacement is estimated on the highlighted node in Fig. 81. The graphs, in Fig. 92 and Fig. 93, show the evolution of stresses and strains, in the direction normal to the bed joints, on the most tensioned and compressed side of the wall, respectively. The former graph refers to the highlighted finite element in Fig. 82 and the latter to the highlighted finite element in Fig. 83. Stresses and strains are estimated on the integration points. The output curves represent the analysis results. The input curves are drawn, according to the material model (Table 2). [47] The juxtaposition shows that the curves match. The stresses on the cross-section of the wall, in the direction normal to the bed joints, when the maximum wind load is applied (orange dot on the curve in Fig. 91), are shown in Fig. 94. Fig. 95 shows the respective strains. The width, in the direction normal to the bed joints of the masonry wall, and the depth of the cracks are shown in Fig. 96.

The influence of geometrically non-linear effects on the capacity of the URM wall is shown in the graph in Fig. 97. Second-order effects can reduce significantly the maximum wind load, that the wall can withstand, when it is subjected to a certain vertical load. Additionally, the graph in Fig. 93 and the stress state, which is shown in Fig. 94, prove that the case study of URM wall behaves as slender, under the applied loads. The wall fails before the compressive capacity of the material is attained.

As it has already been mentioned, a certain mesh size and integration scheme were specified, for the model with the plane strain elements, so as to avoid divergence or non-convergence, at the early steps of the non-linear analysis. In this analysis, only, physically non-linear effects were activated. Further, in the FE analysis of URM walls, of different geometrical and material properties, the geometrical non-linearity will be taken into account, since its influence is considerable for slender walls. It is important to know whether the results of the non-linear FE analysis are influenced by the defined characteristics (Table 16) as well as the properties of the finite elements (Table 12). It is concluded that the size of the load increments, for the non-linear analysis, as well as the size of the finite elements and the integration scheme do not affect the results of the analysis. Particularly, the load – displacement curves are reviewed, since the scope of the analysis is the definition of the maximum wind load, that the URM wall can withstand, when it is subjected to a certain vertical load. In Appendix C, the curves for different size of load increments, different mesh size or different integration scheme are juxtaposed. Assessing whether the choice of linear instead of quadratic interpolation functions, for the elements, can differentiate the analysis results, would be interesting. However, according to DIANA-FEA support team, strain considerations in linear plane strain elements are not compatible with geometrically non-linear analysis. This is, also, the reason why quadratic elements were used in all three FE models, even when, only physically non-linear effects were activated for the analysis.

Table 16 Characteristics of the Non-linear analysis, with geometrically non-linear effects, of the Model with Plane Strain Elements

Analysis	<u>Structural Non-Linear</u>	
	Non-Linear Effects	Physically Non-linear
		Geometrically Non-linear
	Equilibrium Iteration	
	Iterative Method	
	Maximum Number of iterations	200
	Method	Secant (Quasi-Newton)
	Type	BFGS
	First Tangent	Tangential
	Convergence Norm	
	Satisfy all specified norms	Yes
	Displacement	Yes
	Convergence Tolerance	0.01
	No Convergence	Terminate
	Force	Yes
	Convergence Tolerance	0.01
	No Convergence	Terminate
	Load Steps	
	Masonry Weight (Load Case 1)	1
	Load from floors and walls above (Load Case 2)	1
	Wind Load (Load Case 3)	0.5(10)
		0.1(3)
		0.1(4) 0.02(50) Arc-length control activated for the unrestrained nodes, at the mid-height of the wall, in the horizontal direction (direction of application of wind load)
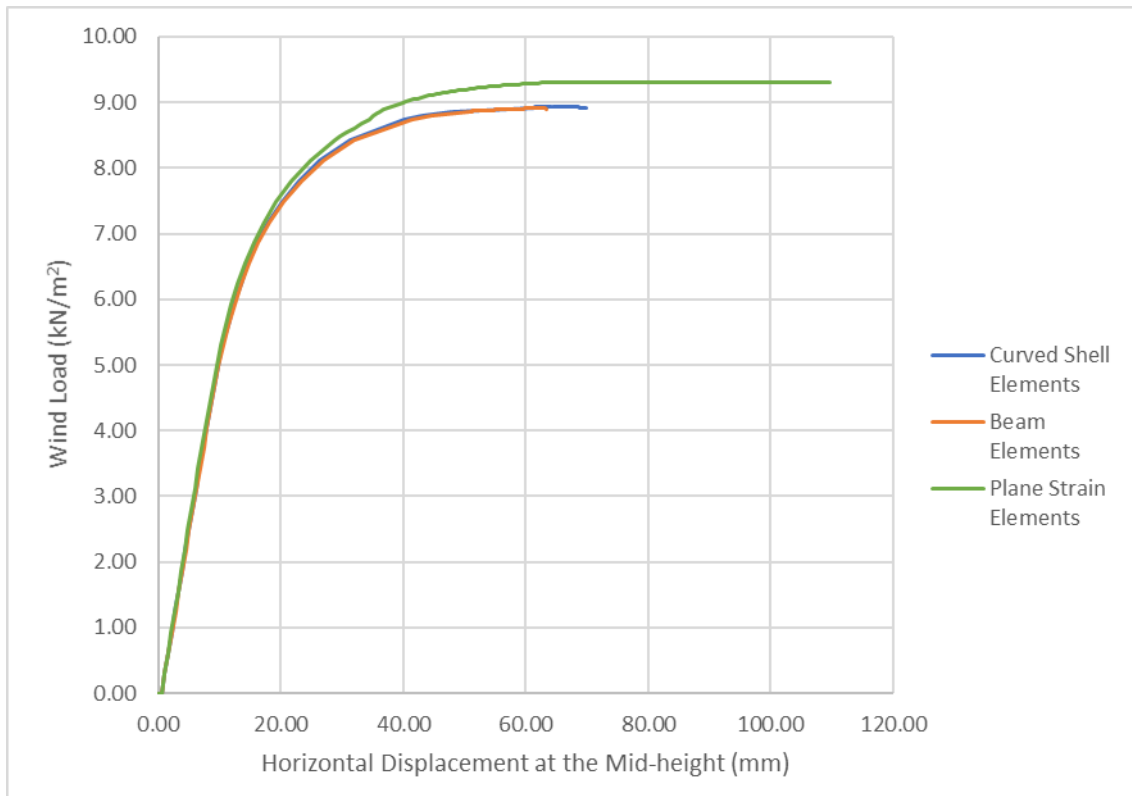
Fig. 90 Reviewing the three FE models based on the Load – Displacement Curve
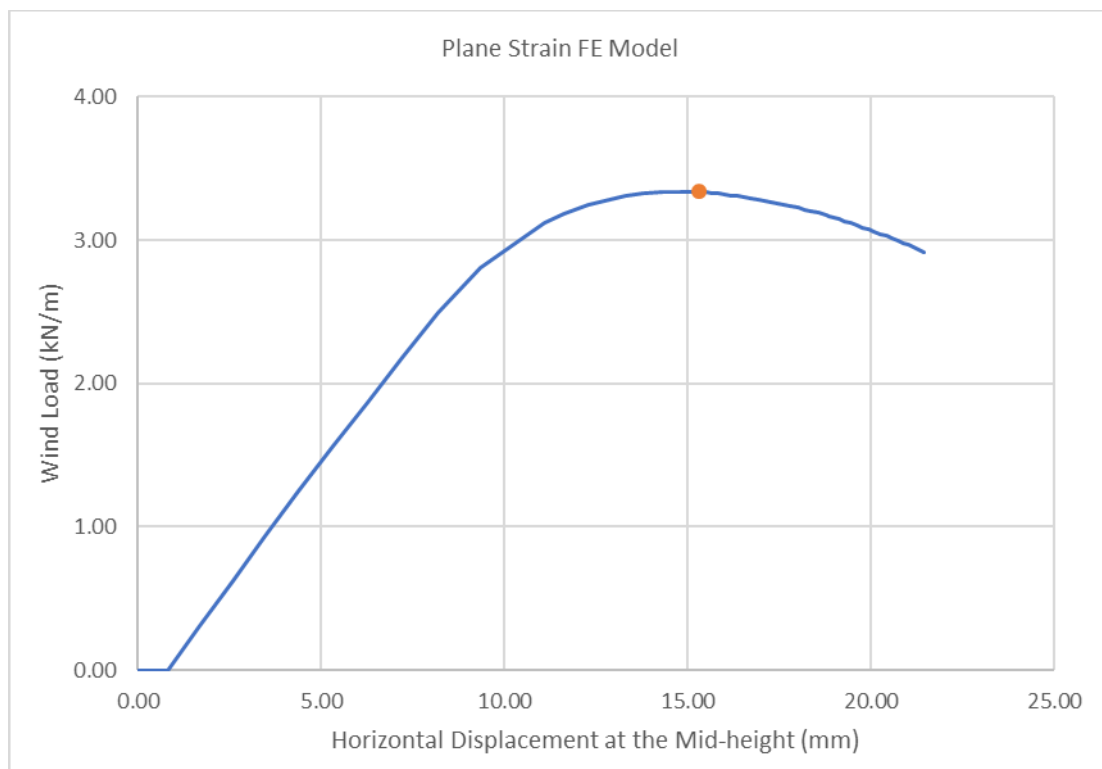
Fig. 91 Load – Displacement Curve for the Model with Plane Strain Elements (geometrically non-linear effects considered)
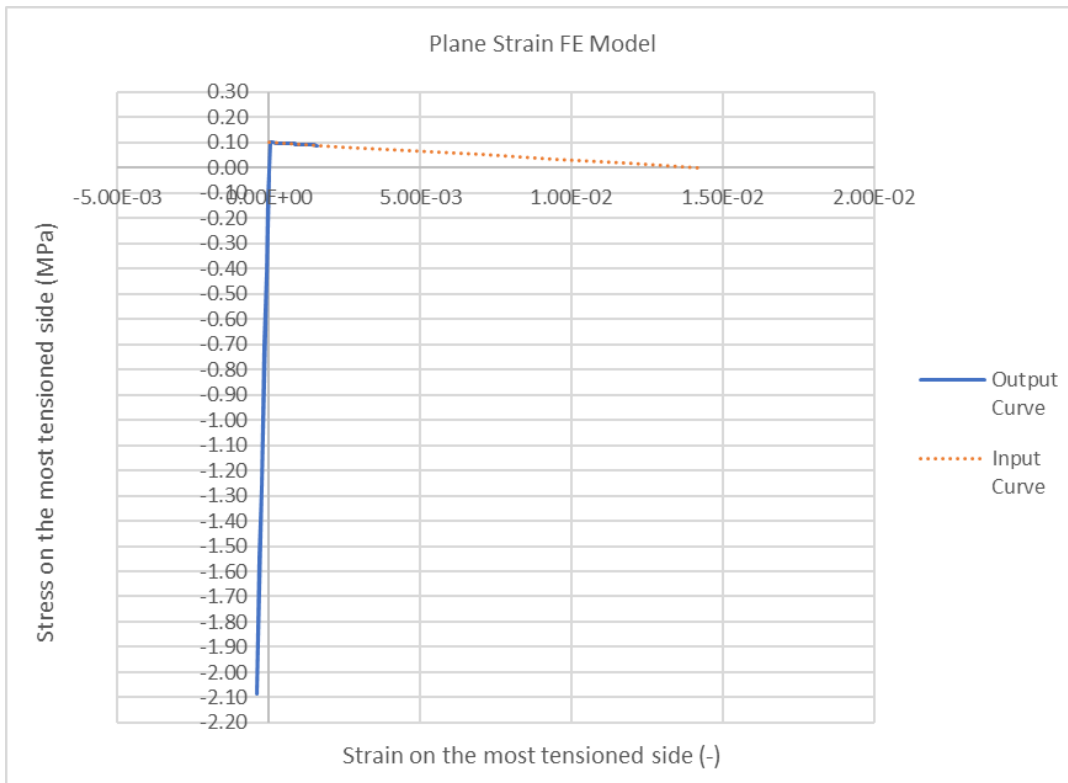
Fig. 92 Stress-Strain Evolution at the most tensioned side of the wall, modelled with Plane Strain Elements (geometrically non-linear effects considered)
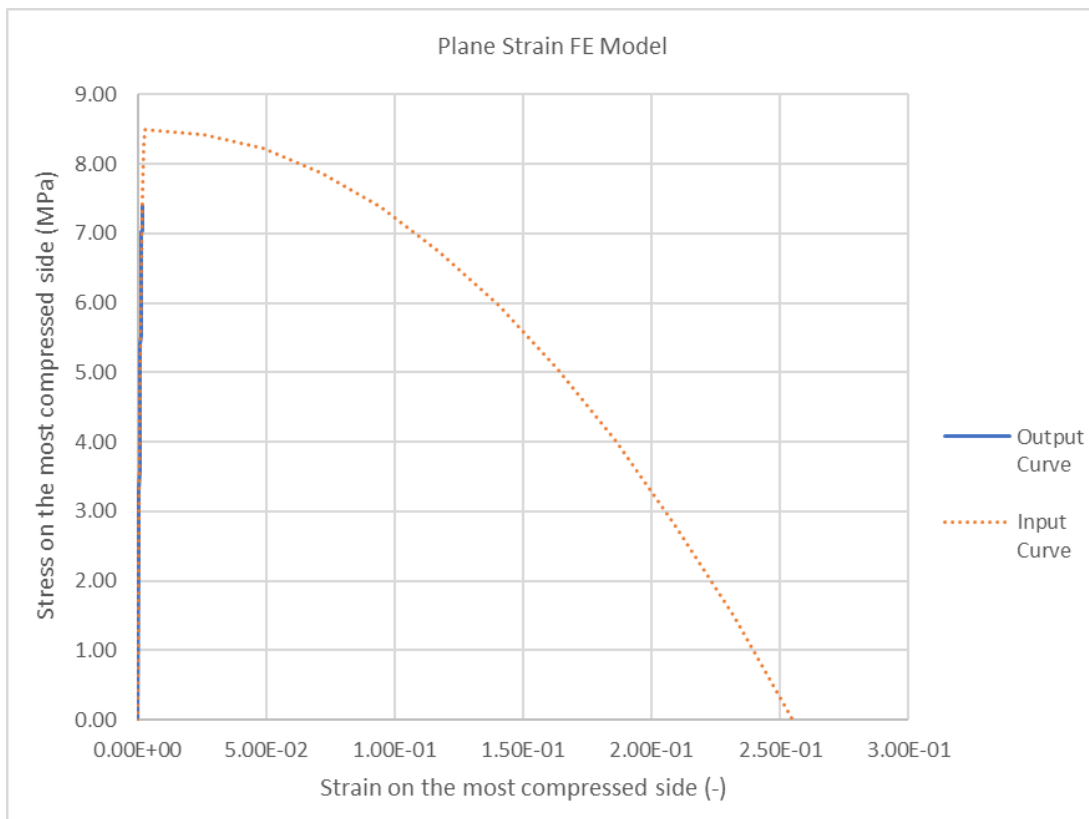
Fig. 93 Stress-Strain Evolution at the most compressed side of the wall, modelled with Plane Strain Elements (geometrically non-linear effects considered)
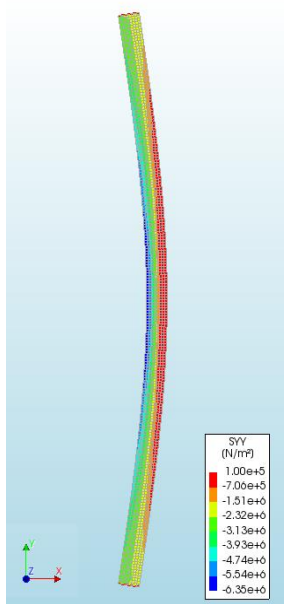
Fig. 94 Stresses on the Wall Modelled with Plane Strain Elements (geometrically non-linear effects considered)
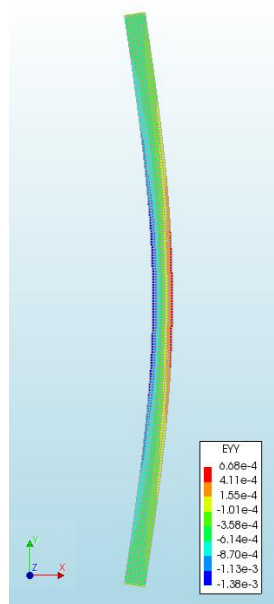
Fig. 95 Strains on the Wall Modelled with Plane Strain Elements (geometrically non-linear effects considered)
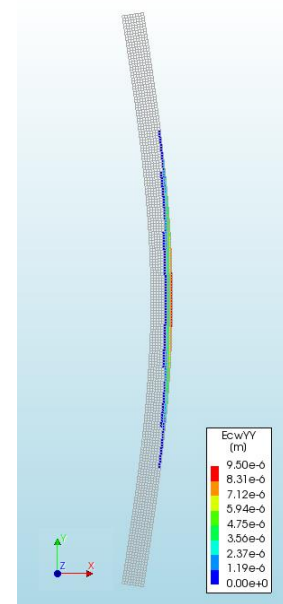
Fig. 96 Crack Widths on the Wall Modelled with Plane Strain Elements (geometrically non-linear effects considered)
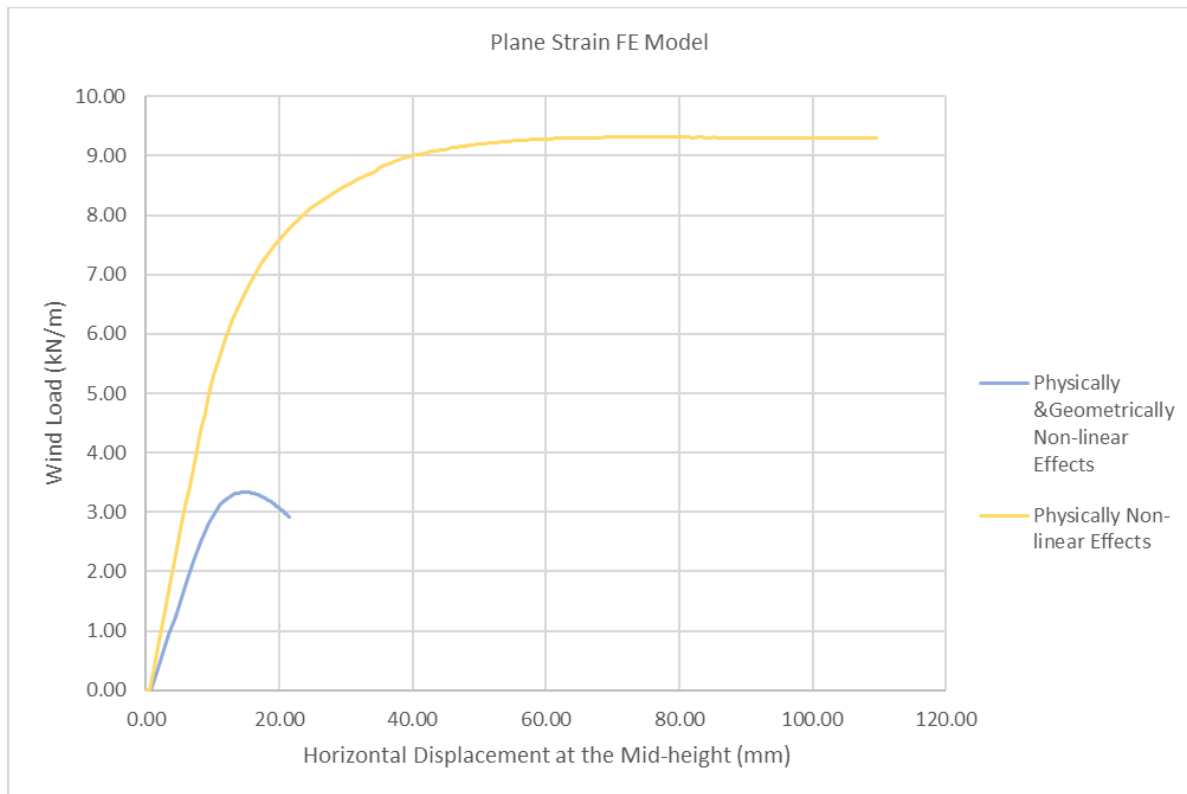
Fig. 97 Load – Displacement Curves for the Model with Plane Strain Elements for different Non-linear Effects

Several FE analyses are performed on the model with the plane strain elements (section 9.1.4). Geometrically non-linear effects are considered for the analyses. Initially, the geometrical properties of the URM wall, are those of the case study (section 8.1). The material properties, that are prescribed in the NPR 9998-2018 norm, are considered (Table 2). As it has been discussed in section 9.1, a small eccentricity at the top and the bottom of the wall is taken into account, just to activate second-order effects on the wall. The first step is to determine the vertical load at the mid-height, for which the wall fails, when zero wind load is applied on it (orange dot in the graph in Fig. 99). Specifically, a non-linear FE analysis is performed, where the self-weight of the wall is, initially, applied, in one step, and then the vertical load (from the floors and the walls on the upper floors) is imposed, in increments, until the wall fails. The sequence of loading and the evolution of the non-linear analysis are shown in Fig. 98. The maximum vertical load (orange dot in the graph in Fig. 98) is added to the self-weight, of the upper half of the wall, to calculate the total load at the mid-height, that leads the wall to failure. This load is, actually, the vertical resistance of the URM wall, for zero wind load. Following, for different values of the vertical load, the value of the wind load, that leads the wall to failure, is determined every time. For every value of the vertical load, a non-linear FE analysis, similar to the one described in section 9.1.4, is performed. The sequence of loading is shown in Fig. 37. The curve in the graph, in Fig. 91, is representative of the evolution of the non-linear analysis, in terms of the relationship load − displacement. The grey dots in the graph, in Fig. 99, are the combinations of vertical load − wind load, that lead the wall to failure. Each time, the vertical load is, actually, the vertical resistance of the URM wall, when it is subjected to the respective wind load.

The research within this thesis focuses on one case, with respect to the boundary conditions of slender URM walls. The walls are simply supported on the top and the bottom edge, as can be seen in Fig. 20. The lateral loading on the wall is caused by the internal wind pressure. Hence, the maximum first-order bending moment, because of the wind load, occurs at the mid-height of the wall. Therefore, the vertical resistance is, also, estimated at the mid-height of the wall. Furthermore, standards and proposed formulas calculate the vertical resistance of URM walls, given the value of the applied wind load. However, it is considered appropriate that the load path, in the FE analysis, is in accordance with the actual load path on the masonry wall. The vertical load on the wall is present when wind load is applied. It is interesting, though, to compare the results with the respective ones from the analysis, with the inverse load path. More specifically, the curve in the graph in Fig. 99 is derived from FE analyses, where the vertical load is applied first, in one step, and, then, the wind load is applied, in small increments, until the wall fails. For values of wind load, within the graph, in Fig. 99, the wall is analyzed for the inverse load path. Initially the self-weight is applied. After that, a vertical load, of certain magnitude, needs to be imposed, so that the analysis proceeds. The curve in the graph, in Fig. 99, shows the combinations of vertical load − wind load, that lead the URM wall to failure. Every combination outside the curve leads to buckling. This explains the necessity of applying a vertical load, in the analysis, before the application of the wind load. Hence, the analysis continues with imposing the wind load, in one step, and then, again, vertical load is applied, in steps, until the wall fails. The results from the analyses, with different load paths, are compared in Appendix D. The respective combinations of vertical load − wind load, that lead the URM wall to failure, show close proximity to each other.

The influence of a number of parameters on the vertical resistance of URM walls, subjected to combined vertical and lateral loading, is sought. Namely, the slenderness ratio (h/t), the modulus of elasticity (E), the characteristic compressive strength (f_k), the tensile strength (f_t), the magnitude of the wind load (w) and the eccentricity at the top or bottom of the wall (e_i). It is, also, interesting to

know the possible combined effects of some of the aforementioned parameters. Particularly, the influence of increasing the tensile strength of masonry (f_t), for different values of slenderness ratio (h/t), as well as the impact of increasing the tensile strength of masonry (f_t), for different values of eccentricity at the top or bottom of the wall (e_i).

The graph in Fig. 100 shows the influence of the slenderness ratio (h/t) of a URM wall on the interaction between wind load and vertical resistance. The wall thickness (t) remains constant. Slender URM walls form the research subject of this thesis. A wall, which is part of the structure of a building block in Amsterdam, is the case study. The technical drawings of the building block, in Fig. 11 and Fig. 12, show that the slenderest walls have a thickness equal to 0.11 m. This value is considered, for the thickness of the URM wall, for every FE model. The wall height (h) is successively increased. For a number of different values of slenderness ratio, equivalent graphs to the one, shown in Fig. 99, are obtained from the FE analysis results. The curves in the graph in Fig. 100 describe the relationship between the vertical resistance and the applied wind load, on existing URM walls, with different values of slenderness ratio (h/t).

As with the case of slenderness ratio, the influence of the material properties, individually, on the interaction between wind load and vertical resistance of existing slender URM walls, needs to be defined. Namely, the short-term secant modulus of elasticity (E), the characteristic and the mean value of the compressive strength (f_k, f'_m) as well as the tensile strength (f_t). The value of one property is altered every time and the rest of the properties remain the same. The properties prescribed in the NPR 9998-2018 norm, for brick masonry constructed before 1945, are considered as reference. Table 17 consists of the different combinations of geometric and material properties, that are assigned to URM walls, which are analyzed with the FE method. The graphs in Fig. 101, Fig. 102 and Fig. 103 show the results of the respective analyses.

The issues of the relationship between the characteristic compressive strength and the short-term secant modulus of elasticity as well as the characteristic and the mean value of the compressive strength have, already, been addressed in sections 5.2.2 and 8.1, respectively. Three values of E/f_k ratio are defined. The first is derived by the suggested values of compressive strength and short-term secant modulus of elasticity, in the NPR 9998-2018 norm. The ratio is equal to *705.88*. This value matches approximately the value of 700, that is suggested in the Dutch national annex to the EN 1996 norm. The other two values of E/f_k ratio, that are used, are *900* and *1000*. This way indicative values of the compressive strength and the short-term secant modulus of elasticity are specified. Components of masonry in buildings, that were built during the end of the 19th - beginning of the 20th century, are of interest within the context of this thesis.

It is a common practice that, codes for the design of masonry structures consider masonry as a non-tension material. However, considering the tensile strength of masonry, in the calculation of the vertical resistance, can enhance significantly the response of URM walls, with large values of slenderness ratio. [20] The curves in the graph, in Fig. 100, are derived for tensile strength of masonry equal to *0.1 MPa*. For three cases of URM walls, with different values of slenderness ratio, half the value of the tensile strength, prescribed in the NPR 9998-2018 norm, is assigned in the respective FE model. Specifically, a value of tensile strength equal to *0.05 MPa* is used.

Three different values of eccentricity, at the top and the bottom, are assigned to the case study of URM wall and relevant FE analyses are performed, in order to obtain the curves in the graph in Fig. 104. The eccentricity at the top and the bottom of the wall (e_i) is equal to the initial eccentricity (e_{init}), which allows for construction imperfections and is assumed for the full height of the wall. [53] The first value of eccentricity is *0.001 m*. It is chosen just to activate second order effects on the wall. The plane

strain FE model, that is created for this eccentricity, consists of finite elements with size *0.014 x 0.014 m* (Table 12). The other two values of eccentricity are defined in such a way, that plane strain FE models with the same size of elements are created. Therefore, two more slender URM walls, with values of eccentricity, at the top and the bottom, equal to *0.015 m* and *0.029 m*, respectively, are analyzed with the FE method. This way, the results from the FE analysis, of models of slender URM walls, with different eccentricity at the top and the bottom, will be comparable.

   Taking into account the actual value of the tensile strength of masonry can enhance, considerably, the calculated value of the vertical resistance of slender URM walls, in cases of large eccentricities at the top or bottom ($e_i \geq 0.1t$). [20] Initially, a value of tensile strength, approximately, equal to zero, was assigned in the material properties of the FE models (Table 2), of the walls with the different values of eccentricity. The intention was to assess the different response of an existing slender URM wall, when the actual tensile strength of masonry is taken into account and when masonry is assumed as a non-tension material. However, for the largest value of eccentricity, large displacements occurred on the top of the FE model of the URM wall, with, approximately, zero tensile strength. Additionally, the following paradox was noticed. The URM wall with, approximately, zero tensile strength had a higher vertical resistance than the wall, with the actual tensile strength, when zero wind load is applied (again for the case of the wall with the largest value of eccentricity). Sandoval et al [13, p. 4395] stated that:

   "An accurate analysis, oriented to predict experimental results, may require the consideration of a realistic value of the tensile strength of masonry in the direction of the applied loads."

Therefore, instead of using a value of tensile strength, approximately, equal to zero, half the value of the prescribed, in the NPR 9998-2018 norm, tensile strength is assigned to the respective FE models. The graph in Fig. 105 shows, how the two different values of tensile strength influence the interaction, between wind load and vertical resistance, for the three values of eccentricity, at the top and the bottom of an existing slender URM wall.
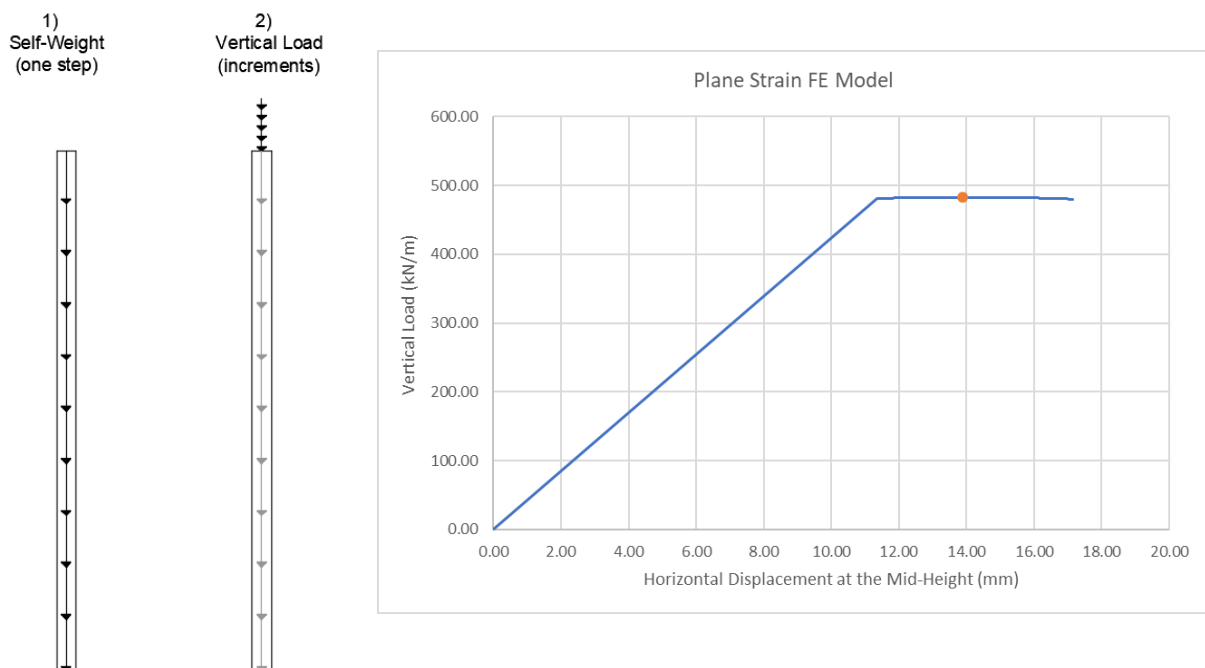
Fig. 98 Sequence of Loading and Evolution of the Non-linear FE Analysis for the definition of the Vertical Load, for which the wall Fails, when Zero Wind Load is applied on it
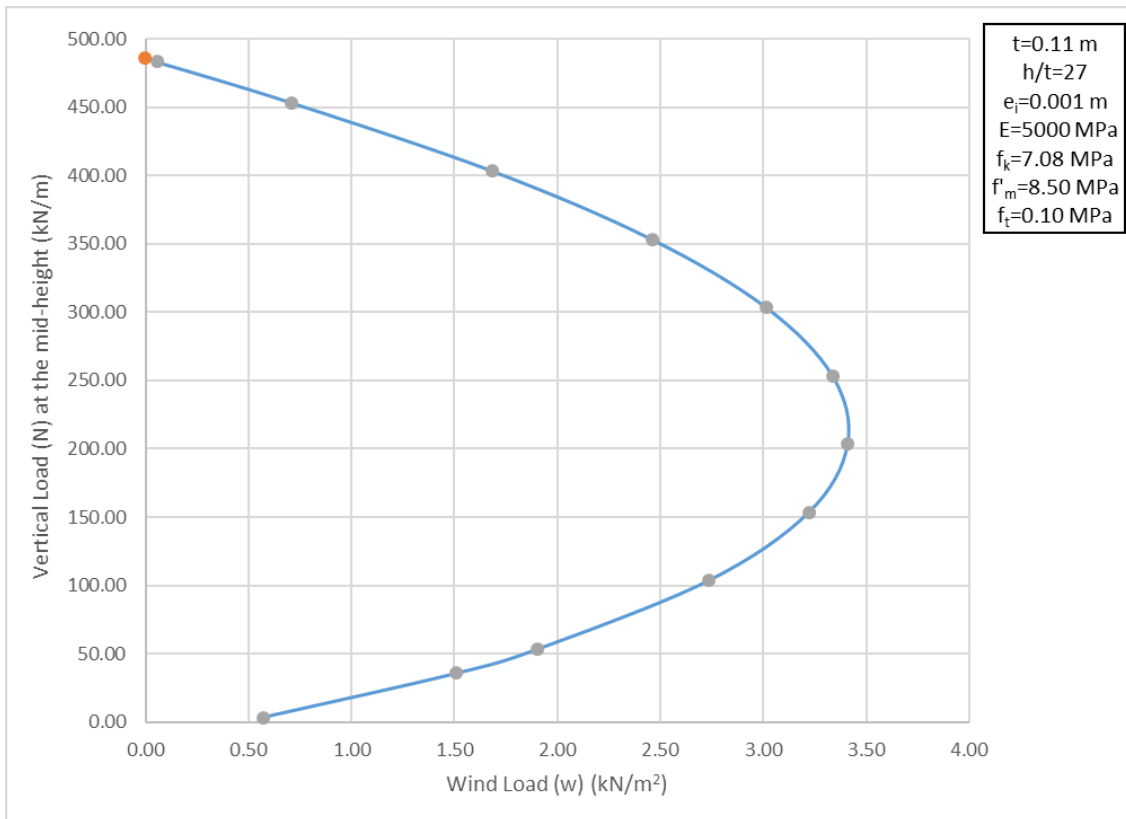
Fig. 99 Combinations of Vertical Load and Wind Load that lead the URM wall to failure
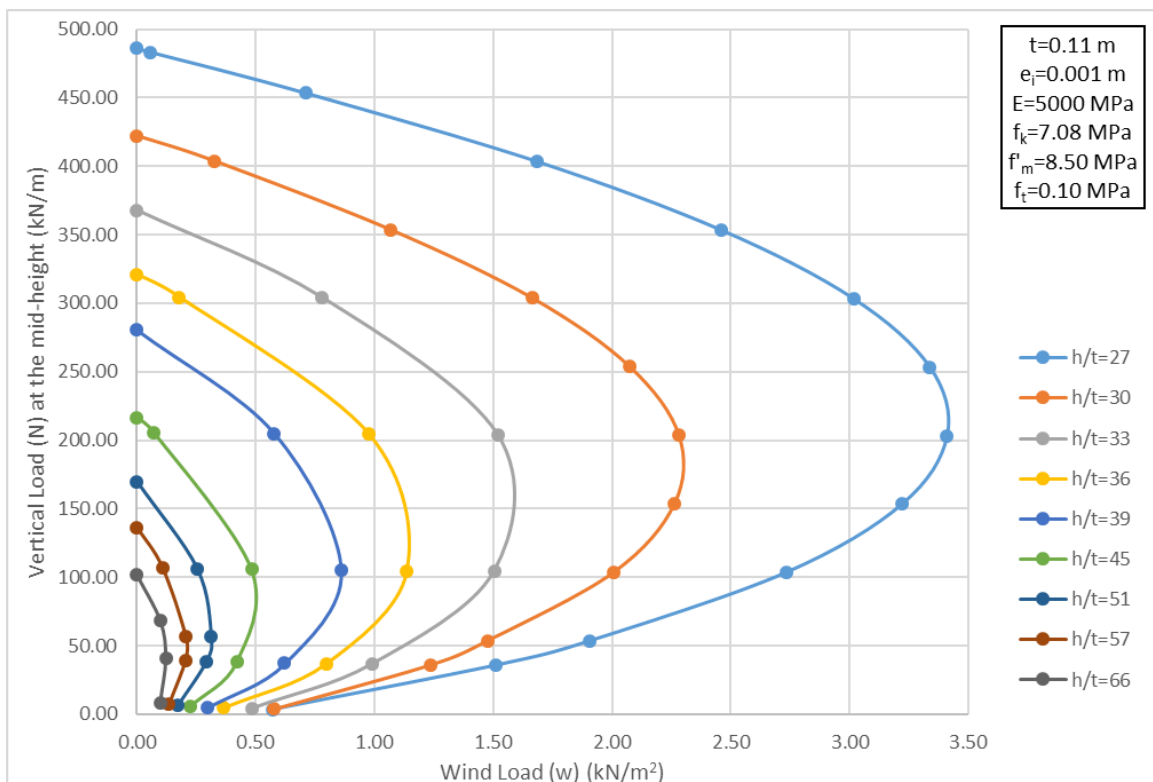
Fig. 100 Influence of slenderness ratio on the interaction between wind load and vertical resistance of a URM wall

Table 17 Geometrical and material properties of analyzed URM walls – Input of FE models

Case	h(m)	t(m)	h/t	e_i (m)	f_k (MPa)	f'_m (MPa)	E(MPa)	E/f_k (-)	f_t (MPa)
1	2.96	0.11	27	0.001	7.08	8.50	5000	700	0.10
2	2.96	0.11	27	0.001	5.56	6.67	5000	900	0.10
3	2.96	0.11	27	0.001	5.00	6.00	5000	1000	0.10
4	2.96	0.11	27	0.001	7.08	8.50	6375	900	0.10
5	2.96	0.11	27	0.001	7.08	8.50	7083	1000	0.10
6	2.96	0.11	27	0.001	7.08	8.50	5000	700	0.05
7	3.30	0.11	30	0.001	7.08	8.50	5000	700	0.10
8	3.30	0.11	30	0.001	5.56	6.67	5000	900	0.10
9	3.30	0.11	30	0.001	5.00	6.00	5000	1000	0.10
10	3.30	0.11	30	0.001	7.08	8.50	6375	900	0.10
11	3.30	0.11	30	0.001	7.08	8.50	7083	1000	0.10
12	3.30	0.11	30	0.001	7.08	8.50	5000	700	0.05
13	4.29	0.11	39	0.001	7.08	8.50	5000	700	0.10
14	4.29	0.11	39	0.001	7.08	8.50	5000	700	0.05
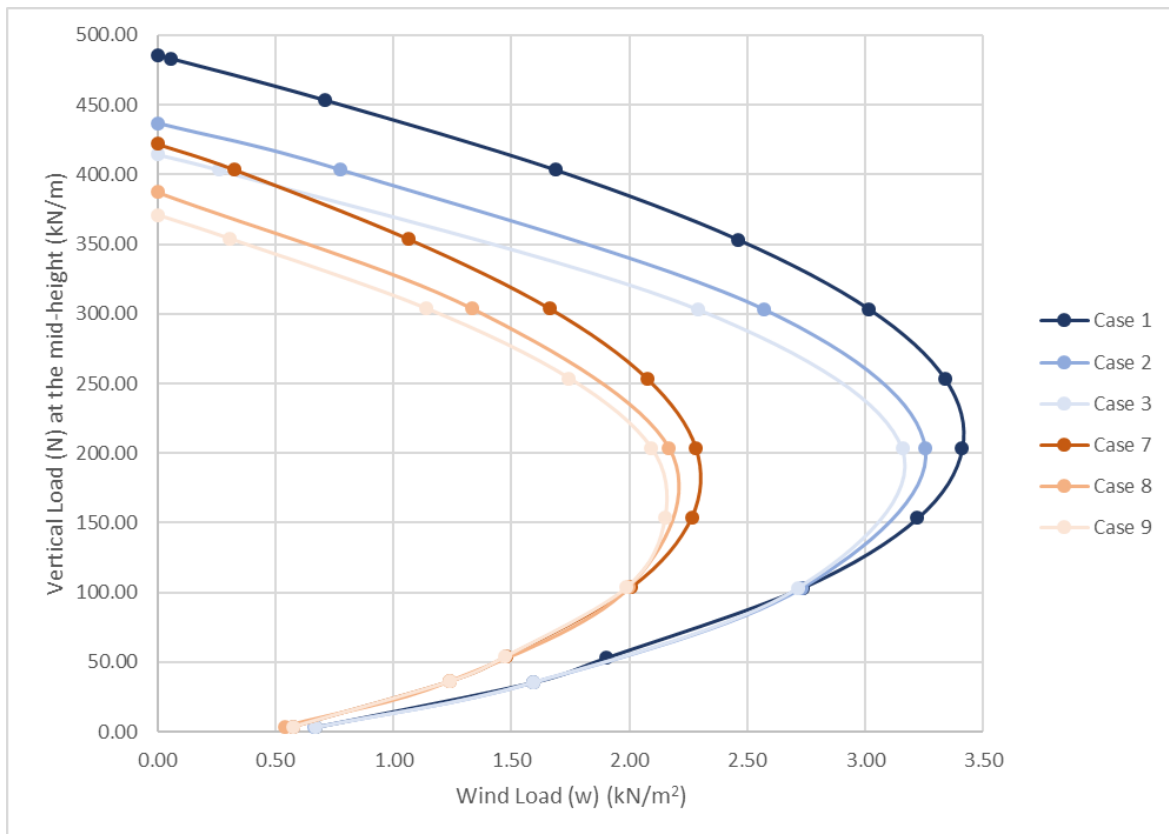
Fig. 101 Interaction between wind load and vertical resistance of a URM wall - constant values of E and f_t & variable value of f_k for two different values of h/t ratio
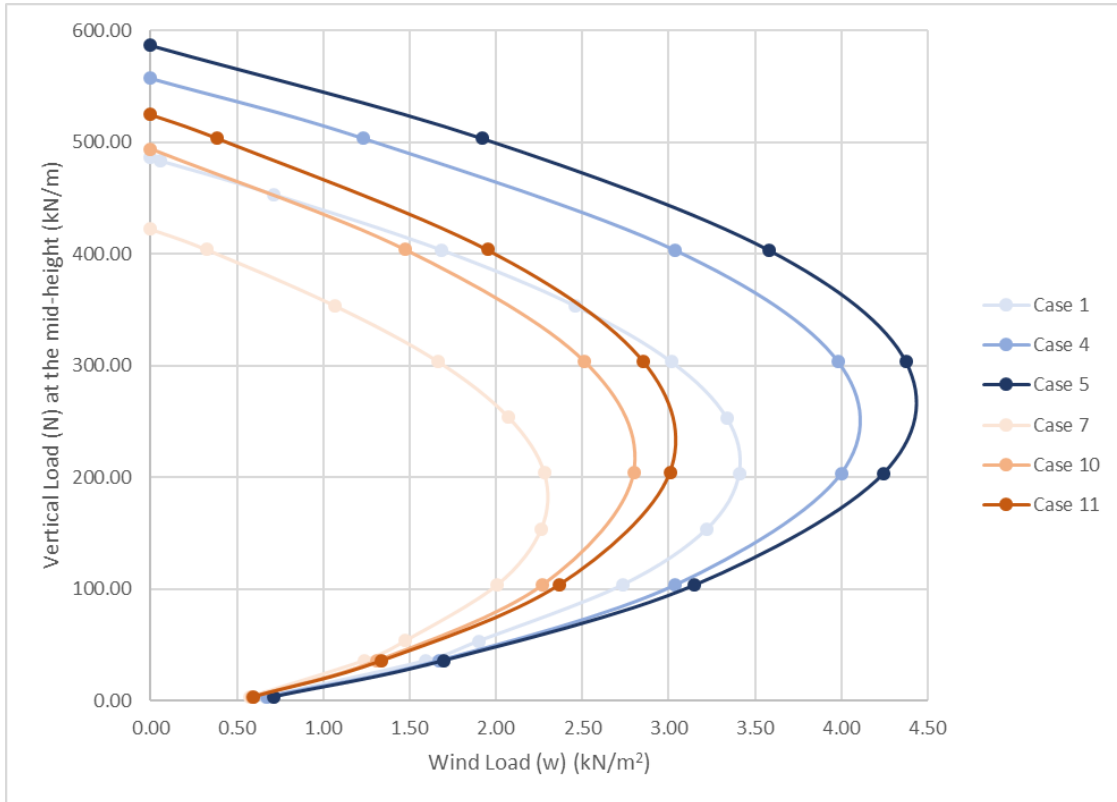
Fig. 102 Interaction between wind load and vertical resistance of a URM wall - constant values of f_k and f_t & variable value of E for two different values of h/t ratio
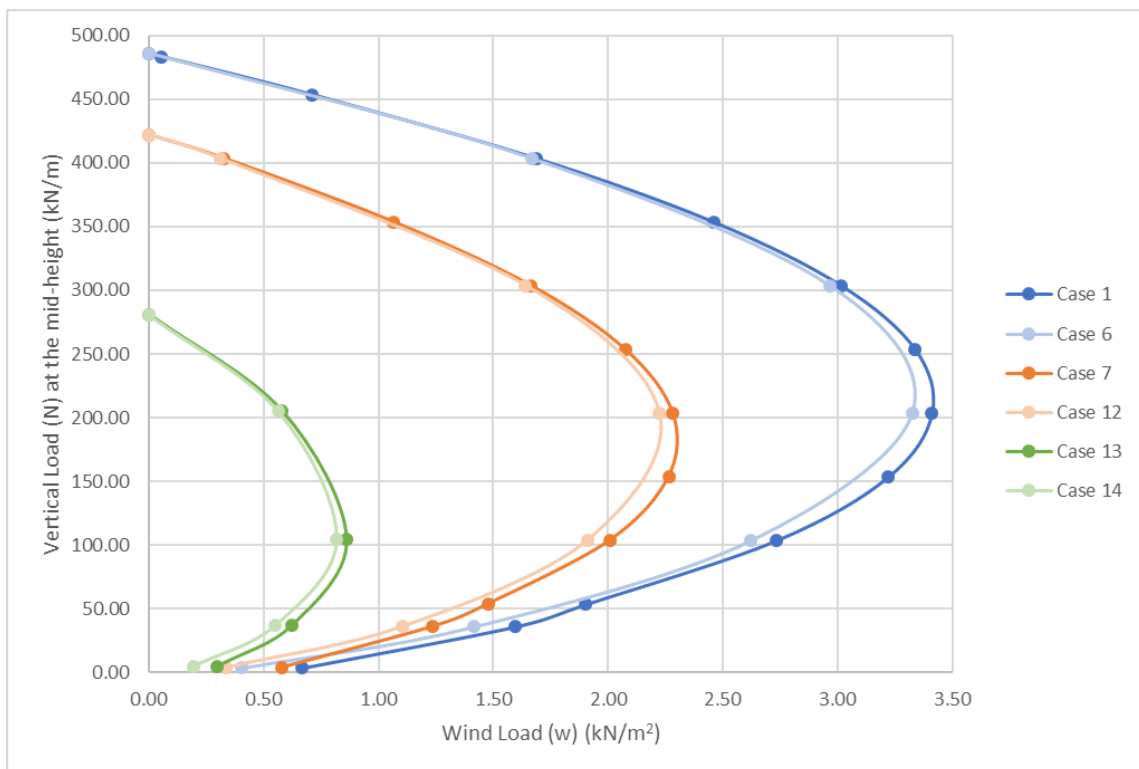
Fig. 103 Interaction between wind load and vertical resistance of a URM wall - constant values of f_k and E & variable value of f_t for three different values of h/t ratio
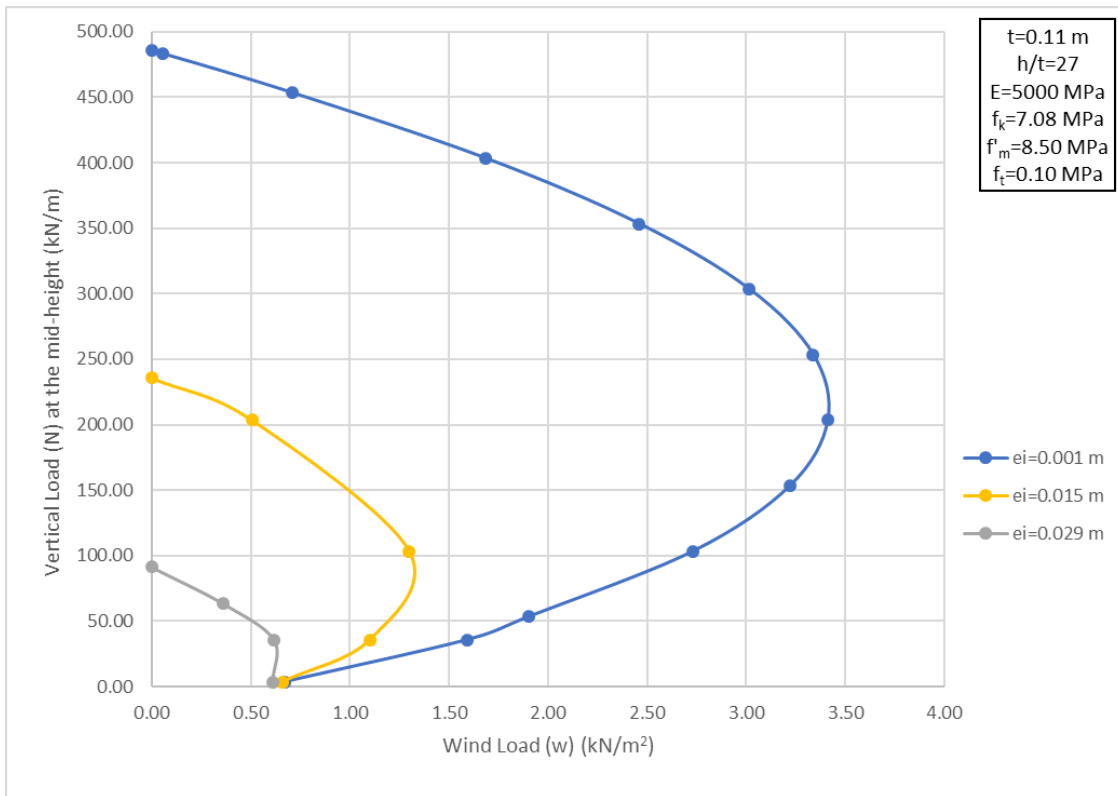
Fig. 104 Influence of eccentricity at the top or bottom of the wall on the interaction between wind load and vertical resistance of a URM wall
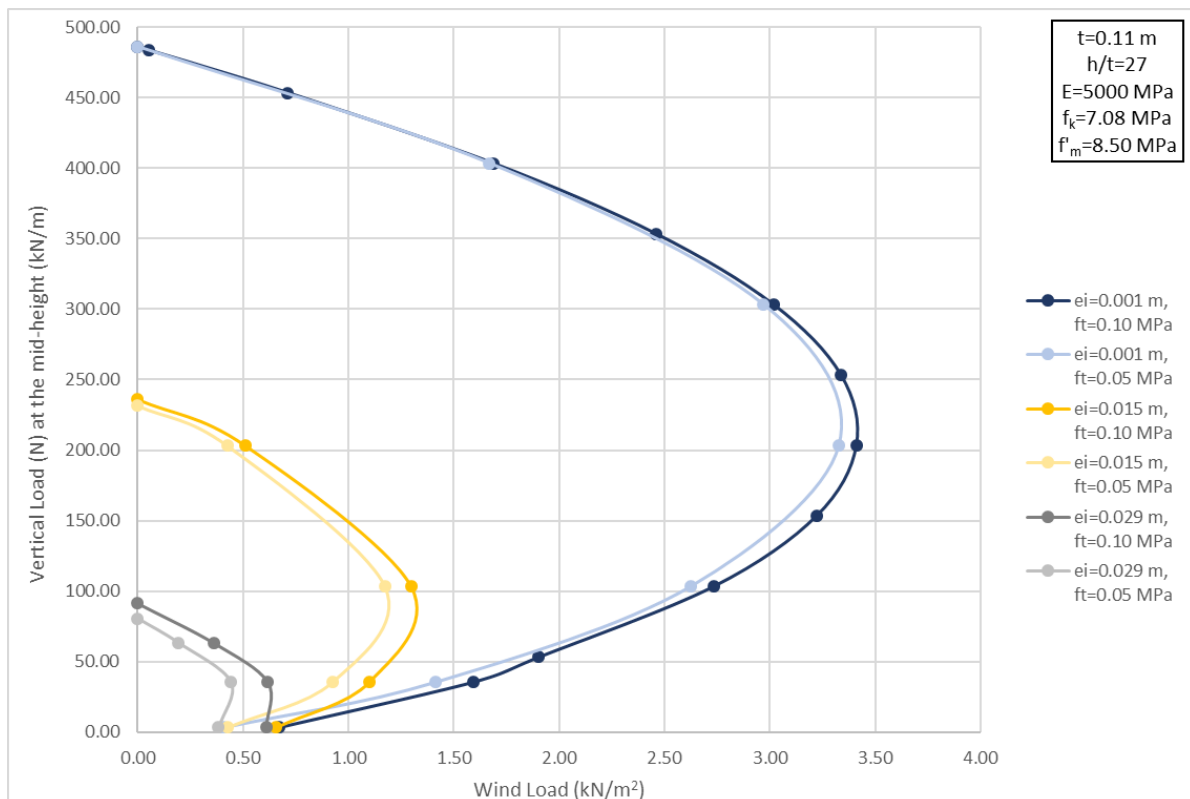
Fig. 105 Interaction between wind load and vertical resistance of a URM wall - variable value of f_t for three different values of eccentricity at the top or the bottom(e_i)

The curves in the graphs, in Fig. 99 - Fig. 105, show the combinations of vertical load and wind load, that can lead an existing slender URM wall to failure. When the self-weight is the only vertical load, that is applied on the wall, the latter can withstand a wind load of low magnitude. Due to the tensile strength of masonry, the wall can resist lateral loads, even if the total vertical load is assumed equal to zero. Increasing the vertical load on the wall, the value of wind load that causes the failure increases. This happens until the maximum value of wind load, that the wall can withstand, is attained. After that point, lower values of wind load lead to failure, as the vertical load on the wall increases. The maximum value of vertical load, that can be applied on the wall, occurs when it is subjected to zero wind load. It is obvious in the graphs that, for every value of wind load, there are two values of vertical load that cause the failure of an existing slender URM wall.

The interaction between the vertical resistance of existing slender URM walls and the applied wind load, according to the results from the FE Analysis, is comparable to the interaction, which is derived from the analytical solutions, for critical axial loads, that Schultz [36] defined for URM members, under the combination of eccentric compression loads and lateral loads. Therefore, the analytical solution (Equation 54) can form the basis, for developing an appropriate formula, for the estimation of the vertical resistance of existing slender URM walls, subjected to combined vertical and lateral loading. As it has already been mentioned, the graphs in section 9.2 show that, for the same value of wind load there might be two values of maximum vertical load at the mid-height – vertical resistance of the URM wall. Schultz [38] distinguishes two regions in the interaction diagrams, between the critical axial load and the moment from lateral loads (Fig. 15). The compression region, where the increase of wind load and, consequently, the bending moment leads to the reduction of the critical load, and the tension region, where the critical axial load increases with the wind load. The distinction criterion is the nature of the axial load. The bending moment is generally caused by variable loads (wind or seismic actions). The response of URM walls, where the axial force, mainly, consists of permanent loads, is described by the compression region of the diagram. On the other hand, the tension region is suitable for URM walls, subjected to axial force, which consists of a significant proportion of variable actions. When assessing the structural capacity of existing masonry building structures, the vertical resistance of URM walls on the lower floors is, generally, estimated. There occur the largest axial loads. A URM wall in the first floor of an existing building (section 8.1) is the case study, since simply supported walls, on the top and the bottom side, are of interest within the context of this thesis. Calculating the design axial load, at the mid-height of the URM wall, according to the provisions in the NEN 8700:2011 norm, it was found that the permanent actions have the major contribution. Therefore, it is considered more appropriate that, a formula for the estimation of the vertical resistance of existing slender URM walls, subjected to combined vertical and lateral loading, is developed to describe the compression region. The general form, that the formula will have, is given in Equation 59.

The formula in Equation 59 is divided in two segments. The first segment '$\alpha N(w = 0)$' entails the impact of the material properties, the geometry of the wall and the eccentricity, at the top or bottom of the wall, on the vertical resistance. It is mentioned, again, that the eccentricity, at the top and the bottom of the studied URM walls, as well as along the full height is equal to the initial eccentricity, which allows for construction imperfections. [53] The influence of the wind load is neglected in the first segment. Literature, relevant to the response of slender masonry walls, under eccentric vertical loads, has already been mentioned. The formula, proposed by Bakeer [19], for the estimation of the capacity reduction factor, at the mid-height of the wall is described by Equation 39. The second expression (below) is relevant for slender walls, where buckling failure is dominant. Given the capacity reduction factor, at the mid-height of the wall, the design value of the vertical resistance can be estimated,

according to Equation 11. Equation 60 and Equation 61 describe the derivation of the design value of the vertical resistance of a slender URM wall, for the capacity reduction factor, proposed by Bakeer [19]. The expressions of critical axial load of URM compression members, under the combination of eccentric vertical loads and lateral loads, defined by Schultz [36], include the estimation of the critical axial load capacity, for members subjected to eccentric vertical loads, only (Equation 51). The radius of gyration of the net section, of the masonry member, is calculated according to Equation 62. Replacing the radius of gyration for a wall segment, of unit length, as well as using the expression for the first Euler Buckling Mode (Equation 45) in Equation 51, an alternative expression is obtained for the critical axial load capacity, for members subjected to eccentric vertical loads, only (Equation 63). Equation 61 and Equation 63 specify a similar influence of the material properties, the geometry of the URM wall and the eccentricity, at the top or bottom of the wall, on the vertical resistance. Hence, they can be used as references, when defining the first segment of the formula in Equation 59.

The influence of the wind load is considered in the second segment '$\left(b + c \sqrt{d - f \frac{e_w}{t}}\right)$' of the formula in Equation 59, as an additional reduction factor to the vertical resistance of an existing slender URM wall, subjected to vertical loading, only. Introducing the magnitude of the wind load in the formula is not the most efficient way to associate vertical resistance and wind load. The effect of wind load depends on the geometry of the wall (height (h) and thickness (t)), the boundary conditions and the applied vertical load. The research within this thesis focuses on one case, with respect to the boundary conditions of slender URM walls. The walls are simply supported, at the top and the bottom edges, as can be seen in Fig. 20. Hence, the maximum first-order bending moment, because of the wind load, occurs at the mid-height of the wall and is calculated according to Equation 64. Both wind loads and eccentrically applied vertical loads cause out-of-plane bending on URM walls. Therefore, the eccentricity, caused by the maximum first-order bending moment on the wall, because of the wind load, can represent the influence of wind load in the formula, for the calculation of the vertical resistance of URM walls. This eccentricity can be calculated according to Equation 48 [38]. The denominator, in Equation 48, is the critical axial load of URM compression members, under the combination of eccentric vertical loads and lateral loads. The latter is, actually, the vertical resistance, that is sought through the formula in Equation 59. Hence, iterating is necessary in order to estimate the vertical resistance. The practicality of such a formula is compromised. In Equation 54, the eccentricity, caused by the maximum first-order bending moment on the wall, because of the wind load, is calculated as M_w/P_e. The critical axial load capacity, for masonry members subjected to eccentric vertical loads, (Equation 51) can be calculated regardless of the applied wind load. This way, iterating is not necessary and the calculation of the critical axial load of unreinforced masonry compression members, under the combination of eccentric vertical loads and lateral loads, becomes easier. Thus, the eccentricity, caused by the maximum first-order bending moment on the wall, because of the wind load, can be calculated according to the expression in Equation 65. The latter expression is introduced in the formula for the estimation of the vertical resistance of existing slender URM walls, subjected to combined vertical and lateral loading (Equation 59). The formula, in the EN 1996 norm, and developed formulas, for the calculation of the vertical resistance of URM walls [19], [36], consider the effect of the eccentricity by the non-dimensional ratio e/t. The effect of the eccentricity, caused by the maximum first-order bending moment on the wall, because of the wind load, can be introduced in a similar way in the formula, that estimates the vertical resistance of existing slender URM walls (Equation 59). The latter comment is in accordance with the calculation of the critical axial load of unreinforced masonry compression members, under the combination of eccentric vertical loads and lateral loads, by Equation 54. Equation 54 makes use of the radius of gyration (Equation 62) whereas Equation 59 uses the thickness of the wall. Since the value of the vertical resistance is calculated per unit length of a URM wall, the radius of gyration is a function of the thickness of the wall, only. [53]

Equation 59 General Form of the Formula for the Estimation of the Vertical Resistance of existing slender URM walls, subjected to Combined Vertical and Lateral Loading

$$N = \alpha \, N(w = 0) \left(b + c \sqrt{d - f \, \frac{e_w}{t}} \right), \text{ where:}$$

a, b, c, d, f: factors to be estimated

N(w=0):   the vertical resistance of a URM wall, subjected to vertical loading only

e$_w$:   the eccentricity at the mid-height of the wall, caused by the maximum first-order bending moment on the wall, because of the wind load (Equation 65)

t: the thickness of the wall

Equation 60 Introducing the Capacity Reduction Factor (Φ) at the Mid-height of the Wall, proposed by Bakeer [19], in Equation 11

$$N_{Rd} = \Phi \, f_d \, t = 0.79 \left(1 - 2 \frac{e_i}{t} \right)^3 \frac{1}{\lambda'^2} \, f_d \, t, \text{ where:}$$

Φ: the capacity reduction factor at the mid-height of the wall (Equation 31)

f_d: the design compressive strength of masonry (Equation 24)

t: the thickness of the wall

e_i: the eccentricity at the top or bottom of the wall (Equation 13)

λ':   a non-dimensional parameter, that takes into account the slenderness and the masonry stiffness (Equation 40)

Equation 61 Design Value of the Vertical Resistance of Slender URM walls, for the capacity reduction factor (Φ) at the mid-height proposed by Bakeer [19]

$$N_{Rd} = \frac{0.79}{\gamma_M} \frac{E \, t_{ef}^3}{h_{ef}^2} \left(1 - 2 \frac{e_i}{t} \right)^3, \text{ where:}$$

γ_M: partial factor for material

E: the short-term secant modulus of elasticity

t_{ef}:   the effective thickness of the wall

h_{ef}:   the effective height of the wall

e_i: the eccentricity at the top or the bottom of the wall (Equation 13)

t: the thickness of the wall

Equation 62 Radius of Gyration of the Net Section of the Masonry Member

$$r = \sqrt{\frac{I_n}{A}}, \text{ where:}$$

I_n: the moment of inertia of the net section of the masonry member

A: the cross-sectional area

Equation 63 Critical Axial Load Capacity for Masonry Member subjected to Eccentric Vertical Loads

$$P_e = 0.822 \frac{E\, t_{ef}^3}{h_{ef}^2} \left(1 - 2\frac{e_i}{t}\right)^3, \text{ where:}$$

E: the short-term secant modulus of elasticity of masonry

t_{ef}:   the effective thickness of the wall

h_{ef}:   the effective height of the wall

e_i: the eccentricity at the top or bottom of the wall (Equation 13)

t: the thickness of the wall

Equation 64 Maximum First-Order Bending Moment on the wall because of the Wind Load

$$M_w = \frac{w\, h^2}{8}, \text{ where:}$$

w: the wind load in kN/m^2

h: the clear storey height

Equation 65 Eccentricity at the Mid-height of the Wall, caused by the Maximum First-Order Bending Moment, because of the Wind Load

$$e_w = \frac{M_w}{N(w=0)}, \text{ where:}$$

M_w: the maximum first-order bending moment on the wall because of the wind load (Equation 64)

N(w=0):   the vertical resistance of a URM wall subjected to vertical loading, only

To elaborate the formula in Equation 59, it is necessary to understand the influence of the parameters, that were discussed in section 9.2, on the vertical resistance of existing slender URM walls, subjected to combined vertical and lateral loading. As it has, already, been mentioned, the formula in Equation 59 is divided in two segments. Each segment will be addressed individually. Initially, it will be assessed whether and how the geometric as well as the material properties, of URM walls, need to be introduced in the second segment of the formula, in Equation 59. Further, the influence of these properties on the vertical resistance of the URM wall, when zero wind load is applied, will specify the expression for the first segment of the formula in Equation 59.

9.3.1   Reduction to the Vertical Resistance of Existing Slender URM Walls due to Wind Load

The second segment of the formula in Equation 59 introduces the influence of the wind load on the vertical resistance of existing slender URM walls, subjected to combined vertical and lateral loading. It has already been mentioned that Equation 54 formed the basis for suggesting Equation 59. In Equation 54 the factors b, c and d are constants. Only the factor f describes the effect of the eccentricity, at the top or bottom of the wall. Schultz [36] defined Equation 54, assuming that masonry is a linear – elastic material with zero tensile strength. These assumptions are not in agreement with the material model, that was used as input for the FE model (Table 2). Therefore, the appropriate consideration of the parameters, that were discussed in section 9.2, within the factors b, c, d and f, will be assessed. Towards that, the second segment is secluded from the rest of the formula in Equation 59. The FE analysis results are depicted in the graphs in section 9.2. The values of the vertical resistance lie on the vertical axis of the graphs. Respectively, new graphs are created, where the vertical axis represents the ratio $N/N(w=0)$. 'N' is the value of the vertical load at the mid-height – vertical resistance of the URM wall, subjected to a specific value of wind load. '$N(w=0)$' is the value of the vertical load at the mid-height – vertical resistance of the URM wall, when zero wind load is applied. The ratio $N/N(w=0)$ is, actually, the reduction, that the wind load causes, to the vertical resistance of an existing slender URM wall, subjected to vertical loading, only. As it has, already, been mentioned, the dimensionless ratio e_w/t represents the influence of the wind load, in the formula for the calculation of the vertical resistance (Equation 59). Therefore, the e_w/t ratios, that are calculated from the respective values of wind load, in the graphs in section 9.2, lie in the horizontal axis of the new graphs. The new graphs are shown in Fig. 106 - Fig. 117.
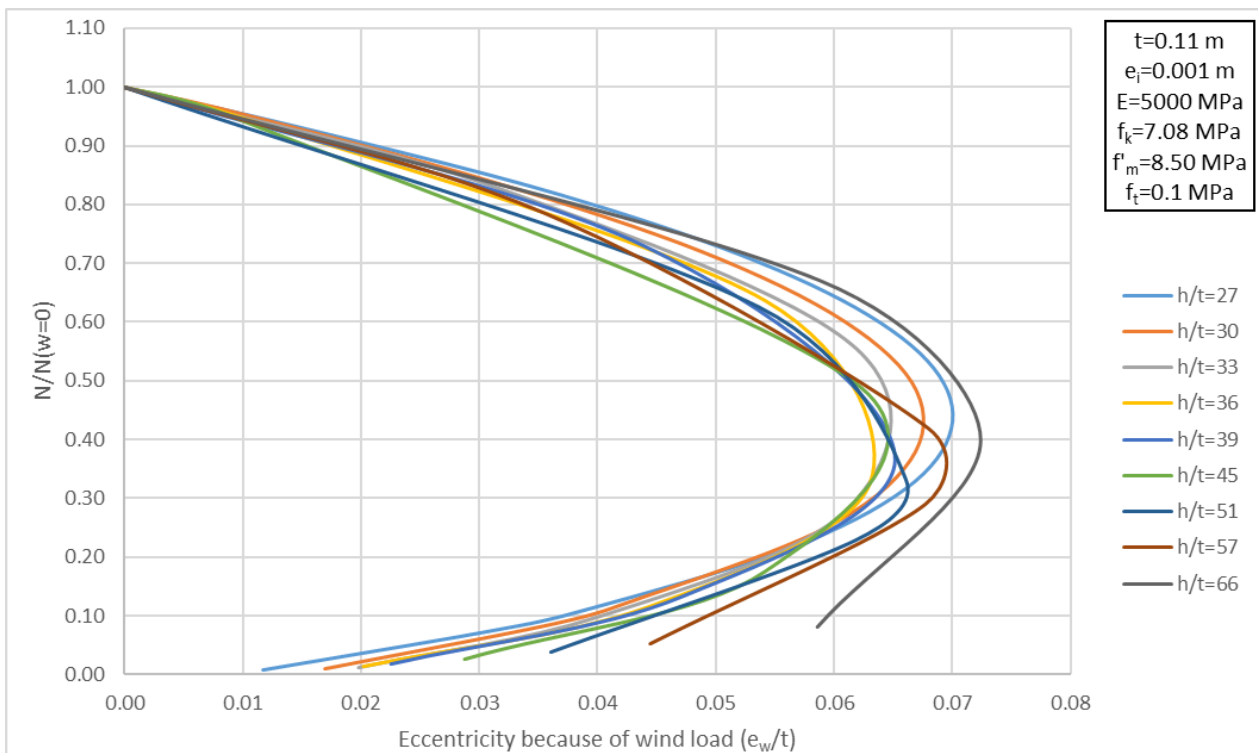
Fig. 106 Reduction to the vertical resistance of URM walls, due to wind load, for different values of slenderness ratio
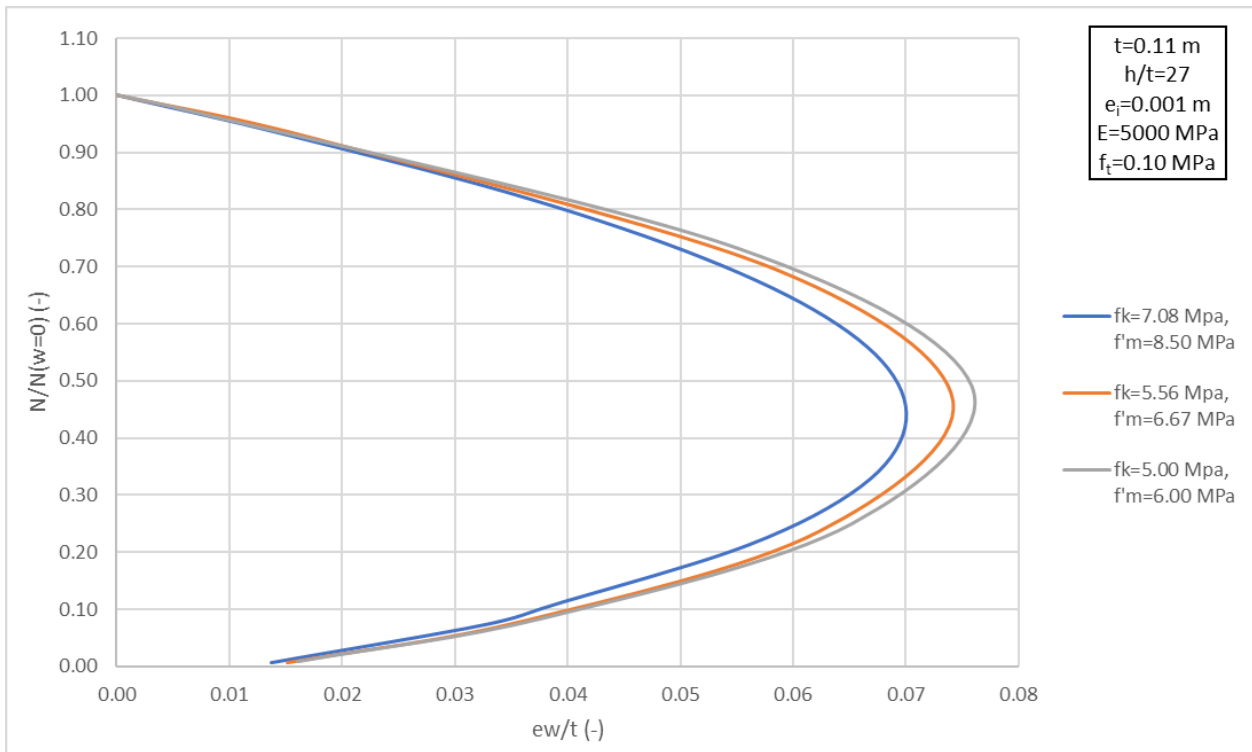
Fig. 107 Reduction to the vertical resistance of URM walls, due to wind load – constant values of E, f_t and variable values of f_k - f'_m for h/t=27
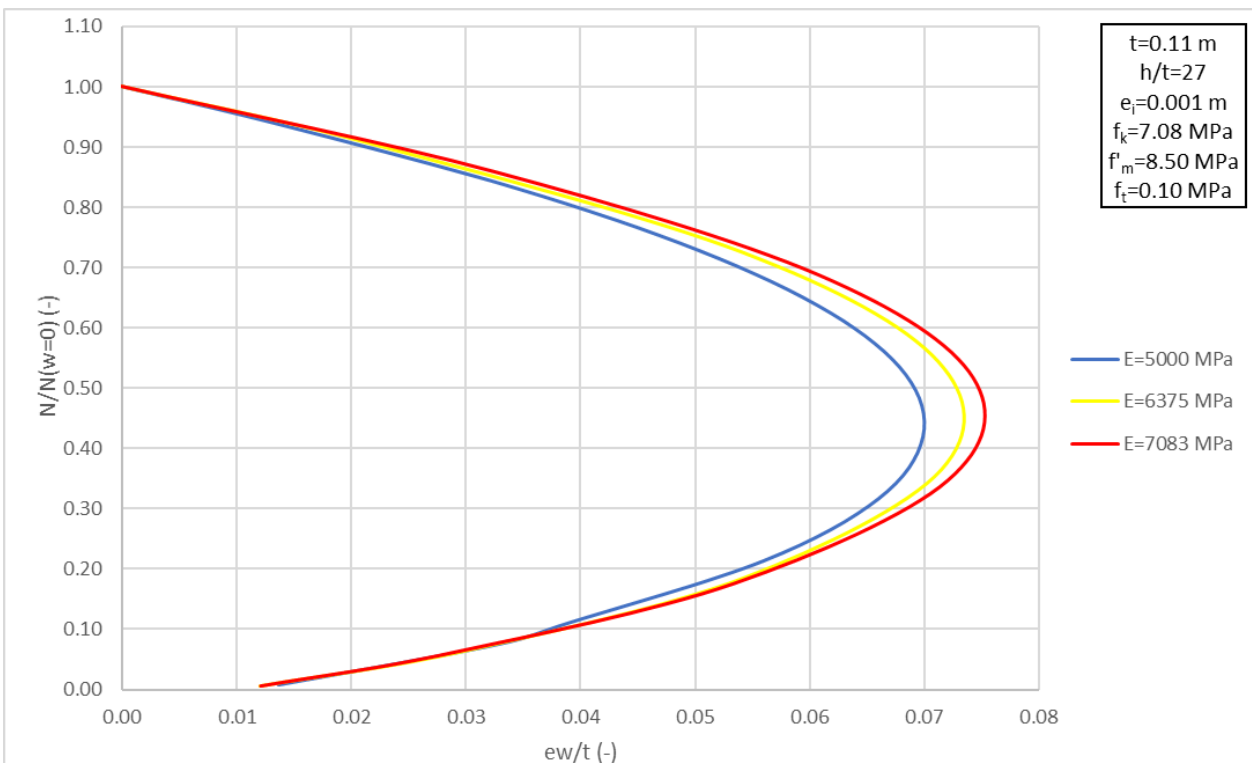
Fig. 108 Reduction to the vertical resistance of URM walls, due to wind load – constant values of f_k - f'_m, f_t and variable value of E for h/t=27
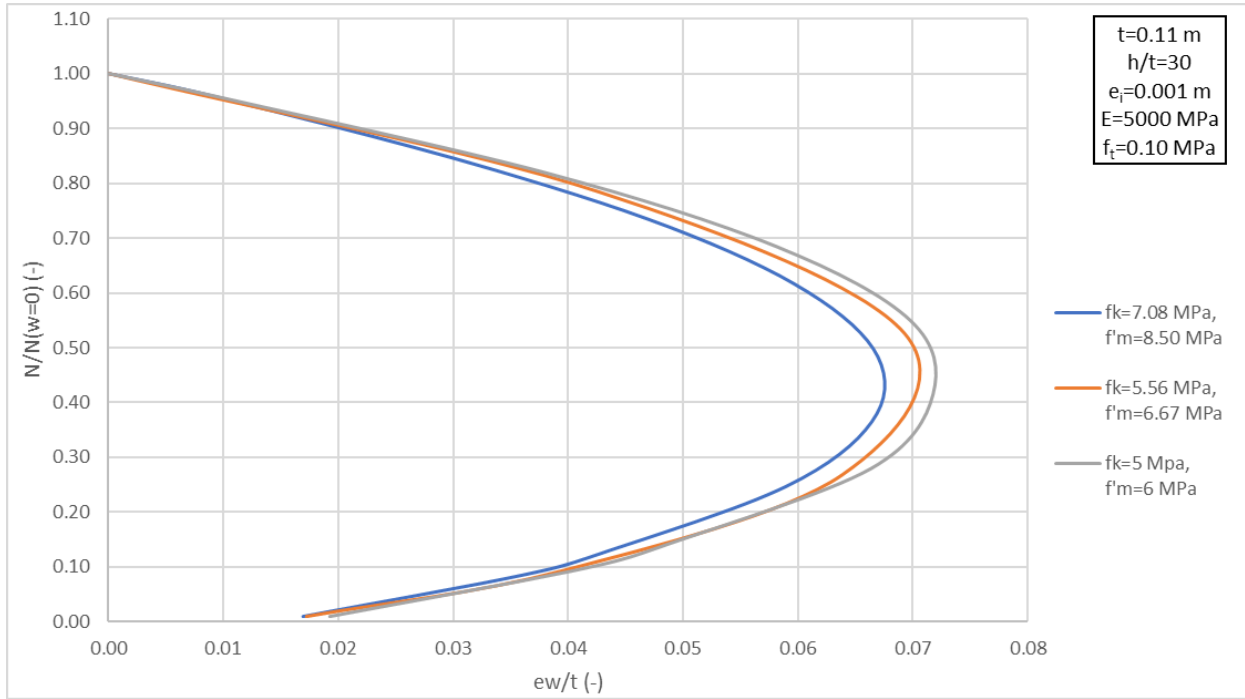
Fig. 109 Reduction to the vertical resistance of URM walls, due to wind load – constant values of E, f_t and variable values of f_k - f'_m for h/t=30
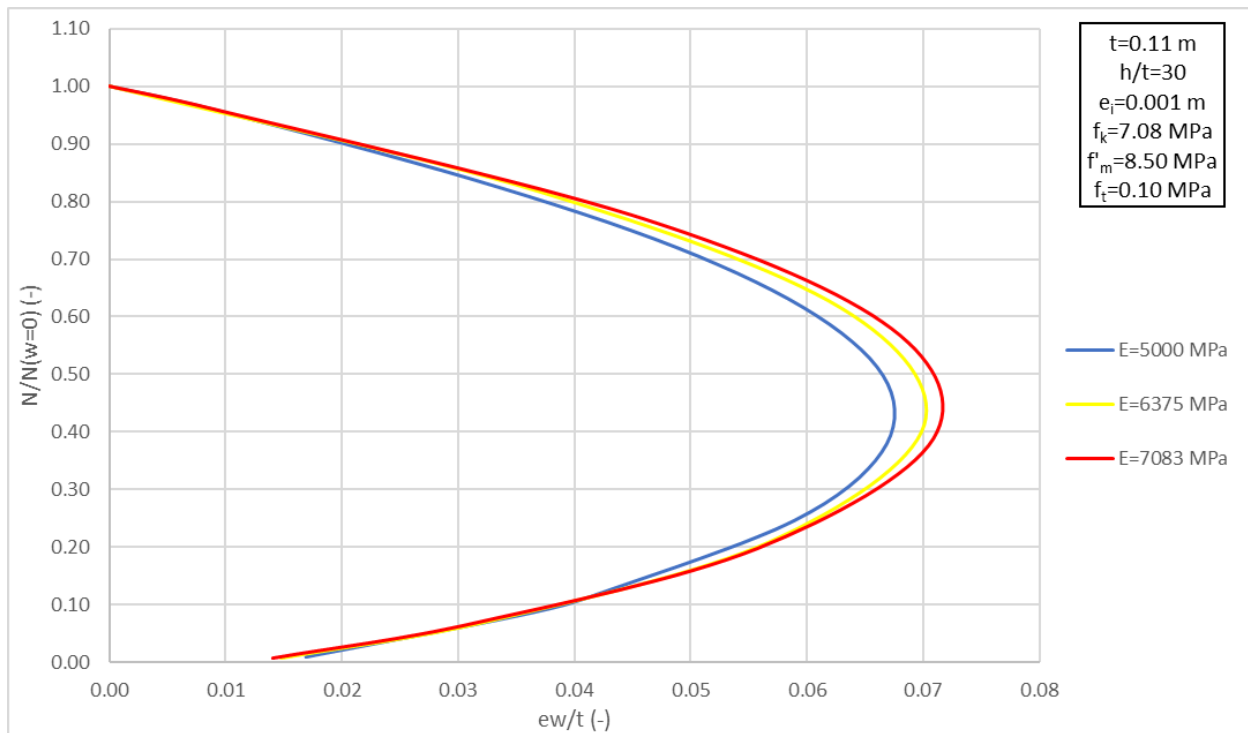
Fig. 110 Reduction to the vertical resistance of URM walls, due to wind load – constant values of f_k - f'_m, f_t and variable value of E for h/t=30
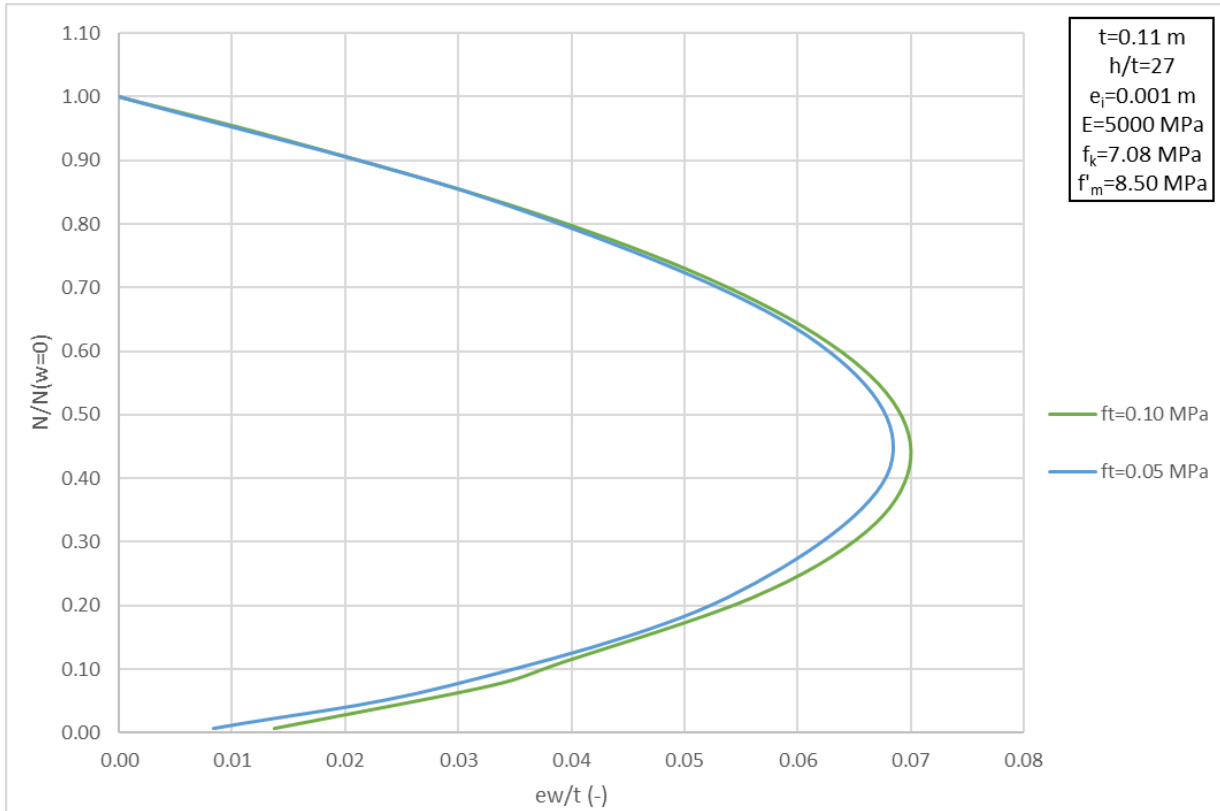
Fig. 111 Reduction to the vertical resistance of URM walls, due to wind load –variable value of f_t for h/t=27
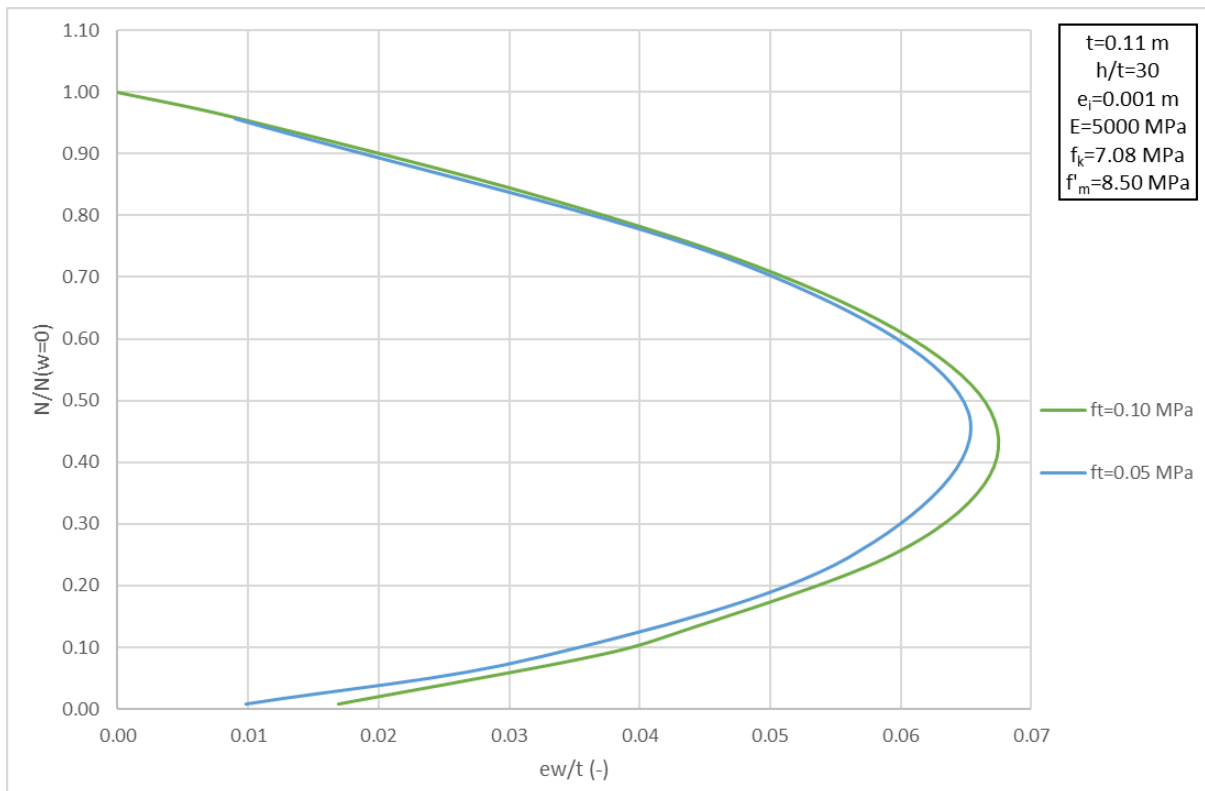
Fig. 112 Reduction to the vertical resistance of URM walls, due to wind load – variable value of f_t for h/t=30
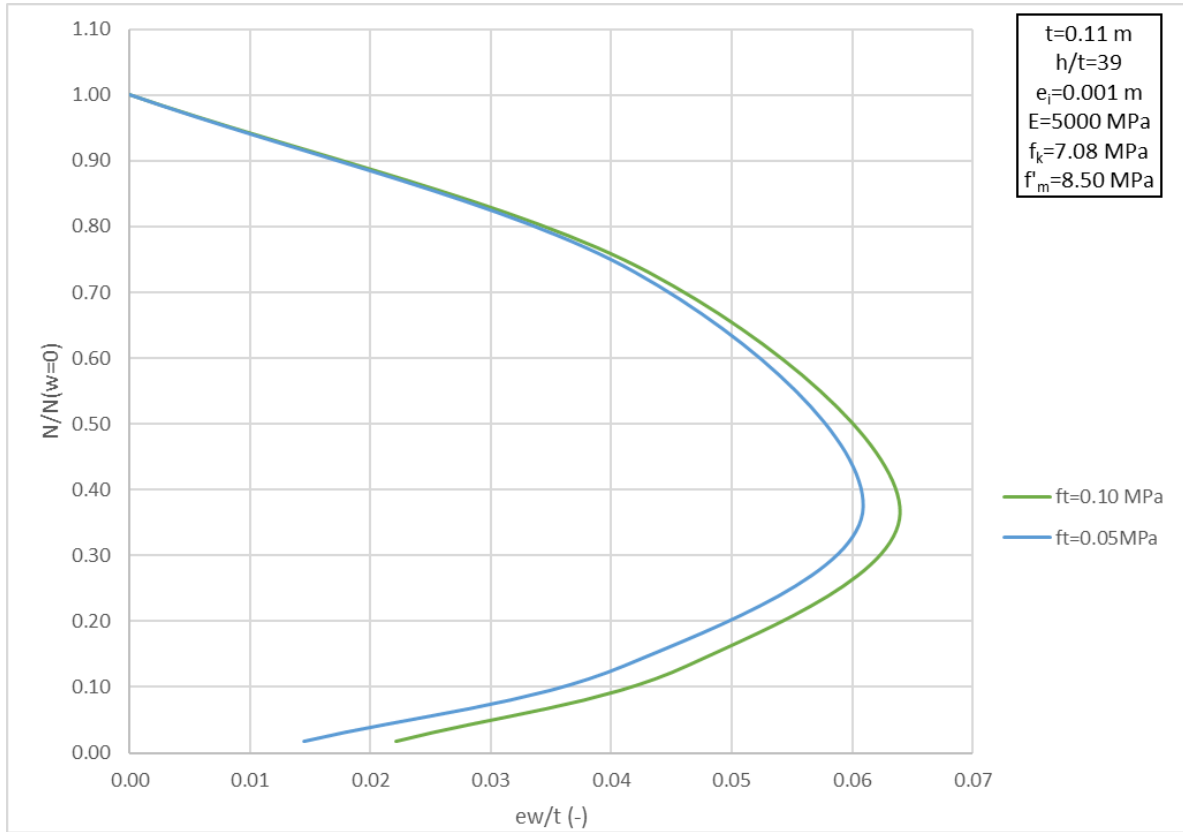
Fig. 113 Reduction to the vertical resistance of URM walls, due to wind load – variable value of f_t for h/t=39
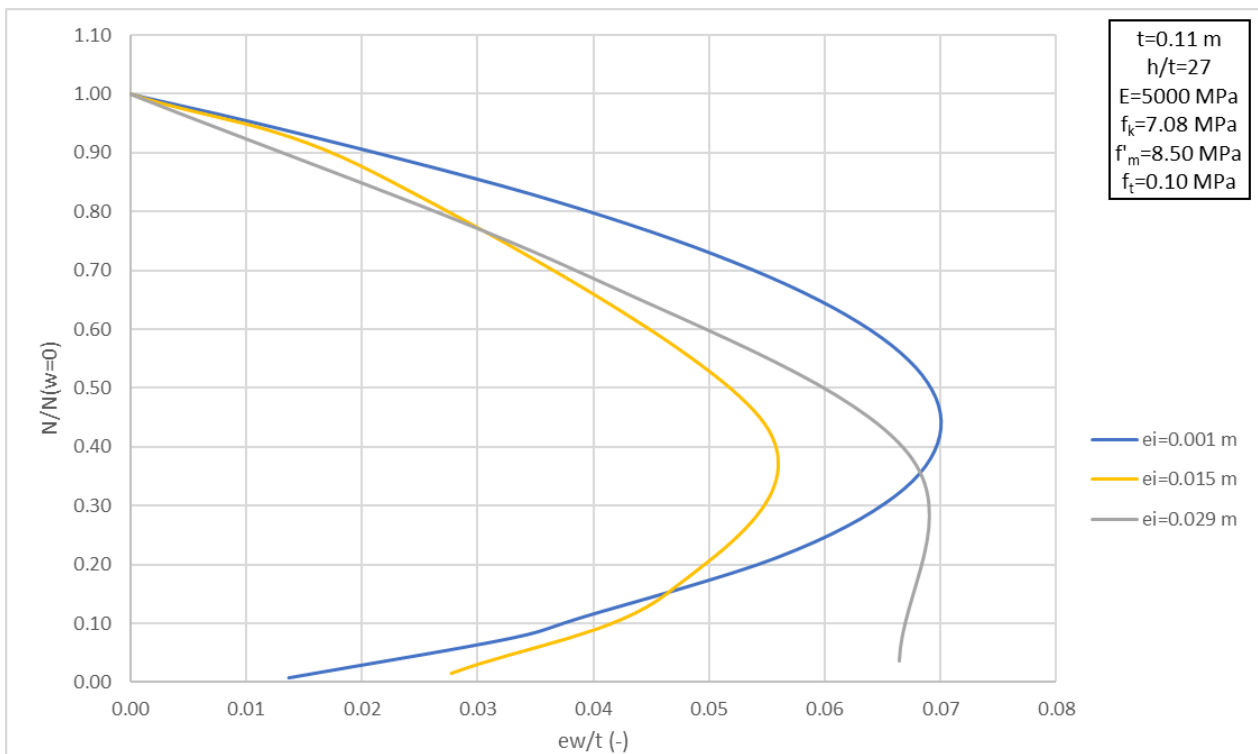
Fig. 114 Reduction to the vertical resistance of URM walls, due to wind load, for different values of eccentricity at the top or bottom of the wall
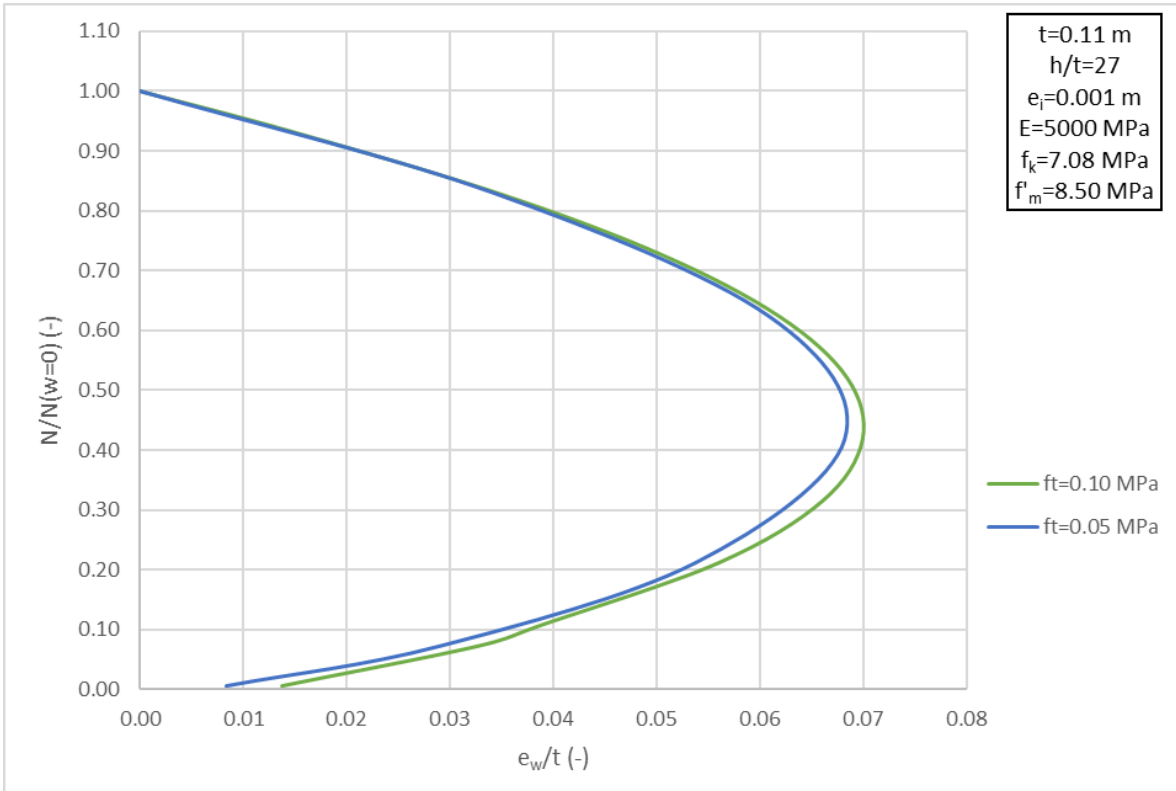
Fig. 115 Reduction to the vertical resistance of URM walls, due to wind load –variable value of f_t e_i=0.001 m
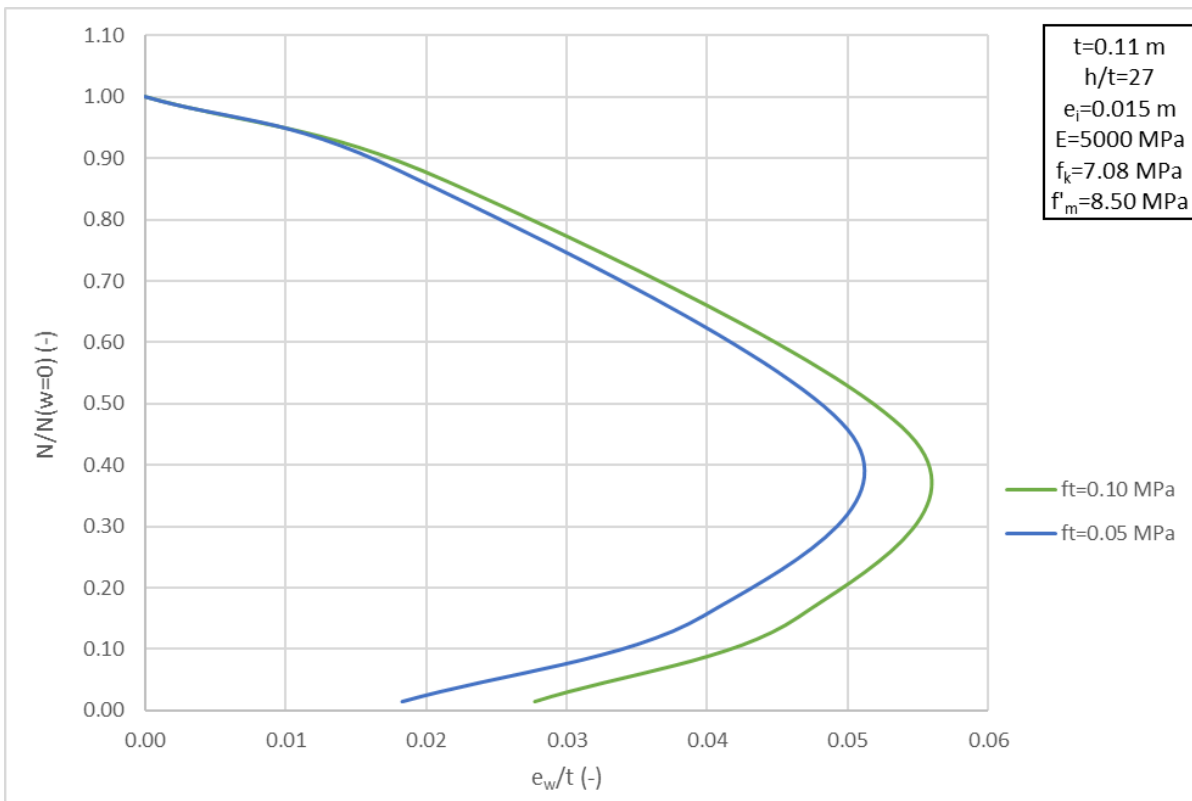
Fig. 116 Reduction to the vertical resistance of URM walls, due to wind load –variable value of f_t for e_i=0.015 m
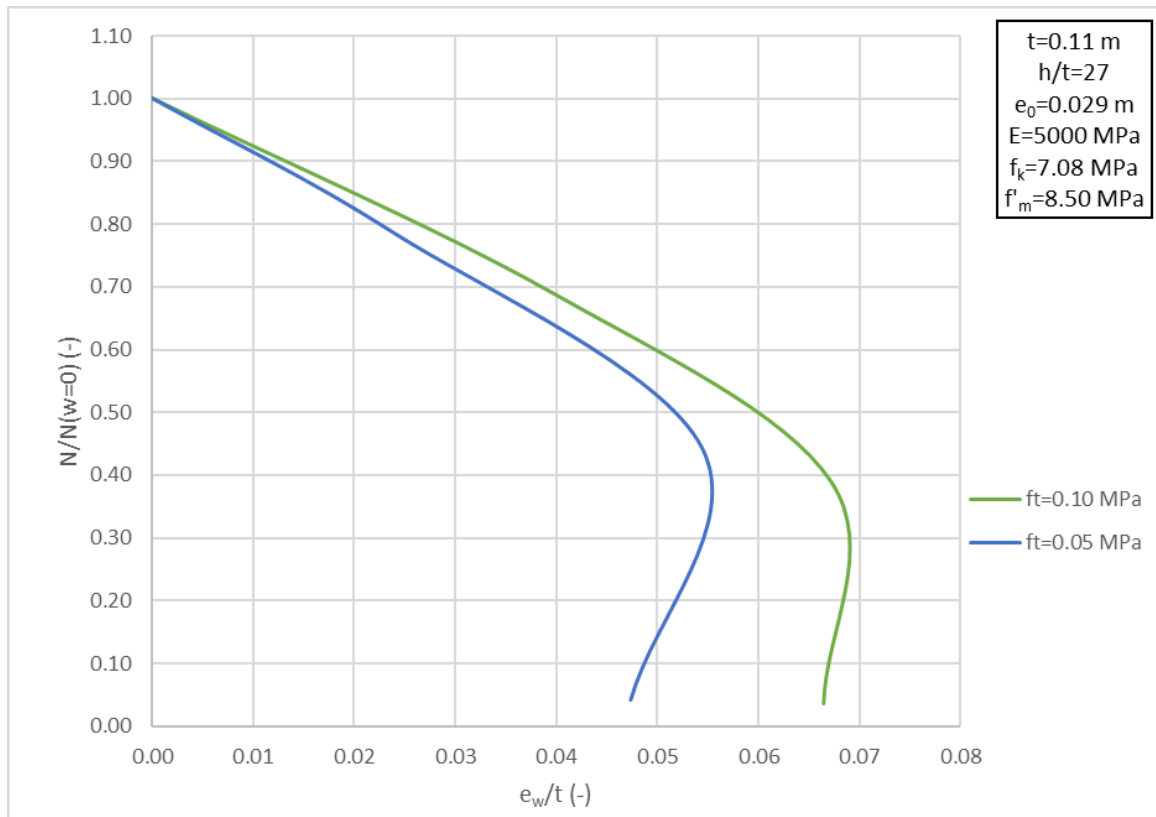
Fig. 117 Reduction to the vertical resistance of URM walls, due to wind load –variable value of f_t for e_i=0.029 m

9.3.1.1 Influence of Slenderness Ratio (h/t)

The curves in the graph in Fig. 106 do not coincide. This means that the influence of the slenderness ratio (h/t) needs to be included in the second segment of the formula in Equation 59.The curves in the graph in Fig. 106 show that, for values of slenderness ratio between 27 and 36, the increase of slenderness ratio results in the decrease of the $N/N(w=0)$ ratio, for the same eccentricity ratio (e_w/t) and vice versa. However, for values of slenderness ratio higher than 39, the response of the URM wall changes, as the slenderness ratio increases. For large values of the eccentricity ratio (e_w/t) (large values of wind load), the increase of slenderness ratio results in the increase of the $N/N(w=0)$ ratio, for the same eccentricity ratio (e_w/t) and vice versa.

The stress state of the URM wall, described by each curve in the graph in Fig. 106, at relevant combinations of applied vertical load - wind load, will provide useful information about the response of the wall. It is noticed that the maximum deviation, between the interaction curves, occurs at the maximum value of wind load. Therefore, the ratio $N/N(w=0)$ is determined, where, approximately, the maximum value of the eccentricity ratio (e_w/t) occurs, for all the interaction curves in the graph in Fig. 106. This value of the ratio $N/N(w=0)$ is equal to *0.40*. A value for the vertical load N is derived from the ratio $N/N(w=0)$, for every curve. Given this vertical load, the maximum wind load, that each wall can withstand, is estimated after a non-linear FE analysis, similar to the one described in section 9.1.4. The curves, with the relationship between the eccentricity ratio (e_w/t) and the horizontal displacement, at the mid-height, that show the evolution of the non-linear analysis, of the URM walls, with values of slenderness ratio equal to 27, 33, 39, 66, are shown in Appendix E. Accordingly, for every FE analysis, graphs can be drawn, with the evolution of stresses and strains, in the direction normal to the bed joints, on the most tensioned and compressed side of the wall. Stresses and strains, on the

most tensioned and the most compressed side of the wall, are estimated at the highlighted finite elements, in Fig. 82 and Fig. 83, respectively. Indicatively, the evolution of stresses and strains on the walls, with values of slenderness ratio equal to 33 and 39, are shown in the graphs in Fig. 118, Fig. 119 and Fig. 120, Fig. 121, respectively. The graphs for the rest of the URM walls can be found in Appendix E. For the same $N/N(w=0)$ ratio, the combination of vertical load – wind load, that leads the URM wall to failure, occurs at a lower compressive stress as the slenderness ratio increases. A lower compressive stress, at the failure, means a larger stiffness of the URM wall.

Another combination of applied vertical load - wind load, that is interesting to know the stress state of the URM walls, is when the wind load is zero and the vertical load is equal to $N(w=0)$. The graphs in Fig. 122 - Fig. 125 show the evolution of stresses and strains, in the direction normal to the bed joints, on the most tensioned and compressed side of the wall. These graphs are the results, from the FE analysis on URM walls, with values of slenderness ratio equal to 33 and 39. The scope of the analysis was the determination of the maximum vertical load on the wall, when zero wind load is applied, as it has already been discussed in section 9.2. Stresses and strains, on the most tensioned and the most compressed side of the wall, are estimated at the highlighted finite elements, in Fig. 82 and Fig. 83, respectively. Appendix E includes the respective graphs, for the remaining cases of URM walls, in the graph in Fig. 106. The level of the compressive stresses on the URM wall, when the maximum vertical load ($N(w=0)$) is applied, gets lower as the slenderness ratio increases. A lower compressive stress at the failure means a larger stiffness of the URM wall. It is, also, noticed that, for zero wind load, the URM walls with values of slenderness ratio equal to 27, 30 and 33, are uncracked when the maximum vertical load is applied. On the contrary, cracks have already initiated at the URM walls, with values of slenderness ratio greater than 36, at the point of maximum vertical load $N(w=0)$.

The stress state results explain the response of the URM walls, that is shown in the graph in Fig. 106, and has been discussed. Especially, the fact that the URM walls with values of slenderness ratio equal to 27, 30 and 33, are uncracked at the combination of maximum vertical load – zero wind load, while walls with greater values of slenderness ratio have already been cracked. The value of 36 is, approximately, the limit, that distinguishes two different patterns, for the influence of the slenderness ratio on the interaction between the vertical load and the wind load, that lead an existing URM wall to failure. Therefore, it does not seem possible that, including a relevant expression for the slenderness ratio in the second segment of the formula in Equation 59, can cover the whole range of values of slenderness ratio of the URM walls, that have been analyzed. Values of slenderness ratio up to 39, which, for a wall thickness equal to 0.11 m, are equivalent to wall heights up to 4.29 m, can be common of masonry building practice. Thus, for values of slenderness ratio between 27 and 39, it is attempted to find an appropriate expression for the influence of the slenderness ratio in the second segment of the formula in Equation 59. The URM walls with values of slenderness ratio greater than 39 are omitted from the graph in Fig. 106. This can be seen in the graph in Fig. 126. For a ratio $N/N(w=0)$ equal to 0.60, the eccentricity ratio (e_w/t) is estimated from the graph, in Fig. 126, for all the different cases of slenderness ratio. This way, the relationship between the slenderness ratio (h/t) and the eccentricity ratio (e_w/t), for the same $N/N(w=0)$ ratio is derived (Fig. 127). The graph in Fig. 127 shows that for the same $N/N(w=0)$ ratio the eccentricity ratio (e_w/t) decreases as the slenderness ratio (h/t) increases. This can be, also, expressed contrariwise. For the same eccentricity ratio (e_w/t), the $N/N(w=0)$ ratio decreases as the slenderness ratio (h/t) increases. Therefore, multiplying the eccentricity ratio (e_w/t) with the slenderness ratio (h/t) can introduce the effect of slenderness ratio in the second segment of the formula in Equation 59. and, thus, make the curves in the graph in Fig. 126 coincide. According to the curve in the graph in Fig. 127, the slenderness ratio needs to be raised to a power, which is approximately equal to 0.4. Trying different values for the power, the value of 0.38 seems to be the most appropriate. This is shown in the graph in Fig. 128. The curves for different slenderness ratios match within the compression region, which will be described by the formula in Equation 59, as it has,

already been discussed in section 9.3. For large values of the eccentricity ratio (e_w/t), only, the interaction curve, that refers to the URM wall with value of slenderness ratio equal to 39, deviates. Attention will be paid when defining the final form of the formula in Equation 59, so that it describes conservatively the interaction, between the vertical resistance, of the existing URM wall, and the applied wind load, for every case of slenderness ratio., compared to the respective FE analysis results
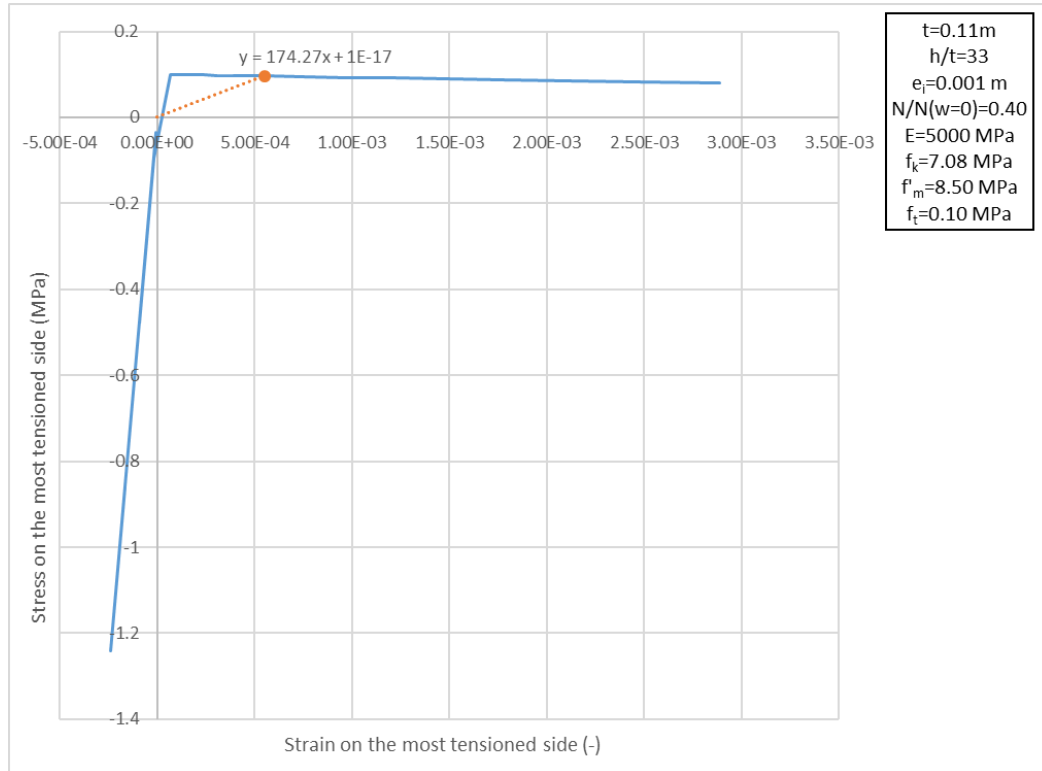
Fig. 118 Stress-Strain Evolution at the most tensioned side of the URM wall with h/t=33 – the dot represents the stress-strain state at the highlighted point on the respective curve in the graph in Fig. E. 1
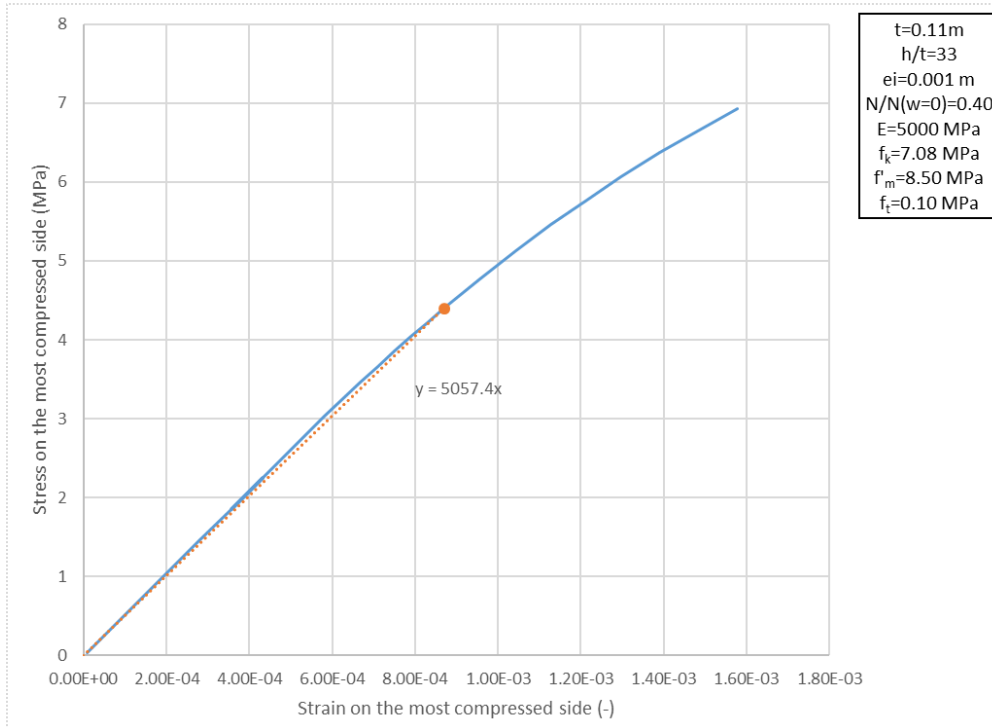
Fig. 119 Stress-Strain Evolution at the most compressed side of the URM wall with h/t=33 – the dot represents the stress-strain state at the highlighted point on the respective curve in the graph in Fig. E. 1

Fig. 120 Stress-Strain Evolution at the most tensioned side of the URM wall with h/t=39 – the dot represents the stress-strain state at the highlighted point on the respective curve in the graph in Fig. E. 1

t=0.11 m
h/t=39
e_i=0.001 m
N/N(w=0)=0.40
E=5000 MPa
f_k=7.08 MPa
f'_m=8.50 MPa
f_t=0.10 MPa

y = 5181x

Fig. 121 Stress-Strain Evolution at the most compressed side of the URM wall with h/t=39 — the dot represents the stress-strain state at the highlighted point on the respective curve in the graph in Fig. E. 1

t=0.11 m
h/t=33
e_i=0.001 m
w=0
E=5000 MPa
f_k=7.08 MPa
f'_m=8.50 MPa
f_t=0.10 MPa

y = 5208.7x
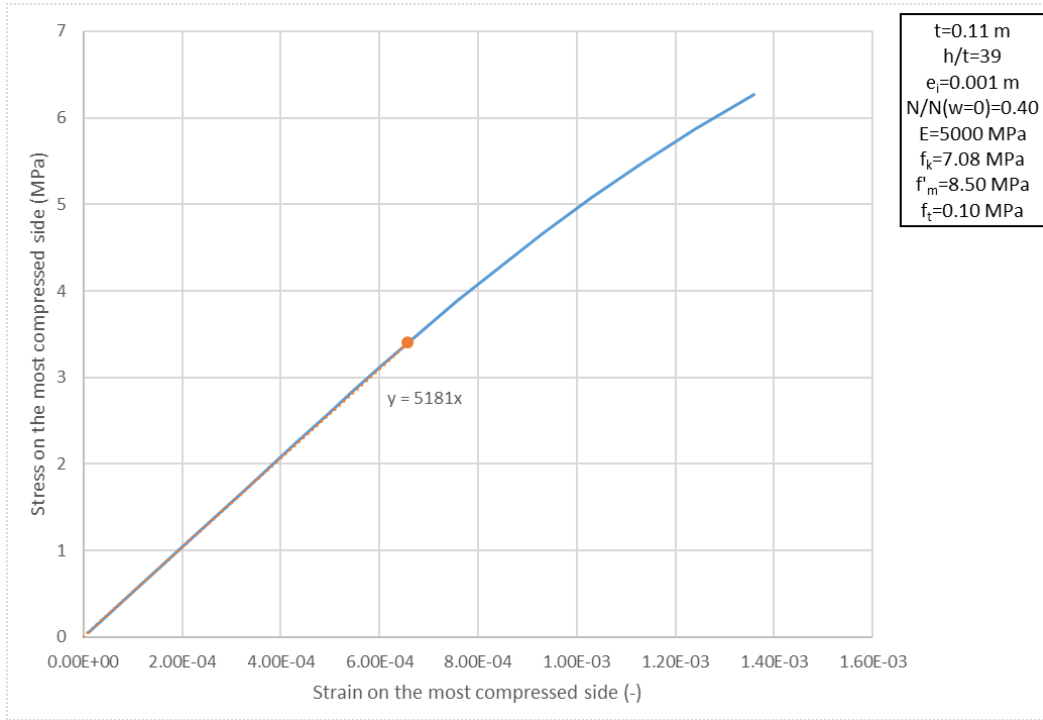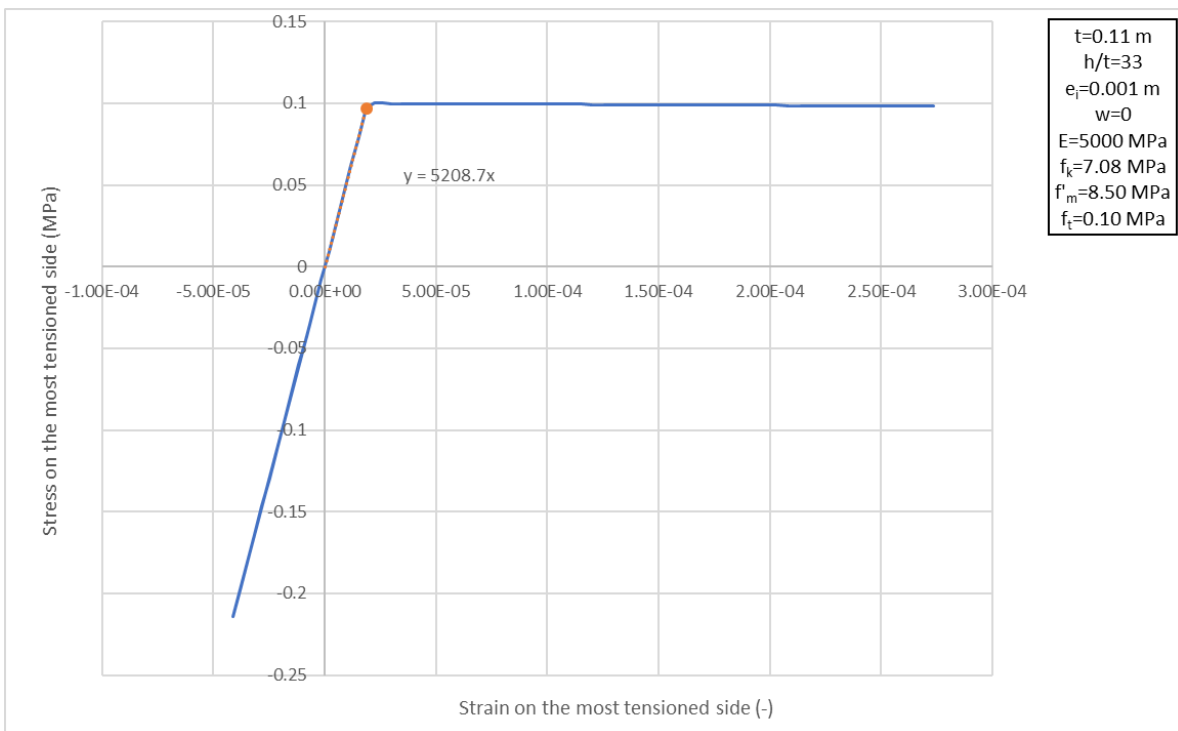
Fig. 122 Stress-Strain Evolution at the most tensioned side of the URM wall with h/t=33 — the dot represents the stress-strain state, when the maximum vertical load N(w=0) is attained
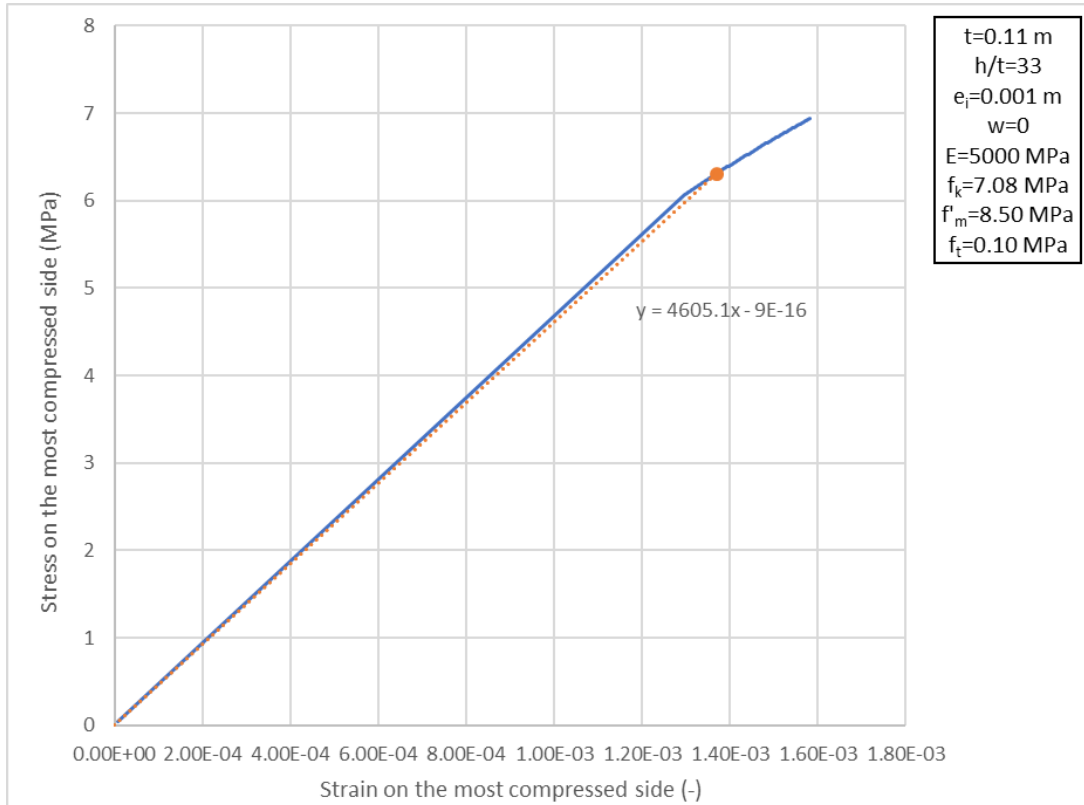
Fig. 123 Stress-Strain Evolution at the most compressed side of the URM wall with h/t=33 – the dot represents the stress-strain state, when the maximum vertical load N(w=0) is attained
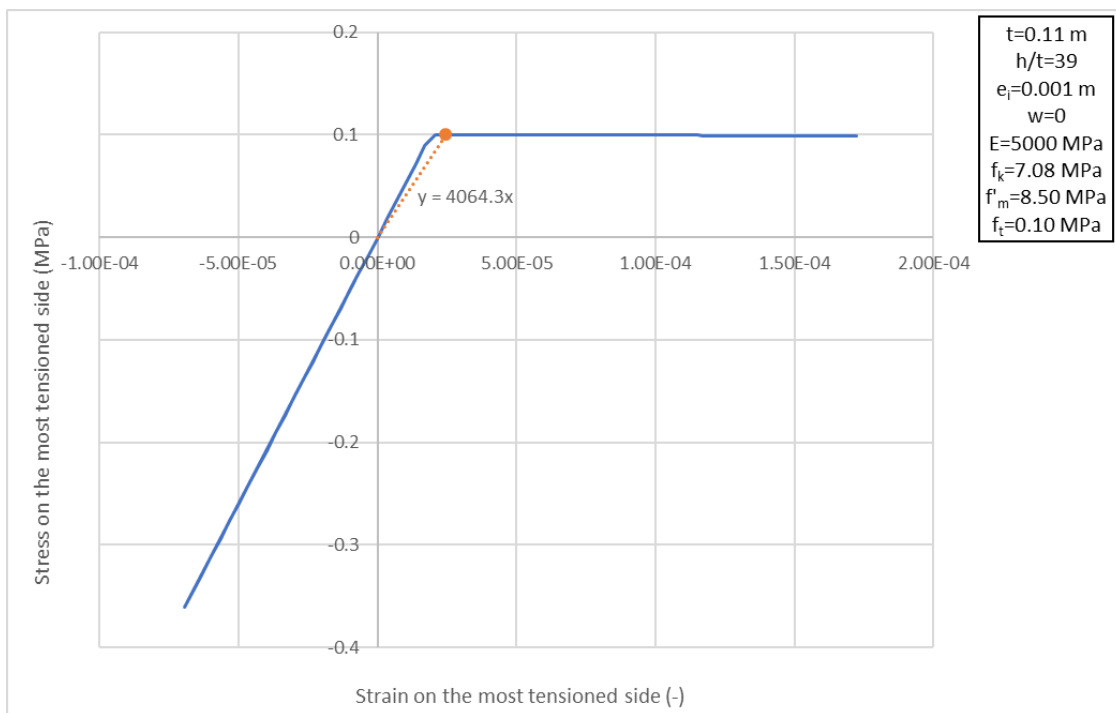
Fig. 124 Stress-Strain Evolution at the most tensioned side of the URM wall with h/t=39 – the dot represents the stress-strain state, when the maximum vertical load N(w=0) is attained
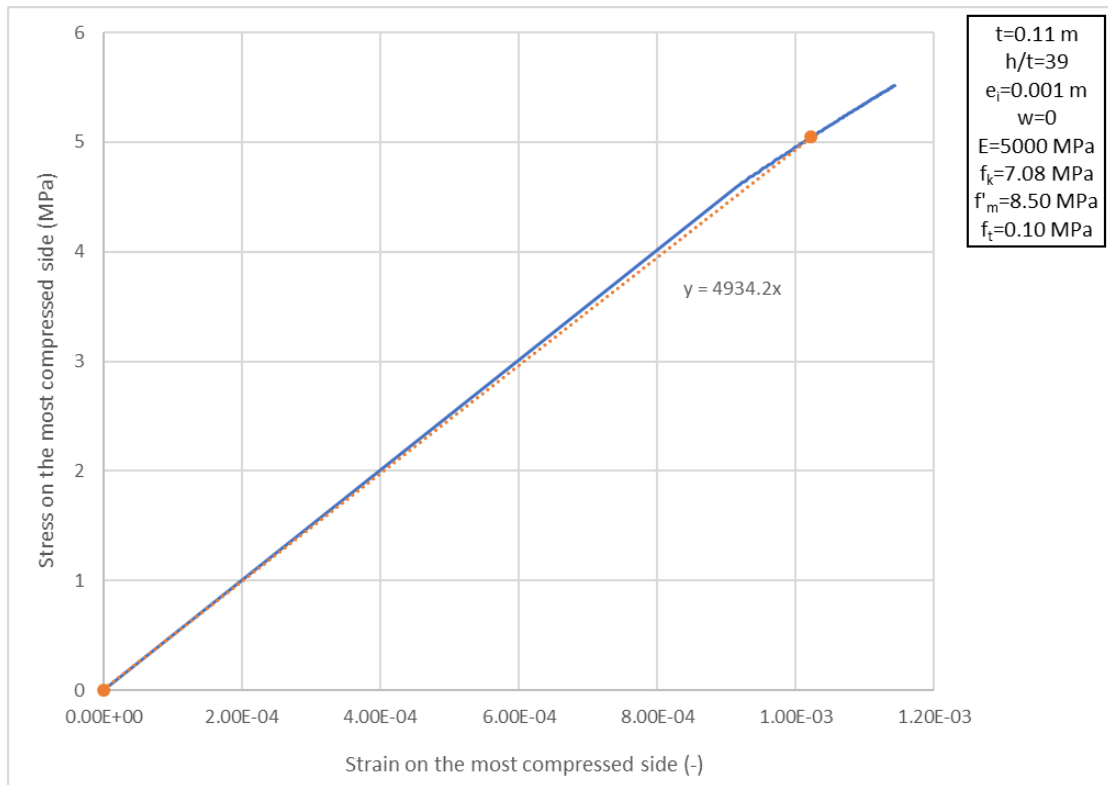
Fig. 125 Stress-Strain Evolution at the most compressed side of the URM wall with h/t=39 – the dot represents the stress-strain state, when the maximum vertical load N(w=0) is attained
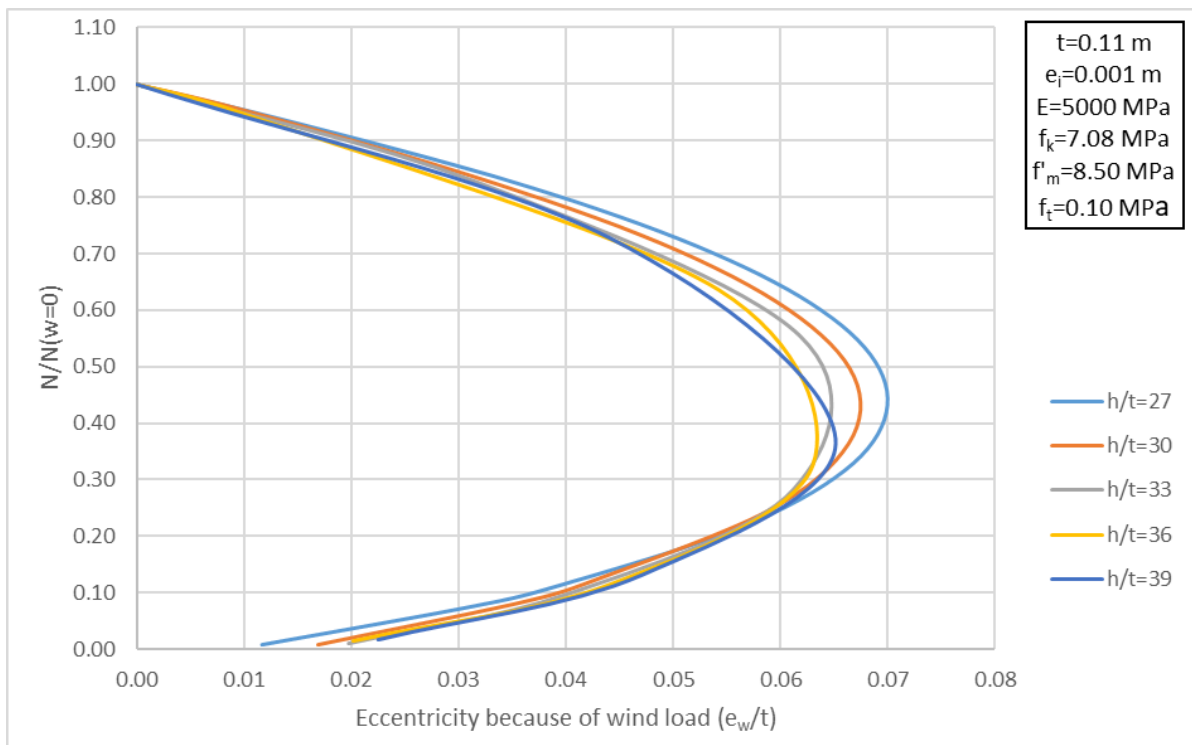
Fig. 126 Reduction factor to the vertical resistance of URM walls, due to wind load, for values of h/t between 27 and 39
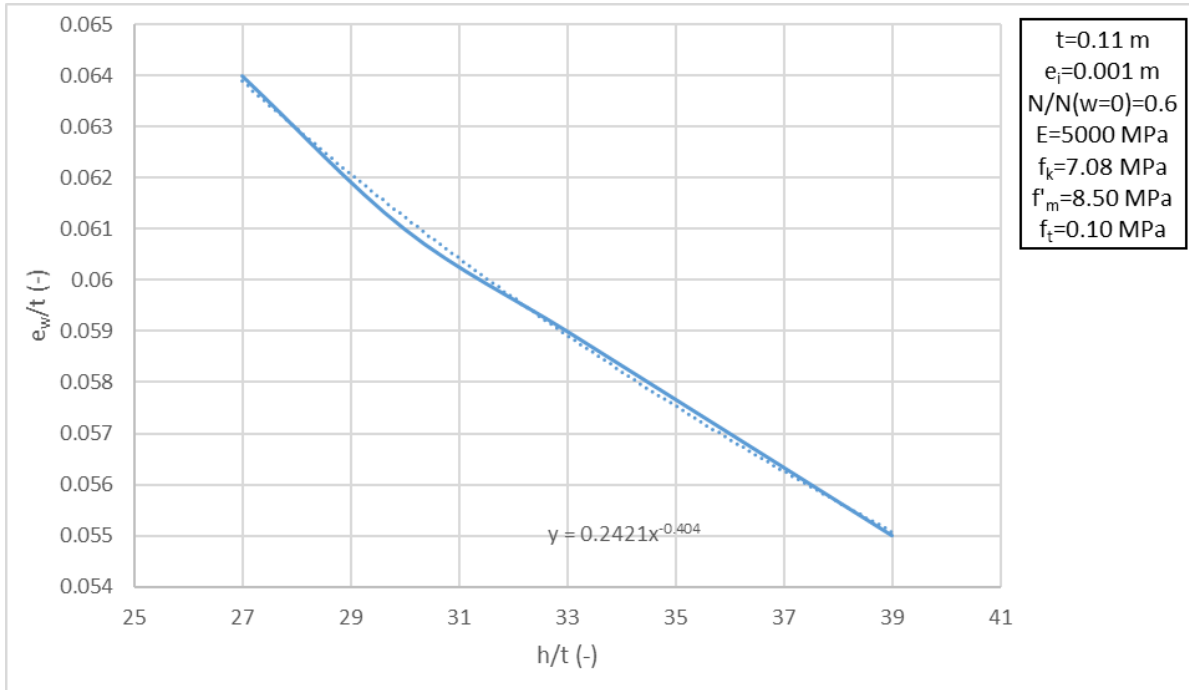
Fig. 127 Relationship between h/t and e_w/t of a URM wall for the same N/N(w=0)
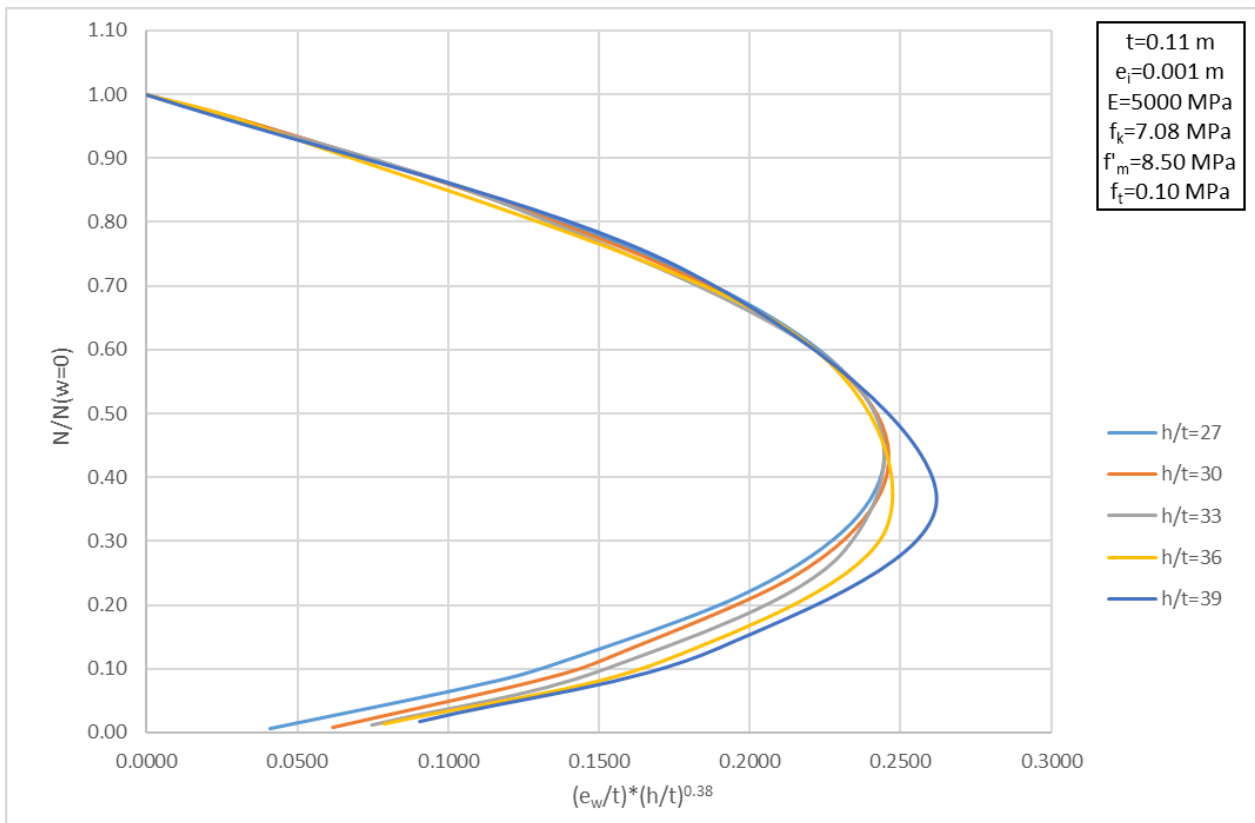
Fig. 128 Reduction factor to the vertical resistance of URM walls, due to wind load, considering the influence of h/t, for values of h/t between 27 and 39

9.3.1.2 Influence of Masonry Stiffness (E/f_k)

The curves in the graphs in Fig. 107 - Fig. 110 do not coincide. This means that the influence of the masonry stiffness (E/f_k) needs to be included in the second segment of the formula in Equation 59.The

curves in the graphs, in Fig. 107 and Fig. 109, show that, increasing the characteristic compressive strength (f_k), while keeping the short-term secant modulus of elasticity (E) constant, results in the decrease of the $N/N(w=0)$ ratio, for the same eccentricity ratio (e_w/t), and vice versa. The curves in the graphs, in Fig. 108 and Fig. 110, describe the different response of a URM wall, when the short-term secant modulus of elasticity (E) changes and the characteristic compressive strength (f_k) remains constant. The increase of the short-term secant modulus of elasticity (E) leads to the increase of the $N/N(w=0)$ ratio, for the same eccentricity ratio (e_w/t), and vice versa. Defining the stiffness of masonry (E/f_k) for every curve in the graphs in Fig. 107 - Fig. 110, it is noticed that the latter has a common influence on the response of the URM walls. The increase of the masonry stiffness leads to the increase of the $N/N(w=0)$ ratio, for the same eccentricity ratio (e_w/t), and vice versa. Combining the curves in the graphs in Fig. 107 and Fig. 108, the graphs in Fig. 129 and Fig. 130 are created, for the same value of masonry stiffness. In a similar way the graphs in Fig. 131 and Fig. 132 are created, for a value of slenderness ratio equal to 30, in this case. It is inferred that, for the same value of slenderness ratio, the value of masonry stiffness has the same influence on the curves, with the interaction between $N/N(w=0)$ and e_w/t, regardless of the values of the short-term secant modulus of elasticity (E) and the characteristic compressive strength (f_k), individually.

A suitable expression is sought for the influence of the masonry stiffness (E/f_k) in the second segment of the formula in Equation 59. For a ratio $N/N(w=0)$ equal to *0.60*, the eccentricity ratio (e_w/t) is estimated from the graph, in Fig. 107, for all the different cases of masonry stiffness. This way, the relationship between the masonry stiffness (E/f_k) and the eccentricity ratio (e_w/t), for the same $N/N(w=0)$ ratio, is derived (Fig. 133). The graph in Fig. 133 shows that, for the same N/N(w=0) ratio, the eccentricity ratio (e_w/t) increases as the masonry stiffness (E/f_k) increases. This can be, also, expressed contrariwise. For the same eccentricity ratio (e_w/t), the $N/N(w=0)$ ratio increases as the masonry stiffness (E/f_k) increases. Therefore, dividing the eccentricity ratio (e_w/t) with the masonry stiffness (E/f_k) or multiplying it with the inverse ratio (f_k/E) can introduce the effect of masonry stiffness, in the second segment of the formula in Equation 59. and, thus, make the curves in the graphs in Fig. 107 - Fig. 110 coincide. According to the curve in the graph in Fig. 133, the masonry stiffness needs to be raised to a power, which is approximately equal to 0.25. Trying different values for the power, the value of 0.23 seems to be the most appropriate. This is shown in the graphs in Fig. 134- Fig. 137. The curves, for different combinations of $E - f_k$, seem to match within the compression region, which will be described by the formula in Equation 59, as it has, already been discussed in section 9.3. Only for large values of the eccentricity ratio (e_w/t), the interaction curves deviate slightly. Attention will be paid when defining the final form of the formula in Equation 59, so that it describes conservatively the interaction between the vertical resistance, of the existing slender URM wall, and the applied wind load, for every combination of $E - f_k$, compared to the respective FE analysis results
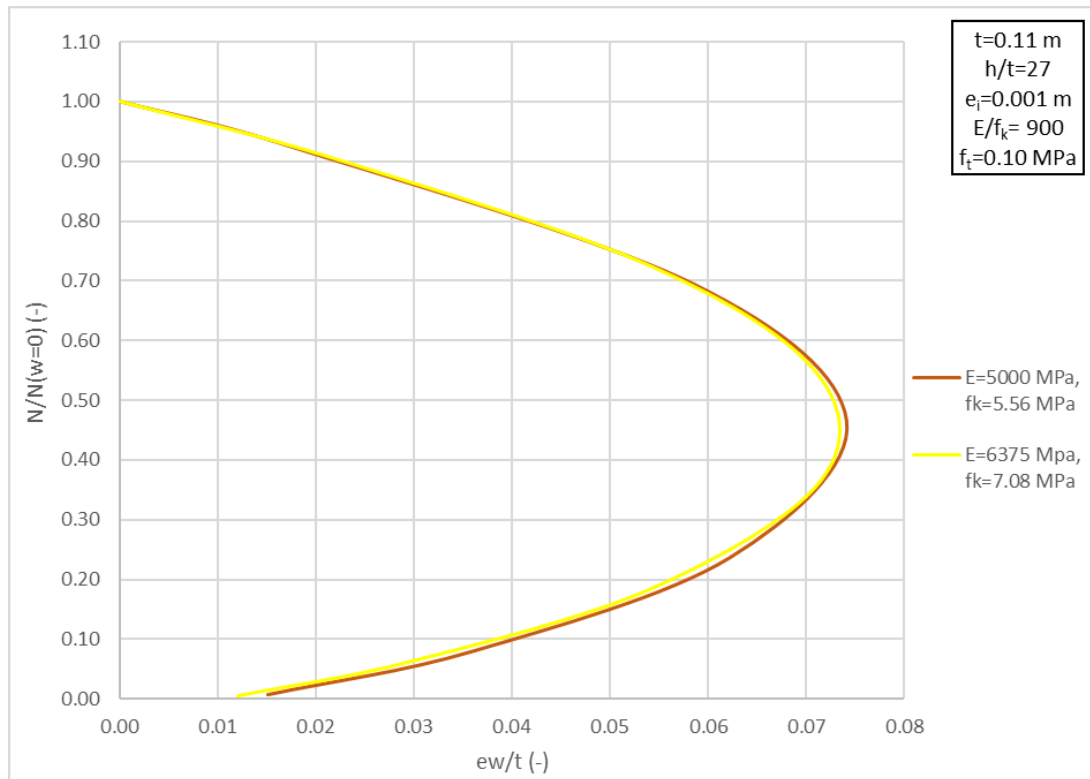
Fig. 129 Reduction factor to the vertical resistance of URM walls, due to wind load –h/t=27 and E/f$_k$=900
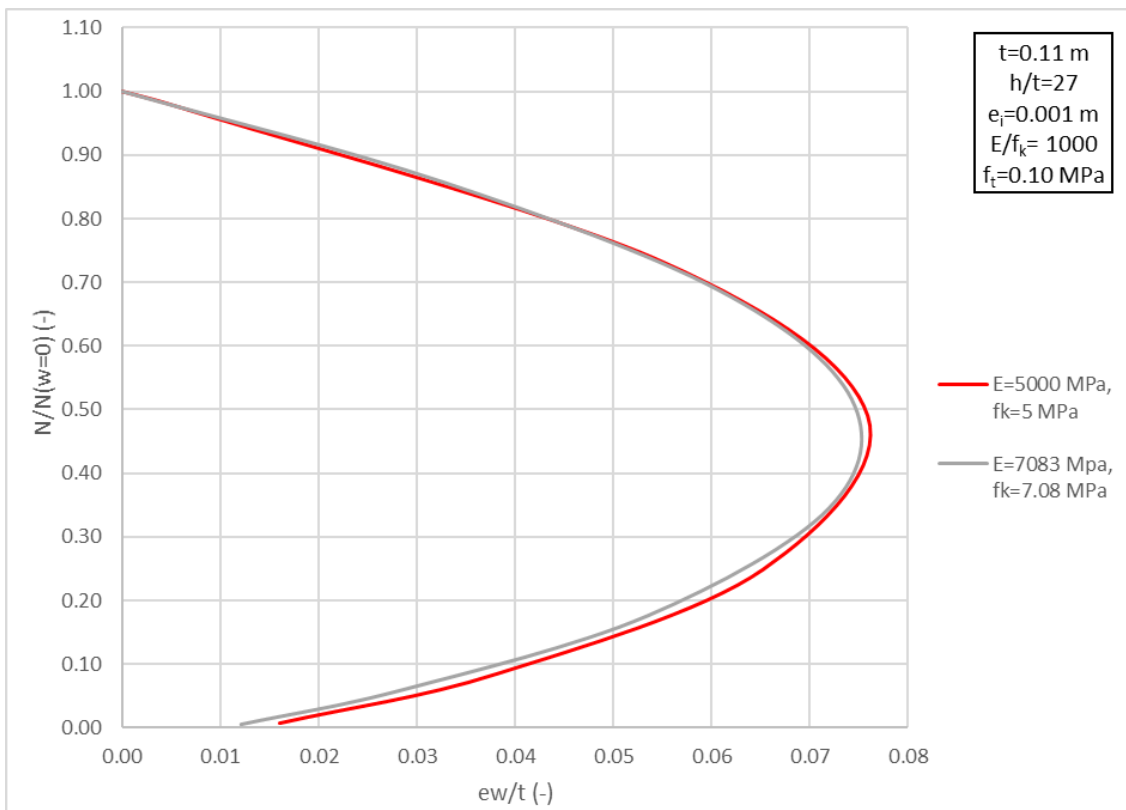
Fig. 130 Reduction factor to the vertical resistance of URM walls, due to wind load – h/t=27 and E/f$_k$=1000
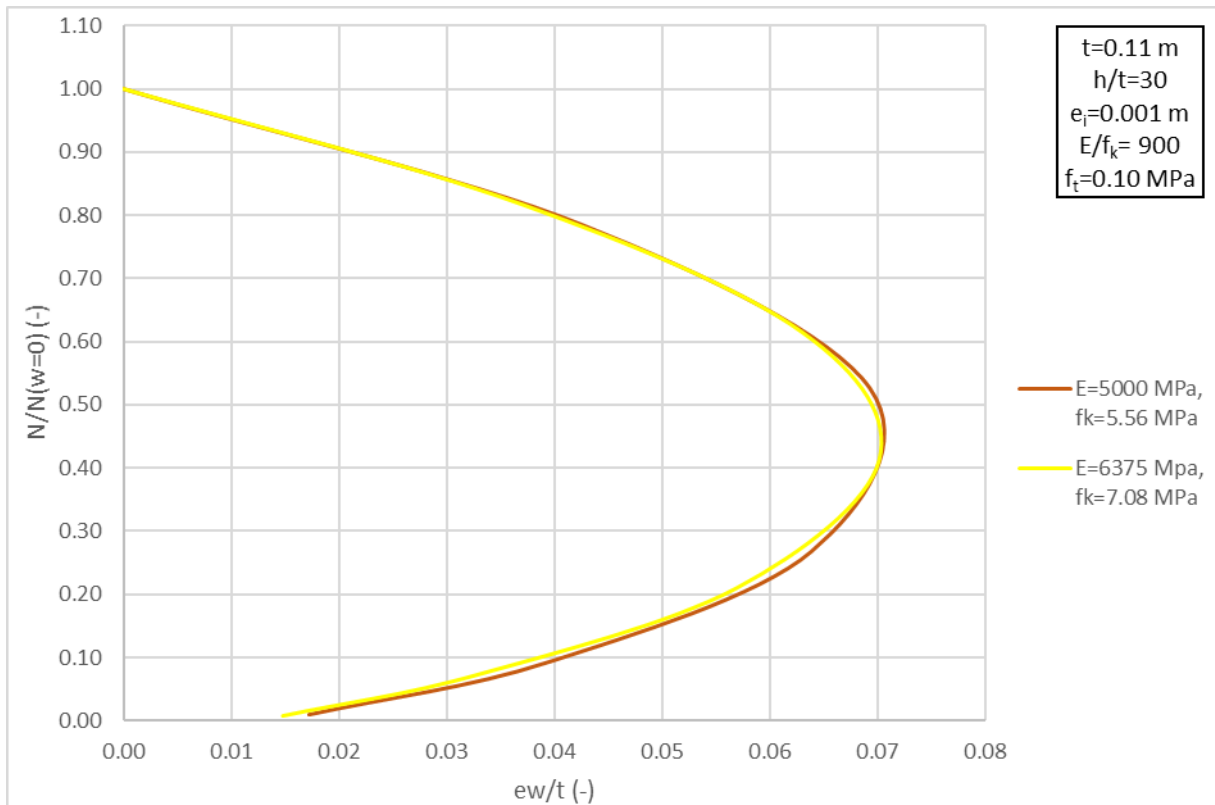
Fig. 131 Reduction factor to the vertical resistance of URM walls, due to wind load –h/t=30 and E/f$_k$=900
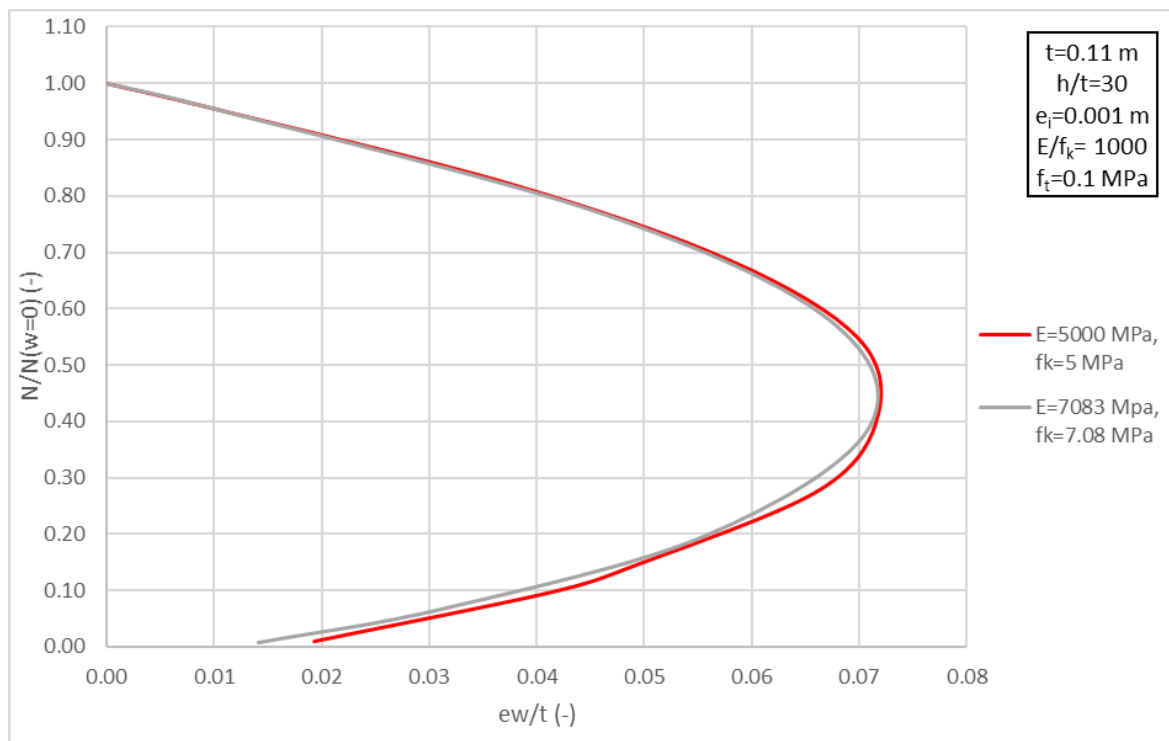
Fig. 132 Reduction factor to the vertical resistance of URM walls, due to wind load –h/t=30 and E/f$_k$=1000
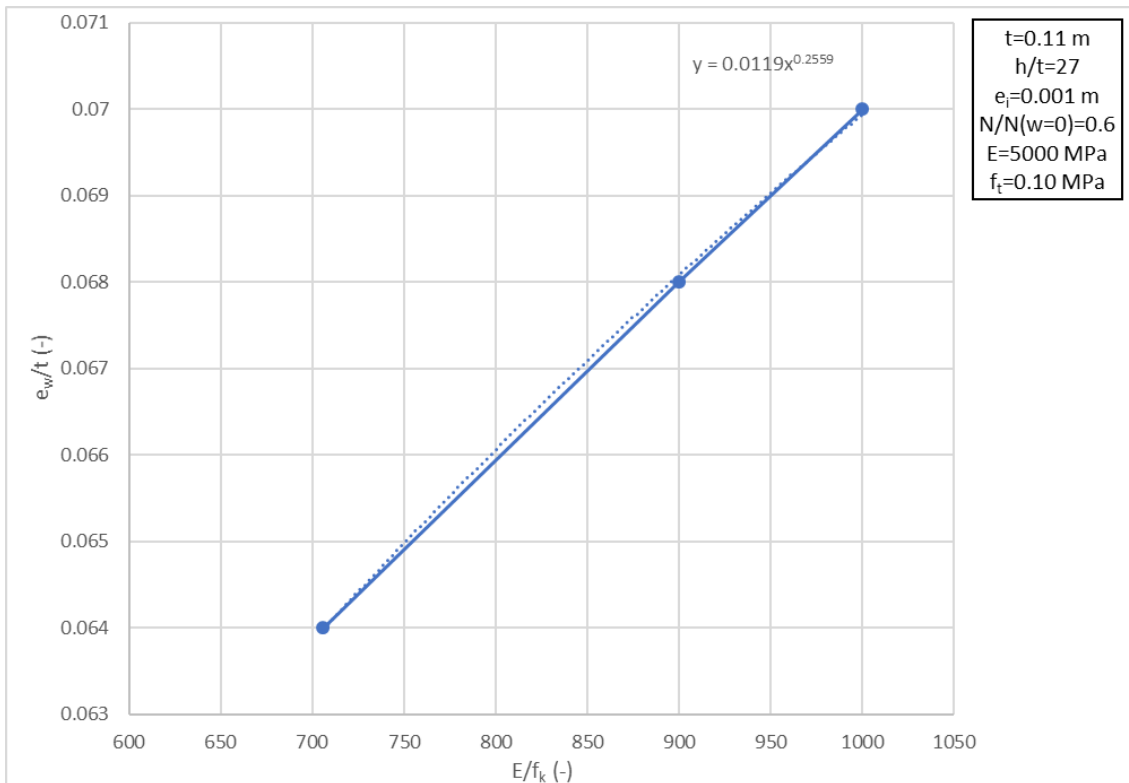
Fig. 133 Relationship between E/f_k and e_w/t of a URM wall for the same N/N(w=0)
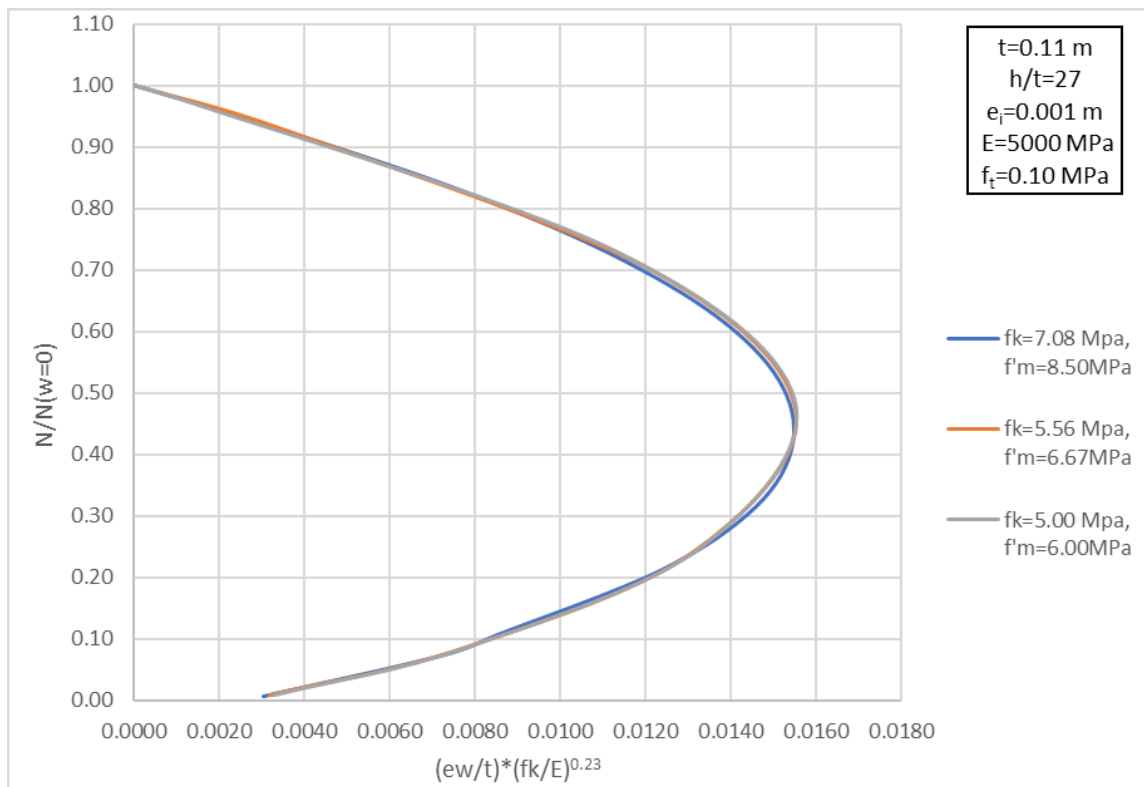
Fig. 134 Reduction factor to the vertical resistance of URM walls, due to wind load, considering the influence of E/f_k – constant values of E, f_t and variable values of f_k - f'_m for h/t=27
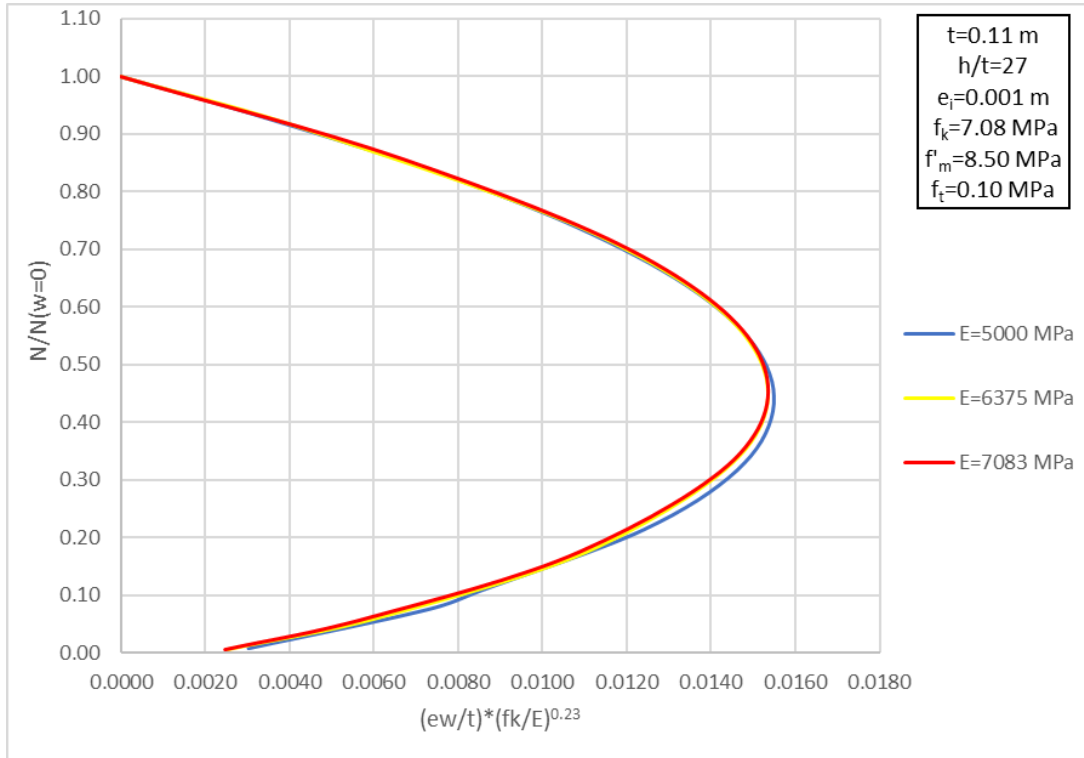
Fig. 135 Reduction factor to the vertical resistance of URM walls, due to wind load, considering the influence of E/f_k – constant values of f_k - f'_m, f_t and variable value of E for h/t=27
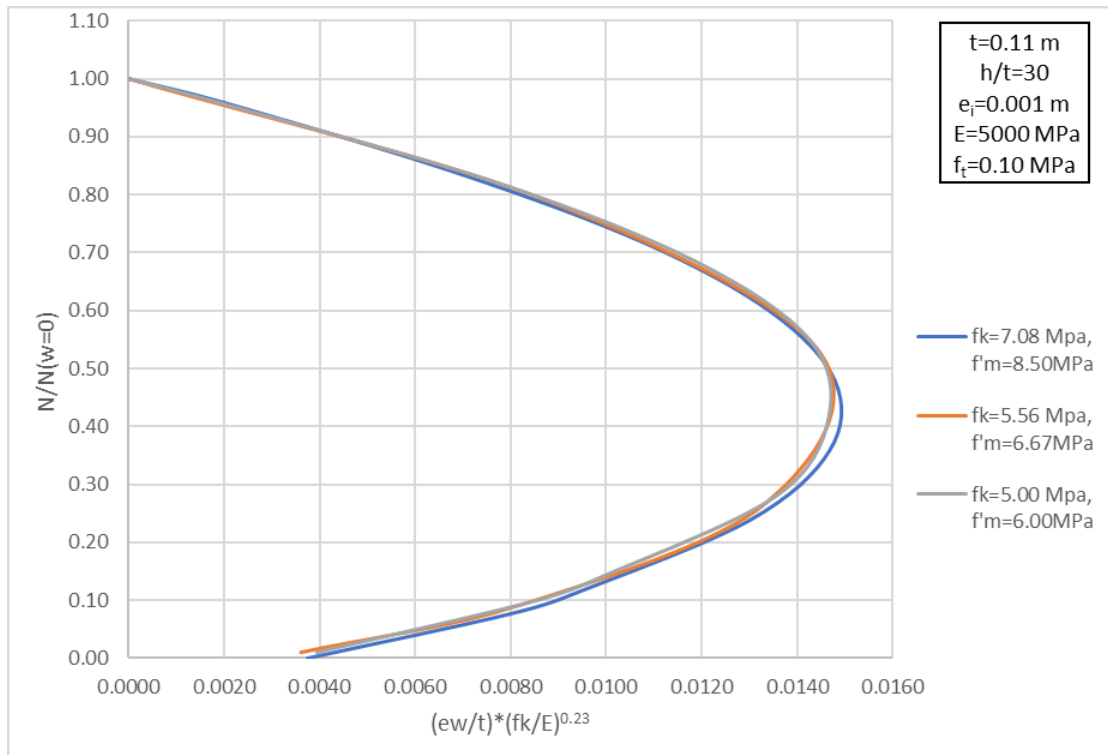
Fig. 136 Reduction factor to the vertical resistance of URM walls, due to wind load, considering the influence of E/f_k – constant values of E, f_t and variable values of f_k - f'_m for h/t=30
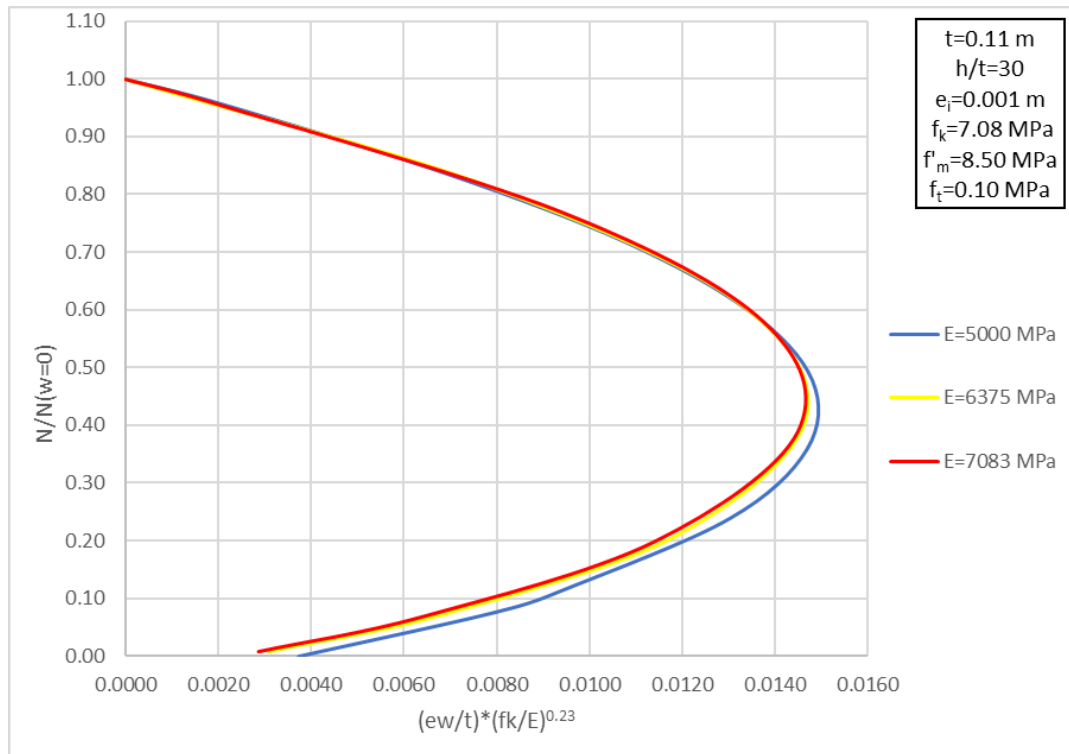
Fig. 137 Reduction factor to the vertical resistance of URM walls, due to wind load, considering the influence of E/f_k – constant values of f_k - f'_m, f_t and variable value of E for h/t=30

9.3.1.3 Influence of Eccentricity at the Top or the Bottom of the URM wall (e_i)

The eccentricity, at the top and the bottom of the studied URM walls (e_i) as well as along the full height, is equal to the initial eccentricity, which allows for construction imperfections. [53] The graph in Fig. 114 shows the different interaction, between the ratios $N/N(w=0)$ and e_w/t, for three different values of e_i. Since the interaction curves do not coincide, the influence of the eccentricity, at the top and the bottom of the URM wall (e_i), needs to be included in the second segment of the formula in Equation 59. The curves in the graph in Fig. 114 show that, increasing the value of the eccentricity (e_i), from 0.001 m to 0.015 m, results in the decrease of the $N/N(w=0)$ ratio, for the same eccentricity ratio (e_w/t), and vice versa. However, increasing the value of the eccentricity (e_i), from 0.015 m to 0.029 m, results in the increase of the $N/N(w=0)$ ratio for the same eccentricity ratio (e_w/t) and vice versa. The latter happens for values of the eccentricity ratio (e_w/t) larger than 0.03.

The stress state of the URM wall, described by each curve in the graph in Fig. 114, at relevant combinations of applied vertical load - wind load, will provide useful information about the response of the wall. It is noticed that the maximum deviation, between the interaction curves, occurs at the maximum value of wind load. Therefore, the ratio $N/N(w=0)$ is determined, where, approximately, the maximum value of the eccentricity ratio (e_w/t) occurs, for all the interaction curves in the graph in Fig. 114. This value of the ratio $N/N(w=0)$ is equal to 0.36. A value for the vertical load N is derived from the ratio $N/N(w=0)$ for every curve. Given this vertical load, the maximum wind load, that each wall can withstand, is estimated after a non-linear FE analysis, similar to the one described in section 9.1.4. The curves, with the relationship between the eccentricity ratio (e_w/t) and the horizontal displacement, at the mid-height, that show the evolution of the non-linear FE analysis, for the URM walls, described by the curves in the graph in Fig. 114, are shown in Appendix E. Accordingly, for every FE analysis, graphs can be drawn, with the evolution of stresses and strains, in the direction normal to

the bed joints, on the most tensioned and compressed side of the wall. Stresses and strains, on the most tensioned and most compressed side of the wall, are estimated at the highlighted finite elements in Fig. 82 and Fig. 83, respectively. The evolution of stresses and strains on the URM walls, described by the curves in the graph in Fig. 114, are shown in the graphs in Fig. 138 - Fig. 143. For the same *N/N(w=0)* ratio, the combination of vertical load – wind load, that leads the URM wall to failure, occurs at a lower compressive stress, as the eccentricity (e_i) increases. A lower compressive stress at the failure means a larger stiffness of the URM wall.

Another combination of applied vertical load - wind load, that is interesting to know the stress state of the URM walls, is when the wind load is zero and the vertical load is equal to *N(w=0)*. The graphs, in Fig. 144 - Fig. 147, show the evolution of stresses and strains, in the direction normal to the bed joints, on the most tensioned and compressed side of the wall. These graphs are the results, from the FE analysis, on URM walls, with values of eccentricity (e_i) equal to *0.015 m* and *0.029 m*. The scope of the analysis was the determination of the maximum vertical load on the wall, when zero wind load is applied, as it has, already, been discussed in section 9.2. Stresses and strains, on the most tensioned and most compressed side of the wall, are estimated at the highlighted finite elements in Fig. 82 and Fig. 83, respectively. The respective graphs for the URM wall, with eccentricity (e_i) equal to *0.001 m*, are shown in Appendix E (Fig. E. 6, Fig. E. 7). The level of the maximum compressive stress on the URM wall, when the maximum vertical load (*N(w=0)*) is applied, gets lower as the eccentricity (e_i) increases. A lower compressive stress at the failure means a larger stiffness of the URM wall. Additionally, it seems that, for zero wind load, the URM wall with eccentricity (e_i) equal to 0.001 m is uncracked, when the maximum vertical load is applied. On the contrary, cracks have already initiated at the URM walls, with values of eccentricity (e_i) equal to 0.015 m and 0.029 m, at the point of maximum vertical load (*N(w=0)*).

The increase of the eccentricity (e_i) from 0.001 m to 0.015 m has a different impact on the curve, with the combinations of vertical load and the wind load, that lead the URM wall to failure, compared to the respective impact, from the increase of the eccentricity (e_i) from 0.015 m to 0.029 m. This might be explained by the fact that, at the point of maximum vertical load *N(w=0)*, when zero wind load is applied, the URM wall, with eccentricity (e_i) equal to 0.001 m, is uncracked whereas the URM walls, with values of eccentricity (e_i) equal to 0.015 m and 0.029 m, have, already, been cracked. Therefore, it does not seem possible that, including a relevant expression for the eccentricity (e_i), in the second segment of the formula in Equation 59, it can cover a range of values of eccentricity (e_i) from 0.001 m to 0.029 m. As it has, already, been mentioned the eccentricity at the top and the bottom of the wall (e_i) is equal to the initial eccentricity (e_{init}), which allows for construction imperfections and is assumed for the full height of the wall. [53] The studied URM walls are simply supported, at the top and the bottom side, and the loads from the floors are applied in the center of the wall section. The EN 1996 norm suggests that the initial eccentricity is assumed equal to $h_{ef}/450$. For the URM walls, described by the curves in the graph in Fig. 114, this is, approximately, equal to $e_i=0.007\ m$. Alternatively, it is proposed, by the Dutch national annex to the EN 1996 norm, to consider a first-order eccentricity, which is constant over the height of the wall and has a value equal to the maximum of *0.010 m* or $h_{ef}/300$. For the URM walls, described by the curves in the graph in Fig. 114, this is equal to $e_i=0.010$ *m*. Hence, values of eccentricity (e_i) between 0.001 m and 0.015 m are relevant for the context of the thesis. Within this range of values of eccentricity (e_i), it is attempted to find an appropriate expression, for the influence of the eccentricity (e_i), in the second segment of the formula in Equation 59. In Equation 54, the eccentricity ratio (e_w/t) is divided by the expression $1 - 0.577 \frac{e_i}{r}$. Replacing the radius of gyration, according to Equation 62, the expression becomes $1 - 2 \frac{e_i}{t}$. Trying different values for the constant factor, which is equal to *2*, in the latter expression, the value of *2.10* seems to be the most appropriate, regarding the curves in the graph in Fig. 114. This is shown in the graph in Fig. 148. The

curves for different values of eccentricity (e_i) show close proximity within the compression region, which will be described by the formula in Equation 59, as it has, already been discussed in section 9.3.

As it has been mentioned in section 9.2, the three values of eccentricity (e_i) (0.001, 0.015, 0.029 m) have been defined in such a way, that plane strain FE models with the same size of finite elements are created. It has been verified that the size of the finite elements does not affect the results of the FE analysis (Appendix C). Therefore, a URM wall, with the properties of the walls, described by the curves in the graph in Fig. 114, and a value of eccentricity (e_i) equal to 0.010 m, is analyzed with the FE method (see section 9.1.4). The value of 0.010 m for the eccentricity (e_i) is the one suggested by the Dutch national annex to the EN 1996 norm. The created model consists of plane strain elements with size *0.009 x 0.009 m²* (see Table 12). Fig. 149 shows the results of the FE analyses. The interaction curve in the graph in Fig. 149 is inserted in the graph in Fig. 104 and the updated graph is shown in Fig. 150. Replacing the vertical load (N), at the mid-height, with the ratio *N/N(w=0)*, on the vertical axis, and the wind load (w) with the eccentricity ratio (e_w/t), on the horizontal axis, results in the graph in Fig. 151. Further, the graph, in Fig. 152, is derived by dividing the eccentricity ratio (e_w/t) with the expression $1 - 2.10 \frac{e_i}{t}$. The curves, for values of eccentricity *e_i=0.001 m* and *e_i=0.010 m*, seem to match, within the compression region, while the curve, for *e_i=0.015 m*, shows close proximity to the other two curves in the graph, in Fig. 152. For large values of the eccentricity ratio (e_w/t), only, the interaction curve for eccentricity *e_i=0.015 m* deviates. Attention will be paid when defining the final form of the formula in Equation 59, so that it describes conservatively the interaction, between the vertical resistance, of the slender existing URM wall, and the applied wind load, for every value of eccentricity (e_i), compared to the respective FE analysis results.
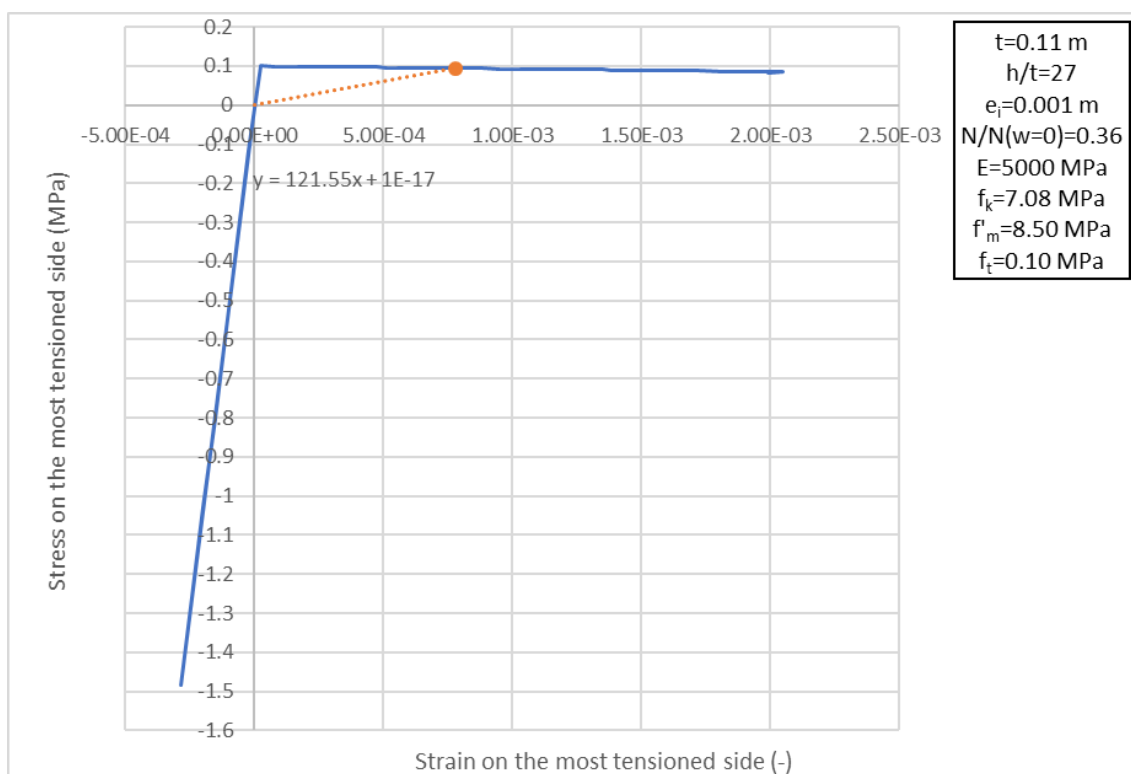
Fig. 138 Stress-Strain Evolution at the most tensioned side of the URM wall with e_i=0.001m – the dot represents the stress-strain state at the highlighted point on the respective curve in the graph in Fig. E. 20
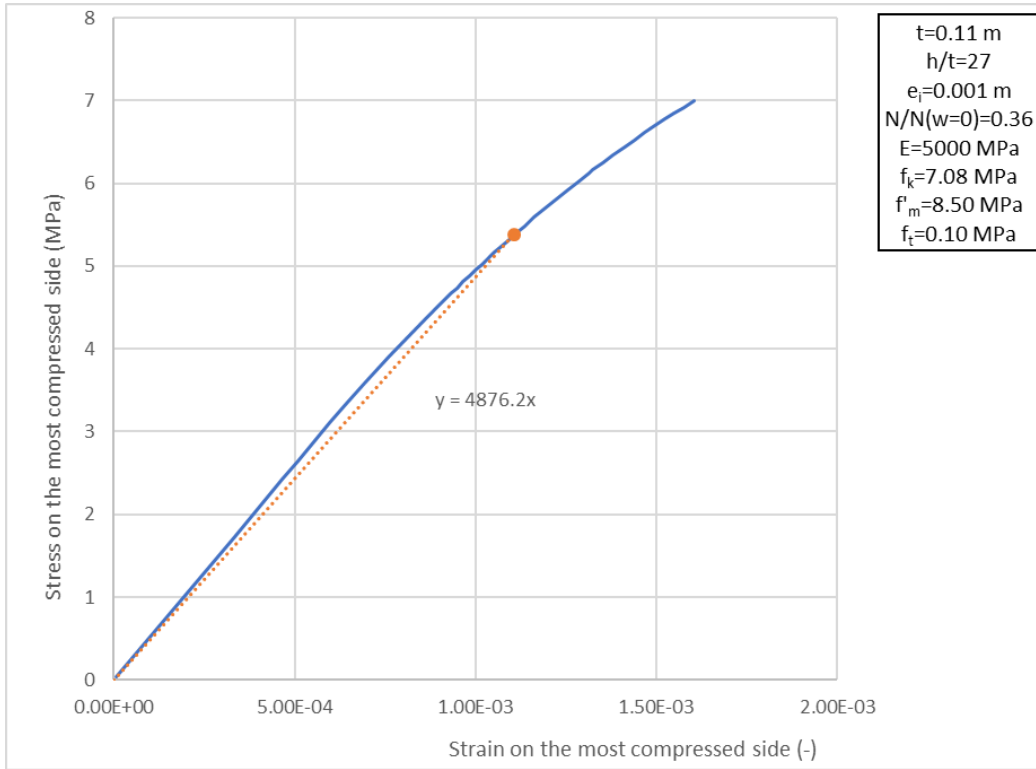
Fig. 139 Stress-Strain Evolution at the most compressed side of the URM wall with e_i=0.001m – the dot represents the stress-strain state at the highlighted point on the respective curve in the graph in Fig. E. 20
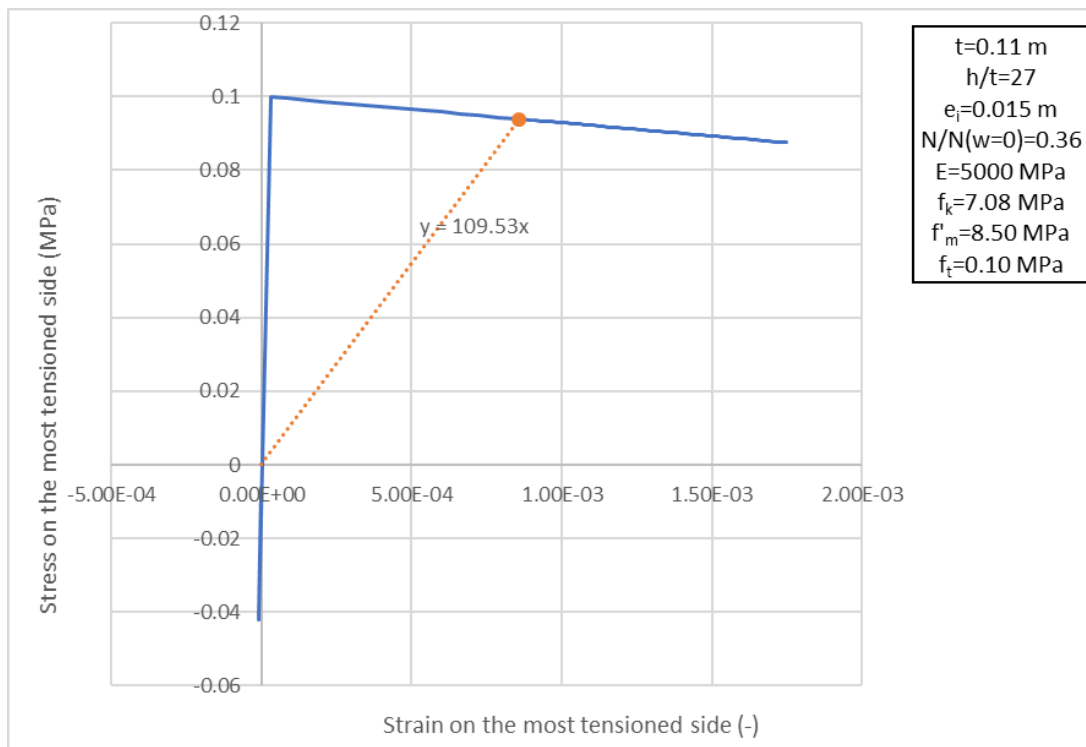
Fig. 140 Stress-Strain Evolution at the most tensioned side of the URM wall with e_i=0.015m – the dot represents the stress-strain state at the highlighted point on the respective curve in the graph in Fig. E. 20
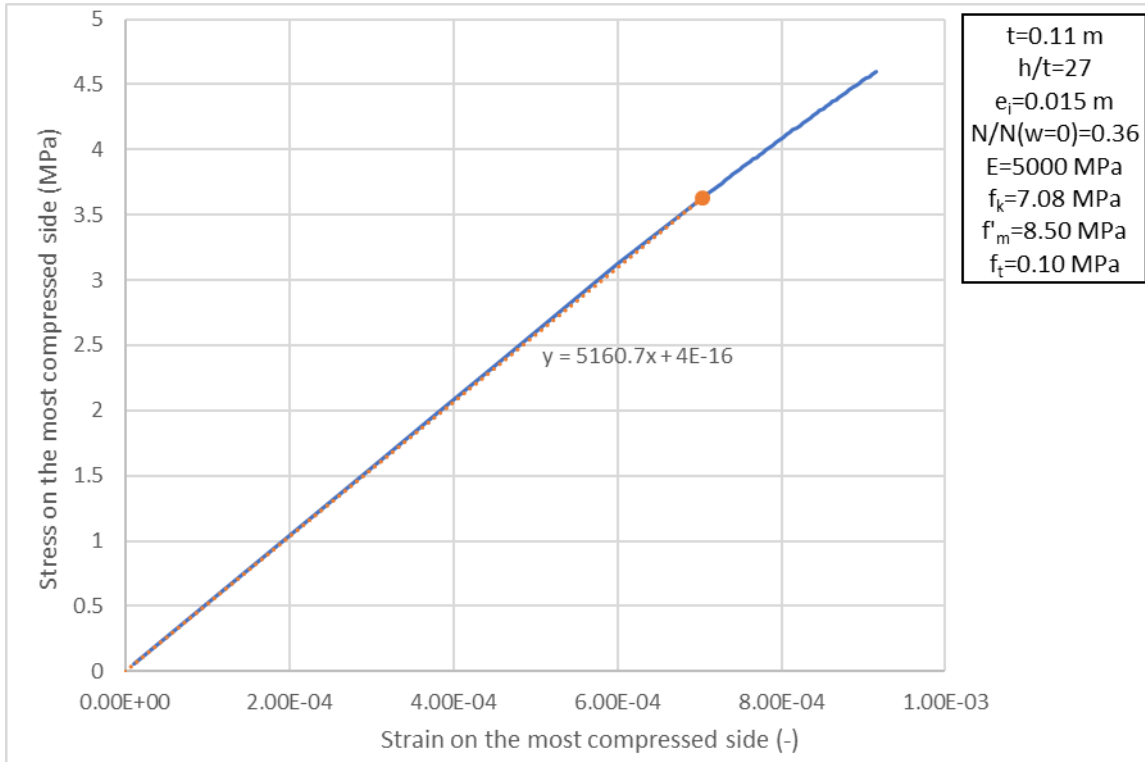
Fig. 141 Stress-Strain Evolution at the most compressed side of the URM wall with e_i=0.015m – the dot represents the stress-strain state at the highlighted point on the respective curve in the graph in Fig. E. 20
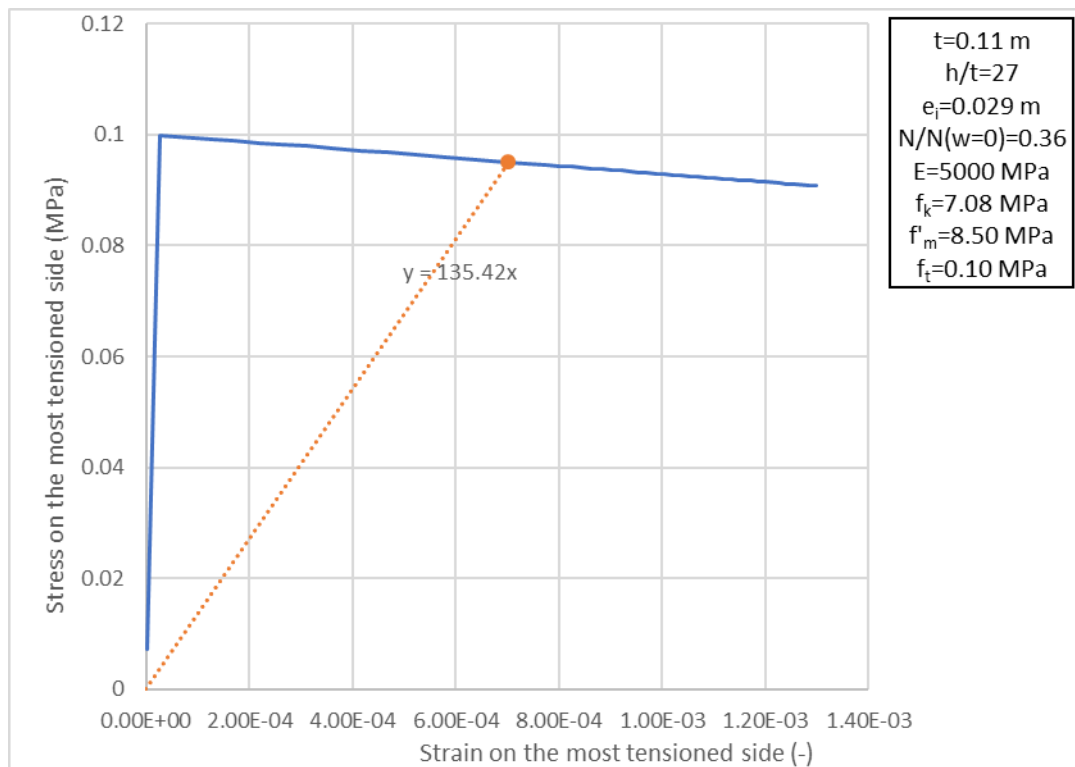
Fig. 142 Stress-Strain Evolution at the most tensioned side of the URM wall with e_i=0.029m – the dot represents the stress-strain state at the highlighted point on the respective curve in the graph in Fig. E. 20
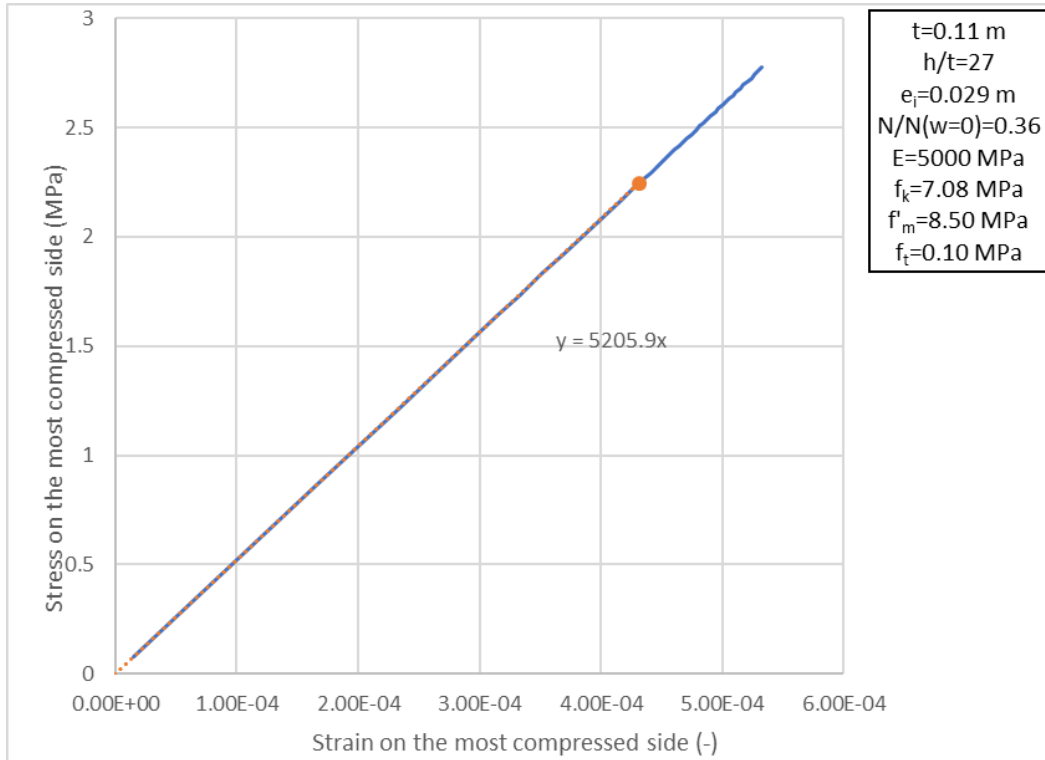
Fig. 143 Stress-Strain Evolution at the most compressed side of the URM wall with e_i=0.029m – the dot represents the stress-strain state at the highlighted point on the respective curve in the graph in Fig. E. 20
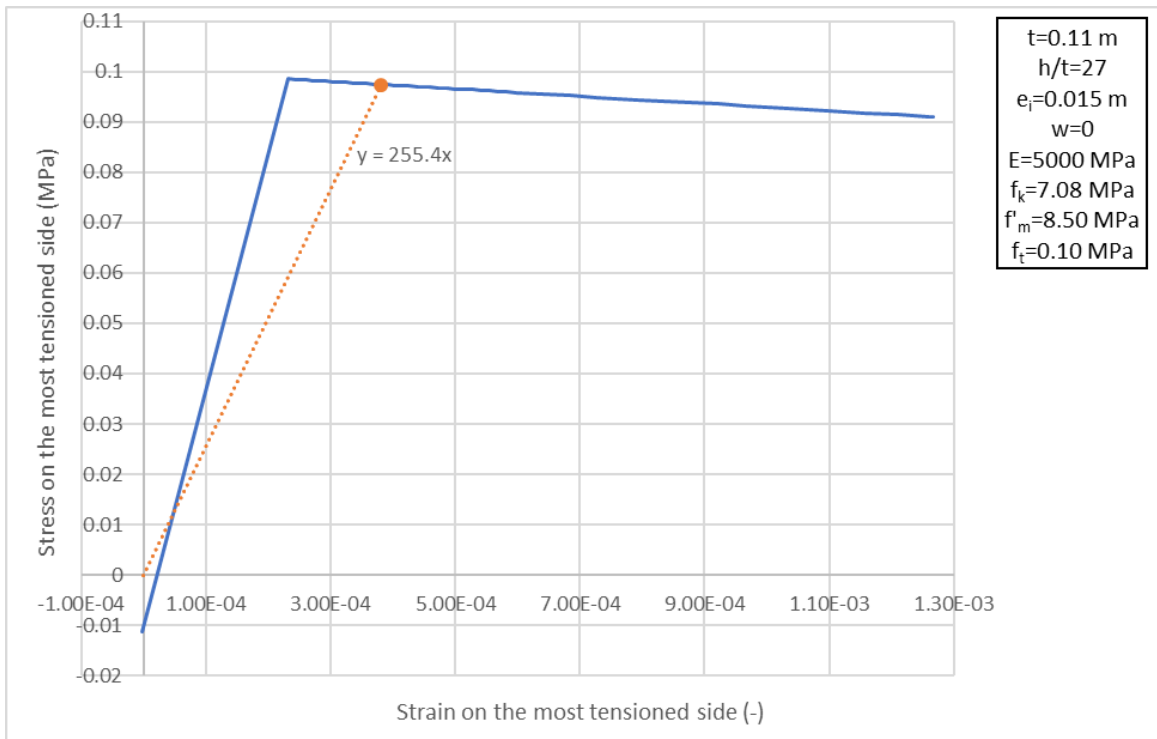
Fig. 144 Stress-Strain Evolution at the most tensioned side of the URM wall with e_i=0.015m – the dot represents the stress-strain state, when the maximum vertical load N(w=0) is attained
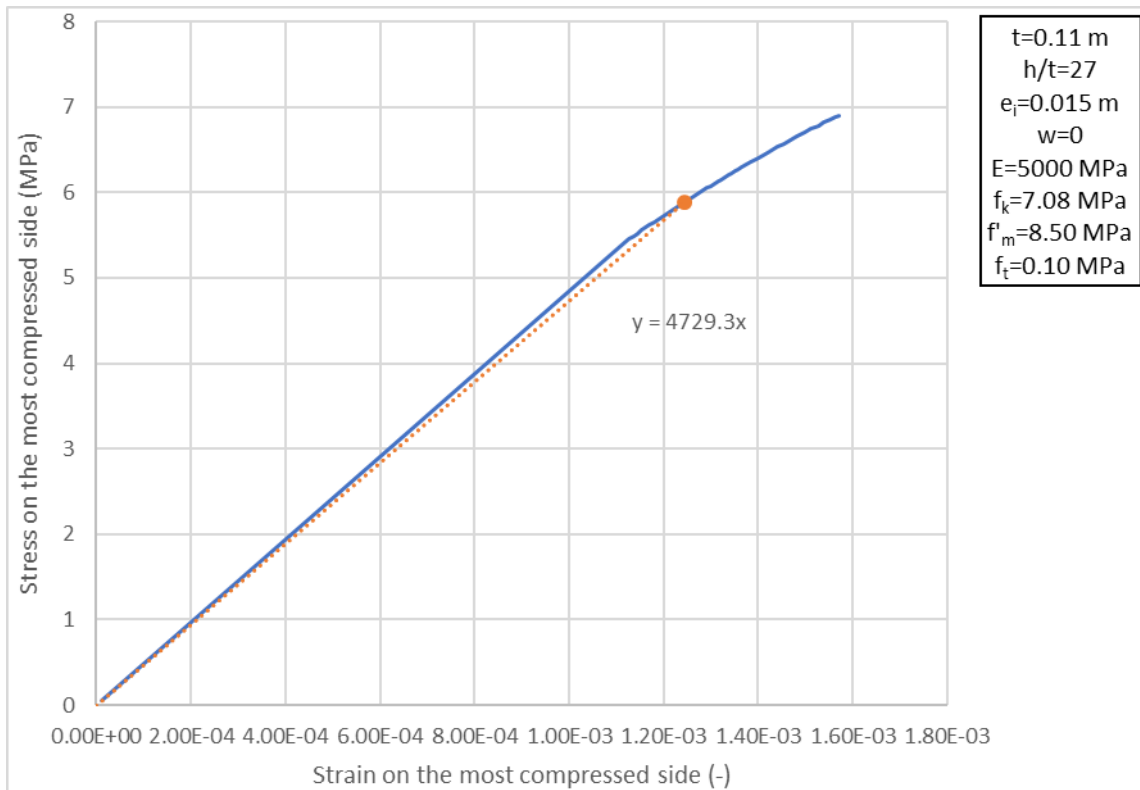
Fig. 145 Stress-Strain Evolution at the most compressed side of the URM with e_i=0.015m – the dot represents the stress-strain state, when the maximum vertical load N(w=0) is attained
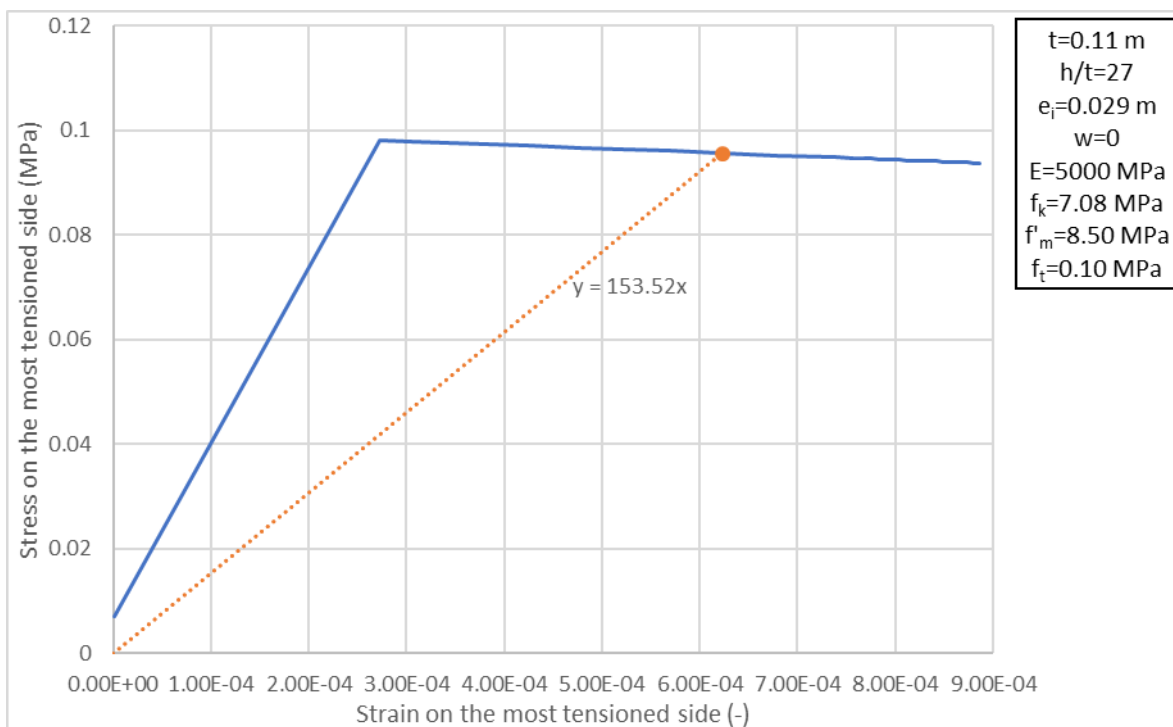
Fig. 146 Stress-Strain Evolution at the most tensioned side of the URM wall with e_i=0.029m – the dot represents the stress-strain state, when the maximum vertical load N(w=0) is attained
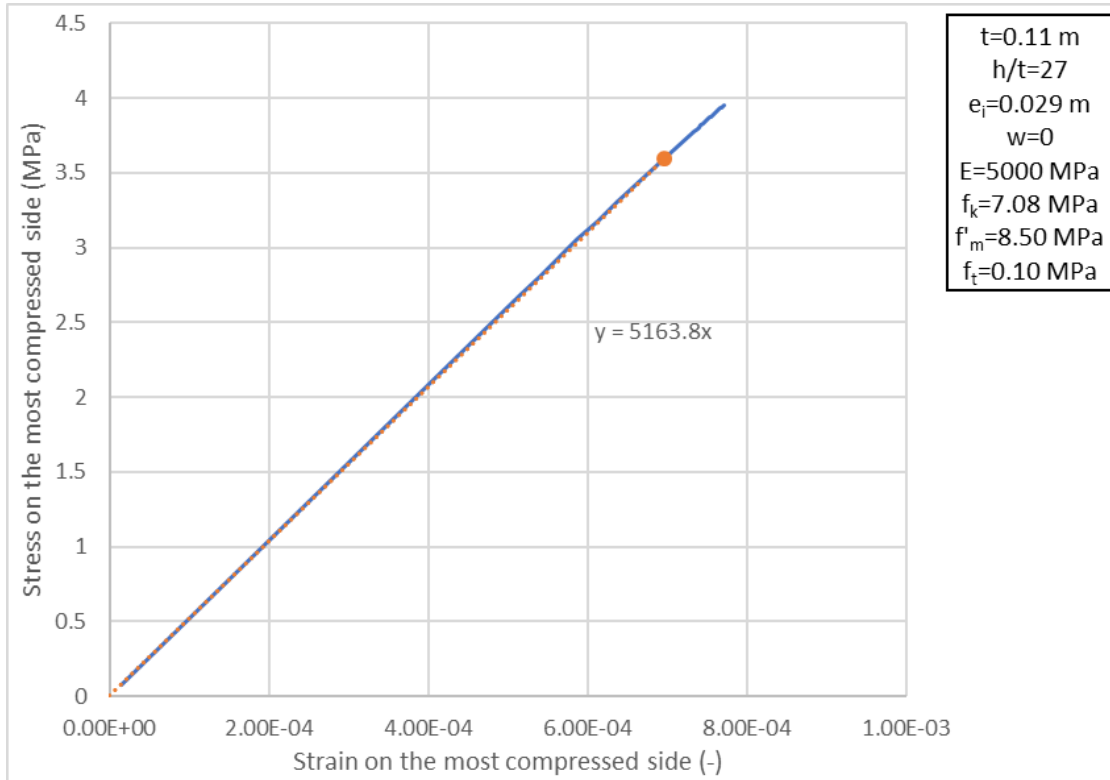
Fig. 147 Stress-Strain Evolution at the most compressed side of the URM with e_i=0.029m – the dot represents the stress-strain state, when the maximum vertical load N(w=0) is attained
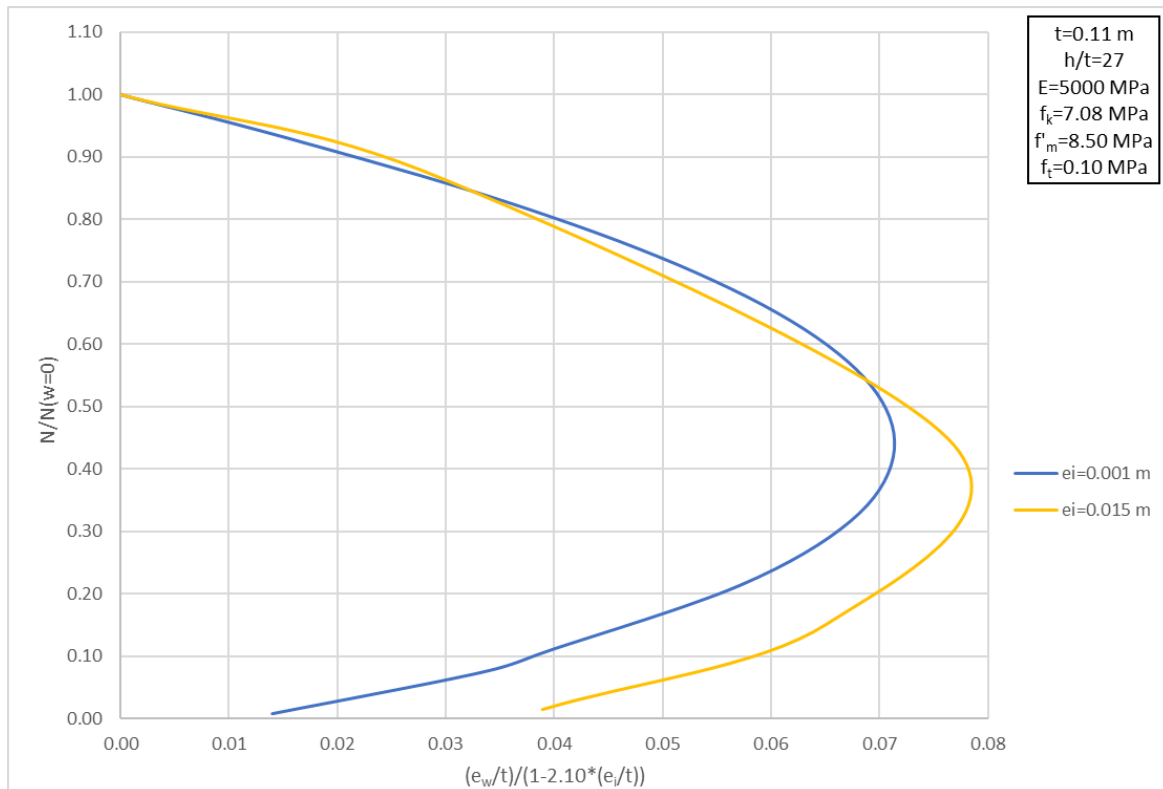
Fig. 148 Reduction factor to the vertical resistance of URM walls, due to wind load, considering the influence of e_i, for values of e_i between 0.001 m and 0.015 m
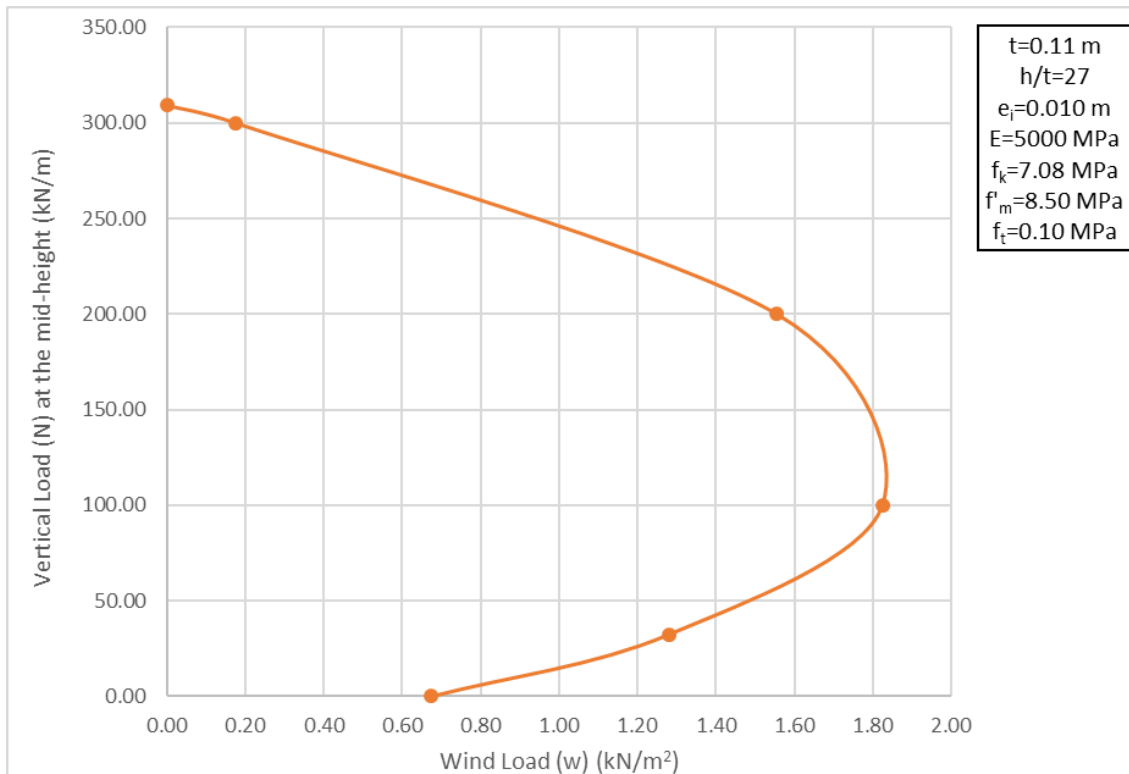
Fig. 149 Combinations of Vertical Load and Wind Load that lead the URM wall with eccentricity e_i=0.010 m to failure
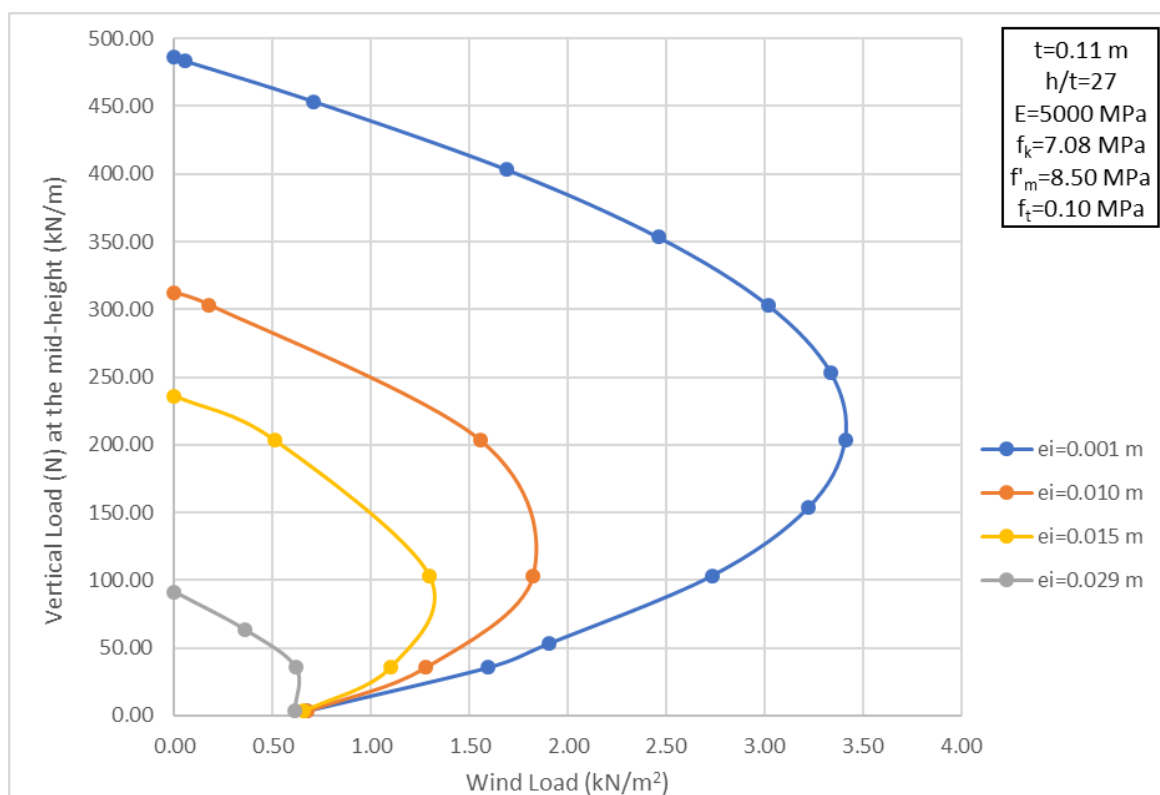
Fig. 150 Influence of eccentricity at the top or bottom of the wall on the interaction between wind load and vertical resistance of a URM wall (includes e_i=0.010 m)
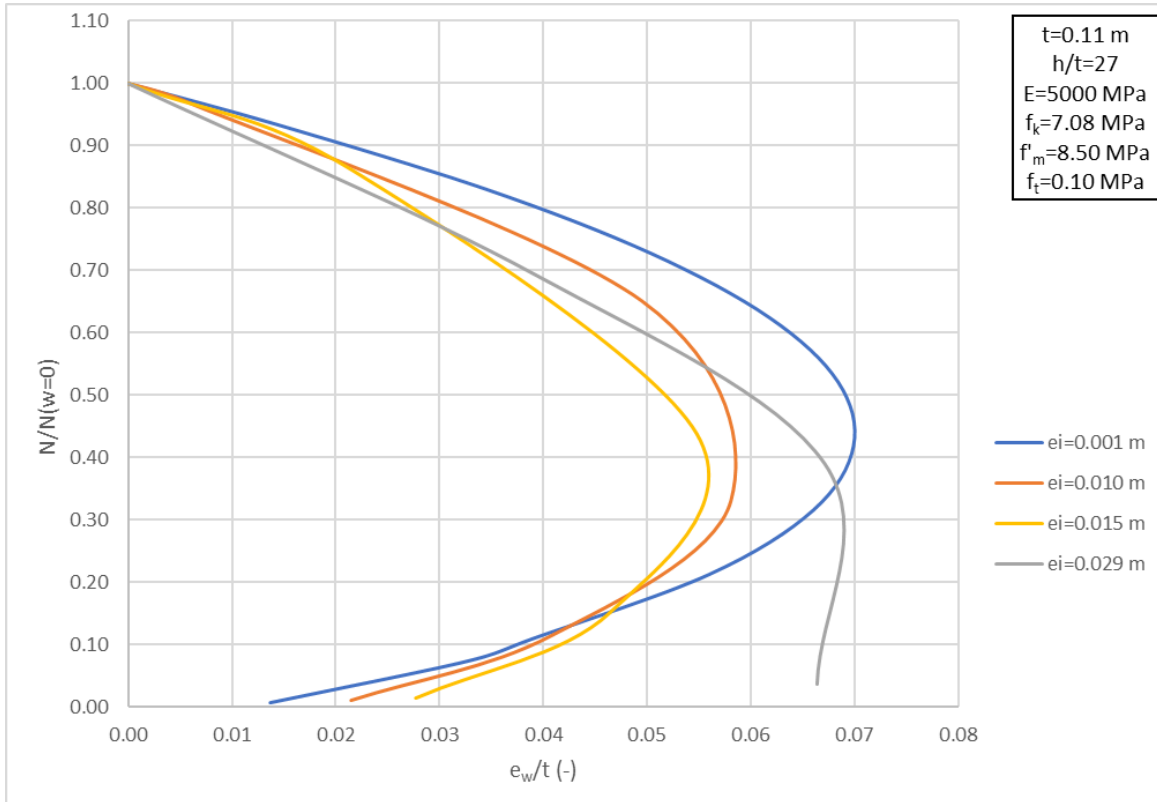
Fig. 151 Reduction factor to the vertical resistance of URM walls, due to wind load, for different values of eccentricity at the top or bottom of the wall (includes e_i=0.010 m)
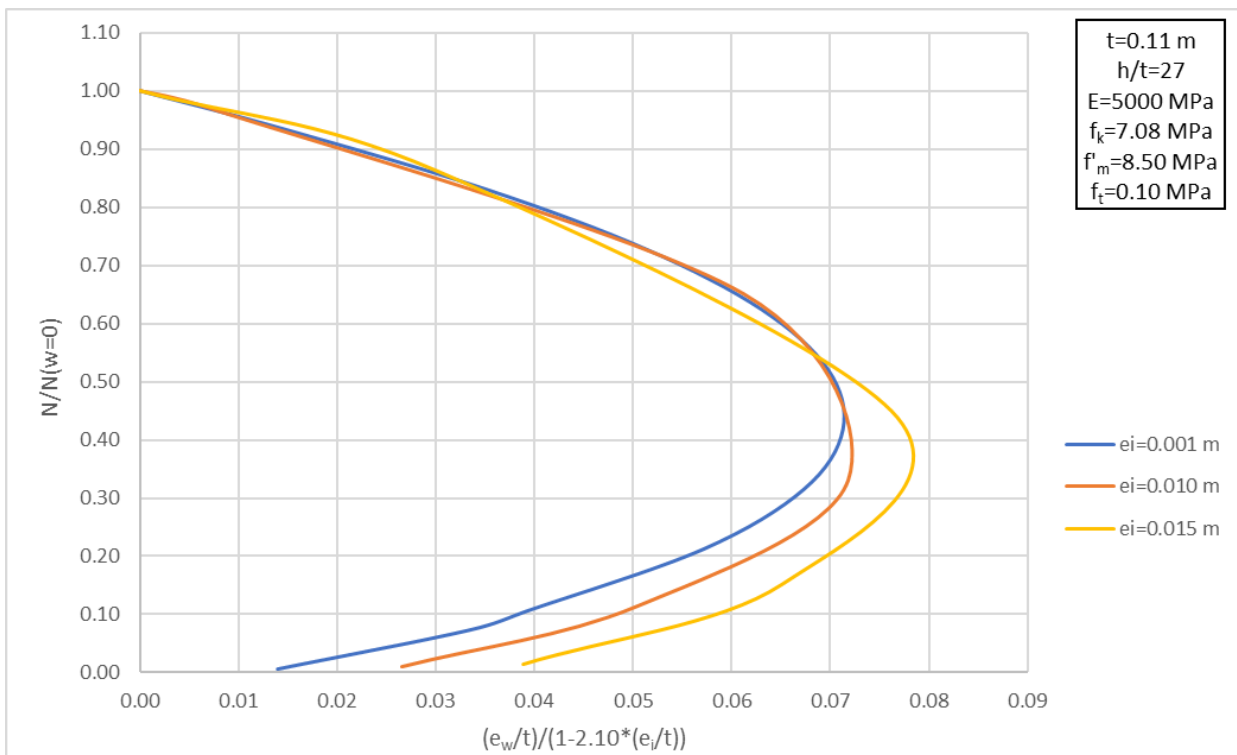
Fig. 152 Reduction factor to the vertical resistance of URM walls, due to wind load, considering the influence of e_i, for values of e_i between 0.001 m and 0.015 m (includes e_i=0.010 m)

9.3.1.4 Influence of Tensile Strength (f_t)

The graphs in Fig. 111 - Fig. 113 show the influence of halving the tensile strength of masonry, on the reduction to the vertical resistance, due to wind load, for different values of slenderness ratio (h/t). For values of slenderness ratio $h/t=27$ and $h/t=30$, the curves, for different values of tensile strength of masonry, seem to match within the compression region. The compression region will be described by the formula in Equation 59, as it has, already been discussed in section 9.3. Only for large values of the eccentricity ratio (e_w/t), the curves deviate. The deviation between the respective curves starts for smaller values of the eccentricity ratio (e_w/t), in the case of slenderness ratio $h/t=39$.

The graphs in Fig. 115 - Fig. 117 show the influence of halving the tensile strength of masonry, on the reduction to the vertical resistance, due to wind load, for different values of eccentricity, at the top or the bottom of the URM wall (e_i). For the value of eccentricity $e_i=0.001\ m$ the curves seem to match within the compression region, which will be described by the formula in Equation 59. Only for large values of the eccentricity ratio (e_w/t), the curves deviate. The deviation, between the respective curves, starts for smaller values of the eccentricity ratio (e_w/t) and gets larger in magnitude, as the eccentricity (e_i) increases ($e_i=0.015\ m$, $e_i=0.029\ m$).

For the value of slenderness ratio $h/t=39$ and the values of eccentricity, at the top or the bottom of the wall, $e_i=0.015\ m$ and $e_i=0.029\ m$, it is noticed that, the value of the tensile strength of masonry (f_t) affects the compression region of the curves, with the interaction between the ratios $N/N(w=0)$ and e_w/t. The interaction curve, that refers to the URM wall, with value of slenderness ratio equal to 39, deviates from the rest of the curves in the graph in Fig. 128, for large values of the eccentricity ratio (e_w/t). Therefore, it was mentioned, in section 9.3.1.1, that the final form of the formula, in Equation 59, will be developed in such a way that, it describes conservatively the interaction between the vertical resistance, of the existing URM wall, and the applied wind load, for every value of slenderness ratio (h/t), compared to the respective FE analysis results. The expression for the influence of the eccentricity, at the top or the bottom of the wall (e_i), in the second segment of the formula in Equation 59, is valid for values of eccentricity (e_i) between 0.001 m and 0.015 m (section 9.3.1.3). Additionally, the curve for $e_i=0.015\ m$ shows close proximity with the other two curves, in the graph in Fig. 152,. but deviates for large values of the eccentricity ratio (e_w/t). To deal with this deviation, attention will be paid, again, when developing the final form of the formula in Equation 59. The formula should describe conservatively the interaction between the vertical resistance, of the slender existing URM wall, and the applied wind load, for every value of eccentricity, at the top or the bottom of the wall (e_i), compared to the respective FE analysis results. Taking the aforementioned remarks into consideration, the influence of the tensile strength will not be introduced in the second segment of the formula, in Equation 59. The curves in the graphs in Fig. 103 and Fig. 105, for $f_t=0.05\ MPa$, will be compared with the respective curves of the final form of the formula in Equation 59. An appropriate formula should result in more conservative curves, compared to the respective curves for $f_t=0.05\ MPa$.

9.3.2   Vertical Resistance of Existing Slender URM Walls subjected to Vertical Loading

It has already been mentioned, that, the influence of the wind load is considered in the second segment '$\left(b + c\ \sqrt{d - f\ \frac{e_w}{t}}\right)$' of the formula in Equation 59, as an additional reduction factor to the vertical resistance of an existing slender URM wall, subjected to vertical loading, only. The vertical resistance of a URM wall, subjected to vertical loading, only, is, thus, calculated by the first segment '$\alpha\ N_{Rd}(w = 0)$', of the formula in Equation 59. The impact of the material properties, the geometry of the wall and the eccentricity, at the top or bottom, are taken into consideration. As, already, discussed in

Schultz [36] defined Equation 51, assuming that masonry is a linear – elastic material with zero tensile strength. Equation 63 is an alternative expression for Equation 51 (section 9.3). The capacity reduction factor, at the mid-height of slender URM walls (second expression in Equation 39), was derived, assuming that the equivalent modulus of elasticity, of the non-linear material model, is equal to the short-term secant modulus of elasticity, of the linear material model. The influence of the tensile strength of masonry is neglected in this case, too. [19] Equation 61 makes use of the aforementioned capacity reduction factor. Hence, both expressions, in Equation 61 and Equation 63, do not consider the non-linearity as well as the tensile strength of masonry. Therefore, the only material property, that is included in the expressions, is the modulus of elasticity. This parameter is crucial for the stability failure, that is relevant to slender URM walls. [19] Equation 63 makes use of the short-term secant modulus of elasticity, while Equation 61 introduces the initial characteristic modulus of elasticity. The initial characteristic modulus of elasticity is equal to the short-term secant modulus of elasticity (Equation 43) The material model, that was used as input for the FE model (Table 2), describes the actual behavior of masonry. Thus, except for the short-term secant modulus of elasticity (E), the FE analysis results provide the influence of the rest of the material properties, on the vertical resistance of URM walls, subjected to vertical loading, only. Namely, the characteristic compressive strength (f_k) and the tensile strength (f_t) of masonry. The influence of each material property will define whether and how it will be introduced, in the first segment of the formula in Equation 59.

Expressions with the geometrical properties of the wall, namely the height (h) and the thickness (t), as well as the eccentricity (e_i), at the top or the bottom, are included in Equation 61 and Equation 63. These expressions depend on the influence, of the respective parameter, on the vertical resistance of URM walls. It will be assessed whether the influence of each parameter (h, t, e_i) on the vertical resistance, that is specified by Equation 61 and Equation 63, matches with the respective results from the FE analysis. In case it is necessary, the expressions for the aforementioned parameters will be adjusted and introduced in the first segment of the formula in Equation 59.

9.3.2.1 Influence of Slenderness Ratio (h/t)

The values of the vertical resistance of existing URM walls, with different values of slenderness ratio (h/t), when zero wind load is applied, can be obtained from the graph in Fig. 100. An expression for the influence of the slenderness ratio, in the second segment of the formula in Equation 59, has been defined in section 9.3.1.1. This expression is valid for values of slenderness ratio between 27 and 39. The first segment of the formula in Equation 59 will be, also, relevant to the same range of values of slenderness ratio.

The dependence of the value of *N(w=0)* on the slenderness ratio (h/t) is shown in the graph in Fig. 153. *N(w=0)* is the vertical resistance of the URM wall, when zero wind load is applied. It seems that the vertical resistance *N(w=0)* is an expression of the slenderness ratio (h/t), raised to a negative power, which is approximately equal to *-1.48*. This means that the inverse ratio (*t/h*) can be introduced in the first segment of the formula in Equation 59, raised to a power, approximately, equal to *1.48*. Trying different values for the power, the value of *1.46* seems to be the most appropriate. Dividing the values of the vertical resistance *N(w=0)*, for different values of slenderness ratio, from the graph in Fig. 100, with the expression $(\frac{t}{h})^{1.46}$, results in the best proximity among the quotients.
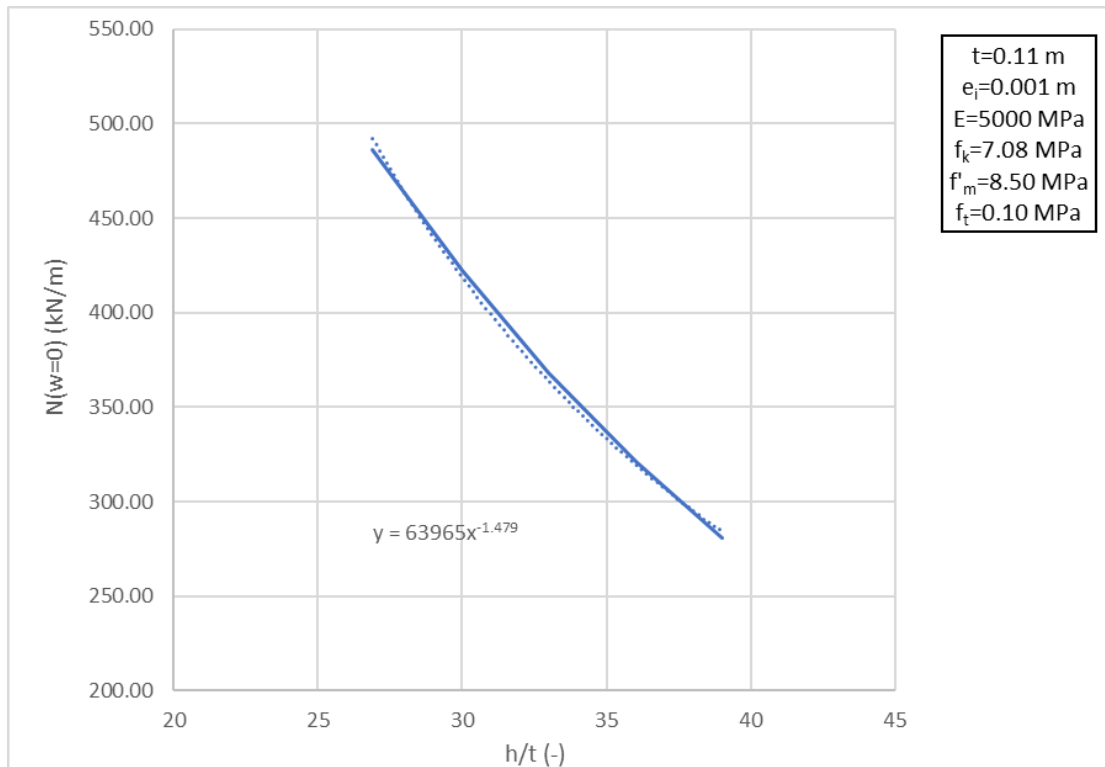
Fig. 153 Relationship between h/t and N(w=0)

9.3.2.2 Influence of the Short-Term Secant Modulus of Elasticity (E) & the Characteristic Compressive Strength (f_k)

The graph in Fig. 101 shows the different curves, with the combinations of vertical load-wind load, that lead an existing slender URM wall to failure, when the short-term secant modulus of elasticity (E) remains constant and the characteristic compressive strength (f_k) is variable. Two values of slenderness ratio (h/t) were considered. A graph is created in Fig. 154, which shows the influence of the characteristic compressive strength on the vertical resistance *N(w=0)*, for a constant value of the short-term secant modulus of elasticity and two different values of the slenderness ratio. It seems that the vertical resistance N(w=0) is an expression of the characteristic compressive strength (f_k), raised to a power. An average value of the power, for the two different values of the slenderness ratio, is approximately equal to 0.4.

The graph in Fig. 102 shows the different curves, with the combinations of vertical load-wind load, that lead an existing slender URM wall to failure, when the characteristic compressive strength (f_k) remains constant and the short-term secant modulus of elasticity (E) is variable. Two values of slenderness ratio (h/t) were considered. A graph is created in Fig. 155, which shows the influence of the short-term secant modulus of elasticity on the vertical resistance *N(w=0)*, for a constant value of the characteristic compressive strength and two different values of the slenderness ratio. It seems that the vertical resistance *N(w=0)* is an expression of the short-term secant modulus of elasticity (E), raised to a power. An average value of the power, for the two different values of the slenderness ratio, is approximately equal to 0.6.

According to the FE analysis results, the characteristic compressive strength (f_k) influences the vertical resistance *N(w=0)* of a slender URM wall, subjected to vertical loading, only. Additionally, it seems that the vertical resistance *N(w=0)* does not have a linear relationship with the short-term secant modulus

of elasticity (E), as the expressions in Equation 61 and Equation 63 suggest. The expression for the vertical resistance N(w=0) should include both the short-term secant modulus of elasticity and the characteristic compressive strength, each raised to a power. It is noticed in the graphs, in Fig. 154 and Fig. 155, that, for each value of slenderness ratio, the summation of the values of power, to which the short-term secant modulus of elasticity and the characteristic compressive strength are raised, equals one. This relationship between the values of power, to which the short-term secant modulus of elasticity and the characteristic compressive strength are raised, seems reasonable for developing the expression for the vertical resistance $N(w=0)$, in the first segment of the formula in Equation 59. In Equation 61 and Equation 63 the ratios $(\frac{t_{ef}}{h_{ef}})^2$ and $\frac{e_i}{t}$ are dimensionless. The short-term secant modulus of elasticity (E) is expressed in *MPa* and the remaining, from the ratio $\frac{t_{ef}^3}{h_{ef}^2}$, effective thickness ($t_{ef}$) is expressed in *m*. The final product, which is the vertical resistance $N(w=0)$, is expressed in *MN/m* and is transformed in *kN/m*. The expression for the slenderness ratio in the first segment of the formula in Equation 59 has been defined in section 9.3.2.1. It is a dimensionless ratio. The eccentricity, at the top or bottom of the URM wall, will be introduced by the no-dimensionless ratio $\frac{e_i}{t}$. Hence, the effective thickness, the short-term secant modulus of elasticity and the characteristic compressive strength will be the unitized parameters in the expression for the vertical resistance $N(w=0)$, in the first segment of the formula in Equation 59. The product of the short-term secant modulus of elasticity and the characteristic compressive strength, each raised to a power, should be expressed in *MPa* so that the vertical resistance $N(w=0)$ is expressed in *MN/m*. Therefore, the summation of the values of power should equal to one, since the values, of the short-term secant modulus of elasticity and the characteristic compressive strength, are expressed in *MPa*, each. The power of 0.60 and the power of 0.40 seem to be the most appropriate, for the expressions of the short-term secant modulus of elasticity and the characteristic compressive strength, respectively. For each value of the slenderness ratio, dividing the values of the vertical resistance $N(w=0)$, from the graphs in Fig. 101 and Fig. 102, with the expression $E^{0.60} f_k^{0.40}$, results in the best proximity among the quotients.
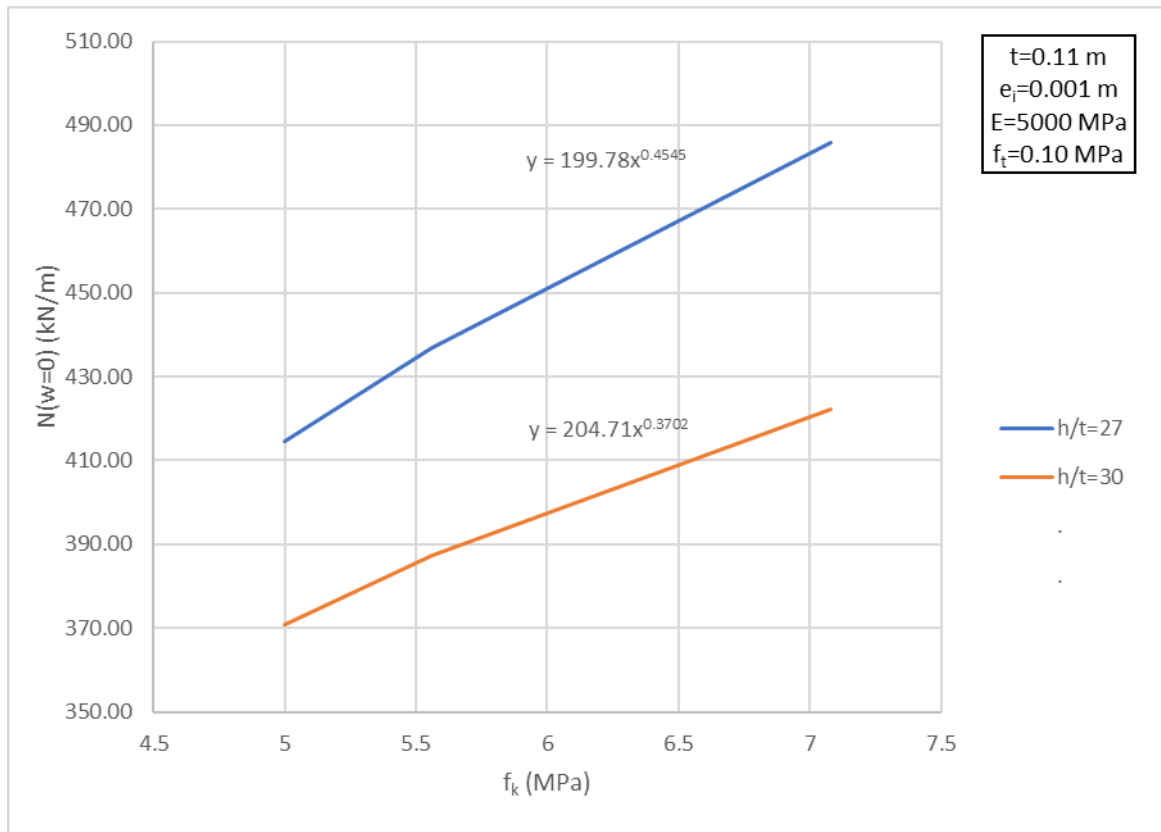
Fig. 154 Relationship between f_k and N(w=0)
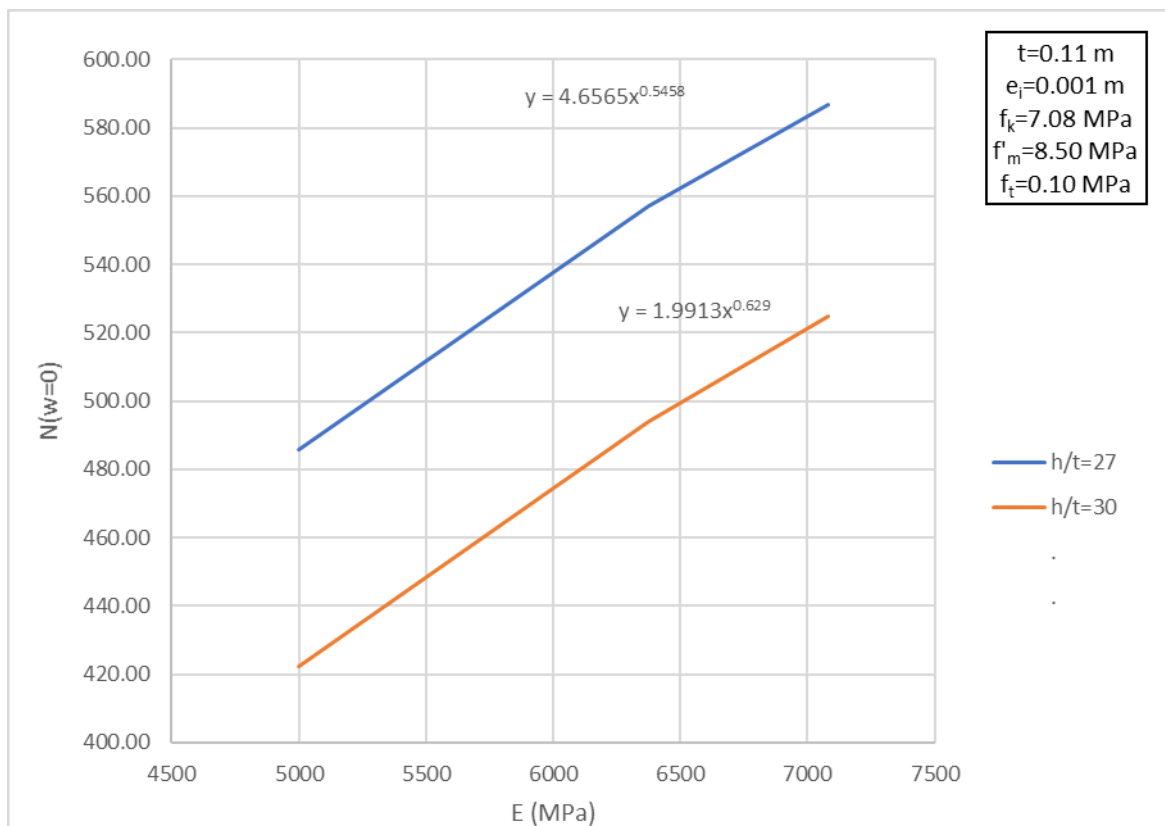
Fig. 155 Relationship between E and N(w=0)

9.3.2.3 Influence of Eccentricity at the Top or the Bottom of the URM Wall (e_i)

It has, already been mentioned that the eccentricity, at the top and the bottom of the studied URM walls (e_i) as well as along the full height, is equal to the initial eccentricity, which allows for construction imperfections. [53] The values of the vertical resistance of existing slender URM walls, with different values of eccentricity (e_i), when zero wind load is applied, can be obtained from the graphs in Fig. 104 and Fig. 150. The graph in Fig. 150 entails the curve with the combinations of vertical load – wind load, that lead a URM wall, with eccentricity $e_i=0.010\ m$, to failure. This curve was added in the graph in Fig. 104, after the remarks, that were made in section 9.3.1.3. In that section, an expression for the influence of the eccentricity (e_i) on the second segment of the formula, in Equation 59, has, also, been defined. The expression is valid for values of eccentricity (e_i) from 0.001 m to 0.015 m. The first segment of the formula in Equation 59 will be, also, relevant to the same range of values of eccentricity (e_i).

Equation 61 and Equation 63 suggest the use of the expression $\left(1 - 2\frac{e_i}{t}\right)^3$, for the influence of the eccentricity (e_i) on the vertical resistance of URM walls, subjected to vertical loading, only. It is attempted to adjust the constant factor, that is multiplied with the ratio $\frac{e_i}{t}$, as well as the power of *3*, in the aforementioned expression. The expression $\left(1 - 2\frac{e_i}{t}\right)^{2.40}$ seems to be the most appropriate to introduce the influence of eccentricity (e_i), in the first segment of the formula in Equation 59. Dividing the values of *N(w=0)*, for $e_i=0.001\ m$, $e_i=0.010\ m$ and $e_i=0.015\ m$, from the graph in Fig. 150, with the latter expression, results in the best proximity between the quotients. *N(w=0)* is the vertical resistance of the URM wall, when zero wind load is applied.

9.3.2.4 Influence of Tensile Strength (f_t)

The graph in Fig. 103 shows the influence of halving the tensile strength of masonry, on the curves with the combinations of vertical load – wind load, that lead an existing URM wall to failure, for different values of slenderness ratio (h/t). The curves seem to match within the compression region, which will be described by the formula in Equation 59, as it has, already been discussed in section 9.3. Only for large values of wind load (*w*), the curves deviate. Therefore, the influence of the tensile strength seems to be relevant to the second segment of the formula in Equation 59, where the effect of wind load is introduced. This issue has been addressed in section 9.3.1.4.

The graph in Fig. 105 shows the influence of halving the tensile strength of masonry, on the curves with the combinations of vertical load – wind load, that lead an existing slender URM wall to failure, for different values of eccentricity, at the top or the bottom of the wall (e_i). For the value of eccentricity $e_i=0.001\ m$, the curves seem to match within the compression region, which will be described by the formula in Equation 59. For large values of wind load (*w*), only, the curves deviate. Therefore, the influence of the tensile strength seems to be relevant to the second segment of the formula in Equation 59, where the effect of wind load is introduced. This issue has been addressed in section 9.3.1.4.

The expressions for the influence of the eccentricity at the top or the bottom of the wall (e_i), in the first and the second segment of the formula in Equation 59, are valid for values of eccentricity (e_i) between 0.001 m and 0.015 m (sections 9.3.1.3 and 9.3.2.3). For the value of eccentricity $e_i=0.015\ m$, deviation between the curves is noticed in the graph in Fig. 105, even when the wind load is zero. This response of the URM wall is in agreement with the theory, that the tensile strength of masonry has a considerable contribution to the capacity of slender walls, for values of eccentricity (e_i) larger than *0.1t*. [20] For the studied walls, which have a thickness of *0.11 m*, the product *0.1t* equals *0.011 m*, which is smaller than the eccentricity $e_i=0.015\ m$. The deviation between the curves, for $e_i=0.015\ m$,

in the graph in Fig. 105, becomes larger in magnitude as the value of the wind load (w) increases. The influence of the tensile strength seems to be, also, relevant to the second segment of the formula in Equation 59, where the effect of wind load is introduced. This issue has been addressed in section 9.3.1.4

Sandoval & Roca [20] suggested an expression (Equation 34), for estimating the contribution of the tensile strength to the vertical resistance of slender URM walls. This expression is introduced in the formula, for the calculation of the capacity reduction factor, for slenderness and eccentricity, at the mid-height of the wall, according to Equation 33. Including the influence of the tensile strength, in the capacity reduction factor, is suggested for values of eccentricity $0.1t \leq e_i \leq 0.3t$. The expression, in Equation 34, seems rather cumbersome, considering that it introduces the effect of one single parameter, in the formula for the calculation of vertical resistance of slender URM walls. It is considered appropriate that, the influence of the tensile strength is not taken into consideration in the first segment of the formula in Equation 59. A suitable formula should result in a more conservative estimation of the vertical resistance $N(w=0)$, of an existing slender URM wall, subjected to vertical loading, only, compared to the respective result from the FE analysis. Moreover, it is intended that the value of the vertical resistance, which is calculated from the first segment of the formula in Equation 59, is smaller than the respective value of resistance, that results from the FE analysis, with $f_t=0.05$ MPa.

10 Proposed Formula for the Estimation of the Vertical Resistance of Existing Slender URM Walls

In section 9.3, a general form of the formula, for the estimation of the vertical resistance of existing slender URM walls, subjected to combined vertical and lateral loading, was suggested (Equation 59). This formula was considered suitable to describe the compression region of the curves, with the combinations of vertical load – wind load, that lead the studied URM walls to failure. These curves are the outcome of several FE analyses, that were performed on existing slender URM walls, with various geometrical and material properties. The formula in Equation 59 is divided in two segments. The first segment estimates the vertical resistance of an existing slender URM wall, subjected to vertical loading, only. The second segment introduces the influence of the wind load, as an additional reduction factor to the vertical resistance. Reviewing the FE analysis results, the impact of a number of parameters, on the first and the second segment of the formula, in Equation 59, was specified, in sections 9.3.2 and 9.3.1, respectively. The considered parameters are the geometrical properties of the URM wall, namely the height (h) and the thickness (t), the eccentricity at the top or the bottom of the wall (e_i) as well as the properties of masonry and, specifically, the short-term secant modulus of elasticity (E), the characteristic compressive strength (f_k) and the tensile strength (f_t). As a result, appropriate expressions were defined, for introducing every parameter into each segment of the formula. Hence, the formula in Equation 59 is developed into the respective one in Equation 66. The constants need to be estimated. A value for the constant a equal to *1.49* seems appropriate. This way, the estimation of the vertical resistance of the studied URM walls, when they are only subjected to vertical loading, is conservative compared to the respective FE analysis results. In the case of zero wind load the expression '$\left(b + c \sqrt{d - f \left(\frac{h_{ef}}{t_{ef}} \right)^{0.38} \left(\frac{f_k}{E} \right)^{0.23} \frac{\frac{e_w}{t}}{1 - 2.10 \frac{e_i}{t}}} \right)$' should equal 1. Hence, the constant d should equal 1 and adding b and c must result in the number 1, too. Suitable values for the constants b, c and f are 0.41, 0.59 and 18.20, respectively. Equation 67 gives the final form of the formula, for the estimation of the vertical resistance of an existing slender URM wall, subjected to combined vertical and lateral loading. Further, section 10.1 includes the graphs with the comparison between the curve, from the formula in Equation 67, and the respective curve, from the FE analysis results, for every case of the studied URM walls.

Equation 66 Proposed Formula for the Estimation of the Vertical Resistance of Existing Slender URM walls, subjected to Combined Vertical and Lateral Loading, with unspecified constant factors

$$N = a\, E^{0.60}\, f_k^{\,0.40} \left(\frac{t_{ef}}{h_{ef}}\right)^{1.46} t \left(1 - 2\,\frac{e_i}{t}\right)^{2.40} \left(b + c\,\sqrt{d - f\left(\frac{h_{ef}}{t_{ef}}\right)^{0.38} \left(\frac{f_k}{E}\right)^{0.23} \frac{\frac{e_w}{t}}{1 - 2.10\,\frac{e_i}{t}}}\right),$$

where:

a, b, c, d, f:	constants to be estimated
E:	the short-term secant modulus of elasticity
f_k:	the characteristic compressive strength
t_{ef}:	the effective thickness of the wall
h_{ef}:	the effective height of the wall
t:	the thickness of the wall
e_i:	the eccentricity at the top or the bottom of the wall
e_w:	the eccentricity at the mid-height of the wall, caused by the maximum first-order bending moment on the wall, because of the wind load

Equation 67 Proposed Formula for the Estimation of the Vertical Resistance of Existing Slender URM walls, subjected to Combined Vertical and Lateral Loading

$$N = 1.49\, E^{0.60}\, f_k^{\,0.40} \left(\frac{t_{ef}}{h_{ef}}\right)^{1.46} t \left(1 - 2\,\frac{e_i}{t}\right)^{2.40} \left(0.41 + 0.59\,\sqrt{1 - 18.20\left(\frac{h_{ef}}{t_{ef}}\right)^{0.38} \left(\frac{f_k}{E}\right)^{0.23} \frac{\frac{e_w}{t}}{1 - 2.10\,\frac{e_i}{t}}}\right),$$

where:

E:	the short-term secant modulus of elasticity
f_k:	the characteristic compressive strength
t_{ef}:	the effective thickness of the wall
h_{ef}:	the effective height of the wall
t:	the thickness of the wall
e_i:	the eccentricity at the top or the bottom of the wall
e_w:	the eccentricity at the mid-height of the wall, caused by the maximum first-order bending moment on the wall, because of the wind load (Equation 68)

Equation 68 Eccentricity at the mid-height of the wall, caused by the maximum first-order bending moment on the wall, because of the wind load

$$e_w = \frac{M_w}{1.49\,E^{0.60}\,f_k{}^{0.40}\left(\frac{t_{ef}}{h_{ef}}\right)^{1.46} t\left(1-2\,\frac{e_i}{t}\right)^{2.40}},$$

where:

M_w: the bending moment at the mid-height of the wall because of the wind load (Equation 64)

E: the short-term secant modulus of elasticity

f_k: the characteristic compressive strength

t_{ef}: the effective thickness of the wall

h_{ef}: the effective height of the wall

t: the thickness of the wall

e_i: the eccentricity at the top or the bottom of the wall

10.1 Verification of the Proposed Formula with the FE Analysis Results

For different values of slenderness ratio (h/t), the graphs, in Fig. 156 - Fig. 164, show the comparison between the curve, from the formula in Equation 67, and the respective curve, from the FE analysis results (Fig. 100). The formula in Equation 67 is valid for values of slenderness ratio from 27 to 39. Within this range of values of slenderness ratio, the formula leads to a conservative calculation of the vertical resistance of existing URM walls. This is confirmed by the curves in the graphs in Fig. 156 - Fig. 160. However, the formula in Equation 67 cannot estimate, accurately, the vertical resistance of URM walls, which are subjected to combined vertical and lateral loading and have a value of slenderness ratio larger than 39. This is obvious in the graphs in Fig. 161 - Fig. 164. The formula overestimates the vertical resistance of URM walls with values of slenderness ratio from 45 to 66.

Table 17 consists of the different combinations of geometrical and material properties, that were assigned to existing slender URM walls. These walls have been analyzed with the FE method. The graphs in Fig. 101, Fig. 102 and Fig. 103 show the results of the respective analyses. The influence of changing the characteristic compressive strength (f_k), while keeping the short-term secant modulus of elasticity (E) constant, on the interaction curves is shown in the graph in Fig. 101. The curves, in the graph in Fig. 101, are compared with the respective curves, from the formula in Equation 67, in the graphs in Fig. 156, Fig. 157, Fig. 165, Fig. 166, Fig. 169 and Fig. 170. The graph in Fig. 102 shows the curves, with the combinations of vertical load – wind load, that lead a URM wall to failure, for the same value of characteristic compressive strength (f_k) and a different value of short-term secant modulus of elasticity (E), each time. The graphs in Fig. 156, Fig. 157, Fig. 167, Fig. 168, Fig. 171 and Fig. 172 juxtapose the curves, in the graph in Fig. 102, with the respective curves, from the formula in Equation 67. For all the combinations $E - f_k$, that have been studied, the formula in Equation 67 estimates the vertical resistance of the URM wall conservatively.

Three different values of eccentricity at the top and the bottom (e_i) have been assigned to the case study of URM wall and relevant FE analyses were performed, in order to obtain the curves in the graph in Fig. 104. As it has been mentioned in 9.3.1.3, a URM wall with eccentricity e_i=0.010 m was, also, analyzed with the FE method. After that, the graph in Fig. 150 was created. The latter graph shows the different curves with the combinations of vertical load – wind load, that lead an existing slender URM

wall to failure, for different values of eccentricity (e_i). These curves are compared with the respective curves, from the formula, in Equation 67, in the graphs in Fig. 156, Fig. 173, Fig. 174 and Fig. 175. The formula in Equation 67 is valid for values of eccentricity (e_i), from 0.001 m to 0.015 m. The graphs in, Fig. 156, Fig. 173 and Fig. 174, show that the formula leads to a conservative calculation of the vertical resistance of existing slender URM walls, for values of eccentricity (e_i), within the aforementioned range. The vertical resistance of a wall, with eccentricity $e_i=0.029\ m$, which is subjected to combined vertical and lateral loading, is underestimated by the formula in Equation 67. Additionally, the formula defines a maximum value for the wind load, that the wall can bear, which is significantly lower than the actual capacity of the wall. These remarks result from the graph in Fig. 175.

Sections 9.3.2.4 and 9.3.1.4 address the issue of the influence of the tensile strength of masonry (f_t) in the first and the second segment of the formula in Equation 59, respectively. Including expressions, that introduce the effect of the tensile strength, in the two segments of the formula, in Equation 59, is not preferred. As it has been mentioned, a suitable formula should result in more conservative interaction curves, compared to the respective curves for $f_t=0.05\ MPa$. Therefore, the curves, from the formula in Equation 67, in the graphs in Fig. 156, Fig. 157, Fig. 160, Fig. 174 and Fig. 175, are juxtaposed with the respective curves, for $f_t=0.05\ MPa$. The latter curves are included in the graphs in Fig. 103 and Fig. 105. The juxtaposition is shown in the graphs in Fig. 176 - Fig. 180. The formula in Equation 67 overestimates the vertical resistance of the wall, only for the case of eccentricity $e_i=0.015\ m$. This overestimation is small in magnitude and occurs for a restricted range of values of wind load, as the graph in Fig. 179 shows. Additionally, the curves in the graphs, in section 9.2, are formed from the combinations of vertical load – wind load, that lead a URM wall to failure. These combinations are defined after non-linear FE analysis. It is obvious in the graph, in Fig. 179, that, the formula in Equation 67 results in more conservative failure combinations, compared to the respective ones from the FE analysis. Therefore, the formula in Equation 67 is assumed to be appropriate for the estimation of the vertical resistance of existing slender URM walls, subjected to combined vertical and lateral loading. Furthermore, it is concluded from the graph in Fig. 180, that the curve, from the formula in Equation 67, describes a conservative response of the wall with eccentricity $e_i=0.029\ m$, even compared to the respective FE analysis results, for $f_t=0.05\ MPa$.

The reference value of the tensile strength of masonry ($f_t=0.10\ MPa$) was obtained from the Dutch practice guideline NPR 9998:2018. FE models of slender URM walls, with half the value of the tensile strength ($f_t=0.05\ MPa$), which is prescribed in the NPR 9998:2018 norm, were analyzed. The results were compared with the respective results, of the analysis of walls, with the reference value of the tensile strength. This way the influence of the tensile strength was assessed. The formula in Equation 67 results in more conservative estimation of the vertical resistance, compared to the respective results of the FE analysis, for $f_t=0.05\ MPa$. Therefore, it is considered appropriate for the estimation of the vertical resistance of existing slender URM walls, subjected to combined vertical and lateral loading. The last conclusion could fail in bringing the design, of new slender URM walls, to the safe side. The tensile strength often becomes negligible, due to microcracks on masonry. [12] However, the definition of the formula, in Equation 67, was based on the analysis of FE models, of existing slender URM walls. Properties of masonry building constructions, during the late 19th – early 20th century, were assigned in the material model. It has already been mentioned that, the EN 1996 norm underestimates the vertical resistance of existing slender URM walls. Frequently, the calculated capacity is not adequate for the applied loads. Nevertheless, the walls have been standing for approximately 100 years. Taking into consideration the properties of high-lime mortars, that were addressed in section 5.2.3, the tensile strength could be an asset for the capacity of existing slender URM walls. The latter remark justifies the choice of comparing the results from the formula, in Equation 67, with the respective results of the FE analysis, for $f_t=0.05\ MPa$, in order to verify the proposed formula.

The graphs in section 9.2 show the results from the FE analysis of URM walls, with different geometrical and material properties. Every time, the value of one parameter, that affects the vertical resistance of the wall, changes, while the values of the rest of the parameters remain constant. This way, the influence of every parameter was specified in section 9.3. It is considered useful, for the verification of the proposed formula (Equation 67), to analyze one more case of existing slender URM wall with the FE method (see section 9.1.4). Alternative values to the reference ones, are assigned to two of the parameters, that affect the vertical resistance. Particularly, a slenderness ratio *h/t=33* and an eccentricity, at the top and the bottom of the wall, equal to *e$_i$=0.010 m*, are defined. The properties of masonry are the ones, that are prescribed in the NPR 9998-2018 norm. The results from the FE analysis of the wall are presented in the graph in Fig. 181. The vertical resistance of the wall is, also, calculated with the formula in Equation 67, for different values of wind load. The resulting curve is included in the graph in Fig. 181, too. It seems that the formula in Equation 67 estimates the vertical resistance of the existing slender URM wall conservatively.
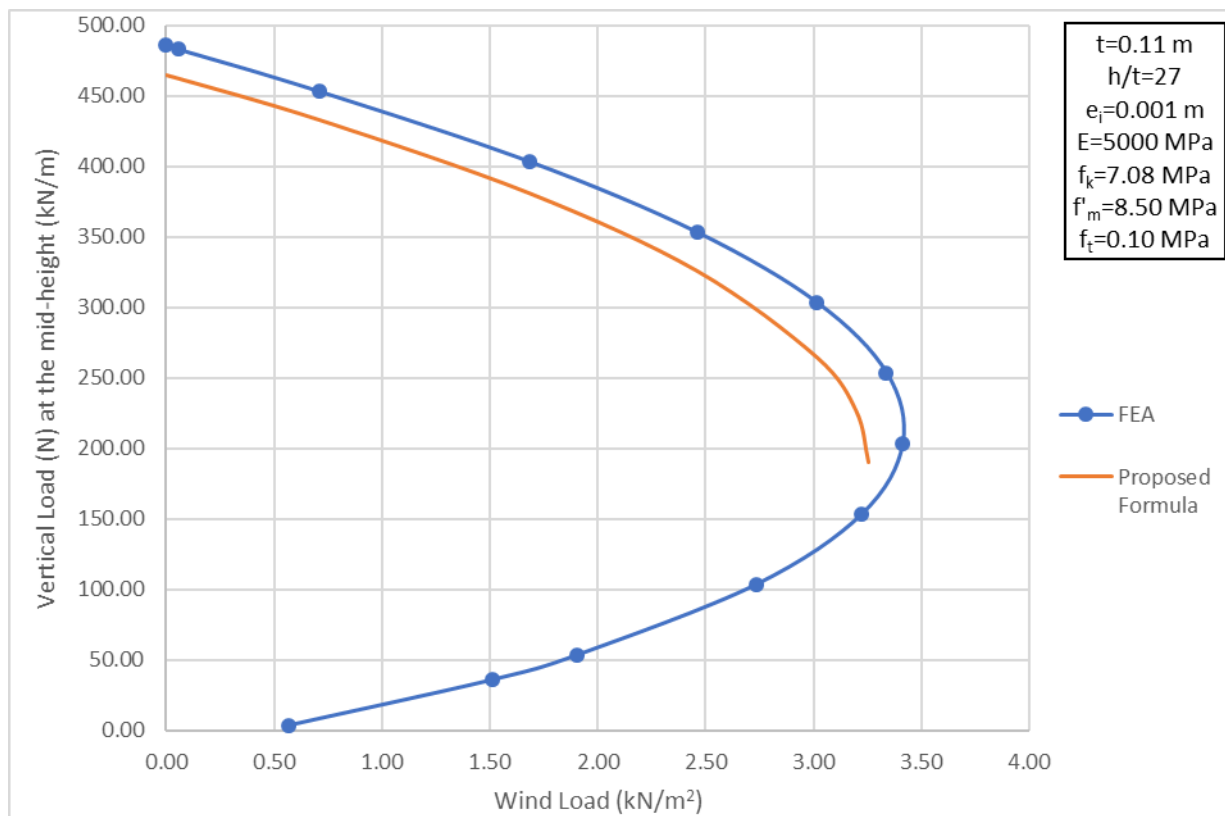
Fig. 156 Verification of the Proposed Formula for a URM Wall with h/t=27
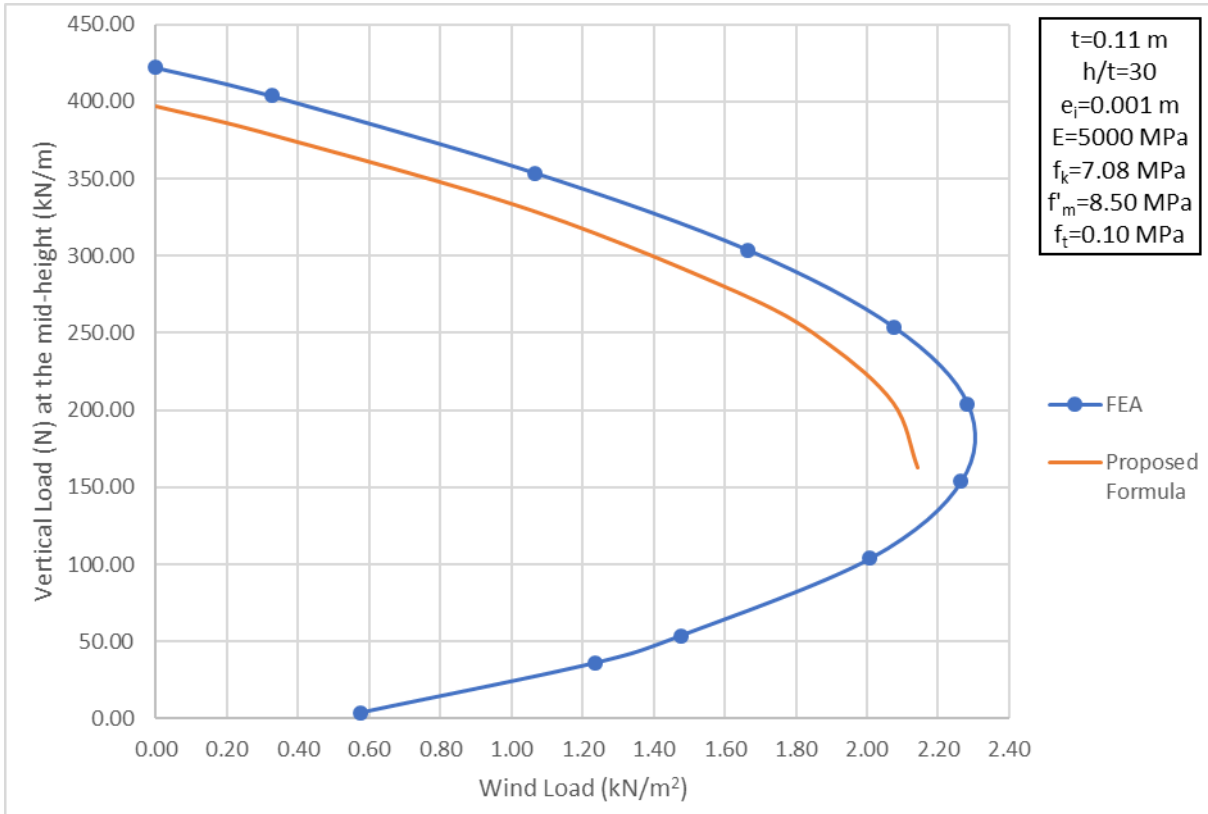
Fig. 157 Verification of the Proposed Formula for a URM Wall with h/t=30
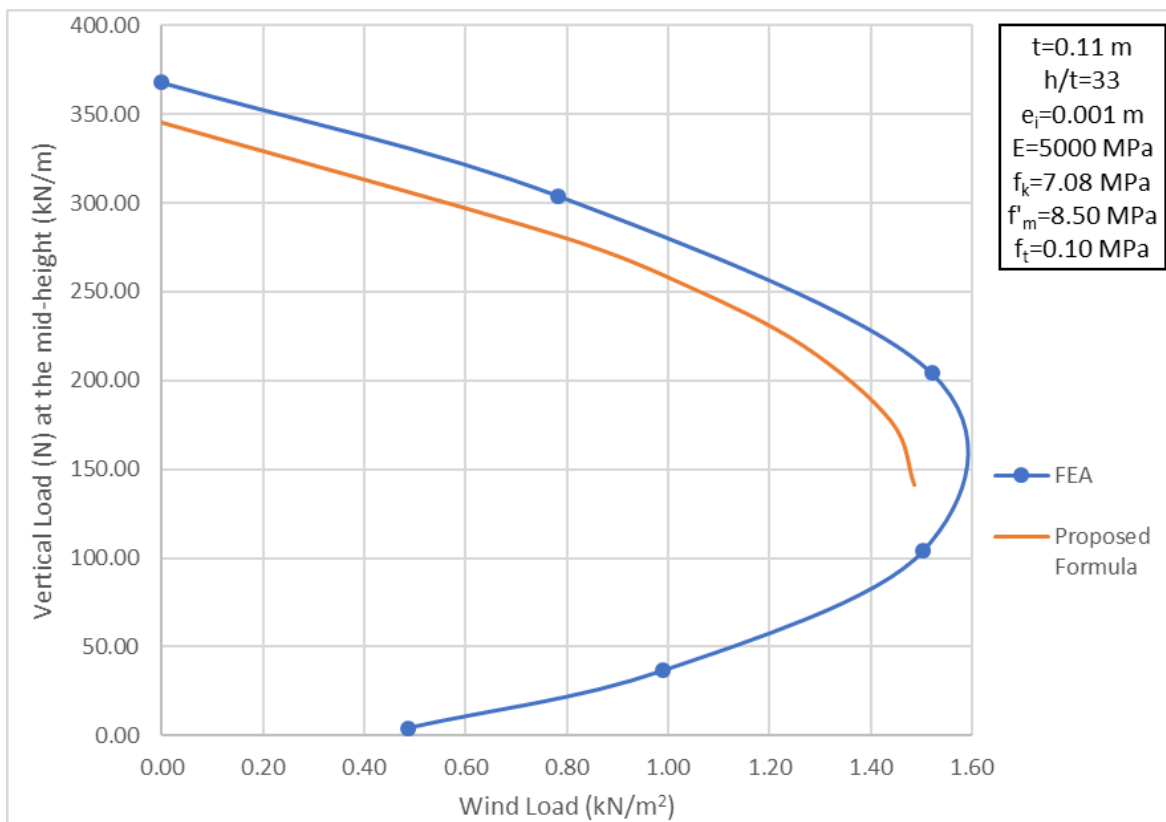
Fig. 158 Verification of the Proposed Formula for a URM Wall with h/t=33
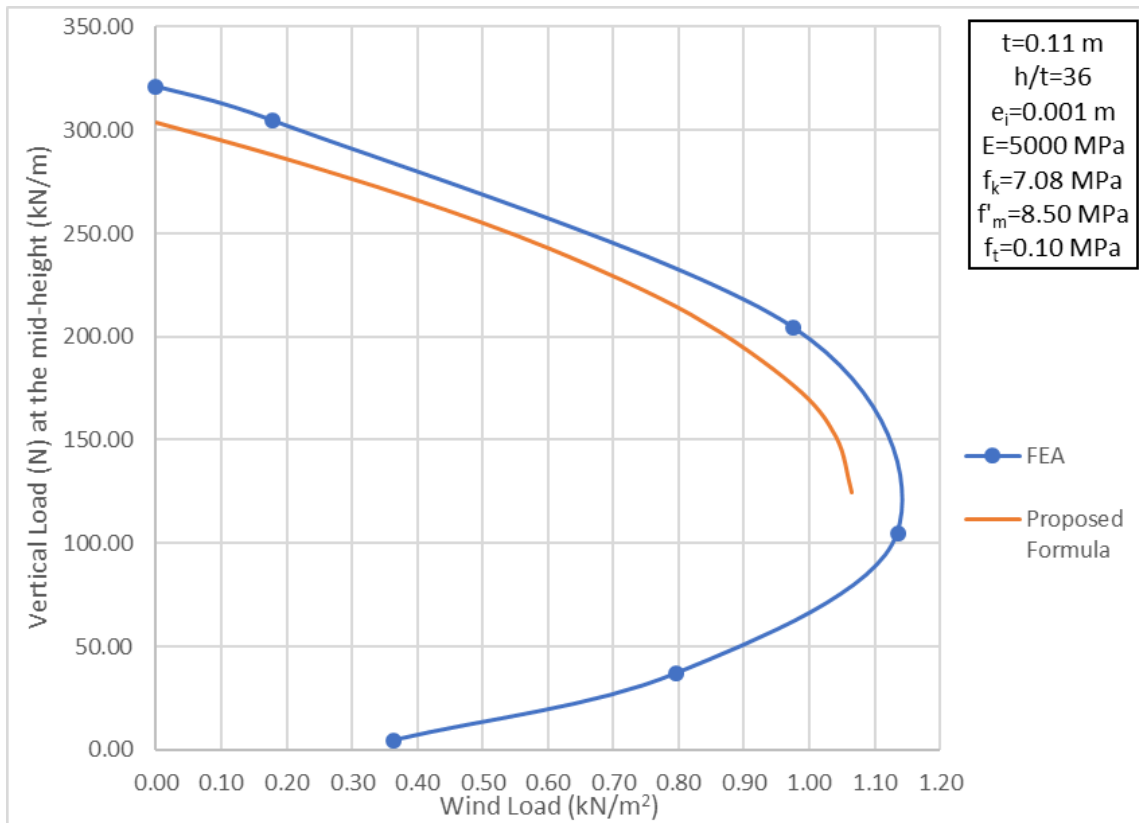
Fig. 159 Verification of the Proposed Formula for a URM Wall with h/t=36
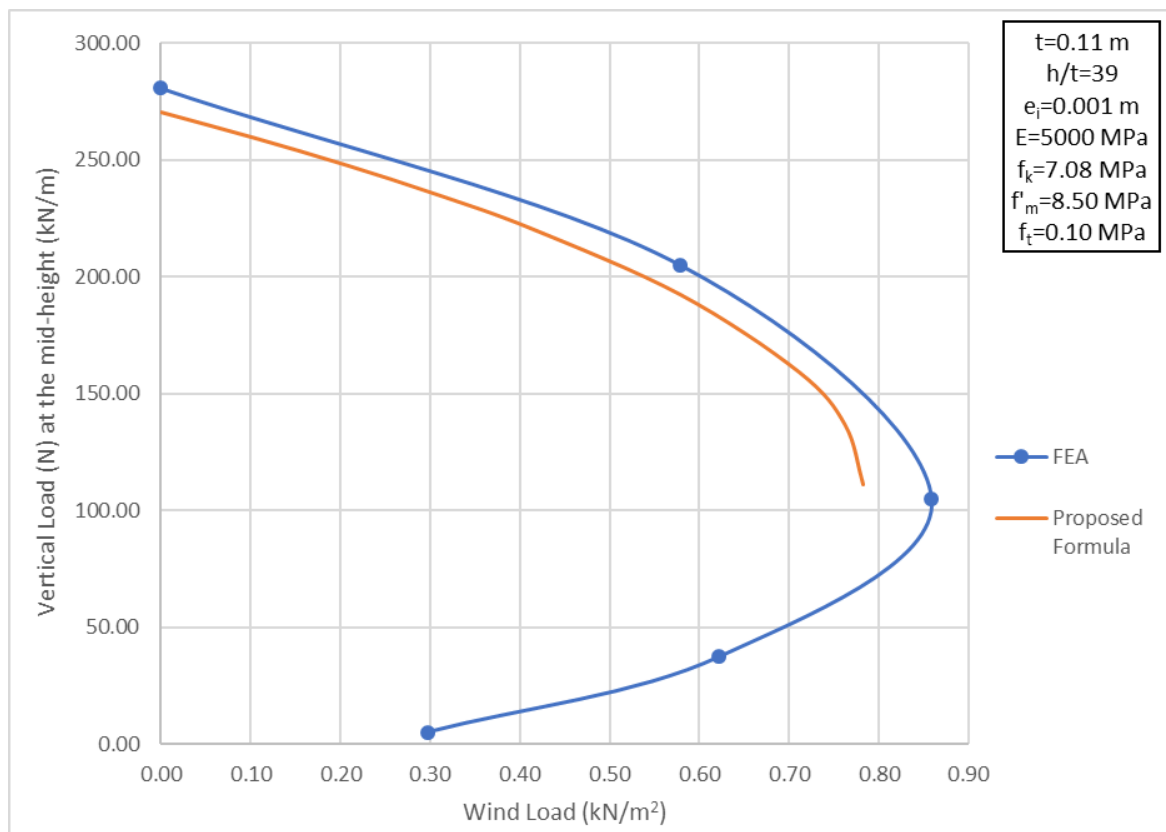
Fig. 160 Verification of the Proposed Formula for a URM Wall with h/t=39
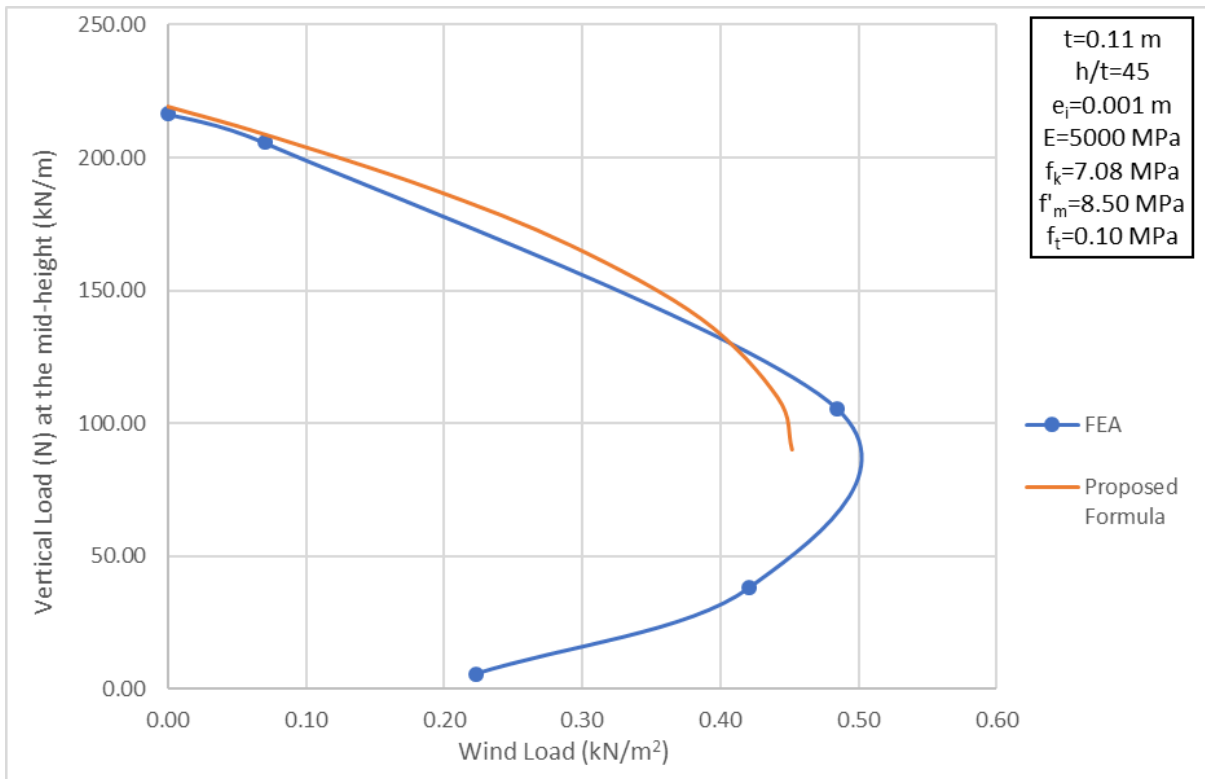
Fig. 161 Verification of the Proposed Formula for a URM Wall with h/t=45
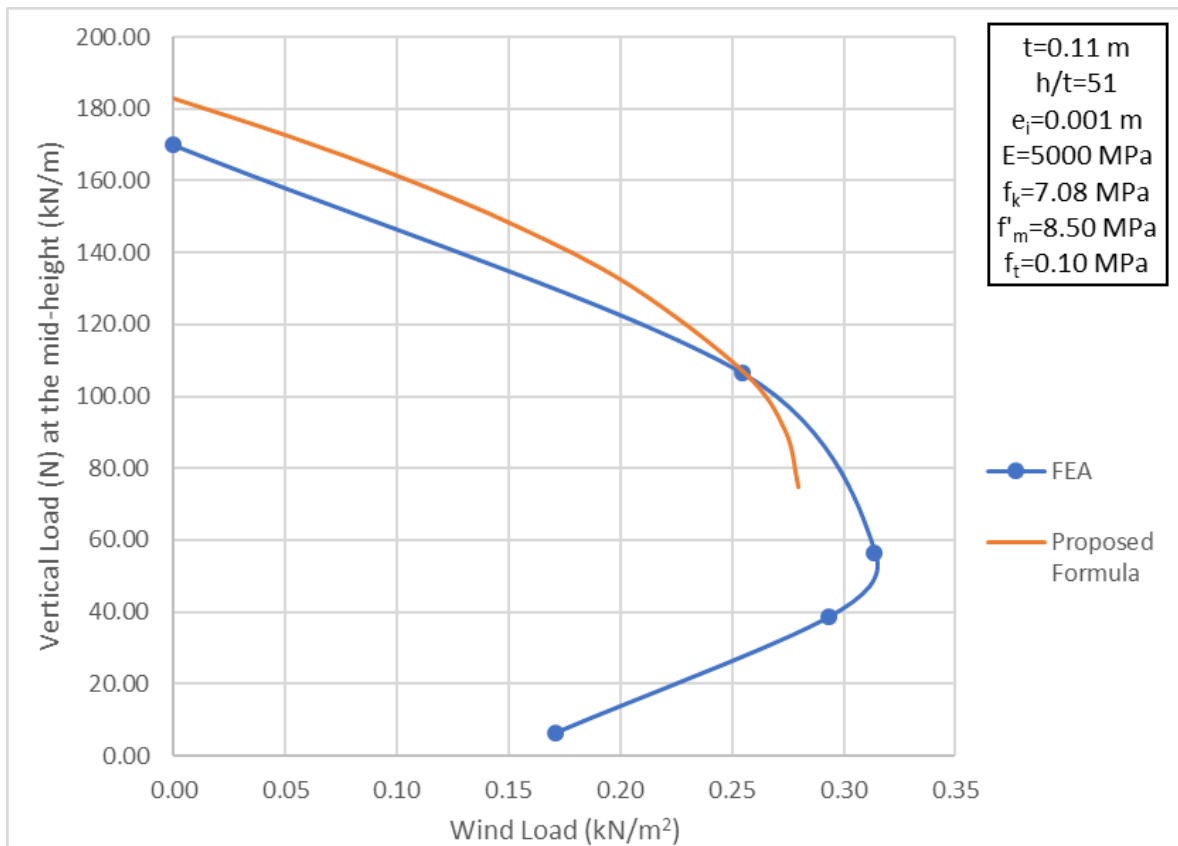
Fig. 162 Verification of the Proposed Formula for a URM Wall with h/t=51
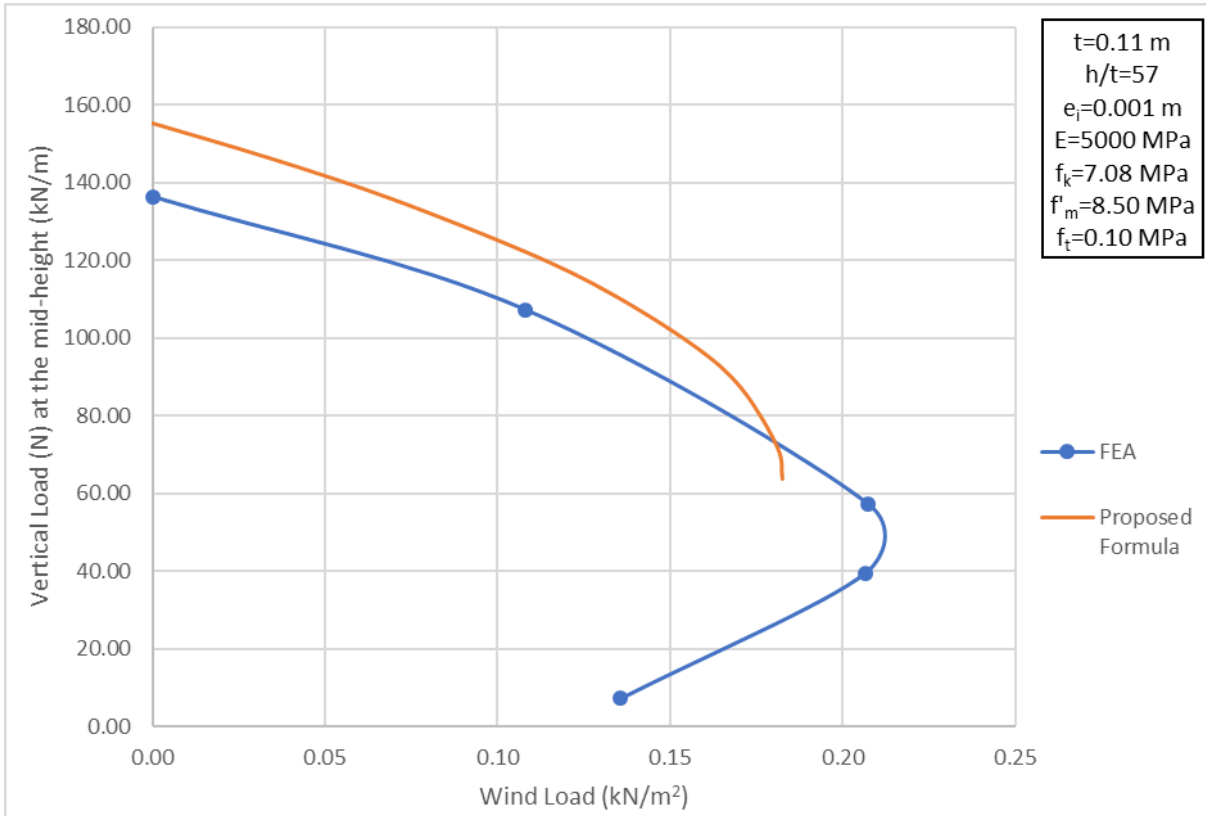
Fig. 163 Verification of the Proposed Formula for a URM Wall with h/t=57
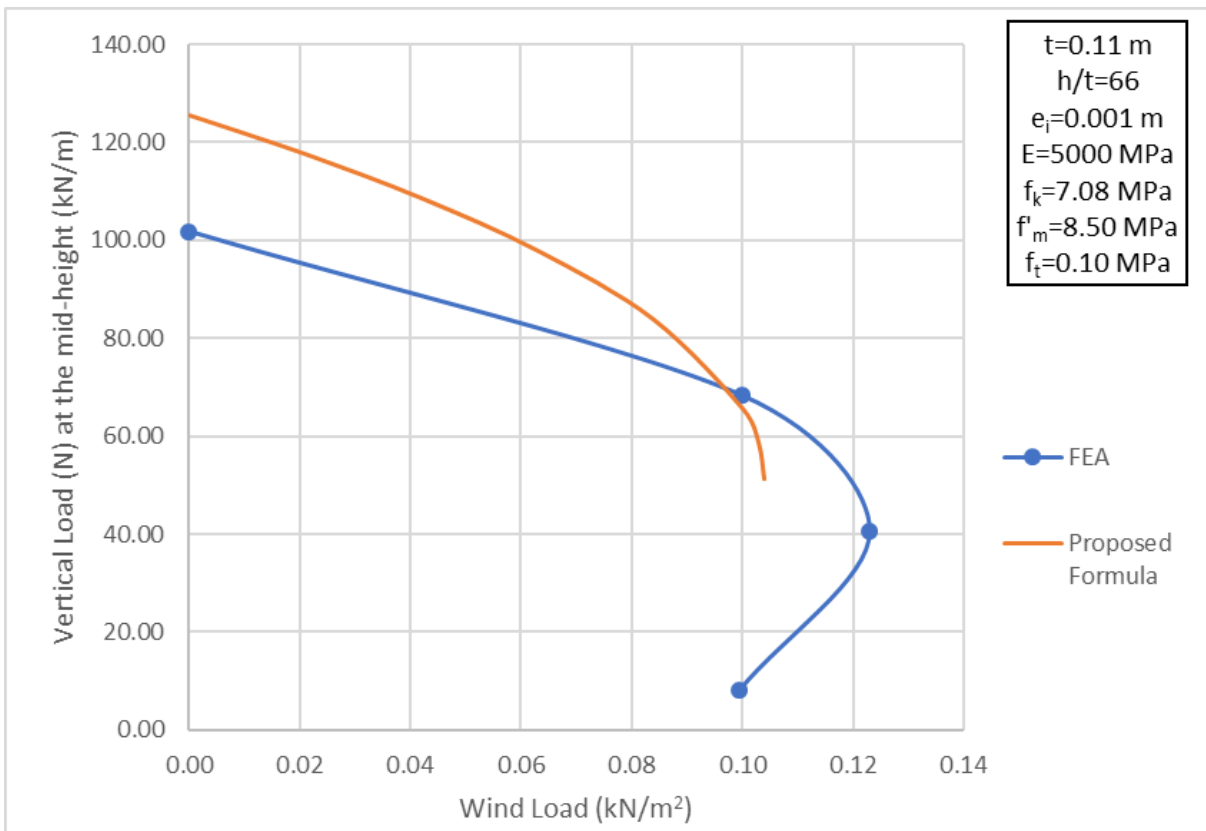
Fig. 164 Verification of the Proposed Formula for a URM Wall with h/t=66
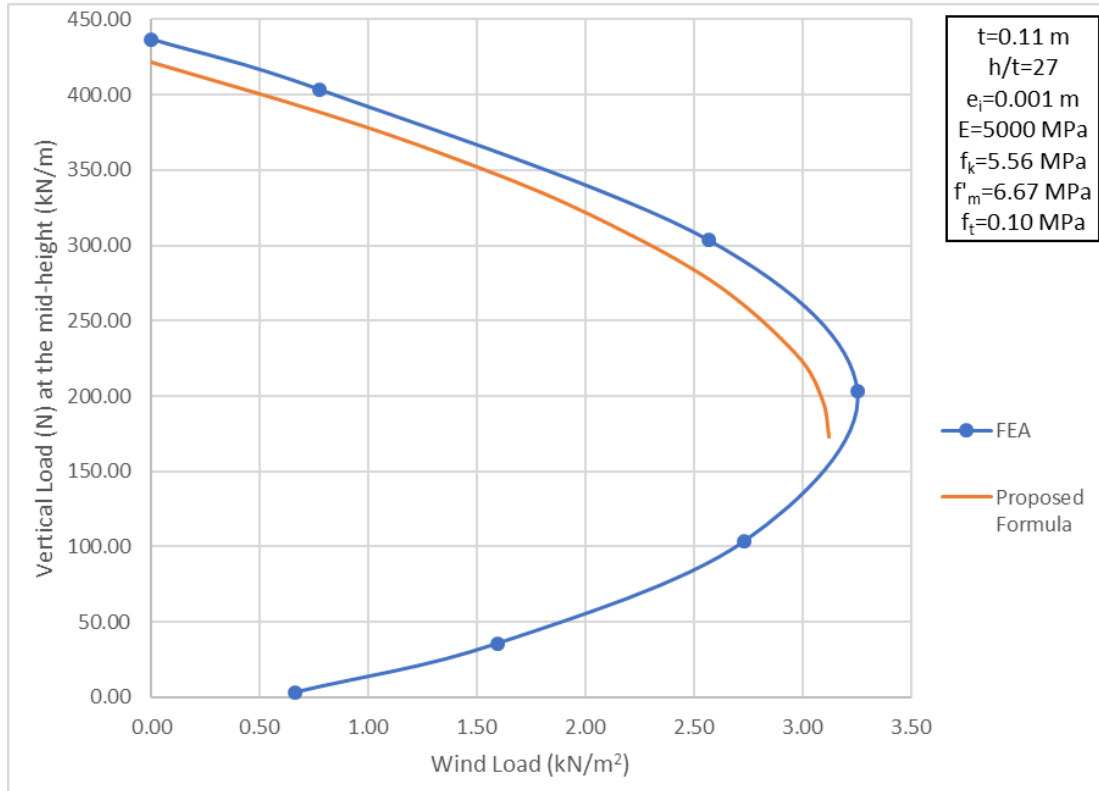
Fig. 165 Verification of the Proposed Formula for a URM Wall with E=5000 MPa, f_k=5.56 MPa and h/t=27
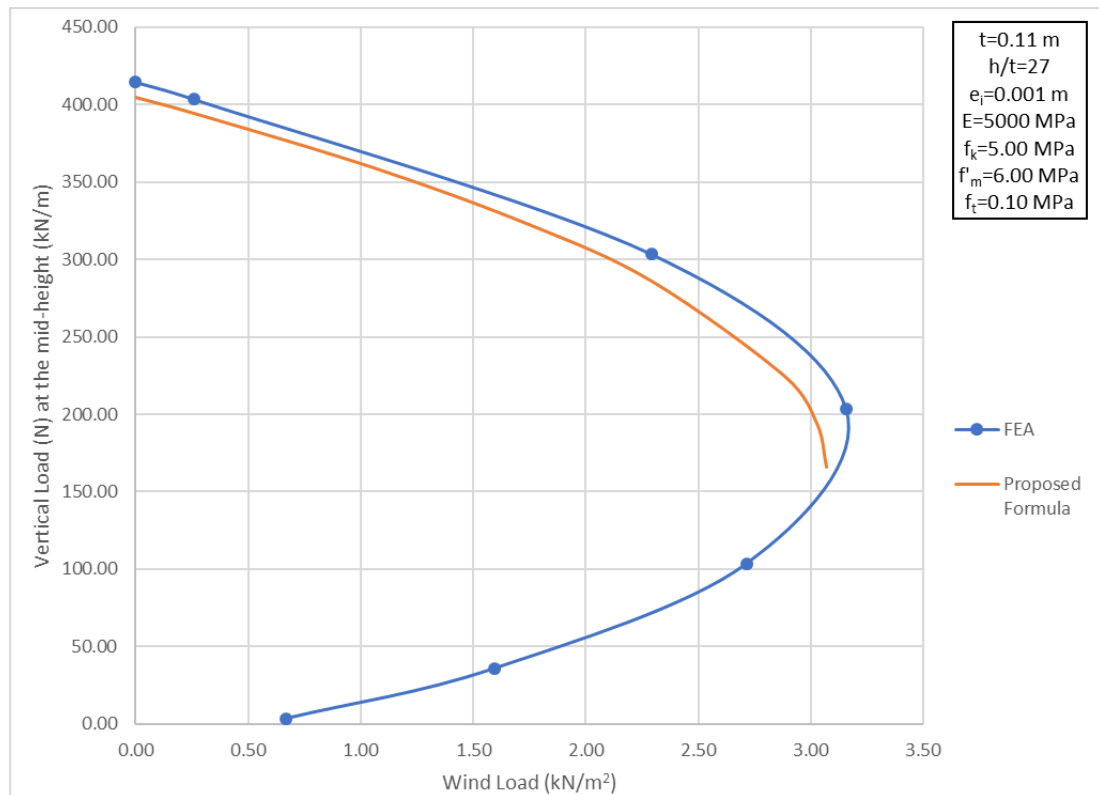
Fig. 166 Verification of the Proposed Formula for a URM Wall with E=5000 MPa, f_k=5.00 MPa and h/t=27
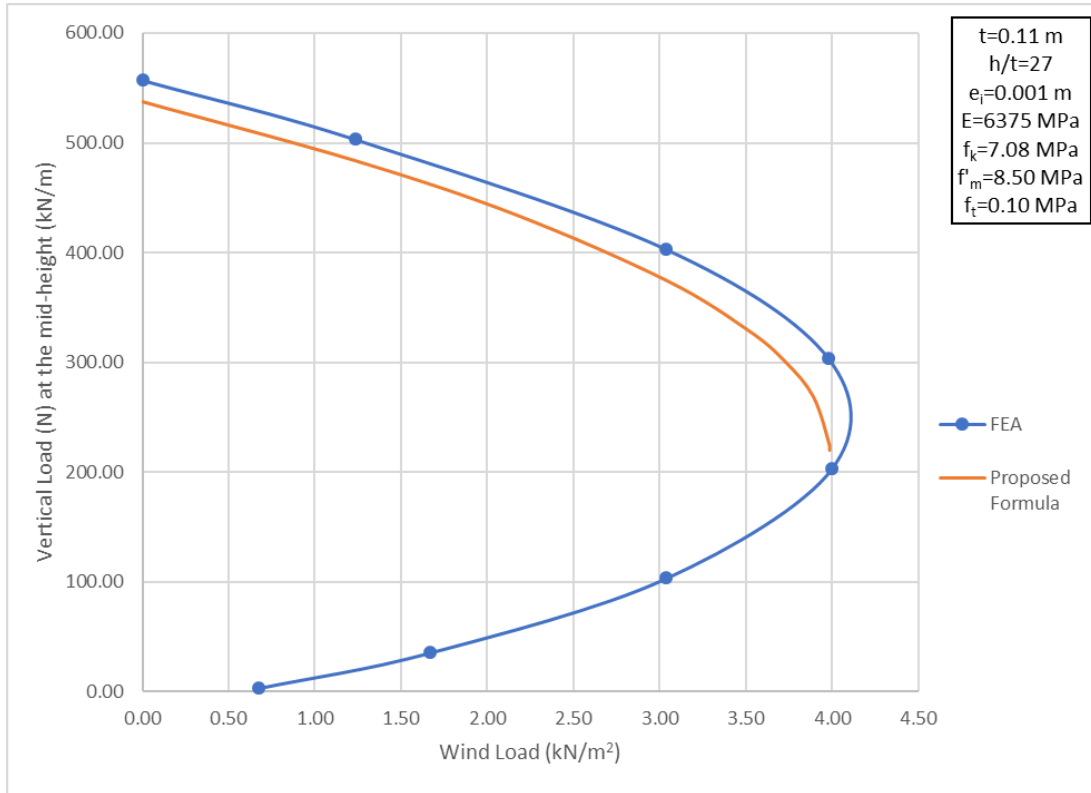
Fig. 167 Verification of the Proposed Formula for a URM Wall with E=6375 MPa, f_k=7.08 MPa and h/t=27
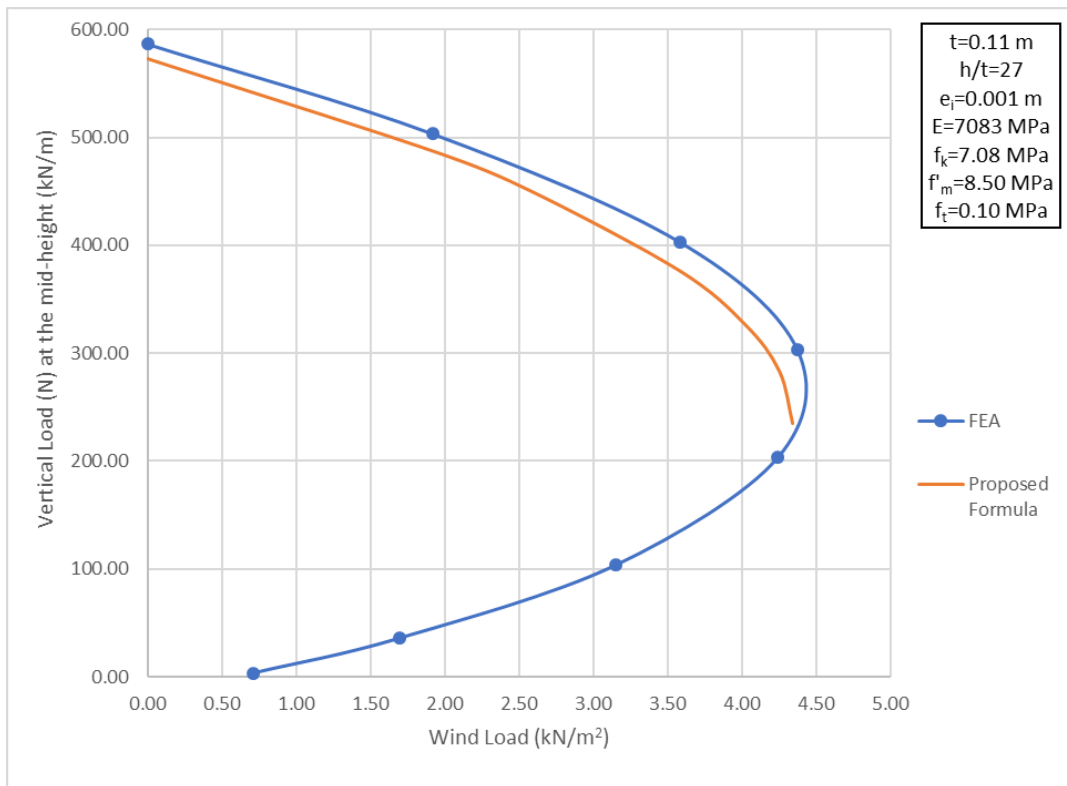
Fig. 168 Verification of the Proposed Formula for a URM Wall with E=7083 MPa, f_k=7.08 MPa and h/t=27
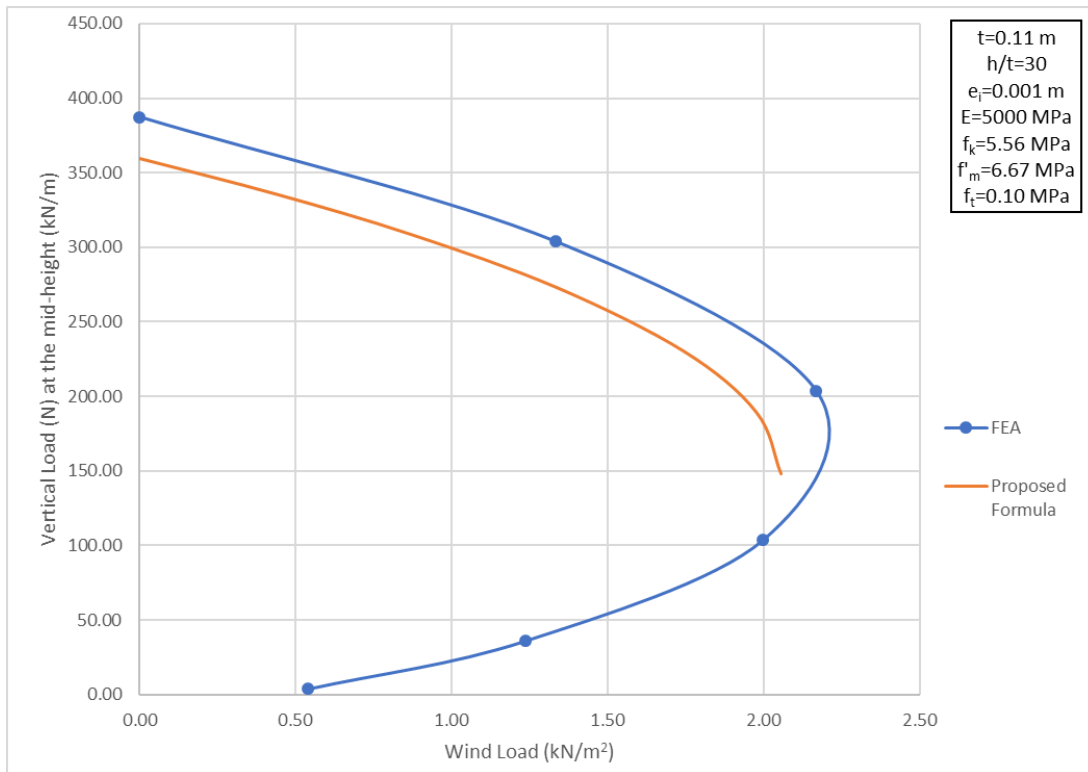
Fig. 169 Verification of the Proposed Formula for a URM Wall with E=5000 MPa, f_k=5.56 MPa and h/t=30
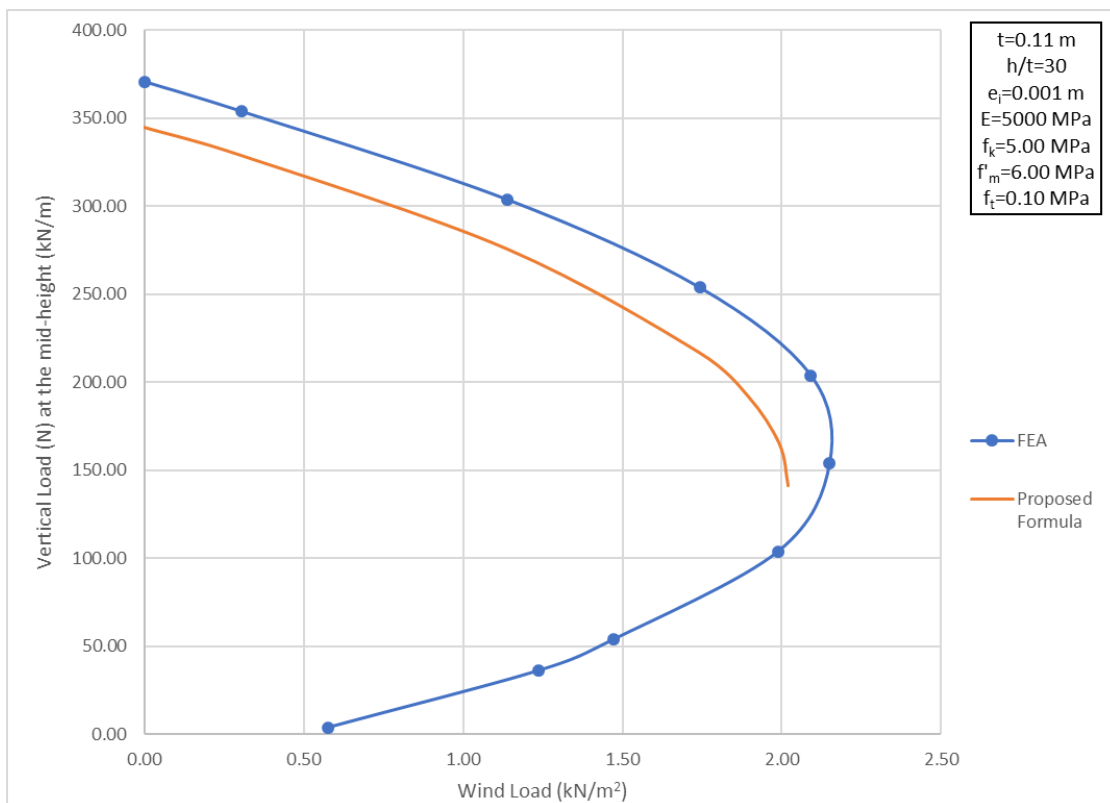
Fig. 170 Verification of the Proposed Formula for a URM Wall with E=5000 MPa, f_k=5.00 MPa and h/t=30
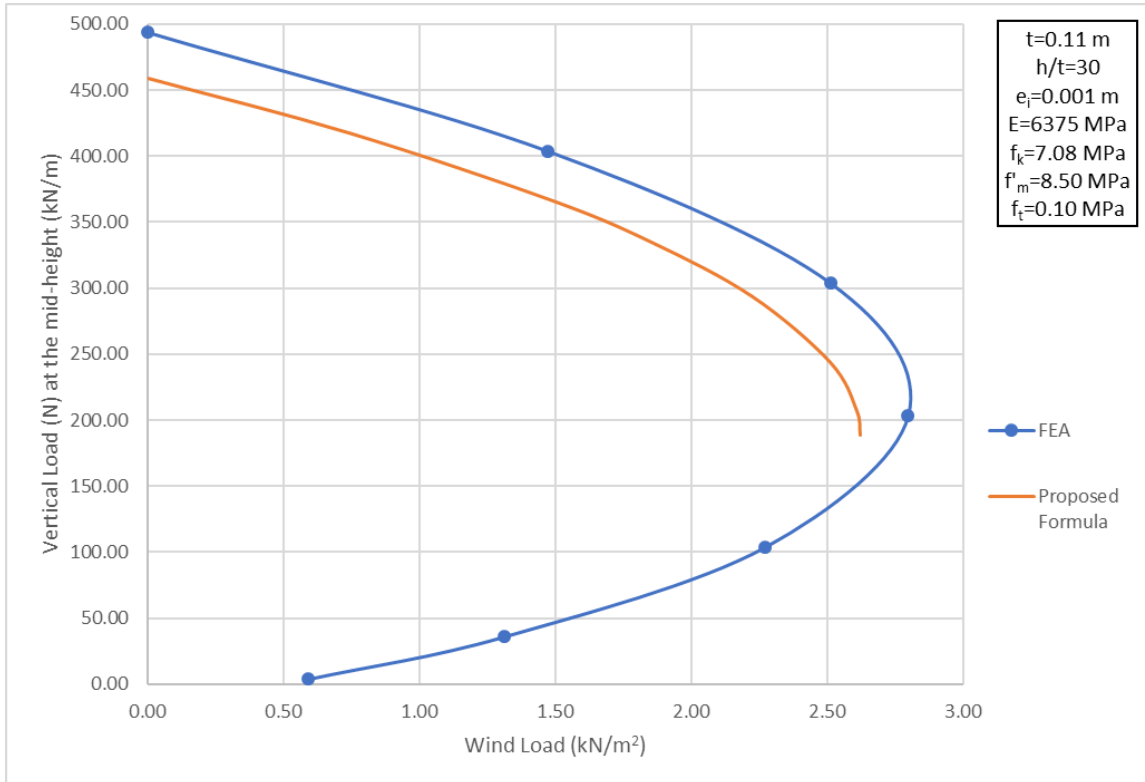
Fig. 171 Verification of the Proposed Formula for a URM Wall with E=6375 MPa, f_k=7.08 MPa and h/t=30
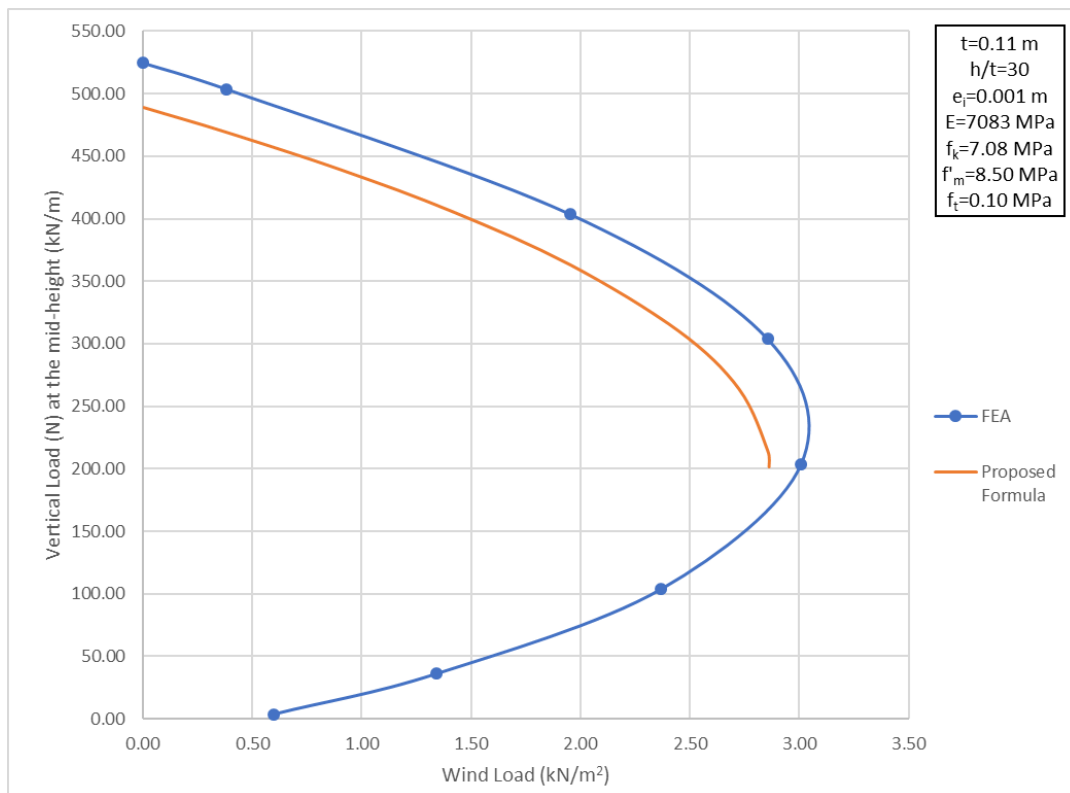
Fig. 172 Verification of the Proposed Formula for a URM Wall with E=7083 MPa, f_k=7.08 MPa and h/t=30
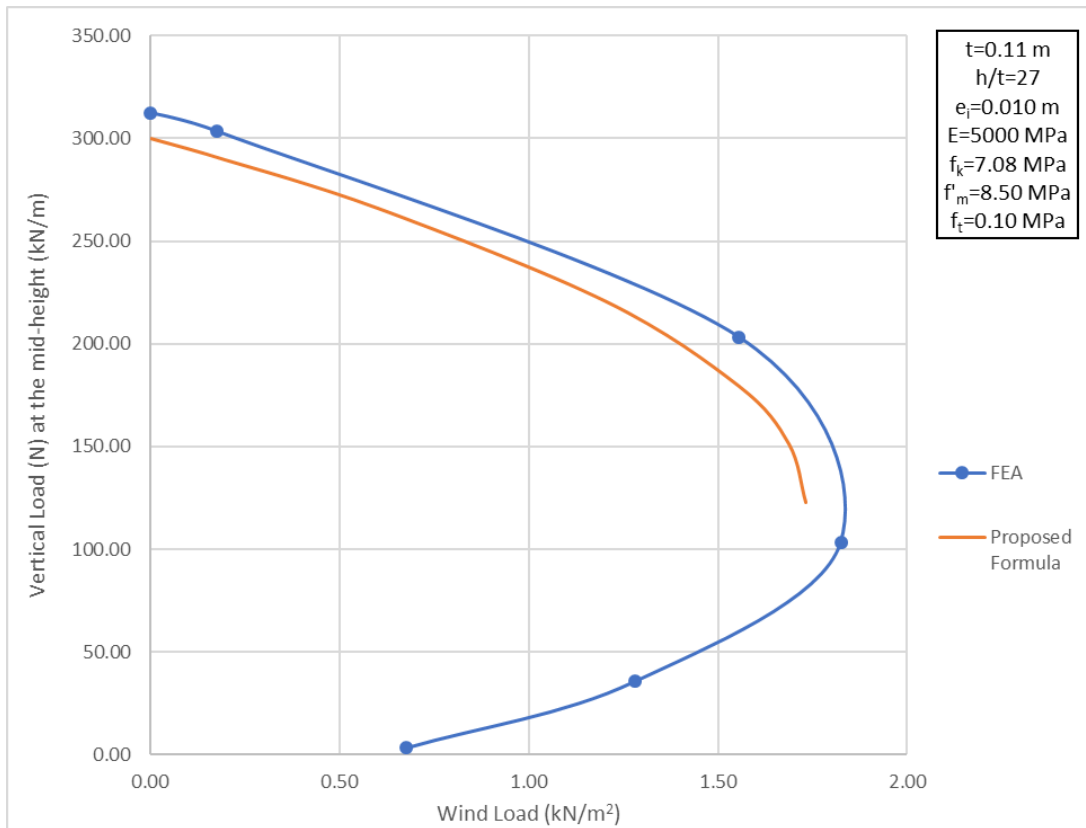
Fig. 173 Verification of the Proposed Formula for a URM Wall with e_i=0.010 m
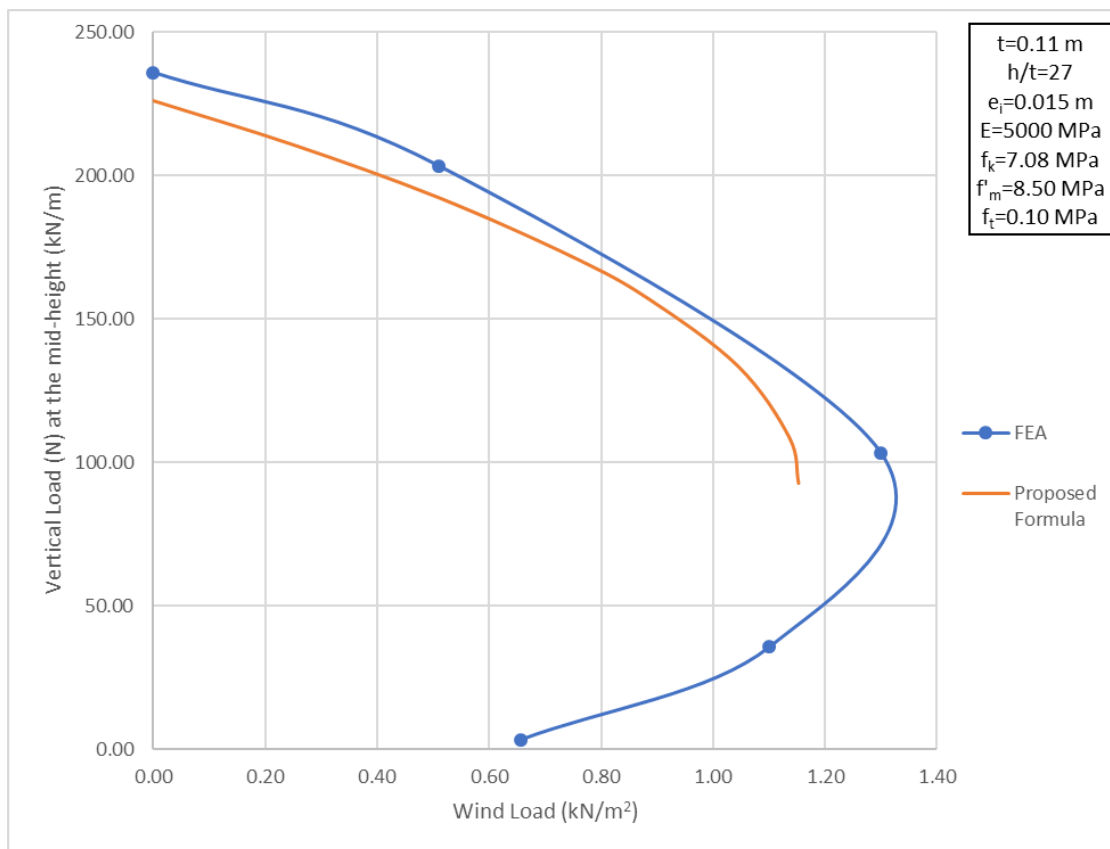
Fig. 174 Verification of the Proposed Formula for a URM Wall with e_i=0.015 m
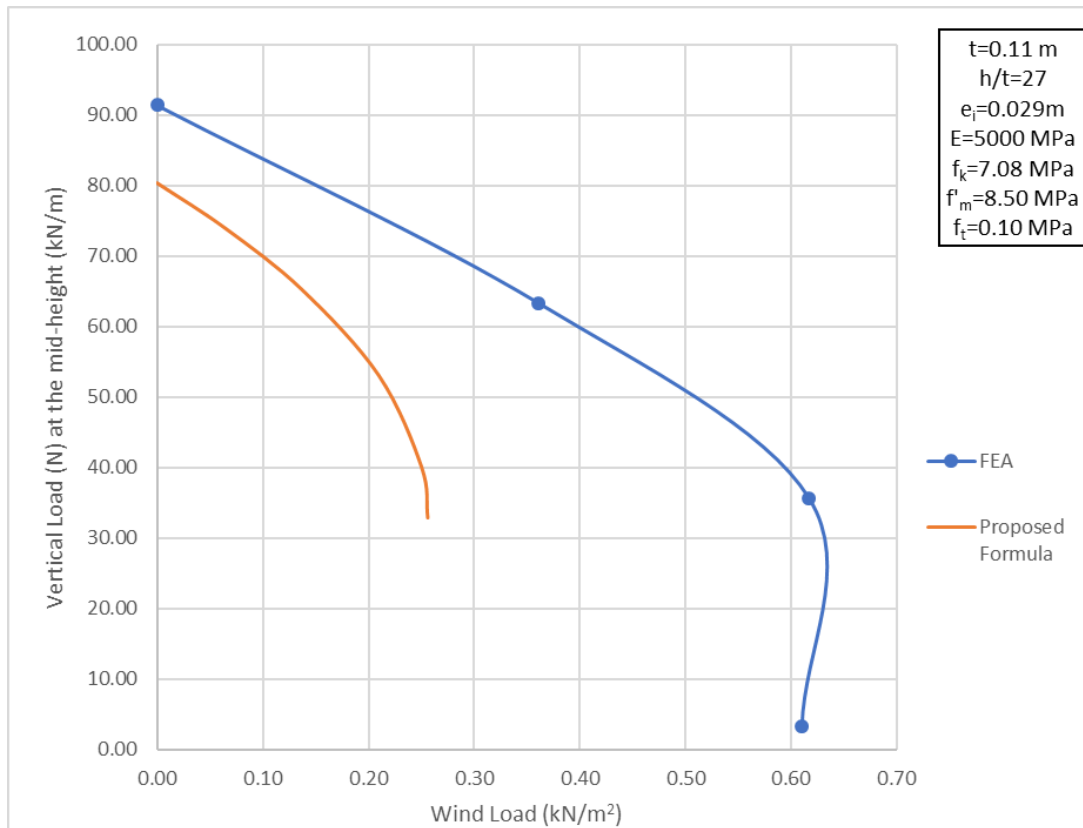
Fig. 175 Verification of the Proposed Formula for a URM Wall with e_i=0.029 m
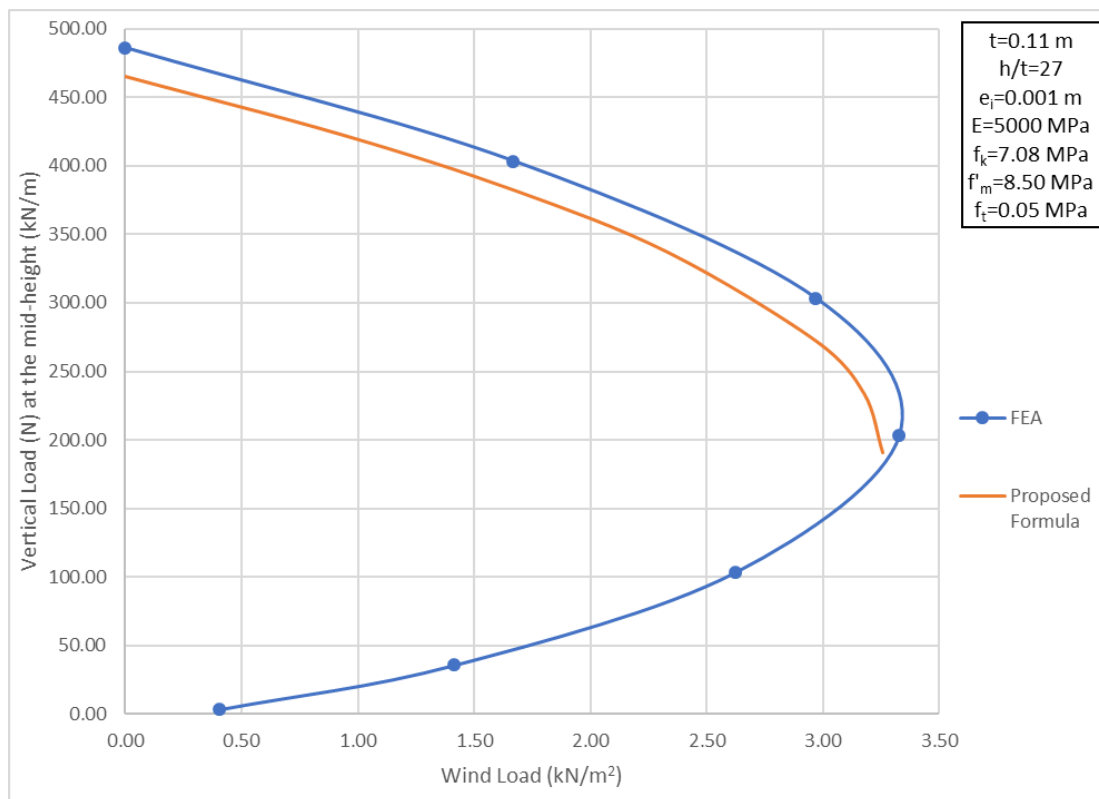
Fig. 176 Verification of the Proposed Formula for a URM Wall with h/t=27 and f_t=0.05 MPa
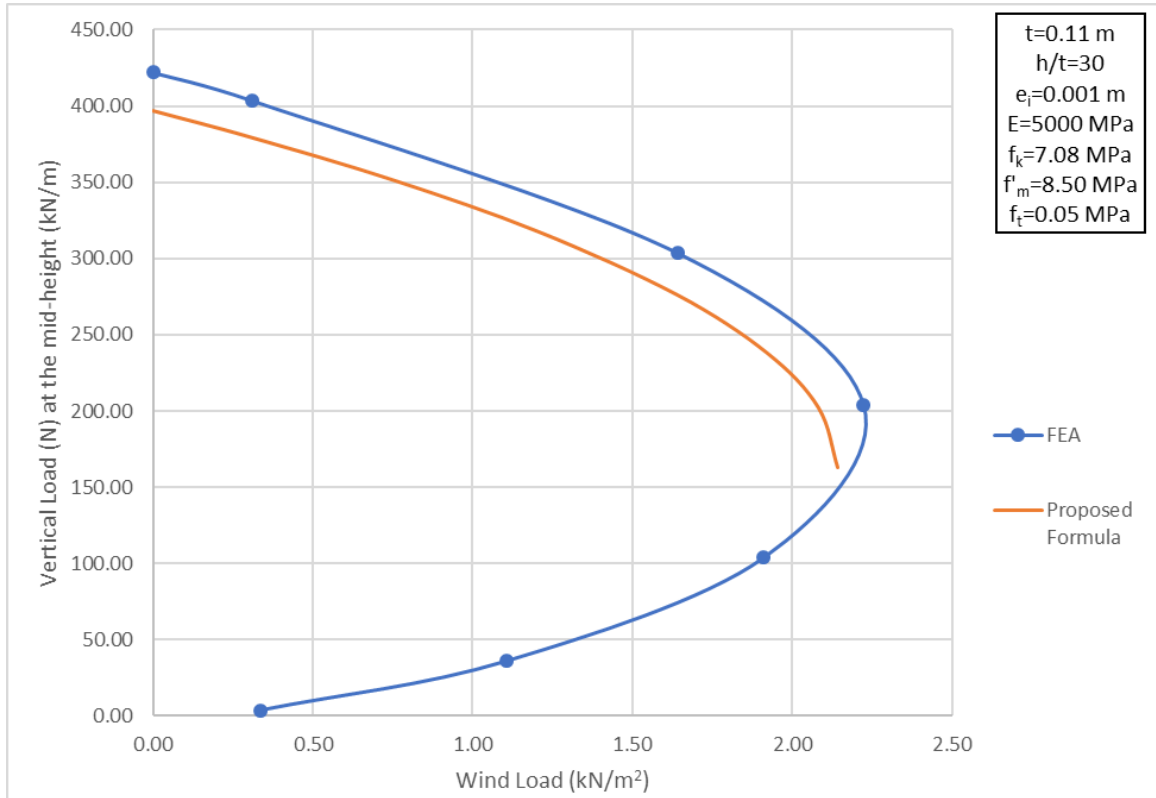
Fig. 177 Verification of the Proposed Formula for a URM Wall with h/t=30 and f_t=0.05 MPa
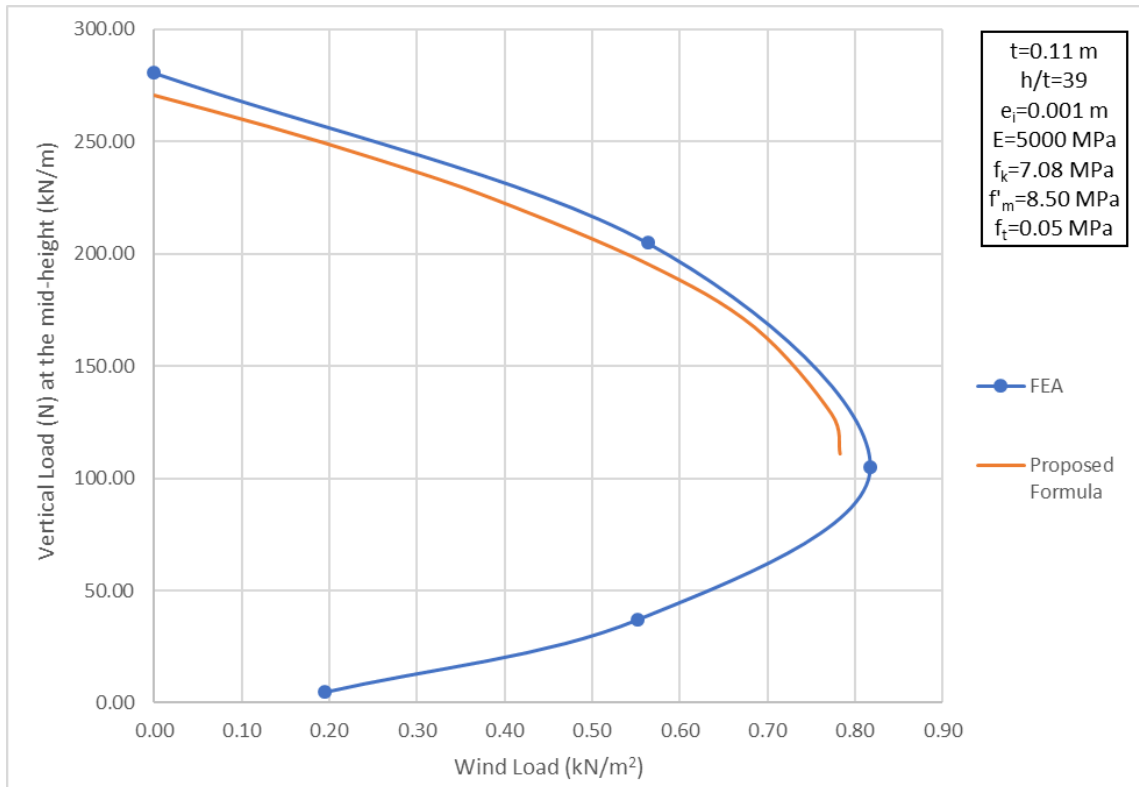
Fig. 178 Verification of the Proposed Formula for a URM Wall with h/t=39 and f_t=0.05 MPa
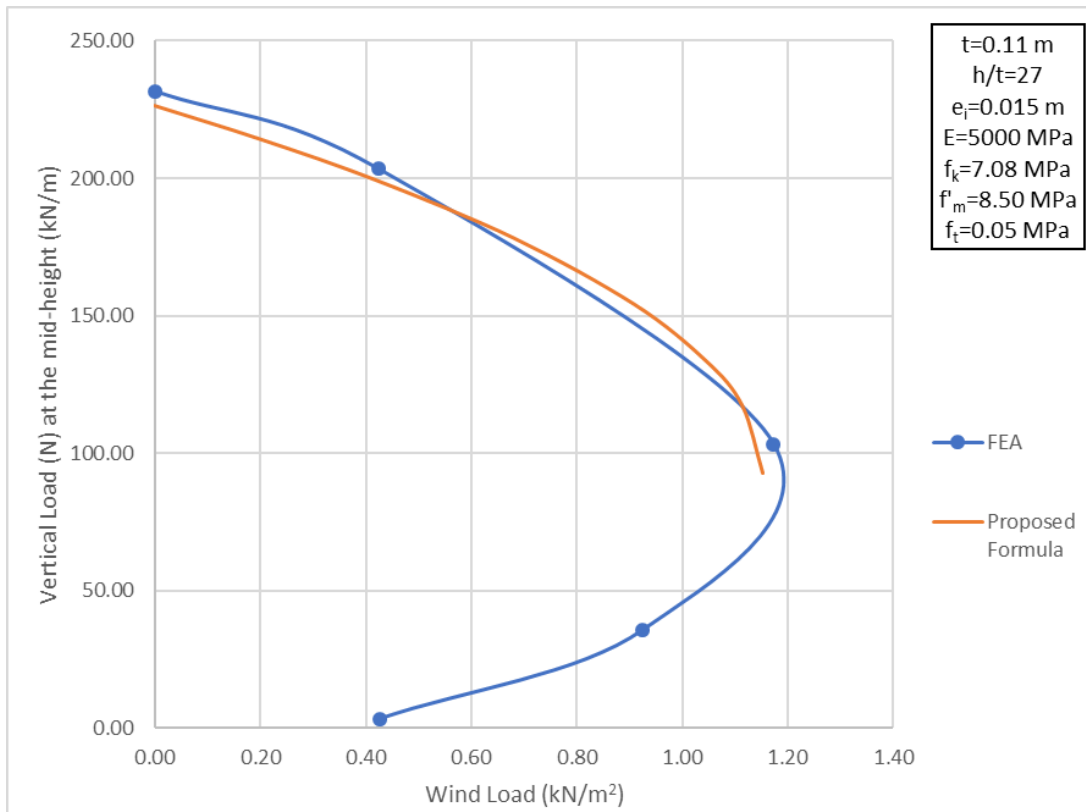
Fig. 179 Verification of the Proposed Formula for a URM Wall with e_i=0.015 m and f_t=0.05 MPa
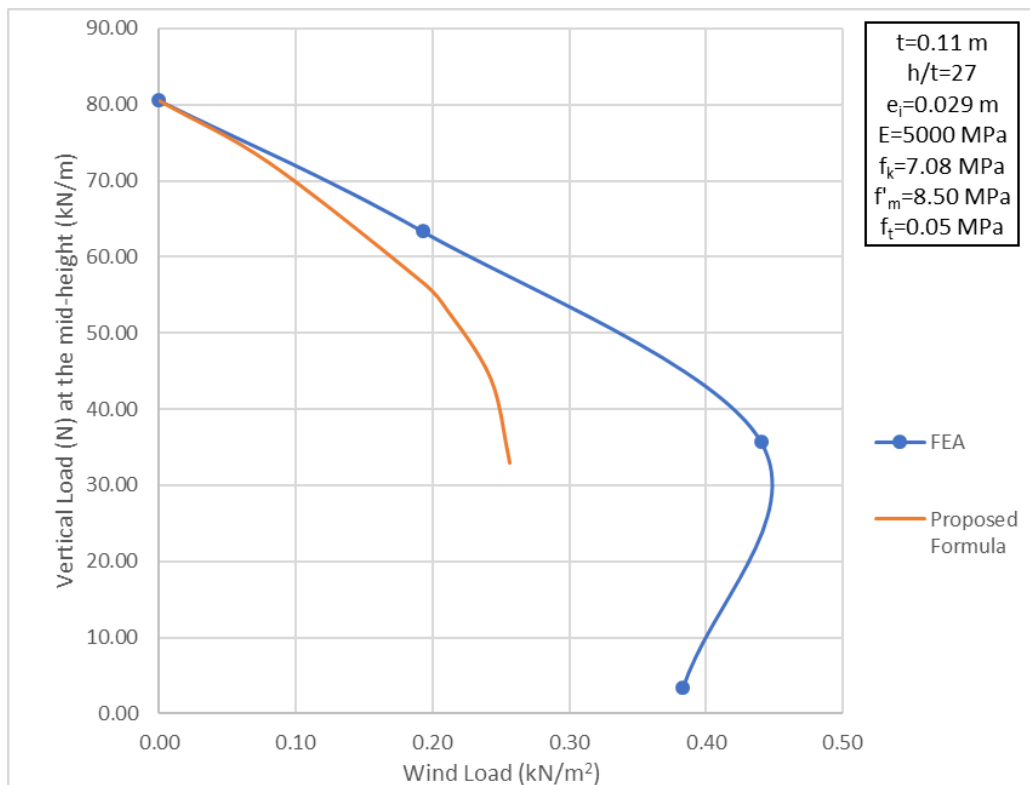
Fig. 180 Verification of the Proposed Formula for a URM Wall with e_i=0.029 m and f_t=0.05 MPa
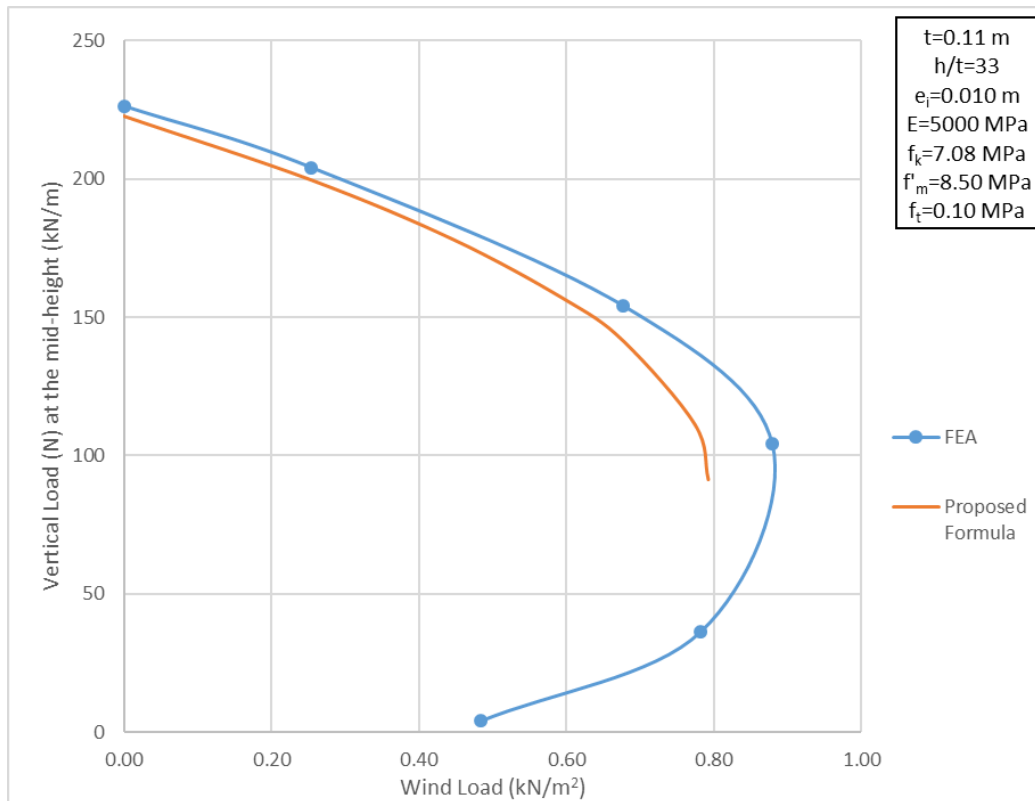
Fig. 181 Verification of the Proposed Formula for a URM Wall with h/t=33 and e_i=0.010 m

10.2 Consideration of the Partial Factor for Material γ_M

The formula in the EN 1996 norm, for the estimation of the vertical resistance of URM walls (Equation 11), makes use of the design compressive strength of masonry. The design compressive strength of masonry is calculated according to Equation 24. That means that, the uncertainty in the compressive strength has the most significant contribution to the uncertainty in the vertical resistance. This is the case for squat walls, where excessive stresses on the material, normally, cause the failure. However, for slender walls, which, usually, fail because of buckling, the uncertainty in the modulus of elasticity, mainly, influences the uncertainty in the vertical resistance. [19] The FE analysis results showed that, both the compressive strength and the modulus of elasticity influence the vertical resistance of slender URM walls. Therefore, both properties are included in the formula in Equation 67. It seems appropriate that, the design value of the vertical resistance is calculated, dividing the expression in Equation 67 with the partial factor for material γ_M. This way, the uncertainty, in the compressive strength, and the uncertainty, in the modulus of elasticity, both affect the uncertainty in the vertical resistance. The design value of the vertical resistance is suggested to be calculated according to Equation 69. For masonry, made with units of category I, and consequences classes CC2 and CC3, the partial factor for material is γ_M=1.70. [42] Furthermore, the design value of the wind load, which is applied on the wall, should be used, for the estimation of the design value of the vertical resistance. Therefore, Equation 68 and Equation 64 are transformed into Equation 70 and Equation 71, respectively.

The graphs, in section 10.1, show the comparison between the curves, from the formula in Equation 67, and the respective curves, from the results from the FE analysis of different cases of existing slender URM walls. The following graphs juxtapose the curves, from the formula in Equation 67, with the respective curves, from the formula in Equation 69. Indicatively, the curves for a certain value of slenderness ratio (h/t), a certain value of eccentricity (e_i), at the top or the bottom of the URM wall, as

well as particular material properties are shown in the graphs in Fig. 182 - Fig. 184. The respective graphs, for the remaining cases, of analyzed URM walls, are included in Appendix F.

Equation 69 Proposed Formula for the Estimation of the Design Value of the Vertical Resistance of existing slender URM walls, subjected to Combined Vertical and Lateral Loading

$$N_{Rd} = \frac{1.49}{\gamma_M} E^{0.60} f_k{}^{0.40} \left(\frac{t_{ef}}{h_{ef}}\right)^{1.46} t \left(1 - 2\frac{e_i}{t}\right)^{2.40} \left(0.41 + 0.59 \sqrt{1 - 18.20 \left(\frac{h_{ef}}{t_{ef}}\right)^{0.38} \left(\frac{f_k}{E}\right)^{0.23} \frac{\frac{e_{wd}}{t}}{1 - 2.10\frac{e_i}{t}}}\right),$$

where:

γ_M: partial factor for material

E: the short-term secant modulus of elasticity

f_k: the characteristic compressive strength

t_{ef}:   the effective thickness of the wall

h_{ef}:   the effective height of the wall

t: the thickness of the wall

e_i: the eccentricity at the top or the bottom of the wall

e_{wd}:   the eccentricity at the mid-height of the wall, caused by the design value of the maximum first-order bending moment on the wall, because of the wind load (Equation 70)

Equation 70 Eccentricity at the mid-height of the URM wall, caused by the design value of the maximum first-order bending moment on the wall, because of the wind load

$$e_{wd} = \frac{M_{wd}}{\frac{1.49}{\gamma_M} E^{0.60} f_k{}^{0.40} \left(\frac{t_{ef}}{h_{ef}}\right)^{1.46} t \left(1 - 2\frac{e_i}{t}\right)^{2.40}},$$

where:

M_{wd}:   the design value of the bending moment at the mid-height of the wall because of the wind load (Equation 71)

γ_M: partial factor for material

E: the short-term secant modulus of elasticity

f_k: the characteristic compressive strength

t_{ef}:   the effective thickness of the wall

h_{ef}:   the effective height of the wall

t: the thickness of the wall

e_i: the eccentricity at the top or the bottom of the wall

Equation 71 Design value of the Maximum First-Order Bending Moment on the wall because of the Wind Load

$$M_{wd} = \frac{w_d \, h^2}{8}, where:$$

w_d: the design value of the wind load

h: the clear storey height
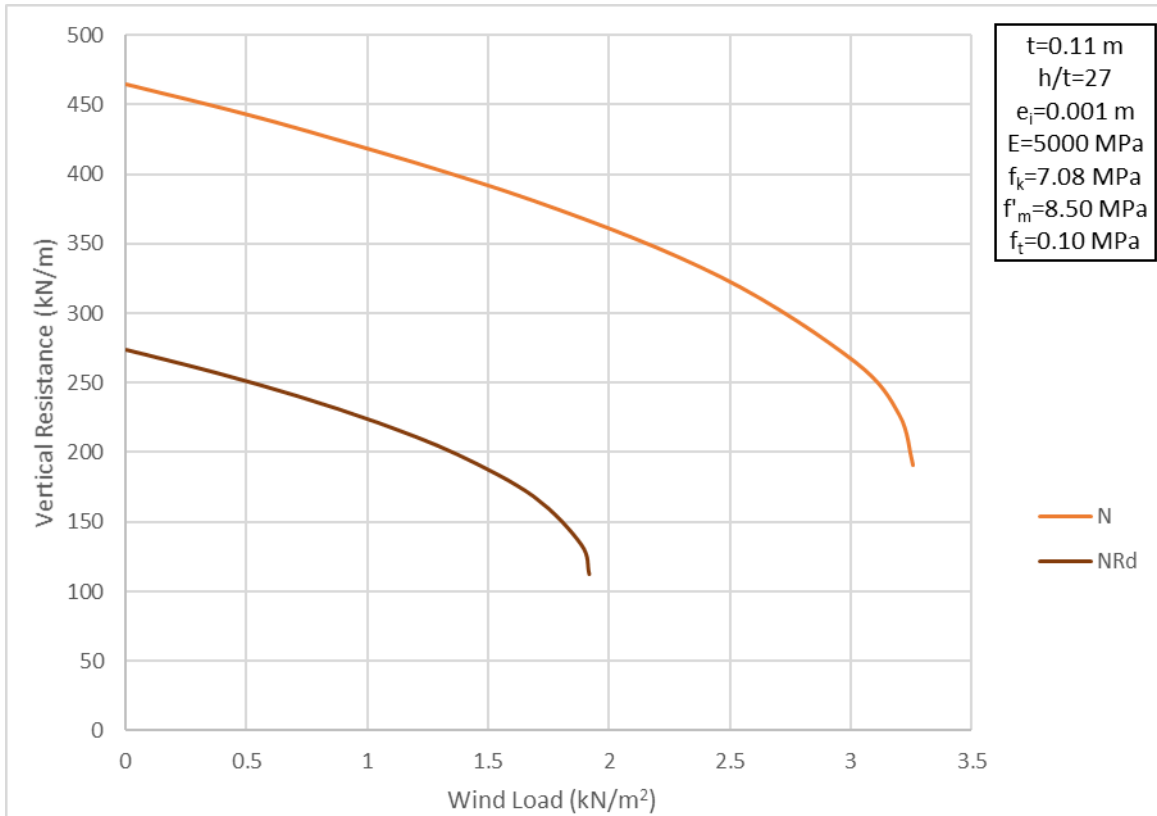
Fig. 182 Curves from formulas in Equation 67 & Equation 69 for a URM wall with h/t=27
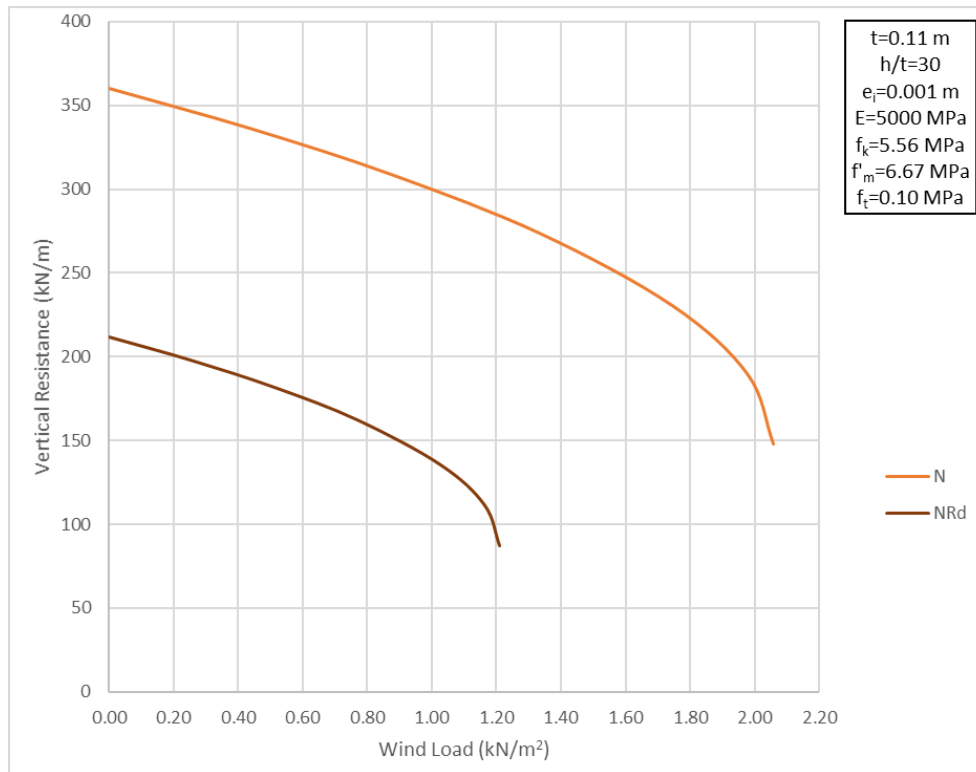
Fig. 183 Curves from formulas in Equation 67 & Equation 69 for a URM Wall with E=5000 MPa, f_k=5.56 MPa and h/t=30
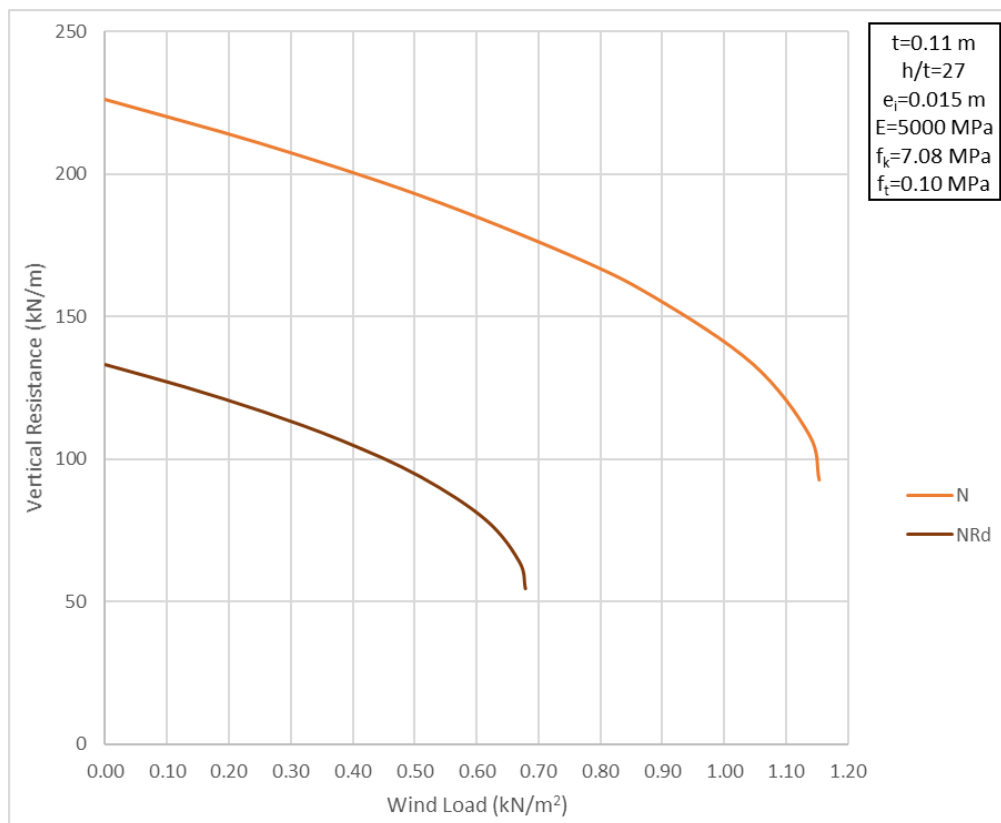
Fig. 184 Curves from formulas in Equation 67 & Equation 69 for a URM Wall with e_i=0.015 m

10.3 Comparison with the EN 1996 Norm

The formula in Equation 69 is proposed as an alternative, to the formula in the EN 1996 norm (Equation 11), for the accurate estimation of the design value of the vertical resistance, of existing slender URM walls, subjected to combined vertical and lateral loading. The walls are in one-way bending. The graphs, in section 10.2, show the curves with the interaction, between the design value of the vertical resistance and the applied wind load, on the URM wall. Different geometrical and material properties of the wall have been considered. It is interesting to compare the results, from the formula in Equation 69, with the respective results, from the formula in the EN 1996 norm (Equation 11). Applying the formula in the EN 1996 norm (Equation 11), respective curves to the ones in the graphs in section 10.2 are created. The juxtaposition of the curves, from the formula in Equation 69, and the respective ones, from the formula in the EN 1996 norm (Equation 11), is shown in the graphs in Fig. 185 - Fig. 201.

The formula, in Equation 69, was derived according to the results, from FE analysis of existing slender URM walls, with different geometrical and material properties (section 9.2). It has been verified that the results, from the formula, are conservative, compared to the respective FE analysis results (section 10.1). The graphs, in Fig. 185 - Fig. 201, show that the EN 1996 norm underestimates the vertical resistance of the analyzed slender URM walls. Especially for large values of wind load, the formula, in Equation 11, results in values of vertical resistance, which are, approximately, equal to zero.
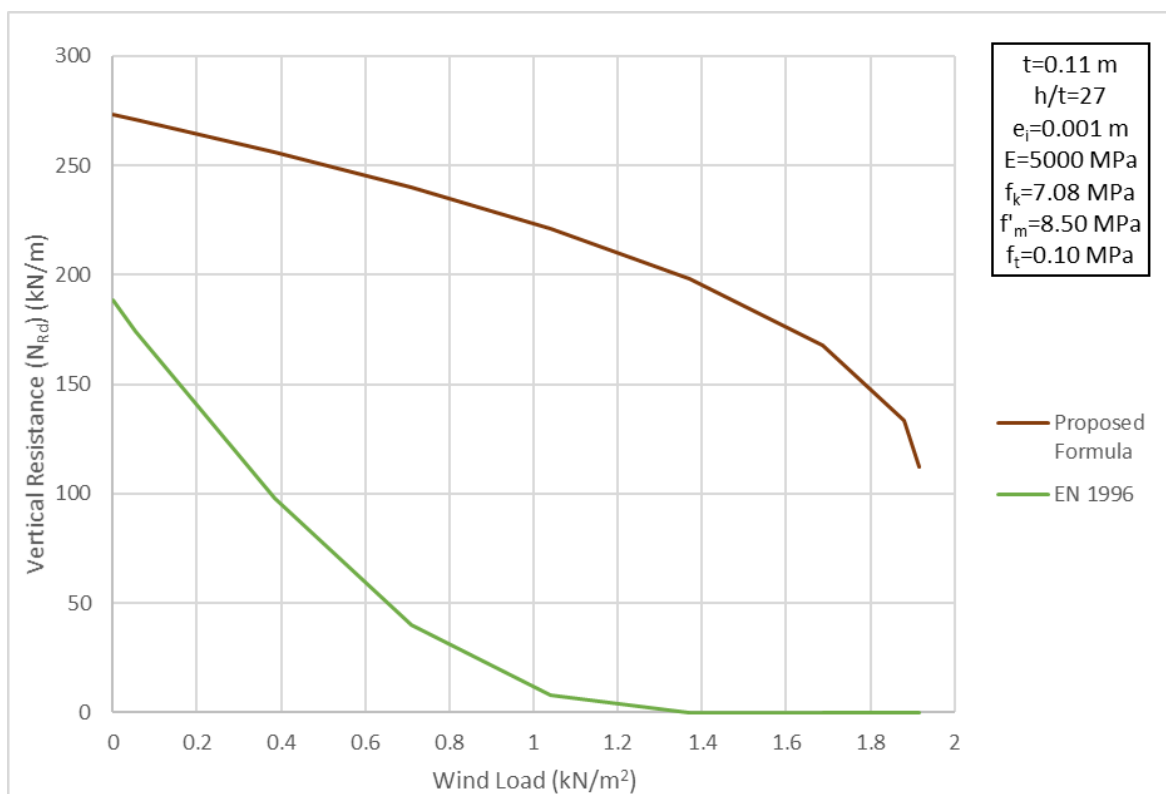
Fig. 185 Comparison between the results from the proposed formula (Equation 69) and the formula in the EN 1996 norm(Equation 11) for a URM wall with h/t=27
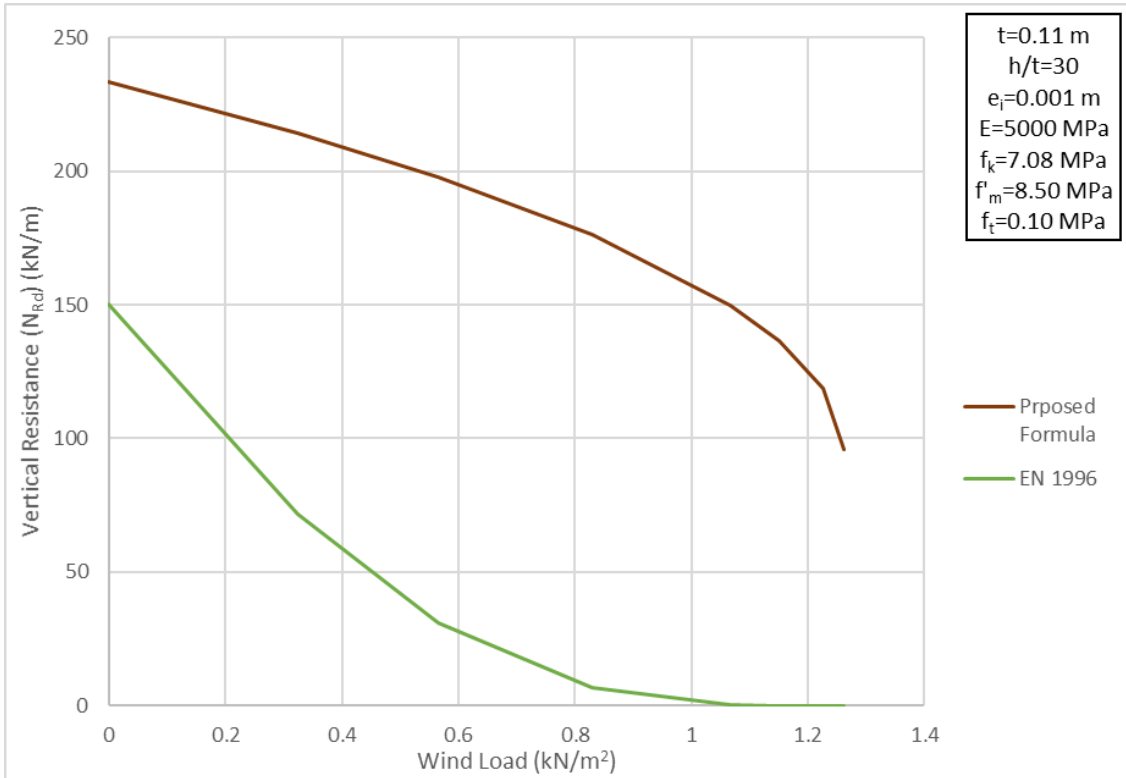
Fig. 186 Comparison between the results from the proposed formula (Equation 69) and the formula in the EN 1996 norm (Equation 11) for a URM wall with h/t=30
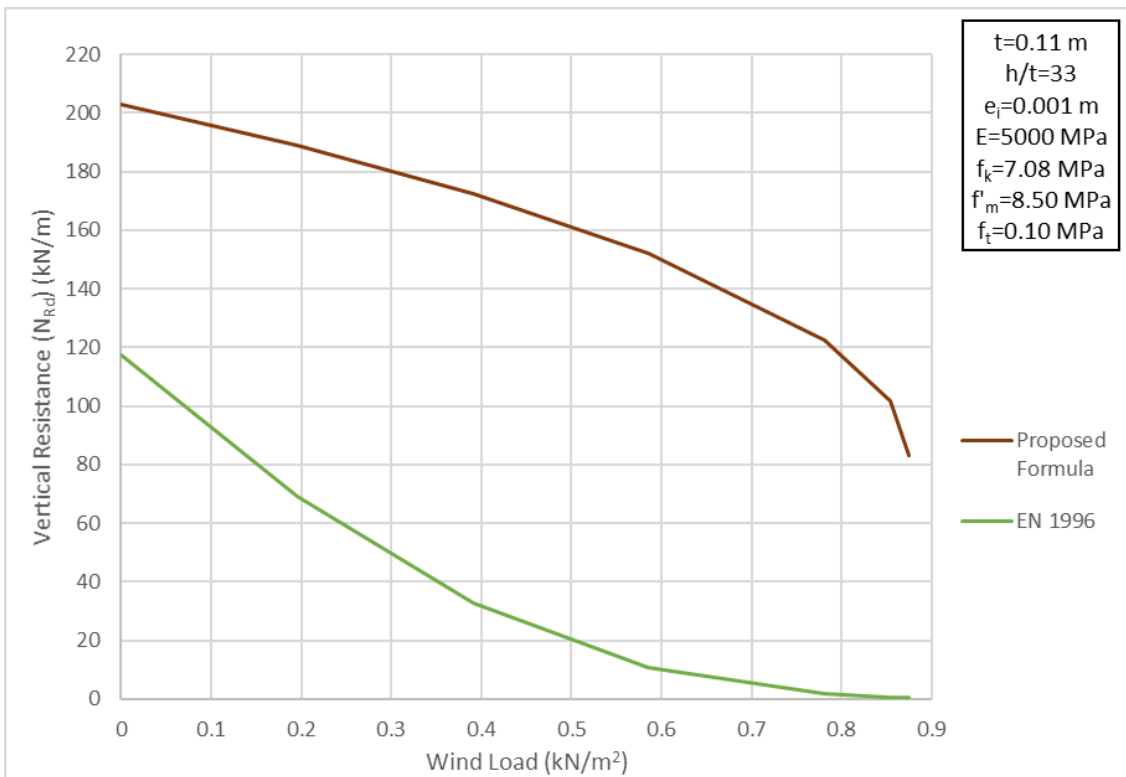
Fig. 187 Comparison between the results from the proposed formula (Equation 69) and the formula in the EN 1996 norm (Equation 11) for a URM wall with h/t=33
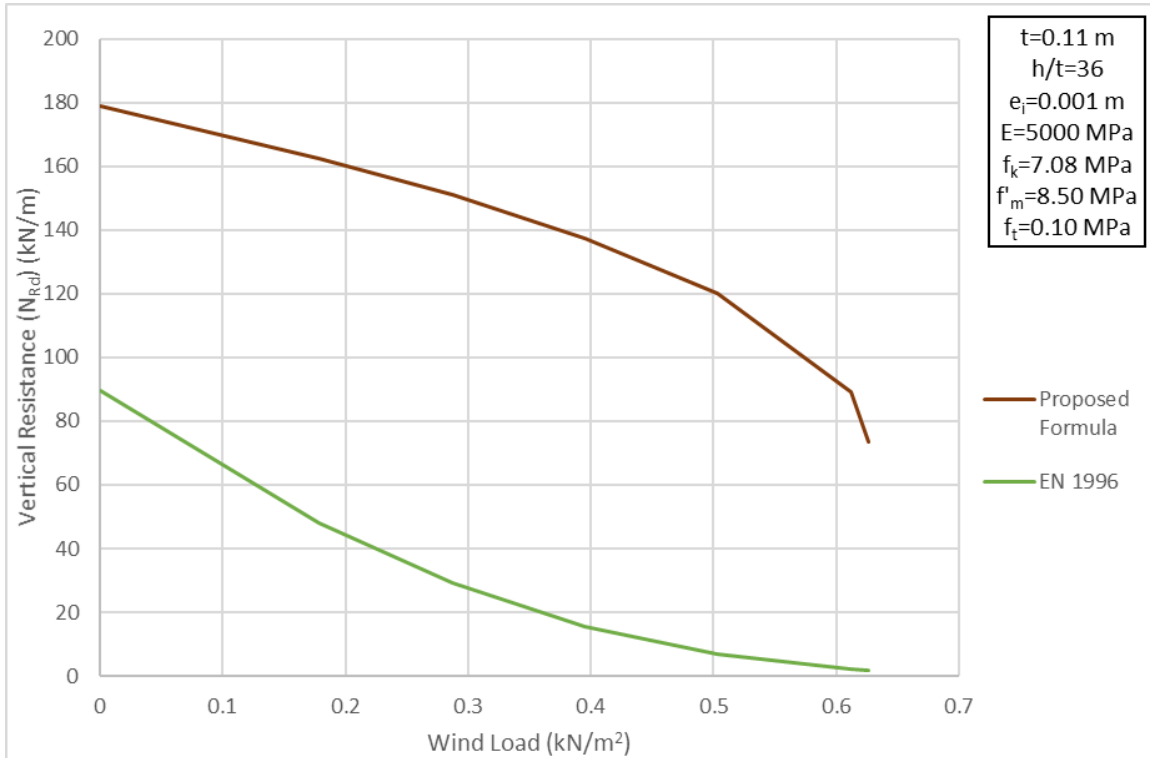
Fig. 188 Comparison between the results from the proposed formula (Equation 69) and the formula in the EN 1996 norm (Equation 11) for a URM wall with h/t=36
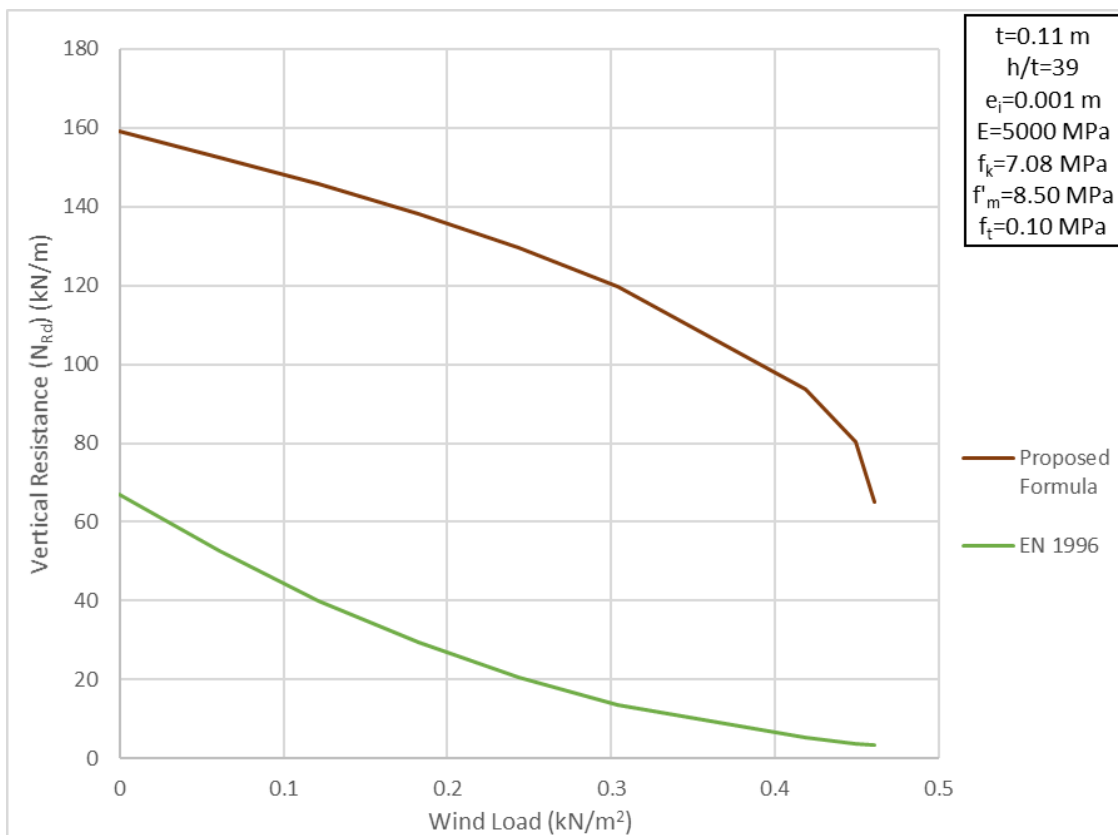
Fig. 189 Comparison between the results from the proposed formula (Equation 69) and the formula in the EN 1996 norm (Equation 11) for a URM wall with h/t=39
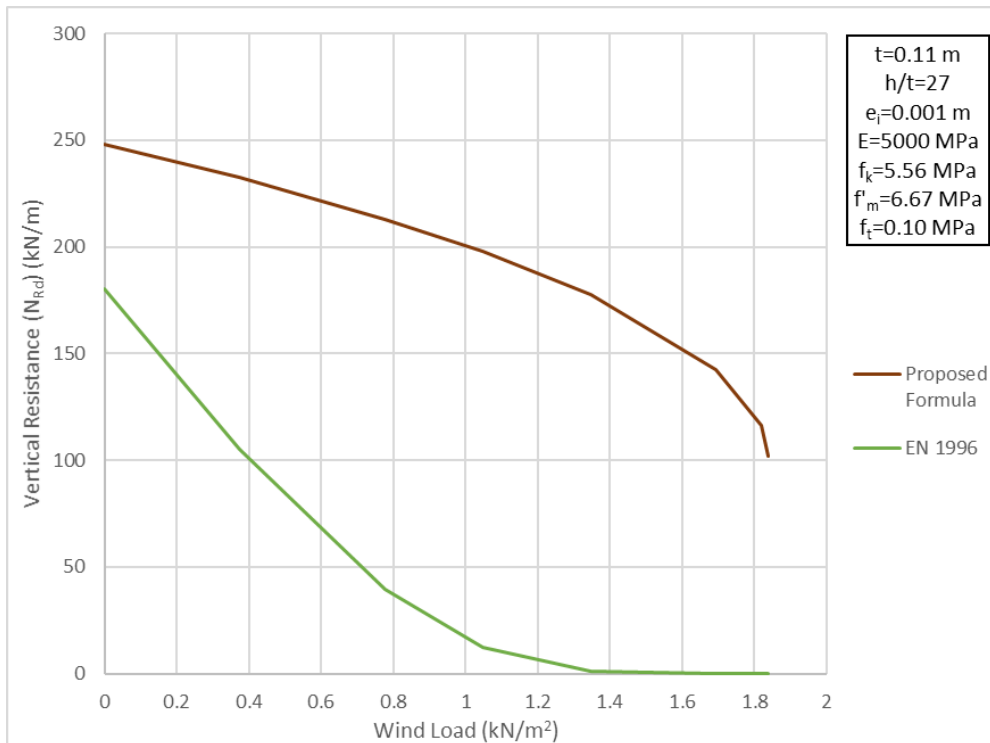
Fig. 190 Comparison between the results from the proposed formula (Equation 69) and the formula in the EN 1996 norm (Equation 11) for a URM wall with E=5000 MPa, f_k=5.56 MPa and h/t=27
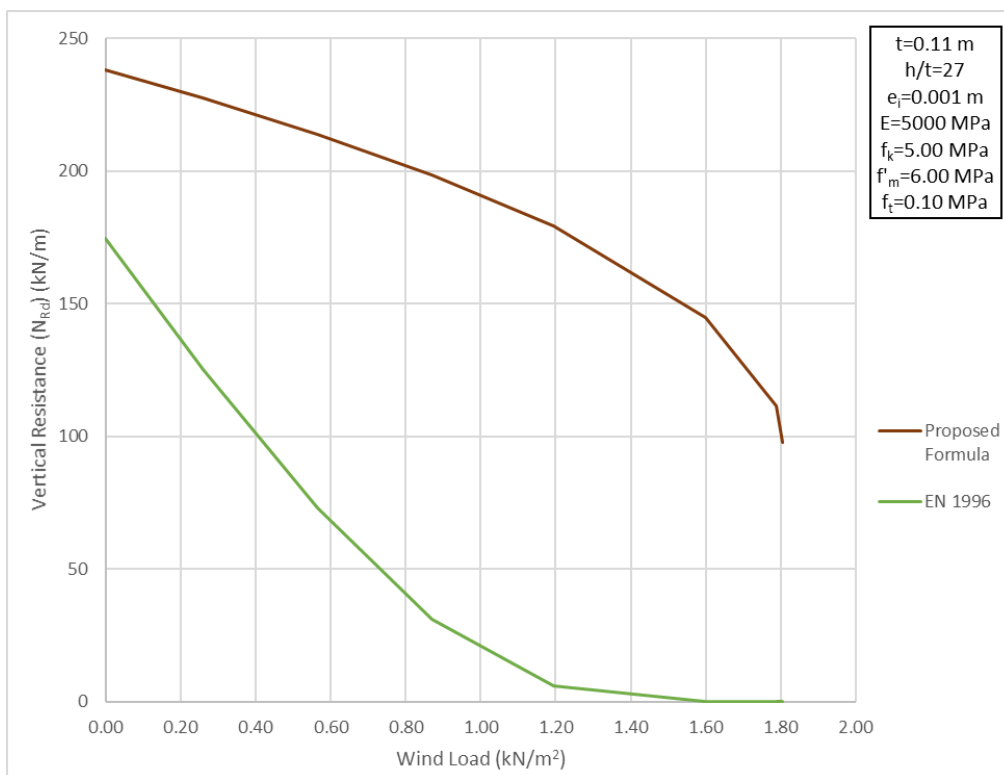
Fig. 191 Comparison between the results from the proposed formula (Equation 69) and the formula in the EN 1996 norm (Equation 11) for a URM wall with E=5000 MPa, f_k=5.00 MPa and h/t=27
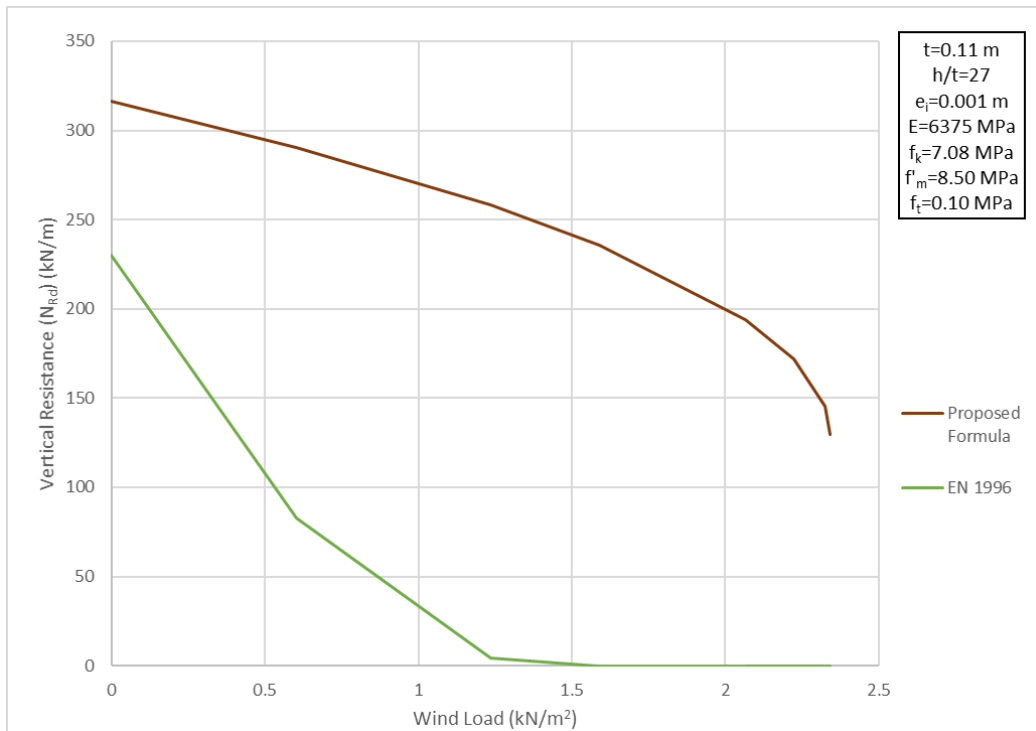
Fig. 192 Comparison between the results from the proposed formula (Equation 69) and the formula in the EN 1996 norm (Equation 11) for a URM wall with E=6375 MPa, f_k=7.08 MPa and h/t=27
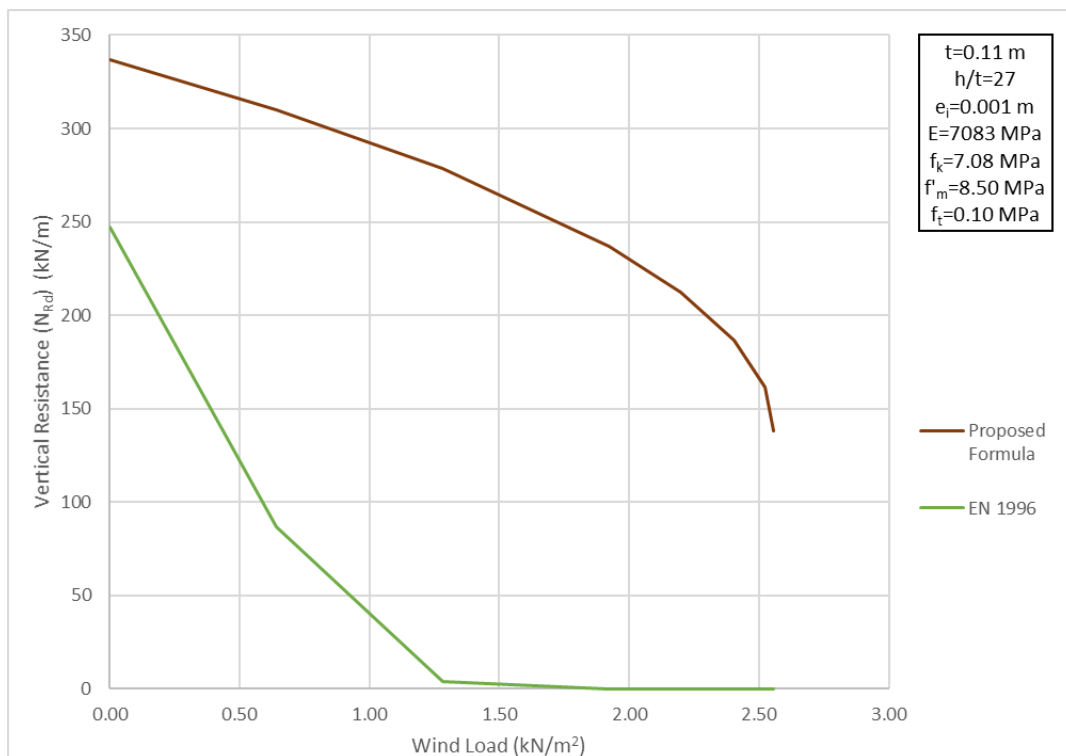
Fig. 193 Comparison between the results from the proposed formula (Equation 69) and the formula in the EN 1996 norm (Equation 11) for a URM wall with E=7083 MPa, f_k=7.08 MPa and h/t=27
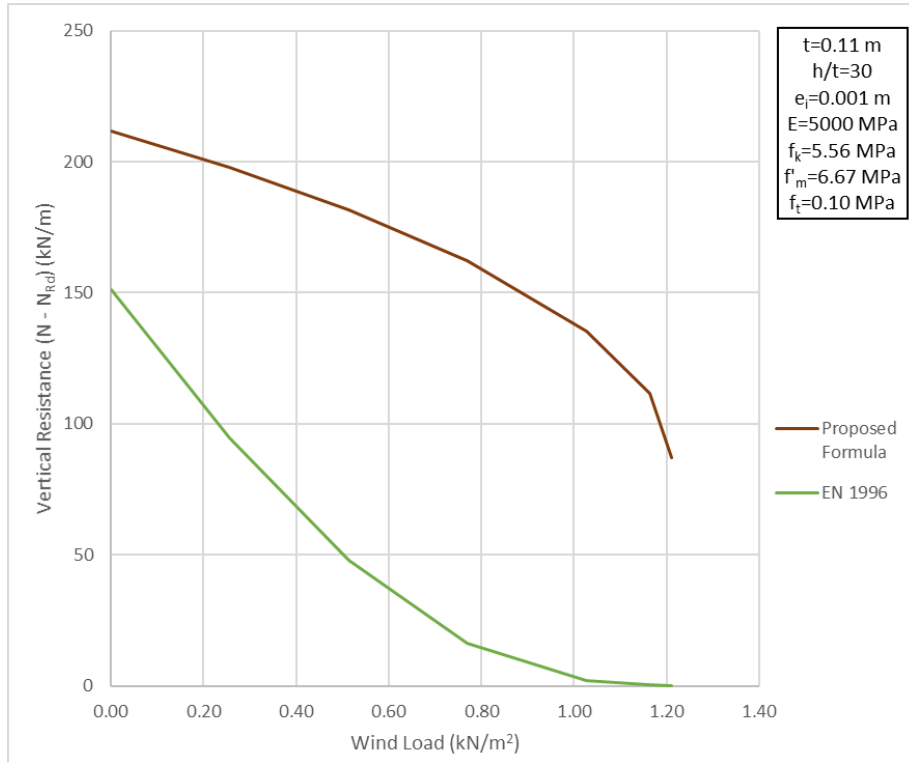
Fig. 194 Comparison between the results from the proposed formula (Equation 69) and the formula in the EN 1996 norm (Equation 11) for a URM wall with E=5000 MPa, f_k=5.56 MPa and h/t=30
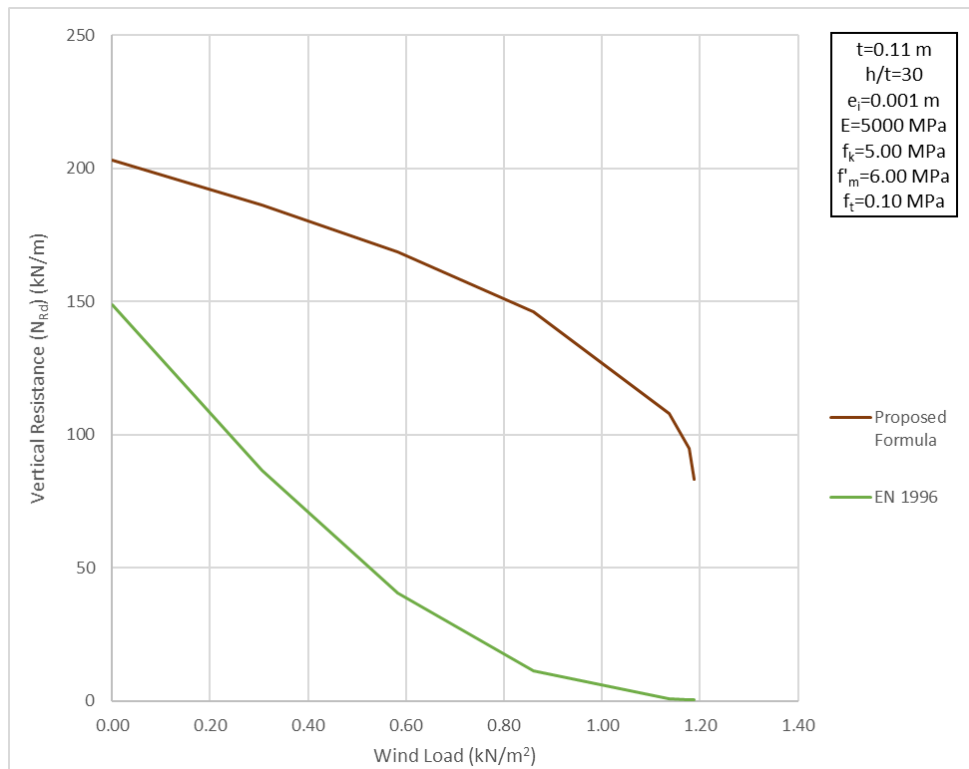
Fig. 195 Comparison between the results from the proposed formula (Equation 69) and the formula in the EN 1996 norm (Equation 11) for a URM wall with E=5000 MPa, f_k=5.00 MPa and h/t=30
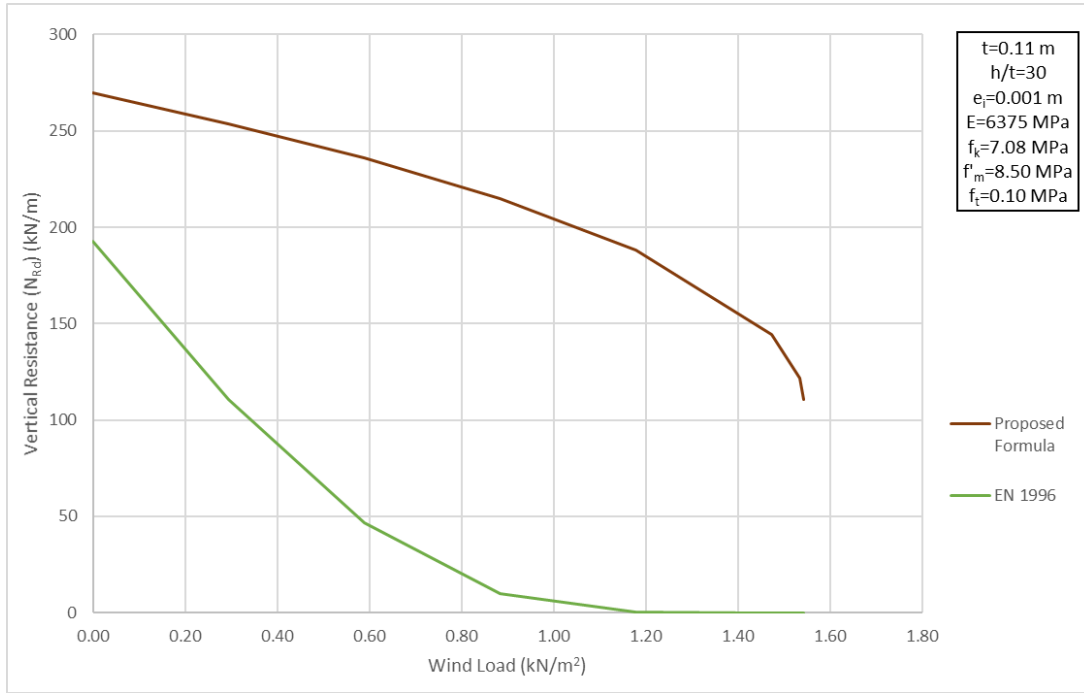
Fig. 196 Comparison between the results from the proposed formula (Equation 69) and the formula in the EN 1996 norm (Equation 11) for a URM wall with E=6375 MPa, f_k=7.08 MPa and h/t=30
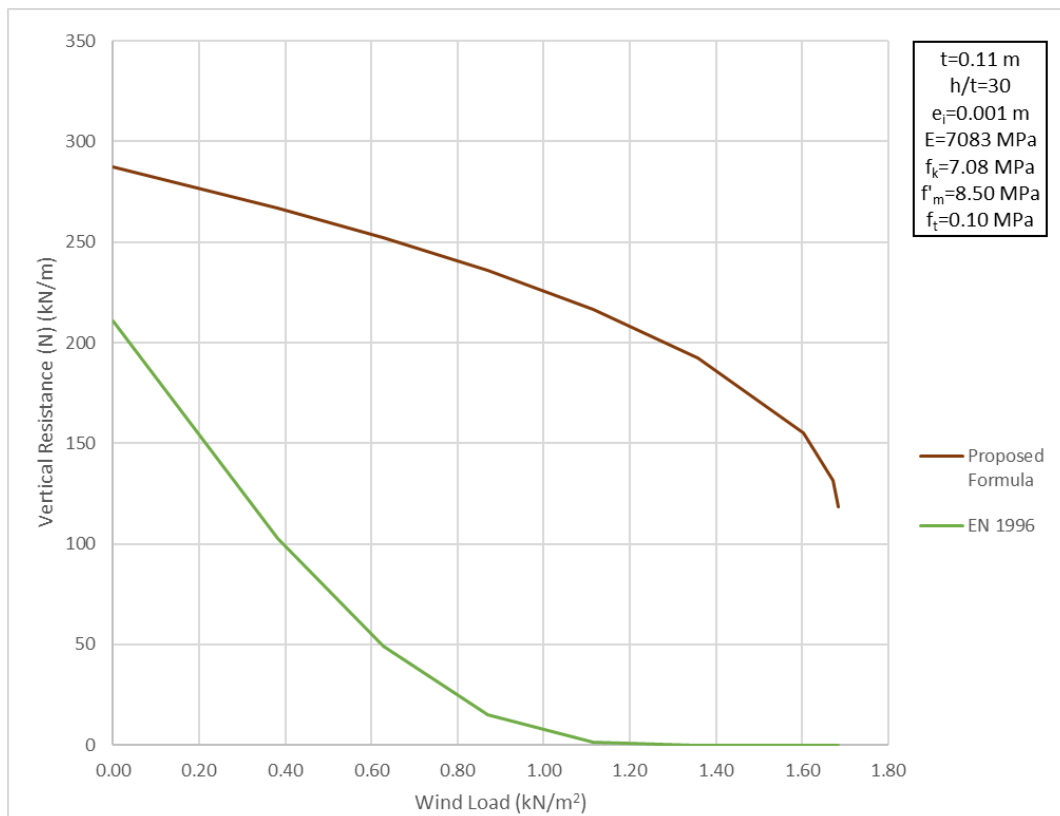
Fig. 197 Comparison between the results from the proposed formula (Equation 69) and the formula in the EN 1996 norm (Equation 11) for a URM wall with E=7083 MPa, f_k=7.08 MPa and h/t=30
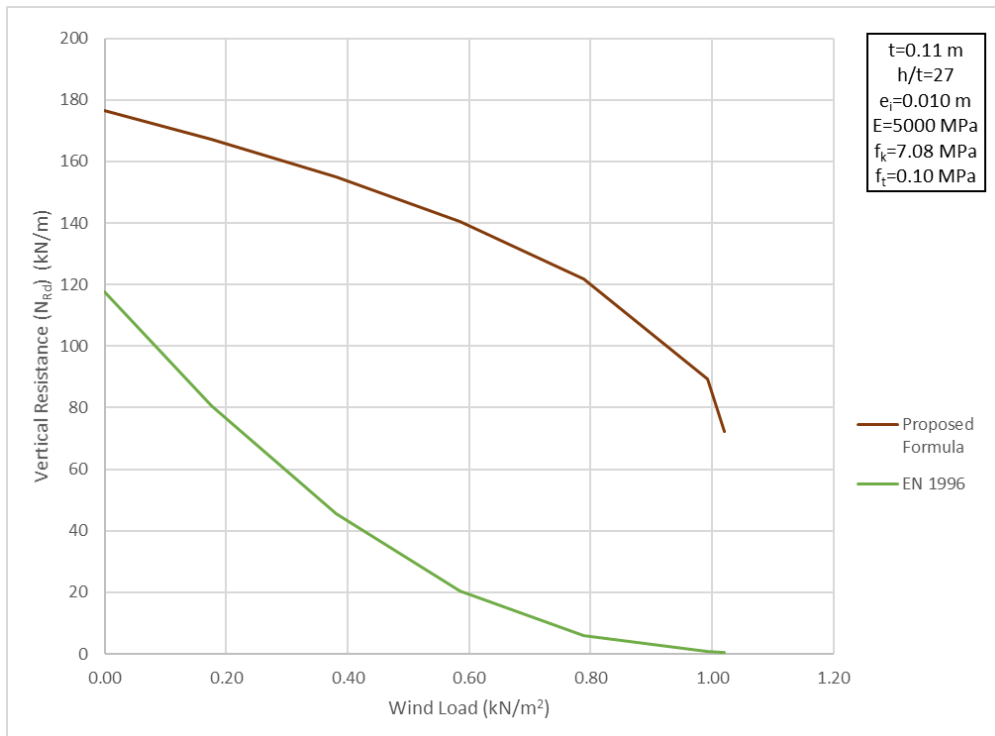
Fig. 198 Comparison between the results from the proposed formula (Equation 69) and the formula in the EN 1996 norm (Equation 11) for a URM wall with e_i=0.010 m
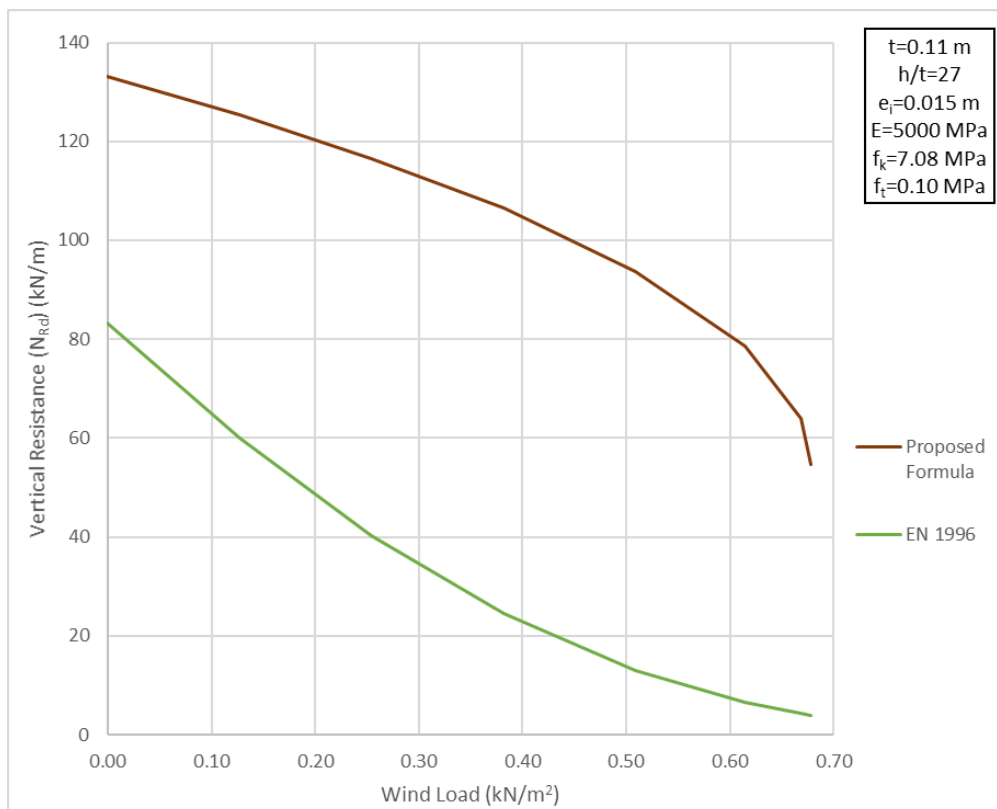
Fig. 199 Comparison between the results from the proposed formula (Equation 69) and the formula in the EN 1996 norm (Equation 11) for a URM wall with e_i=0.015 m
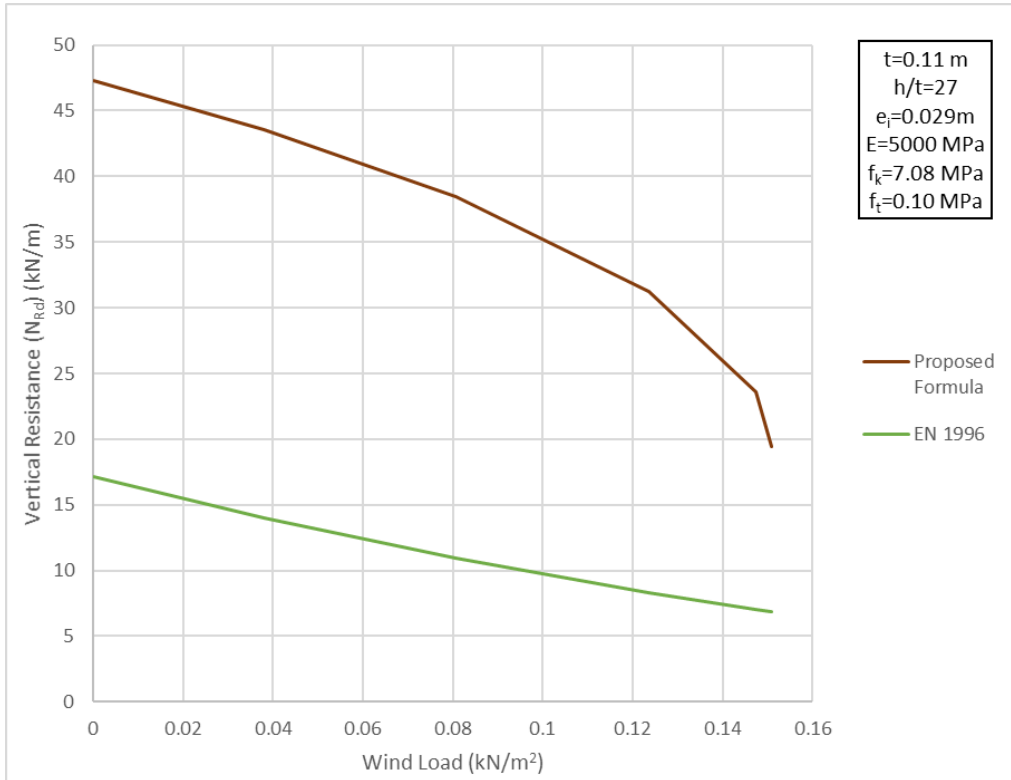
Fig. 200 Comparison between the results from the proposed formula (Equation 69) and the formula in the EN 1996 norm (Equation 11) for a URM wall with e_i=0.029 m
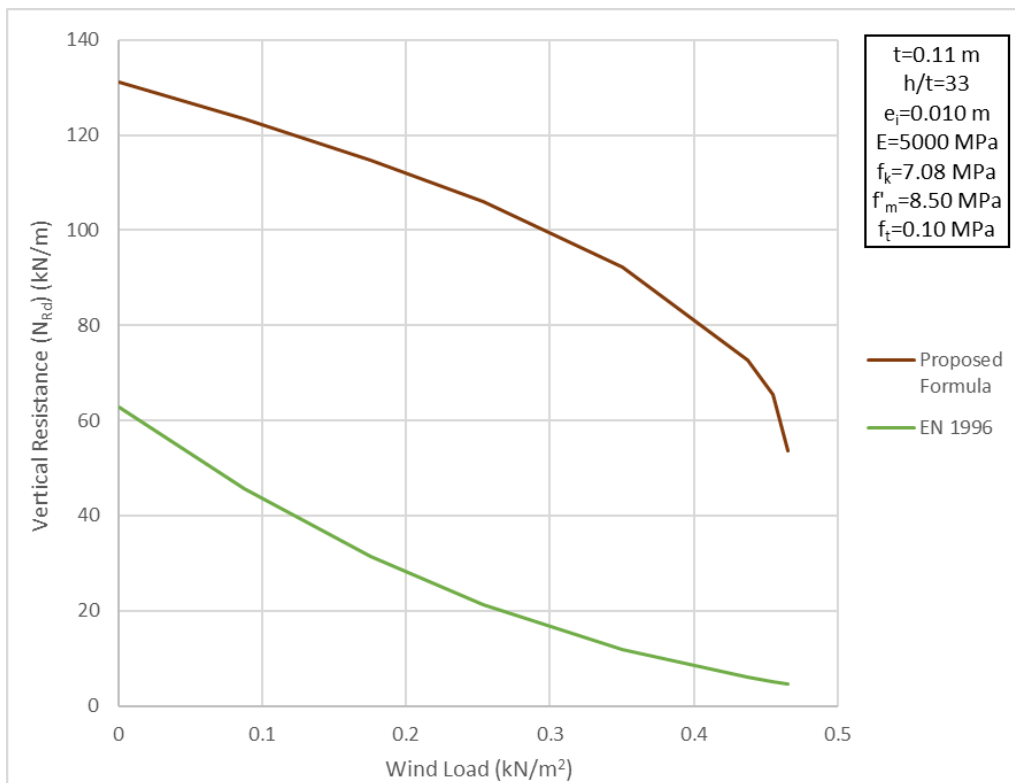
Fig. 201 Comparison between the results from the proposed formula (Equation 69) and the formula in the EN 1996 norm (Equation 11) for a URM wall with h/t=33 and e_i=0.010 m

10.4 Eccentricity due to Creep

According to Equation 15, the EN 1996 norm considers the eccentricity due to creep at the mid-height of URM walls. However, creep effects were not taken into account for the FE analysis (section 9.1.4). Additionally, creep is not addressed in the expressions for eccentricity (e_i, e_w), that the proposed formula, in Equation 69, entails. Therefore, the values of the vertical resistance, that were calculated according to the EN 1996 norm and are shown in the graphs, in section 10.3, were derived, assuming that the eccentricity, at the mid-height of the wall (Equation 15), is caused by loads, only (Equation 16). The eccentricity due to creep was neglected.

The subject of the thesis consists of interior URM walls, restrained on every floor level by timber floors and beams. As it has already been discussed in section 4.3, the beams run through the walls and, therefore, the loads from the floors to the URM walls are applied in the center of the wall section. Additionally, it is considered that the connections, between the timber beams and the URM walls, are not moment resisting. Hence, zero bending moments result at the top and the bottom of the walls, at the floor levels. The eccentricity, at the top or the bottom of the wall (e_i), is caused exclusively by construction imperfections. The latter are taken into consideration with the initial eccentricity (e_{init}). [53] The eccentricity at the mid-height of the wall is equal to the eccentricity at the top or the bottom (e_i), since an initial eccentricity is assumed for the full height of the wall. Introducing the effect of creep, the eccentricity at the mid-height can be estimated according to Equation 72. Creep strains are caused, when the URM wall is subjected to high stresses for a long period of time. [54] As a result, the horizontal displacement of the wall increases. [55] Wind loads are variable actions on structures. [56] Therefore, they cannot create long-term stresses. Thus, it is proposed that the eccentricity due to creep is not added to the eccentricity due to wind load (e_{wd}), at the mid-height of the wall (Equation 70). Furthermore, contrary to the provision in the EN 1996 norm, the eccentricity due to wind load (e_{wd}), at the mid-height of the wall, is not considered in the calculation of the eccentricity due to creep (e_k). This is obvious in Equation 73. Because of the addition of the eccentricity due to creep (Equation 73) to the eccentricity at the mid-height of the wall (Equation 72), the proposed formula, for the estimation of the design value of the vertical resistance of existing slender URM walls, subjected to combined vertical and lateral loading (Equation 69), is modified (Equation 74).

Equation 72 Eccentricity at the mid-height of the wall

$$e_{mk} = e_i + e_k,$$

where:

   e_i: the eccentricity at the top or bottom of the wall

   e_k: the eccentricity due to creep (Equation 73)

Equation 73 Proposed expression for calculating the eccentricity due to creep at the mid-height of the wall

$$e_k = 0.002 \, \varphi_\infty \frac{h_{ef}}{t_{ef}} \sqrt{t_{ef} \, e_i},$$

where:

ϕ_∞: the final creep coefficient

h_{ef}: the effective height of the masonry wall

t_{ef}: the effective thickness of the masonry wall

e_i: the eccentricity at the top or bottom of the wall

Equation 74 Formula for the Estimation of the Design Value of the Vertical Resistance of slender URM walls, subjected to Combined Vertical and Lateral Loading, considering Effects of Creep

$$N_{Rd} = \frac{1.49}{\gamma_M} E^{0.60} f_k^{\ 0.40} \left(\frac{t_{ef}}{h_{ef}}\right)^{1.46} t \left(1 - 2\,\frac{e_{mk}}{t}\right)^{2.40} \left(0.41 + 0.59 \sqrt{1 - 18.20 \, (\tfrac{h_{ef}}{t_{ef}})^{0.38} \, (\tfrac{f_k}{E})^{0.23} \, \frac{\frac{e_{wd}}{t}}{1 - 2.10\frac{e_{mk}}{t}}}\right),$$

where:

γ_M: partial factor for material

E: the short-term secant modulus of elasticity

f_k: the characteristic compressive strength

t_{ef}: the effective thickness of the wall

h_{ef}: the effective height of the wall

t: the thickness of the wall

e_{mk}: the eccentricity at the mid-height of the wall (Equation 72)

e_{wd}: the eccentricity at the mid-height of the wall, caused by the design value of the maximum first-order bending moment on the wall, because of the wind load (Equation 75)

Equation 75 Eccentricity at the mid-height of the URM wall, caused by the design value of the maximum first-order bending moment on the wall, because of the wind load (effects of creep are considered in the eccentricity at the mid-height (e_{mk}))

$$e_{wd} = \frac{M_{wd}}{\frac{1.49}{\gamma_M} E^{0.60} f_k{}^{0.40} \left(\frac{t_{ef}}{h_{ef}}\right)^{1.46} t \left(1 - 2\frac{e_{mk}}{t}\right)^{2.40}},$$

where:

M_{wd}:   the design value of the bending moment at the mid-height of the wall because of the wind load (Equation 71)

γ_M: partial factor for material

E: the short-term secant modulus of elasticity

f_k: the characteristic compressive strength

t_{ef}:   the effective thickness of the wall

h_{ef}:   the effective height of the wall

t: the thickness of the wall

e_{mk}:   the eccentricity at the mid-height of the wall (Equation 72)

11 Conclusions

11.1 General

The major objective of the research, within this master thesis, comprised the definition and validation of an appropriate method, for the verification of slender URM walls in one-way bending, under combined vertical and lateral loading. The verification of walls is a task of the assessment of the structural capacity of existing masonry buildings.

The European Standard EN 1996 is currently the national standard, used by the members of CEN, for the design of masonry structures. The specified maximum value of slenderness ratio is equal to 27, for masonry walls, subjected to mainly vertical loading. Initially, the formula, in the EN 1996 norm, was used for the calculation of the vertical resistance of the case study of URM wall. The case study is one of the slenderest URM walls, that form the structure of an existing building block in Amsterdam. The slenderness ratio of the wall is, approximately, equal to 27. Different properties of masonry have been taken into account. The properties are indicative of existing masonry buildings in the Netherlands, constructed during the late 19th – early 20th century. Although the EN 1996 norm and the Dutch National Annex to the norm suggest certain relationships, between the short-term secant modulus of elasticity (E) and the characteristic compressive strength (f_k) of masonry, different values, of the ratio E/f_k, were considered. Relevant literature mentions, that the assumed range of values, of the ratio E/f_k, have been noticed after experimental tests on brickwork. The results from the proposed formula, in the EN 1996 norm, showed that the vertical resistance of the URM wall decreases while the compressive strength of the masonry increases. More specifically, when the short-term secant modulus of elasticity remains constant and the ratio E/f_k decreases (the characteristic compressive strength increases), the vertical resistance decreases. This is shown in Fig. 202. Hence, the formula for the calculation of the vertical resistance, in the EN 1996 norm, describes a rather paradoxical behavior of masonry walls.
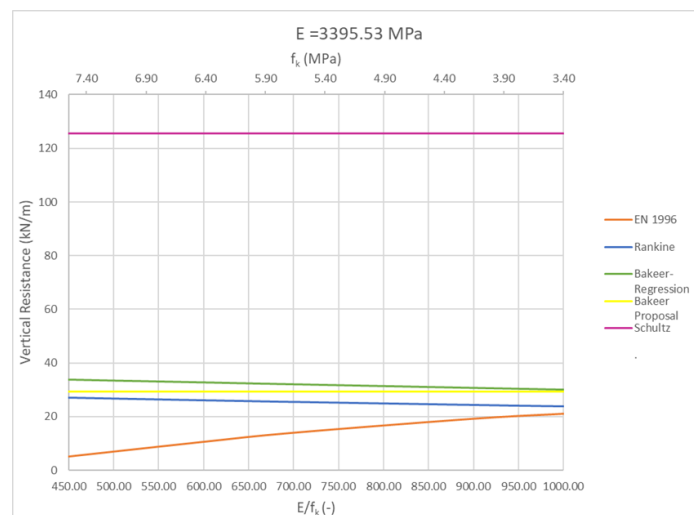
Fig. 202 Variation in the Vertical Resistance when the Compressive Strength Changes and the Modulus of Elasticity is Constant

To develop a formula for the verification of existing slender masonry walls, reference values of the vertical resistance were necessary. Therefore, the response of URM walls, subjected to combined vertical and lateral loading, was estimated according to the results of FE analysis. A macro-model of the wall was created. The model is, actually, the cross-section of the wall. This modeling technique

was considered appropriate for the specific support conditions of the studied wall. The wall is simply supported along its top and bottom edges. The case study of URM wall was the reference for the geometry of the FE model. The properties of masonry, that are prescribed in the NPR 9998-2018 norm, were the input for the initial material model. Every time one parameter, relevant to the resistance of the URM wall, changed in the model. Namely, the slenderness ratio, the eccentricity, at the top and bottom edges, as well as the characteristic compressive strength, the short-term secant modulus of elasticity and the tensile strength of masonry. Graphs with the combinations of vertical load – wind load, that lead the wall to failure, were created for every case of analyzed URM wall. The interaction between vertical load and wind load, according to the results from the FE analysis, is comparable to the interaction, which is derived from the analytical solutions, for critical axial loads, that Schultz defined, for URM members, under the combination of eccentric compression loads and lateral loads. Therefore, the analytical solutions formed the basis, for developing an appropriate formula, for the estimation of the vertical resistance of existing slender URM walls, subjected to combined vertical and lateral loading.

A formula is proposed for calculating the vertical resistance of existing slender URM walls, subjected to combined vertical and lateral loading. The vertical resistance is a function of various parameters. Namely, the slenderness ratio of the wall, the short-term secant modulus of elasticity and the characteristic compressive strength of masonry as well as the eccentricity, at the top and the bottom of the wall, and the eccentricity, caused by the maximum first-order bending moment, due to the wind load. Appropriate expressions introduce the influence, of the aforementioned parameters, in the formula for the estimation of the vertical resistance. The influence of each parameter was defined according to the results of the FE analysis. The proposed formula was verified by comparing its results with the respective results, from the FE analysis. An indicative comparison is shown in Fig. 203.

It was noticed that, the tensile strength of masonry has a considerable effect on the vertical resistance of existing slender URM walls, when the value of eccentricity at the top and the bottom, is large. Additionally, for higher values of slenderness ratio and significant wind load, on the wall, increasing the tensile strength can enhance the vertical resistance. Thus, the tensile strength of masonry has a combined effect, with the slenderness ratio, the eccentricity, at the top and the bottom of the wall, and the magnitude of wind load, on the vertical resistance of existing slender URM walls. Therefore, it becomes complicated to define an appropriate expression for the tensile strength and introduce it in the proposed formula. Furthermore, an attempt, by Sandoval & Roca, to include the contribution of the tensile strength, in the estimation of the vertical resistance, of slender URM walls, resulted in a rather cumbersome expression. Taking everything into consideration, the influence of the tensile strength of masonry is not included in the proposed formula. Some cases of URM walls were analyzed with the FE method, considering half the value of the tensile strength, prescribed in the NPR 9998-2018 norm, for the material model. The results, from the latter analyses, were compared with the results, from the proposed formula. It was noticed that the actual vertical resistance, of existing slender URM walls, when the tensile strength of masonry is halved, is larger than the respective value, which is estimated from the proposed formula. Hence, the proposed formula, for the estimation of the vertical resistance, can bring the structural assessment of slender URM walls, in existing buildings, to the safe side. The latter is concluded, considering the role of the tensile strength in the capacity of existing slender URM walls. The tensile strength could be an asset for the vertical resistance. The bond between the brick and the lime mortar is durable and the extent of bond is, also, significant. Additionally, the tensile strength could be the reason why existing slender URM walls have been standing for approximately 100 years, whereas, according to the EN 1996 norm, their vertical resistance is, frequently, not adequate for the applied loads.
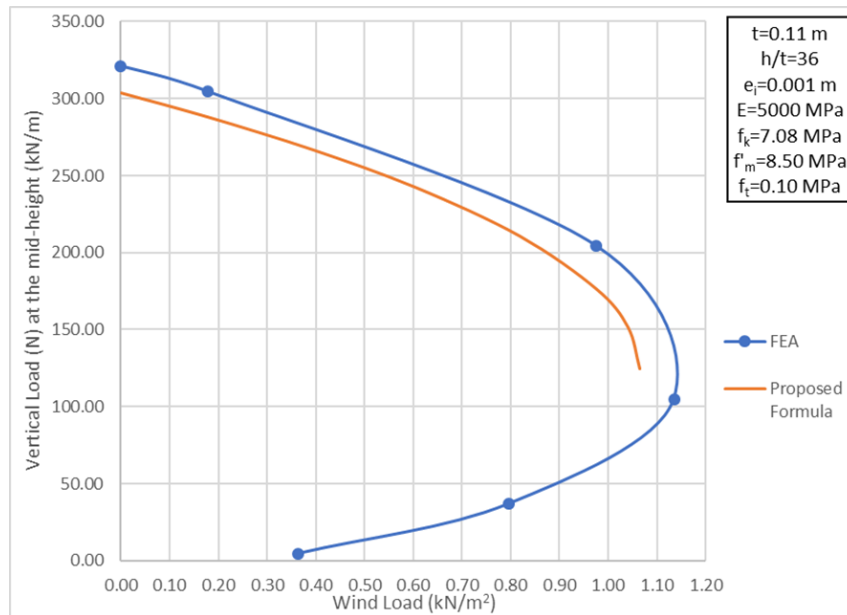
Fig. 203 Verification of the Proposed Formula

The formula in the EN 1996 norm, for the estimation of the design value of the vertical resistance of URM walls, makes use of the partial factor for material γ_M. The latter considers the contribution of the uncertainty in the compressive strength, to the uncertainty in the vertical resistance. The FE analysis results showed that, both the compressive strength and the modulus of elasticity influence the vertical resistance of existing slender URM walls. Mean values of strength and the modulus of elasticity were the input of the material model. Both the compressive strength and the modulus of elasticity were included in the proposed formula. The formula makes use of the characteristic value of the compressive strength and the mean value of the modulus of elasticity. To estimate the design value of the vertical resistance, the expression, in the proposed formula, was divided with the partial factor for material γ_M. This way, the uncertainty, in the compressive strength, and the uncertainty, in the modulus of elasticity, both affect the uncertainty in the vertical resistance.

The design values of vertical resistance, calculated according to the proposed formula and the formula, in the EN 1996 norm, were compared. The graph, in Fig. 204, juxtaposes the respective curves of the aforementioned formulas, by way of illustration. The comparison showed that the EN 1996 norm underestimates the vertical resistance of the analyzed slender URM walls. Especially for large values of wind load, the formula, in the EN 1996 norm, results in values of vertical resistance, which are, approximately, equal to zero.

The definition of the eccentricity at the mid-height, resulting from wind loads, is, probably, the reason why the EN 1996 norm, vastly, underestimates the vertical resistance of URM walls, for large values of wind load. The norm does not, specifically, provide an expression for the eccentricity at the mid-height, resulting from wind loads. It was assumed that the latter is equal to the design value of the first-order bending moment, due to the wind load, divided by the design value of the vertical load, at the mid-height of the wall. This way, the eccentricity, due to wind load, was estimated based on the design value of the vertical load. However, the FE analysis results showed an interaction between the vertical load and the wind load, that lead a slender URM wall to failure. In the proposed formula, the eccentricity at the mid-height of the wall, resulting from wind loads, was defined as the quotient of the maximum first-order bending moment, due to wind load, divided by the design value of the vertical resistance, when the wall is subjected to vertical loading, only. Doing so, the results from the proposed formula were comparable to the respective FE analysis results (Fig. 203). It is mentioned that, the

vertical resistance is calculated at the mid-height of the URM walls, since the maximum first-order bending moment, due to wind load, occurs there.

The EN 1996 norm considers the eccentricity due to creep at the mid-height of the wall. However, creep effects were not taken into account for the FE analysis. Additionally, the eccentricity due to creep, at the mid-height of the wall, was neglected for the comparison between the proposed formula and the formula in the EN 1996 norm. To be in accordance with the current standard, the eccentricity, due to creep, was added to the eccentricity, at the mid-height of the wall, in the proposed formula. The proposed formula is described in Equation 76.
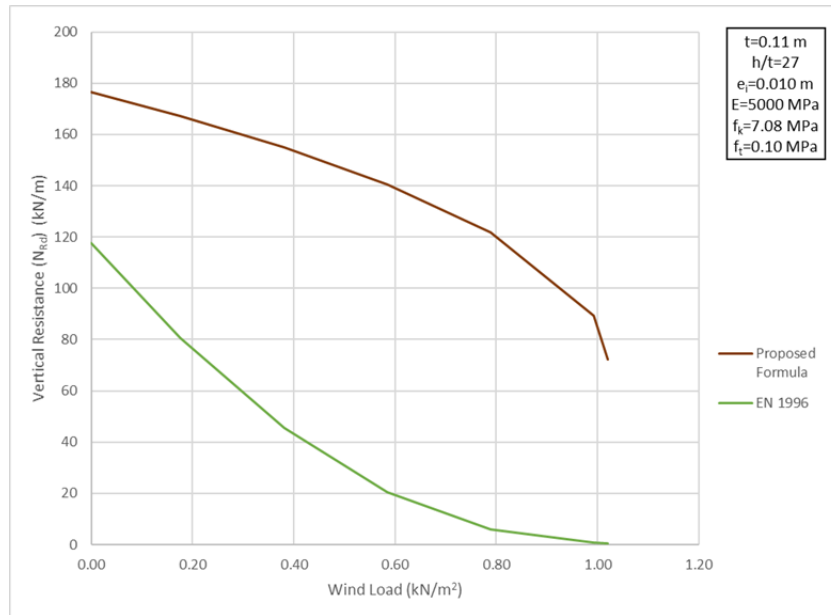
Fig. 204 Comparison between the results from the proposed formula and the formula of the EN 1996 norm

Equation 76 Proposed Formula for the Estimation of the Design Value of the Vertical Resistance of slender URM walls, subjected to Combined Vertical and Lateral Loading

$$N_{Rd} = \frac{1.49}{\gamma_M} E^{0.60} f_k^{\ 0.40} \left(\frac{t_{ef}}{h_{ef}}\right)^{1.46} t \left(1 - 2\,\frac{e_{mk}}{t}\right)^{2.40} \left(0.41 + 0.59 \sqrt{1 - 18.20\,(\frac{h_{ef}}{t_{ef}})^{0.38}\,(\frac{f_k}{E})^{0.23}\,\frac{\frac{e_{wd}}{t}}{1 - 2.10\frac{e_{mk}}{t}}}\right),$$

where:

γ_M: partial factor for material

E: the short-term secant modulus of elasticity

f_k: the characteristic compressive strength

t_{ef}:   the effective thickness of the wall

h_{ef}:   the effective height of the wall

t: the thickness of the wall

e_{mk}:   the eccentricity at the mid-height of the wall (Equation 77)

e_{wd}:   the eccentricity at the mid-height of the wall, caused by the design value of the maximum first-order bending moment on the wall, because of the wind load (Equation 79)

Equation 77 Eccentricity at the mid-height of the wall

$$e_{mk} = e_i + e_k,$$

where:

e_i: the eccentricity at the top or bottom of the wall

e_k: the eccentricity due to creep (Equation 78)

Equation 78 Proposed expression for calculating the eccentricity due to creep at the mid-height of the wall

$$e_k = 0.002\ \varphi_\infty\ \frac{h_{ef}}{t_{ef}}\ \sqrt{t_{ef}\ e_i},$$

where:

ϕ_∞:   the final creep coefficient

Equation 79 Eccentricity at the mid-height of the URM wall, caused by the design value of the maximum first-order bending moment on the wall, because of the wind load

$$e_{wd} = \frac{M_{wd}}{\frac{1.49}{\gamma_M} E^{0.60} f_k^{\ 0.40} \left(\frac{t_{ef}}{h_{ef}}\right)^{1.46} t \left(1 - 2\frac{e_{mk}}{t}\right)^{2.40}},$$

where:

M_{wd}:   the design value of the bending moment at the mid-height of the wall because of the wind load (Equation 80)

Equation 80 Design value of the Maximum First-Order Bending Moment on the wall because of the Wind Load

$$M_{wd} = \frac{w_d\ h^2}{8}, \text{where:}$$

w_d: the design value of the wind load

h: the clear storey height

11.2 Limitations of the Study

The proposed formula, that estimates the vertical resistance of existing slender URM walls, subjected to combined vertical and lateral loading, is applicable for one case of support conditions. Particularly, for walls, that are simply supported along the top and bottom edges. A wall, which is part of the structure of a building block in Amsterdam, is the case study. The wall is located on the first floor and is stiffened on one vertical edge. However, the length of the wall l is $l \geq 15\,t$, where t is the thickness of the wall. Therefore, according to the EN 1996 norm, the wall should be considered as supported, only, at the top and bottom edges. The connections between the timber beams and the URM walls are not moment resisting. Hence, the supports are hinged. Furthermore, only out-of-plane lateral loads are considered. Therefore, it is expected that stresses and deformations do not change along the length of the URM walls.

According to the technical drawings of the building block in Amsterdam, the support conditions, along the bottom edge of the walls, that are located on the ground floor, are different. The bottom edge lies at the foundation level, where bending moments develop. Hence, the walls on the ground floor are clamped, at the bottom edge. The resulting diagram of bending moments, along the height of the wall, will be different, compared to the respective diagram, for a simply supported wall. Additionally, URM walls, that have a length $l < 15\,t$, should be treated as stiffened on one vertical edge. Walls, that are stiffened on both vertical edges, can, also, belong to the structure of existing masonry buildings. In these cases, stresses and deformations do change along the length of the URM walls. The results from the FE analysis, of simply supported walls, described a certain interaction, between the vertical resistance and the applied wind load. This interaction is expressed in the proposed formula. According to the aforementioned remarks, a different interaction, between the vertical resistance and the applied wind load, is expected for URM walls, with different support conditions. Additionally, for URM walls, stiffened on one or two vertical edges, the FE model, that was used for the analysis, is not appropriate.

The proposed formula was derived from and verified with the results, from FE analysis of existing slender URM walls, with certain geometric and material properties. A reliable calculation of the vertical resistance is obtained, when the formula is applied on cases of URM walls, with a range of values of slenderness ratio (h/t) between 27 and 39.

Similarly to the case of slenderness ratio, there are limitations with respect to the eccentricity (e_i), at the top and the bottom of the URM walls. Non-linear structural FE analyses were performed on existing slender URM walls, with a minimum value of eccentricity (e_i), equal to 0.001 m, and a maximum value of eccentricity (e_i), equal to 0.029 m. The proposed formula was developed for values of eccentricity (e_i), from 0.001 m to 0.015 m, and leads to a conservative calculation of the vertical resistance within the aforementioned range. The vertical resistance of an existing slender URM wall, with eccentricity $e_i=0.029\ m$, which is subjected to combined vertical and lateral loading, is underestimated by the proposed formula. Additionally, the formula defines a maximum value for the wind load, that the latter can bear, which is significantly lower than its actual capacity.

As far as the material properties are concerned, the properties prescribed in the NPR 9998-2018 norm, for brick masonry, constructed before 1945, were considered as reference. The different response of an existing slender URM wall, when the characteristic compressive strength (f_k) remains constant and the short-term secant modulus of elasticity (E) changes and vice versa, has been reviewed. Three different values of E/f_k ratio have been defined. The first is derived by the suggested values of compressive strength and short-term secant modulus of elasticity, in the NPR 9998-2018 norm. The ratio is equal to 705.88. The other two values of E/f_k ratio, that have been used, are equal to 900 and 1000. Attention has been paid so that, the properties are indicative of masonry components in buildings, that were constructed in the late 19th – early 20th century. It should be mentioned that, the influence on the vertical resistance, from changing the aforementioned material properties, was assessed for values of slenderness ratio, of the URM wall, equal to 27 and 30. The graph, in Fig. 205, shows the effect of changing the characteristic compressive strength of masonry, while keeping the short-term secant modulus of elasticity constant.
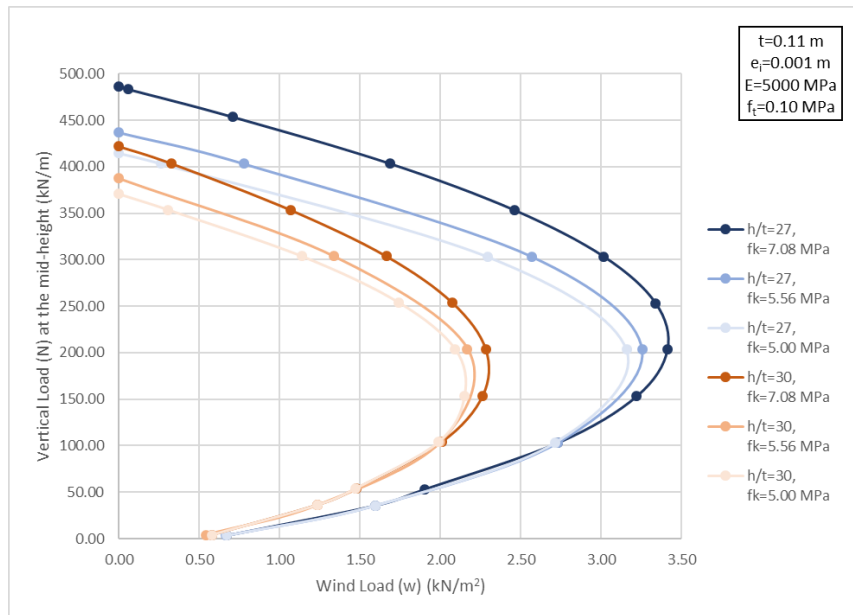
Fig. 205 Influence of Masonry Properties on the Vertical Resistance of Slender URM Walls

11.3 Recommendations for Further Research

The proposed formula was verified by comparing its results with the respective results, from the FE analysis. The reliability of the FE analysis results was reviewed, to the extent possible. Input and output stress-strain curves of the material model seemed to match. Additionally, it was noticed that the size of the load increments, for the non-linear analysis, as well as the size of the finite elements and the integration scheme do not affect the results of the analysis. It is considered necessary, though, to compare the FE analysis results with the results, from relevant experimental testing of existing slender URM walls. The comparison can assess the validity of the proposed formula.

Appropriate expressions, in the proposed formula, introduce the influence of the material properties on the vertical resistance, of existing slender URM walls, subjected to combined vertical and lateral loading. Namely, the characteristic compressive strength and the short-term secant modulus of elasticity of masonry. These expressions were specified according to the FE analysis results. Two different values of slenderness ratio, of the URM wall, were taken into consideration, when the impact of the material properties, on the vertical resistance, was assessed. Particularly, the values 27 and 30. It will be interesting to review, whether the characteristic compressive strength and the short-term secant modulus of elasticity, of masonry, affect the vertical resistance of URM walls, with higher values of slenderness ratio, in a different way.

The proposed formula is applicable to URM walls, with values of slenderness ratio from 27 to 39. The FE analysis results showed that the studied URM walls behaved as slender, under every possible combination of applied vertical load and wind load. The walls failed because of buckling, before the stresses on masonry reach the compressive strength. Johnson and Bakeer specified criteria, for distinguishing slender from squat walls. Particularly, Johnson defines as slender, walls with slenderness ratio $\frac{h}{t} > 28.6$. According to Bakeer, the condition $\lambda \geq 1.26 \left(1 - 2\frac{e_i}{t}\right)$ should be met, for slender masonry walls. The URM wall with value of slenderness ratio, equal to 27, value of eccentricity, at the top and the bottom, equal to 0.001 m, and the properties of masonry, prescribed in the NPR 9998-2018 norm, does not meet the latter condition. However, the non-linear FE analysis results showed that the wall failed because of buckling, for all the combinations of applied vertical load and wind load. Hence, the

aforementioned criteria are not valid for the studied URM walls. Proceeding with the FE analysis of URM walls, with smaller values of slenderness ratio, is recommended. The lower limit of slenderness ratio, for which the proposed formula is valid, can be estimated. Furthermore, an appropriate condition can be specified, for characterizing URM walls, in existing masonry buildings, as squat or slender.

12 References

[1] S. Pasterkamp, "Analysis Of The Structural Design Process Of The Adaptive Reuse Of Building Structures," Mexico City, 2014.

[2] H. Remøy and T. van der Voordt, "Adaptive reuse of office buildings into housing Opportunities and risks," *Building Research and Information,* vol. 42, no. 3, pp. 381-390, 2014.

[3] F. Messali, R. Esposito, S. Jafari, G. Ravenshorst, P. Korswagen and J. Rots, "A Multiscale Experimental Characterization Of Dutch Unreinforced Masonry Buildings," Thessaloniki, 2018.

[4] *Eurocode 6-Design of masonry structures-Part 1-1: General rules for reinforced and unreinforced masonry structures,* Delft: Nederlands Normalisatie-instituut, 2013.

[5] J. Rots ed., Structural Masonry: an experimental/numerical basis for practical design rules, Rotterdam: A.A. Balkema, 1997.

[6] S. Jafari, R. Esposito and J. Rots, "A Comparative Study On The Different Testing Methods: Evaluating The Compression Properties Of Masonry," Milan , 2018.

[7] N. Stas, "The Economics of Adaptive Reuse of Old Buildings: A Financial Feasibility Study & Analysis," Master Thesis - University of Waterloo, Waterloo, 2007.

[8] T. Stathopoulos, D. Surry and A. Davenport, "Internal pressure characteristics of low-rise buildings due to wind action," *Journal of Fluids Engineering,* vol. 97, no. 1, pp. 451-463, 1979.

[9] P. Lourenço, "Computations of historical masonry constructions," *Progress in Structural Engineering and Materials,* vol. 4, no. 3, pp. 301-319, 2002.

[10] T. Bakeer, "Assessment the stability of masonry walls by the transfer-matrix," *Engineering Structures,* no. 110, pp. 1-20, 2016.

[11] A. Simone, *An Introduction to the Analysis of Slender Structures,* Delft: Delft University of Technology, 2011.

[12] G. Manos, *Notes for Unreinforced and Reinforced Masonry Structures,* Thessaloniki: Aristotle University of Thessaloniki, 2005.

[13] C. Sandoval, P. Roca, E. Bernat and L. Gil, "Testing and numerical modelling of buckling failure of masonry walls," *Construction and Building Materials,* vol. 25, no. 12, pp. 4394-4402, 2011.

[14] P. Bullen, "Adaptive reuse and sustainability of commercial buildings," *Facilities,* vol. 25, no. 1/2, pp. 20-31, 2007.

[15] A. F. Thomsen and C. L. van Der Flier, "Replacement or reuse? The choice between demolition and life cycle extension from a sustainable viewpoint.," in *Shrinking Cities, Sprawling Suburbs, Changing Countrysides*, Dublin, Centre for Housing Research, 2008, pp. 1-13.

[16] R. P. Geraedts, T. van der Voordt and H. Remøy, "Conversion Meter: A new tool to assess the conversion potential of vacant office buildings into housing," in *International Conference on Advances on Sustainable Cities and Buildings Development*, Porto, 2017.

[17] S. Huerta, "The analysis of masonry architecture: A historical approach: To the memory of professor Henry J. Cowan," *Architectural Science Review,* vol. 51, no. 4, pp. 297-328, 2008.

[18] K. Stylianidis and C. Ignatakis, *Masonry Constructions (according to Eurocodes 6 and 8) - Lecture Notes,* Thessaloniki: Aristotle University of Thessaloniki, 2010.

[19] T. Bakeer, "Empirical estimation of the load bearing capacity of masonry wallsunder buckling – Critical remarks and a new proposal for the Eurocode 6," *Construction and Building Materials,* no. 113, pp. 376-394, 2016.

[20] C. Sandoval and P. Roca, "Empirical Equations for the assessment of the load-bearing capacity of brick masonry walls," *Construction and Building Materials,* no. 44, pp. 427-439, 2013.

[21] J. Rots, B. Belletti, M. Boonpichetvong and I. S., "Event-by-Event Strategies for Modeling Amsterdam Masonry Structures," in *Structural Analysis of Historical Constructions*, New Delhi, 2006.

[22] J. G. Rots, F. Messali, R. Esposito, S. Jafari and V. & Mariani, "Computational modeling of masonry with a view to Groningen induced seismicity," in *10th international conference on Structural Analysis of Historical Constructions, SAHC*, Leuven, 2016.

[23] M. Stefanidou, I. Papayianni and V. Pachta, "Analysis and characterization of Roman and Byzantine fired bricks from Greece," *Materials and Structures,* vol. 48, no. 7, pp. 2251-2260, 2015.

[24] F. Fernandes, P. Lourenço and F. Castro, "Ancient Clay Bricks: Manufacture and Properties," in *Materials, Technologies and Practice in Historic Heritage Structures*, Dordrecht, Springer, 2010, pp. 29-48.

[25] I. Papayianni and V. Pachta, "Experimental study on the performance of lime-based grouts used in consolidating historic masonries," *Materials and structures,* vol. 48, no. 7, pp. 2111-2121, 2015.

[26] L. Pelà, P. Roca and A. Benedetti, "Mechanical characterization of historical masonry by core drilling and testing of cylindrical samples," *International Journal of Architectural Heritage,* vol. 10, no. 2-3, pp. 360-374, 2016.

[27] E. Kamendere, L. Grava, K. Zvaigznitis, A. Kamenders and A. Blumberga, "Properties of Bricks and Masonry of Historical Buildings as a Background for Safe Renovation Measures," *Energy Procedia,* vol. 95, pp. 119-123, 2016.

[28] V. Pachta and I. Papayianni, "The study of the historic buildings of Eclecticism in Thessaloniki under the prism of sustainability," *Procedia environmental sciences,* vol. 38, pp. 283-289, 2017.

[29] E. Bernat Masó, C. Escrig Pérez and L. Gil Espert, "Study of the compressive response of masonry using non-conventional joint materials," *International journal of masonry research and innovation,* vol. 2, no. 1, pp. 83-103, 2017.

[30] S. Wijte and R. van der Pluijm, "Introduction to the Dutch Masonry Code—TGB Masonry Structures," *Mauerwerk,* vol. 14, no. 5, pp. 311-318, 2010.

[31] E. Bernat, L. Gil, P. Roca and C. Sandoval, "Experimental And Numerical Analysis Of Bending-Buckling Mixed Failure Of Brickwork Walls," *Construction and Building Materials ,* no. 43, pp. 1-13, 2013.

[32] R. S. Boynton and K. A. Gutschick, Bond of mortar to masonry units: factors influencing strength, extent, and durability of bond, Washington D.C.: National Lime Association, 1964.

[33] S. Wijte, "Graphs for the design of braced load bearing masonry walls," in *8th International Masonry Conference*, Dresden, 2010.

[34] *NEN 6790 Technical principles for building structures - TGB 1990 - Masonry structures - Basic requirements and calculation methods,* Delft: Nederlands Normalisatie-instituut, 2005.

[35] C. Sandoval and P. Roca, "Study of the influence of different parameters on the buckling behaviour of masonry walls," *Construction and Building Materials,* no. 35, pp. 888-899, 2012.

[36] A. Schultz, "Solutions for Critical Axial Loads in Eccentrically Compressed and Laterally Loaded Slender URM Members," in *11th North American Masonry Conference*, Minneapolis, 2011.

[37] T. Bakeer and P. D. Christiansen, "Buckling of masonry walls–A new proposal for the Eurocode 6: Knicken von Mauerwerk–Ein neuer Bemessungsvorschlag für den Eurocode 6," *Mauerwerk,* vol. 21, no. 2, pp. 82-89, 2017.

[38] A. E. Schultz and J. G. Mueffelman, "Design considerations for stability of transversely loaded URM walls," *TMS Journal (The Masonry Society),* vol. 21, no. 1, pp. 41-53, 2003.

[39] J. R. B. Popehn, A. E. Schultz, M. Lu, H. K. Stolarski and N. J. Ojard, "Influence of transverse loading on the stability of slender unreinforced masonry walls.," *Engineering Structures,* vol. 30, no. 10, pp. 2830-2839, 2008.

[40] *NEN 8700 Assessment of existing structures in case of reconstruction and disapproval - Basic Rules,* Delft: Nederlands Normalisatie-insituut, 2011.

[41] *EN 1052-1 Methods for test of masonry - Part 1: Determination of compressive strength,* Delft: Nederlands Normalisatie-insituut, 1998.

[42] *NEN-EN 1996-1-1+A1/NB National Annex to Eurocode 6 - Part 1-1,* Delft: Nederlands Normalisatie-instituut, 2018.

[43] "DIANA-9.4.4 User's Manual - Element Library - 21.5 Integration Schemes," TNO DIANA BV, 2012. [Online]. Available: https://dianafea.com/manuals/d944/ElmLib/node628.html. [Accessed 21 November 2019].

[44] "DIANA-10.1 User's Manual - Material Library - 6.6 Crack Bandwidth," DIANA FEA BV, 2017. [Online]. Available: https://dianafea.com/manuals/d101/MatLib/node102.html. [Accessed 21 November 2019].

[45] "DIANA-9.4 User's Manual - Element Library - 10. Curved Shell Elements," TNO DIANA BV, 2010. [Online]. Available: https://dianafea.com/manuals/d94/ElmLib/node267.html. [Accessed 21 November 2019].

[46] "DIANA-10.0 User's Manual - Element Library - 6. Plane Strain Elements," TNO DIANA BV, 2015. [Online]. Available: https://dianafea.com/manuals/d100/ElmLib/node129.html. [Accessed 21 November 2019].

[47] "DIANA-9.4 User's Manual - Material Library - 6.2 Total Strain Crack Models," TNO DIANA BV, 2010. [Online]. Available: https://dianafea.com/manuals/d94/MatLib/node73.html. [Accessed 21 November 2019].

[48] "DIANA-10.1 User's Manual - Material Library - 6.6.1 Rots' Element Based Method," DIANA FEA BV, 2017. [Online]. Available: https://dianafea.com/manuals/d101/MatLib/node103.html#crack:bw:rots. [Accessed 21 November 2019].

[49] G. Magenes and A. Penna, "Existing masonry buildings: general code issues and methods of analysis and assessment.," *Eurocode,* vol. 8, pp. 185-198, 2009.

[50] K. Palacio, "Practical Recommendations for Nonlinear Structural Analysis in DIANA," TNO DIANA BV, Delft, 2013.

[51] "DIANA-9.4.4 User's Manual - Element Library," TNO DIANA BV, 2012. [Online]. Available: https://dianafea.com/manuals/d944/ElmLib/node51.html. [Accessed 21 November 2019].

[52] P. J. B. B. Lourenço, An anisotropic macro-model for masonry plates and shells: Implementation and validation., Delft: Delft University of Technology, Faculty of Civil Engineering, Mechanics and Structures, Computational Mechanics, 1997.

[53] *Eurocode 6: Design of masonry structures-Part 1-1: General rules for reinforced and unreinforced masonry structures,* Delft: Nederlands Normalisatie-instituut, 2013.

[54] A. Taliercio, "An overview of masonry creep," *WIT Transaction on the Built Environment,* vol. 109, pp. 197-208, 2009.

[55] N. G. Shrive and M. R. Taha, "Effects of creep on new masonry structures," in *Learning From Failure, Long-Term Behaviour of Heavy Masonry Structures*, Milan, WIT Press, 2008, pp. 83-108.

[56] *Eurocode 1: Actions on structures - Part 1-4: General Actions - Wind Actions,* Delft: Nederlands Normalisatie-insituut, 2005.

[57] *Eurocode 1: Actions on structures - Part 1-1: General actions - Densities, self-weight, imposed loads for buildings,* Brussels: CEN, 2002.

[58] *Eurocode - Basis of structural design,* Brussels: CEN, 2002.

[59] *NEN-EN 1991-1-4+A1+C2/NB National Annex to Eurocode 1 - Part 1-4,* Delft: Nederlands Normalisatie-insituut, 2011.

[60] *NPR 9998 Assessment of structural safety of buildings in cases of erection, recosntruction and disapproval - Induced Eartquakes - Basis of design, actions and resistances,* Delft: Nederlands Normalisatie-insituut, 2018.

Appendix A

Properties of Masonry												
Compressive strength of masonry units (MPa)	3.20	3.20	7.65	7.65	12.10	12.10	16.55	16.55	21.00	21.00	25.00	-
Compressive strength of mortar (MPa)	0.50	0.70	0.50	0.70	0.50	0.70	0.50	0.70	0.50	0.70	1.90	-
Characteristic Compressive strength of masonry (MPa)	**1.07**	**1.17**	**1.89**	**2.06**	**2.55**	**2.77**	**3.13**	**3.40**	**3.65**	**3.97**	**5.71**	**7.08**
Short-Term Secant Modulus of Elasticity - 300*fc (Mpa)	322.38	350.67	568.06	617.91	765.29	832.45	938.07	1020.39	1095.11	1191.21	1712.47	2125.00
Short-Term Secant Modulus of Elasticity - 450*fc (Mpa)	483.56	526.00	852.09	926.87	1147.93	1248.67	1407.10	1530.58	1642.66	1786.82	2568.70	3187.50
Short-Term Secant Modulus of Elasticity - 600*fc (Mpa)	644.75	701.33	1136.12	1235.82	1530.58	1664.90	1876.13	2040.78	2190.22	2382.43	3424.93	4250.00
Short-Term Secant Modulus of Elasticity - 700*fc (Mpa)	752.21	818.22	1325.48	1441.80	1785.67	1942.38	2188.82	2380.91	2555.26	2779.50	3995.75	4958.33
Short-Term Secant Modulus of Elasticity - 900*fc (Mpa)	967.13	1052.00	1704.18	1853.74	2295.87	2497.35	2814.20	3061.17	3285.33	3573.64	5137.40	6375.00
Short-Term Secant Modulus of Elasticity - 1000*fc (Mpa)	1074.59	1168.89	1893.54	2059.71	2550.96	2774.83	3126.89	3401.30	3650.37	3970.71	5708.22	7083.33
Partial Material Factor γ	1.70											
Design Compressive Strength of Masosnry (Mpa)	0.63	0.69	1.11	1.21	1.50	1.63	1.84	2.00	2.15	2.34	3.36	4.17
Short-Term Secant Modulus of Elasticity (Mpa)	**322.38**	**937.01**	**1551.64**	**2166.27**	**2780.90**	**3395.53**	**4010.16**	**4624.79**	**5239.42**	**5854.05**	**6468.68**	**7083.31**
Characteristic Compressive strength of masonry E/1000 (MPa)	-	0.94	1.55	2.17	2.78	3.40	4.01	4.62	5.24	5.85	6.47	7.08
Characteristic Compressive strength of masonry E/900 (MPa)	-	1.04	1.72	2.41	3.09	3.77	4.46	5.14	5.82	6.50	7.19	-
Characteristic Compressive strength of masonry E/700 (MPa)	-	1.34	2.22	3.09	3.97	4.85	5.73	6.61	-	-	-	-
Characteristic Compressive strength of masonry E/600 (MPa)	-	1.56	2.59	3.61	4.63	5.66	6.68	-	-	-	-	-
Characteristic Compressive strength of masonry E/450 (MPa)	-	2.08	3.45	4.81	6.18	7.55	-	.	-	-	-	-
Characteristic Compressive strength of masonry E/300 (MPa)	1.07	3.12	5.17	7.22	-	-	-	-	-	-	-	-
Design Compressive strength of masonry E/1000 (MPa)	-	0.55	0.91	1.27	1.64	2.00	2.36	2.72	3.08	3.44	3.81	4.17
Design Compressive strength of masonry E/900 (MPa)	-	0.61	1.01	1.42	1.82	2.22	2.62	3.02	3.42	3.83	4.23	-
Design Compressive strength of masonry E/700 (MPa)	-	0.79	1.30	1.82	2.34	2.85	3.37	3.89	-	-	-	-
Design Compressive strength of masonry E/600 (MPa)	-	0.92	1.52	2.12	2.73	3.33	3.93	-	-	-	-	-
Design Compressive strength of masonry E/450 (MPa)	-	1.22	2.03	2.83	3.64	4.44	-	-	-	-	-	-
Design Compressive strength of masonry E/300 (MPa)	0.63	1.84	3.04	4.25	-	-	-	-	-	-	-	-

Fig. A. 1 Indicative Properties of Masonry for the Case Study of URM wall

Appendix B

Formulae	Vertical Resistance	Condition	Additional Parameters	Parameter for slenderness and masonry stiffness 'λ'	Modulus of Elasticity	Eccentricity
EC6	$((1-2*(e_{mk}/t))*e^{(-(u^2)/2)})*t*fd$	-	$u=(\lambda-0.063)/(0.73-1.17*(e_{mk}/t))$	$(hef/tef)*(fk/Es)^{(1/2)}$	Es (although calibrated for Es/fk=1000)	e_{mk}/t (sum of axial load eccentricity and eccentricity due to wind load)
NEN 6790	$\alpha*t*fd$ (α from Table 8-page 50 for slenderness and ecentricity on top and bottom)	-	-	hef/tef	Es=900*fk	e_{mk}/t (sum of axial load eccentricity and eccentricity due to wind load)
Bakeer-Regression	$((1-2*(e_{mk}/t))*(5.1*(e_{mk}/t)^2-2.4*(e_{mk}/t)+1)*atan(1,13*u^2)/1,13*u^2)*t*fd$	-	$u=\lambda/(1-2*(e_{mk}/t))$	$(hef/tef)*(fk/Es)^{(1/2)}$	Es	e_{mk}/t (sum of axial load eccentricity and eccentricity due to wind load)
Bakeer-Proposal	$(1-2*e_{mk}/t-\lambda^2/(3.15*(1-2*e_{mk}/t)))*t*fd$	$\lambda<1.26*(1-2*e_{mk}/t)$	-	$(hef/tef)*(fk/E0k)^{(1/2)}$	E0k=E0mean/1.2=(1.1-1.2)Es/1.2=Es	e_{mk}/t (sum of axial load eccentricity and eccentricity due to wind load)
	$(0.79*(1-2*e_{mk}/t)^3/\lambda^2)*t*fd$	$\lambda>=1.26*(1-2*e_{mk}/t)$				
Rankine Method	$((1-2*e/t)/(1+(12/\pi^2)*(\lambda/(1-2*e/t))^2))*t*fd$	-	-	$(hef/tef)*(fk/Es)^{(1/2)}$	Es (formula can be also derived for Eσ=E*(1-σ/f)) with E the tangent modulus of elasticity at low stress levels	e_{mk}/t (sum of axial load eccentricity and eccentricity due to wind load)
Schultz	$Pe*(0.422+0.578*(1-(5.47*\lambda\_m*Mw/(Pe*r))/(1-0.577*e\_a/r))$	-	$Pe=(\pi^2*E*I/h^2)*(1-0.577(e\_a/r))^3$	-	Em=(0.33fm'-0.05fm')/(ε0.33-ε0.05) -> Es	e_i/r & $\lambda\_m*Mw/(Pe*r)$ (axial load eccentricity and eccentricity due to wind load)

Fig. B. 1 Summary of Assessed Formulas

Appendix C

FE Analysis Results for different Size of Load Increments

Two non-linear analyses are performed on the model with the plane strain elements. The material model, the geometry, the properties of the finite elements and the support conditions are mentioned in sections 9.1 and 9.1.4. Geometrically non-linear effects are activated for the analyses. The load cases and the magnitude of loads are listed in Table C. 3. Table C. 1 and Table C. 2 list the different characteristics of the two analyses. The resulting load-displacement curves are compared in the graph in Fig. C. 1.

	Structural Non-Linear	
	Non-Linear Effects	Physically Non-linear
		Geometrically Non-linear
	Equilibrium Iteration	
	Iterative Method	
	Maximum Number of iterations	200
	Method	Secant (Quasi-Newton)
	Type	BFGS
	First Tangent	Tangential
	Convergence Norm	
	Satisfy all specified norms	Yes
	Displacement	Yes
	Convergence Tolerance	0.01
	No Convergence	Terminate
Analysis 1	Force	Yes
	Convergence Tolerance	0.01
	No Convergence	Terminate
	Load Steps	
	Masonry Weight (Load Case 1)	1
	Loads from floors and masonry above (Load Case 2)	1
	Wind Load (Load Case 3)	0.5(2)
		0.25(4) 0.1(20) Arc-length control activated for the translation of the nodes in the middle of the wall in the horizontal direction (direction of application of wind load)

Table C. 1 Characteristics of the first of the non-linear analyses with different Size of Load Increments

Analysis 2	Structural Non-Linear		
	Non-Linear Effects	Physically Non-linear	
		Geometrically Non-linear	
	Equilibrium Iteration		
	Iterative Method		
	Maximum Number of iterations	200	
	Method	Secant (Quasi-Newton)	
	Type	BFGS	
	First Tangent	Tangential	
	Convergence Norm		
	Satisfy all specified norms	Yes	
	Displacement	Yes	
	Convergence Tolerance	0.01	
	No Convergence	Terminate	
	Force	Yes	
	Convergence Tolerance	0.01	
	No Convergence	Terminate	
	Load Steps		
	Masonry Weight (Load Case 1)	1	
	Loads from floors and walls above (Load Case 2)	1	
	Wind Load (Load Case 3)	0.5(2)	
		0.1(10) 0.05(30) Arc-length control activated for the translation of the nodes in the middle of the wall in the horizontal direction (direction of application of wind load)	

Table C. 2 Characteristics of the second of the non-linear analyses with different Size of Load Increments

Loads	*Masonry Weight (Load Case 1)*	
	Surface force pointing downwards (negative y direction)	20700 N/m^2
	Loads from floors and walls above (Load Case 2)	
	Point force on top vertex	110320 N/m
	Wind Load (Load Case 3)	
	Distributed force on the edge of the element	624 N/m

Table C. 3 Loads on the FE Models for analyses with different Size of Load Increments
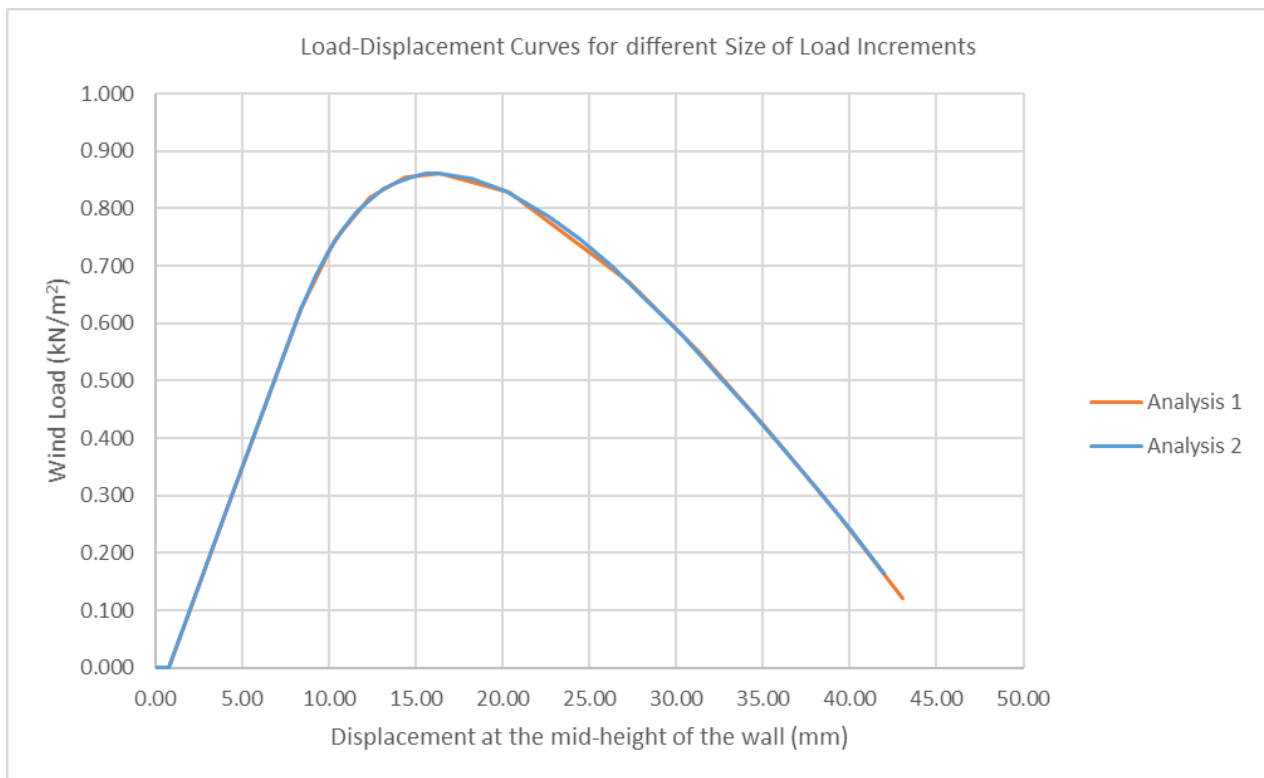
Fig. C. 1 Load – Displacement Curves from FE analyses with different Size of Load Increments

FE Analysis Results for different Size of Finite Elements

Two non-linear analyses are performed on the model with the plane strain elements. The material model, the geometry and the support conditions are mentioned in sections 9.1 and 9.1.4. Geometrically non-linear effects are activated for the analyses. The load cases and the characteristics of the analyses are listed in Table C. 3 and Table C. 1,respectively. Table C. 4 and Table C. 5 list the different properties of the finite elements in each analysis. The resulting load-displacement curves are compared in the graph in Fig. C. 1.

	Class	Plane Strain Elements	
	Geometry	Dimensions	0.014 x 0.014 m2
Element A.1		Type	CQ16E
	Data	DOF	Ux, Uy - 8-noded
		Interpolation Scheme	Quadratic in Ux,Uy
		Integration Scheme	3x3 HIGH
	Class	Infinite Shells	
		Thickness	0.1 m
	Geometry	Shape Definition Type	Flat
Element A.2		Size of Elements	0.014 m
		Type	CL9PE
	Data	DOF	Ux,Uy, Φz - 3-noded
		Interpolation Scheme	Quadratic
		Integration Scheme	2x2 Gauss

Table C. 4 Properties of the Elements for the first of the analyses with different mesh sizes

	Class	Plane Strain Elements	
	Geometry	Dimensions	0.0105 x 0.0105 m2
Element B.1	Data	Type	CQ16E
		DOF	Ux, Uy - 8-noded
		Interpolation Scheme	Quadratic
		Integration Scheme	3x3 HIGH
	Class	Infinite Shells	
	Geometry	Thickness	0.1 m
		Shape Definition Type	Flat
Element B.2		Size of Elements	0.0105 m
	Data	Type	CL9PE
		DOF	Ux,Uy, Φz - 3-noded
		Interpolation Scheme	Quadratic
		Integration Scheme	2x2 Gauss

Table C. 5 Properties of the Elements for the second of the analyses with different mesh sizes
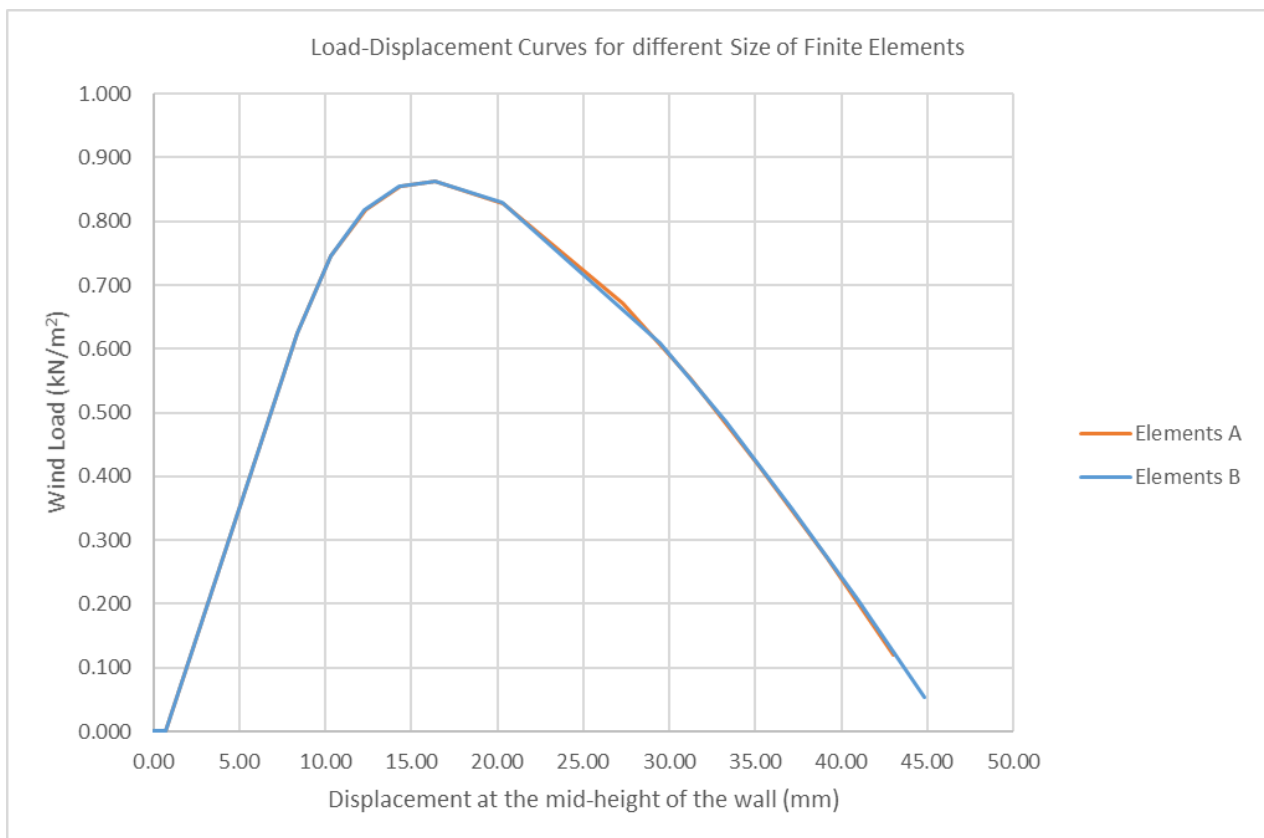
Fig. C. 2 Load – Displacement Curves from FE analyses with different Size of Finite Elements

FE Analysis Results for different Integration Scheme for the Finite Elements

Two non-linear analyses are performed on the model with the plane strain elements. The material model, the geometry and the support conditions are mentioned in sections 9.1 and 9.1.4.

Geometrically non-linear effects are activated for the analyses. The load cases and the characteristics of the analyses are listed in Table C. 6 and Table C. 7, respectively. Table C. 4 and Table C. 8 list the different properties of the finite elements in each analysis. The resulting load-displacement curves are compared in the graph in Fig. C. 3.

Loads	*Masonry Weight (Load Case 1)*	
	Surface force pointing downwards (negative y direction)	20700 N/m2
	Loads from floors and walls above (Load Case 2)	
	Point force on top vertex	226800 N/m
	Wind Load (Load Case 3)	
	Distributed force on the edge of the element	624 N/m

Table C. 6 Loads on the FE Models for analyses with different Integration Schemes

Analysis	Structural Non-Linear	
	Non-Linear Effects	Physically Non-linear
		Geometrically Non-linear
	Equilibrium Iteration	
	Iterative Method	
	Maximum Number of iterations	200
	Method	Secant (Quasi-Newton)
	Type	BFGS
	First Tangent	Tangential
	Convergence Norm	
	Satisfy all specified norms	Yes
	Displacement	Yes
	Convergence Tolerance	0.01
	No Convergence	Terminate
	Force	Yes
	Convergence Tolerance	0.01
	No Convergence	Terminate
	Load Steps	
	Masonry Weight (Load Case 1)	1
	Loads from floors and masonry above (Load Case 2)	1
	Wind Load (Load Case 3)	0.5(10)
		0.1(16) 0.05(40) Arc-length control activated for the translation of the nodes in the middle of the wall in the horizontal direction (direction of application of wind load)

Table C. 7 Characteristics of the non-linear analyses of Models with different Integration Schemes

	Class	Plane Strain Elements	
Element B.1	Geometry	Dimensions	0.014 x 0.014 m2
	Data	Type	CQ16E
		DOF	Ux,Uy - 8-noded
		Interpolation Scheme	Quadratic
		Integration Scheme	2x2 REGULAR
Element B.2	Class	Infinite Shells	
	Geometry	Thickness	0.1 m
		Shape Definition Type	Flat
		Size of Elements	0.0105 m
	Data	Type	CL9PE
		DOF	Ux,Uy, Φz - 3-noded
		Interpolation Scheme	Quadratic
		Integration Scheme	2x2 Gauss

Table C. 8 Properties of the Elements for the second of the analyses with different Integration Schemes
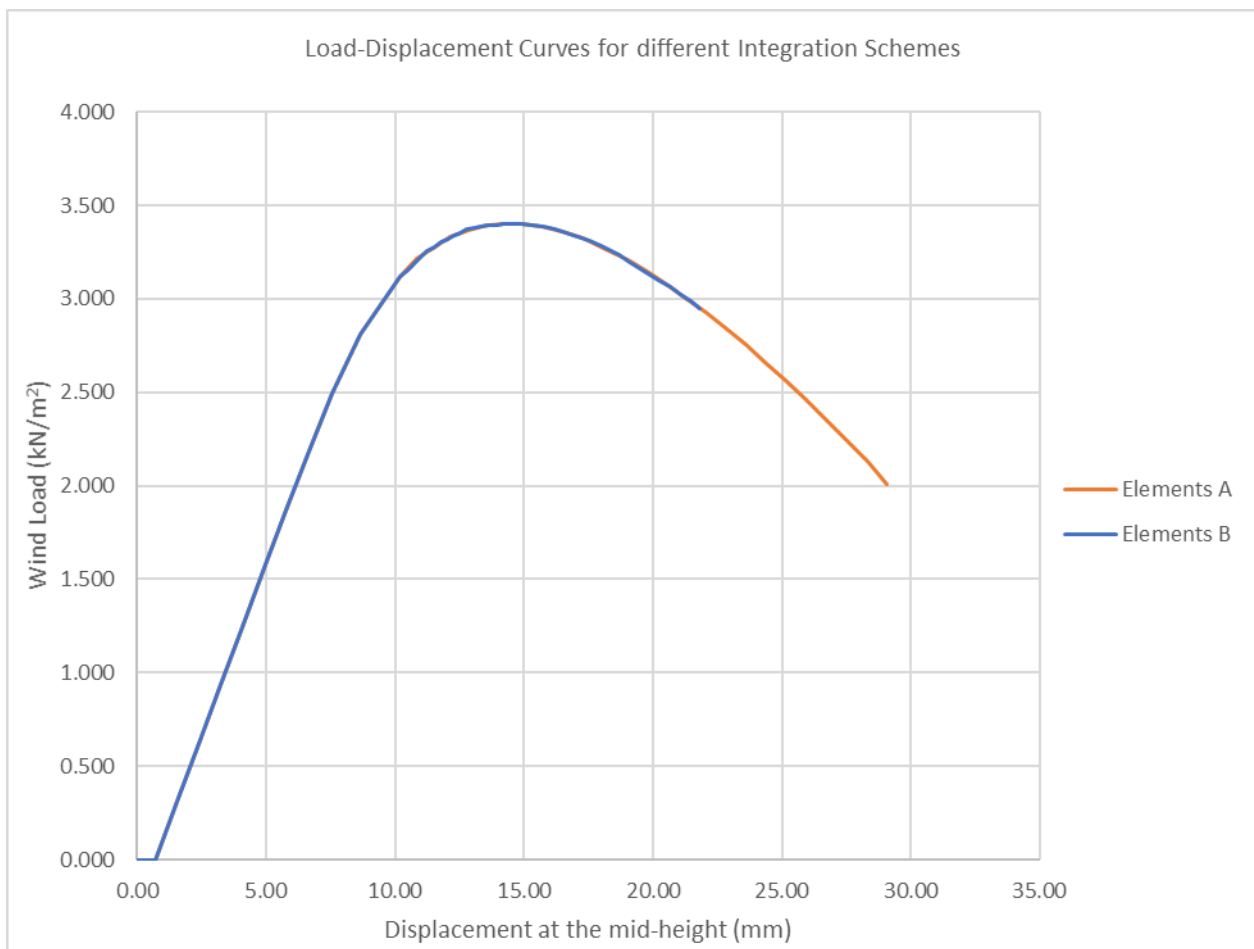
Fig. C. 3 Load – Displacement Curves from analyses with different Integration Schemes for the Finite Elements

Appendix D

The graph in Fig. D. 1 shows two curves, with the combinations of vertical load – wind load, that lead the URM wall to failure. The first curve was derived from FE analyses, where the vertical load is applied first, in one step, and, then, the wind load is applied, in small increments, until the wall fails. It is called 'N-W'. The second curve was derived from FE analyses, where the inverse load path was followed, as discussed in section 9.2. This curve has the title 'W-N'.
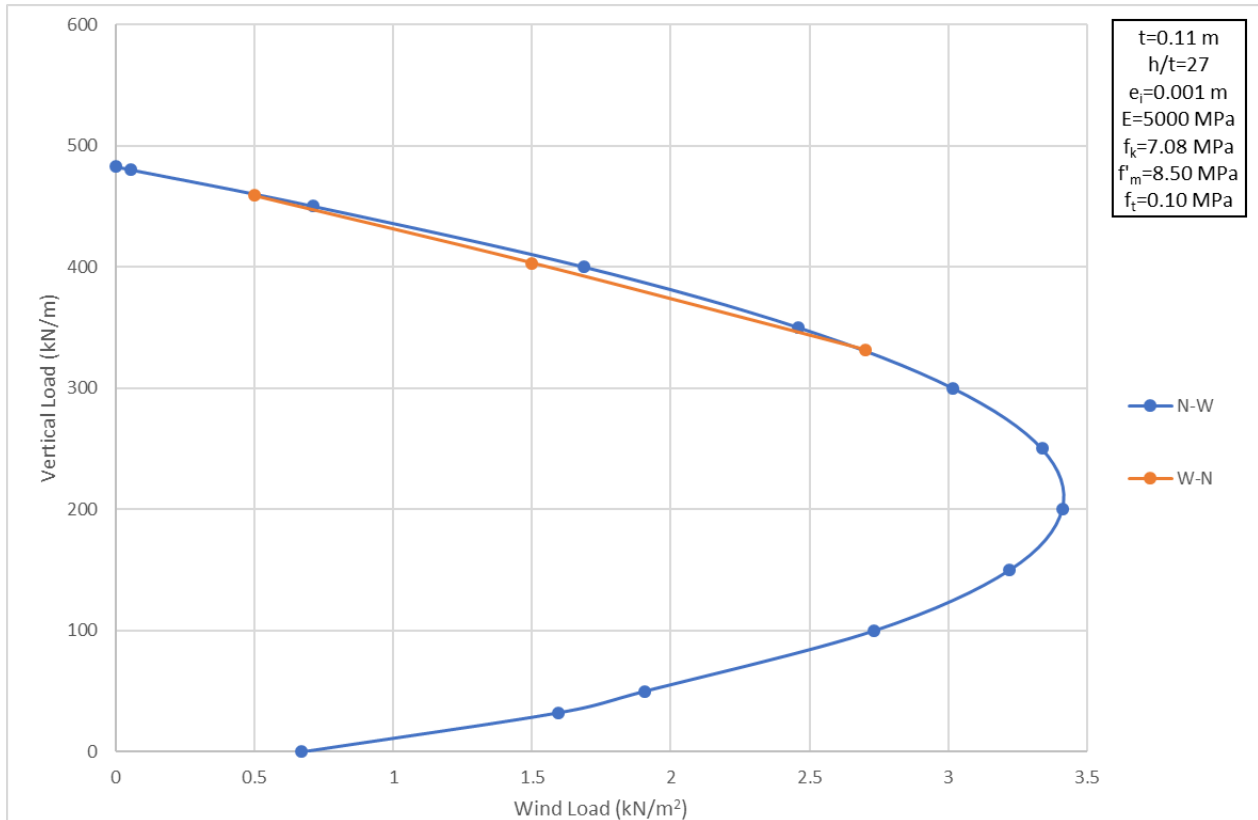
Fig. D. 1 Combinations of Vertical Load and Wind Load that lead the URM wall to failure from FE analyses with different load paths

Appendix E

Results from FE Analysis of URM walls with different values of Slenderness Ratio
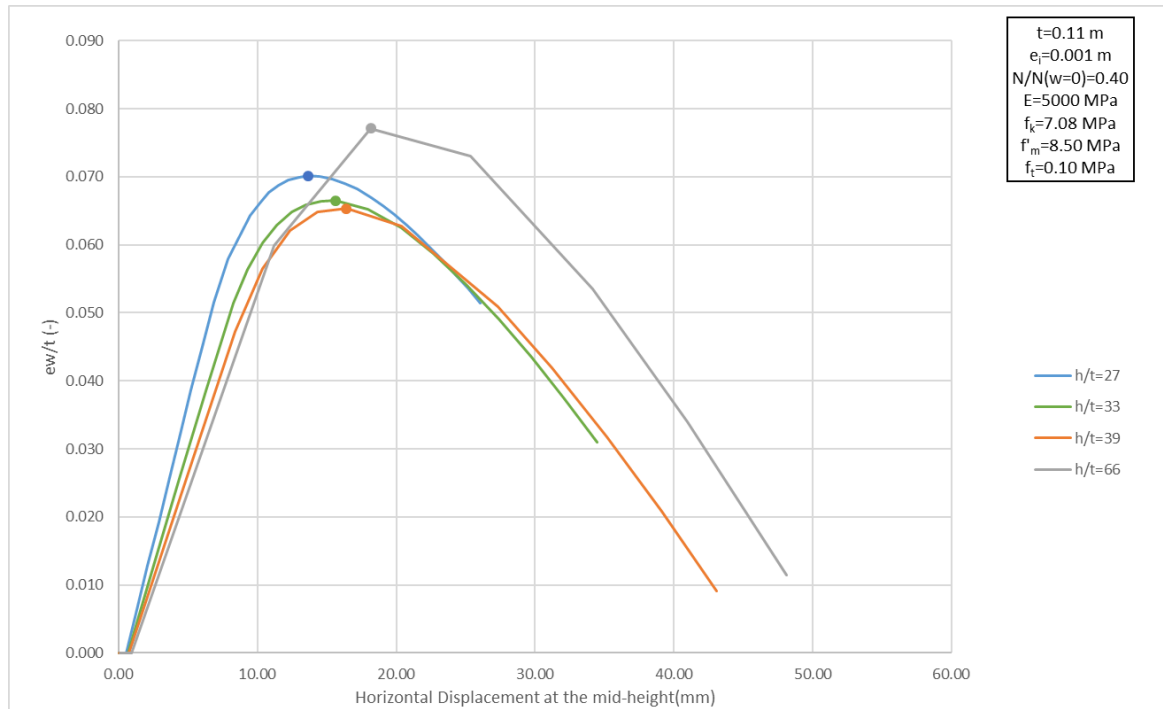
Fig. E. 1 Eccentricity due to wind load – Horizontal Displacement Curves for URM walls with different h/t
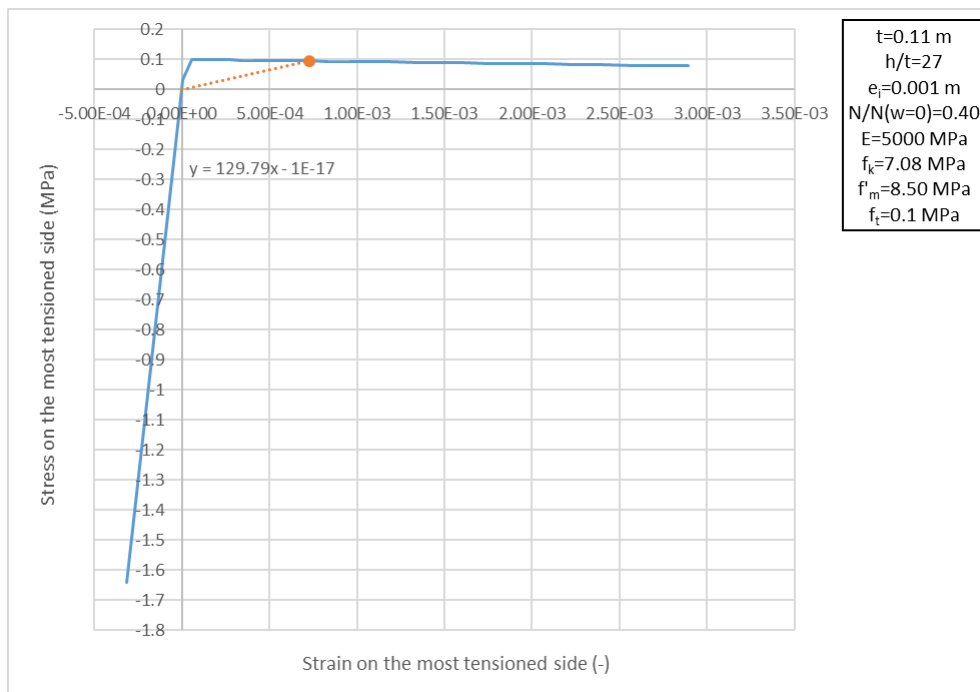
Fig. E. 2 Stress-Strain Evolution at the most tensioned side of the URM wall with h/t=27 – the dot represents the stress-strain state at the highlighted point on the respective curve in the graph in Fig. E. 1
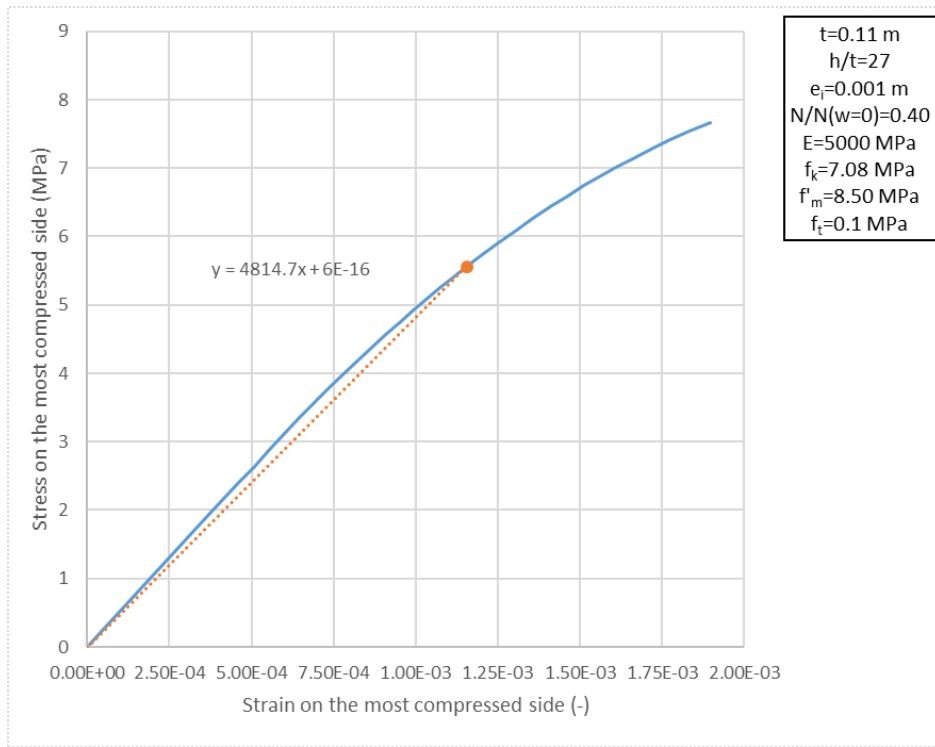
Fig. E. 3 Stress-Strain Evolution at the most compressed side of the URM wall with h/t=27 – the dot represents the stress-strain state at the highlighted point on the respective curve in the graph in Fig. E. 1
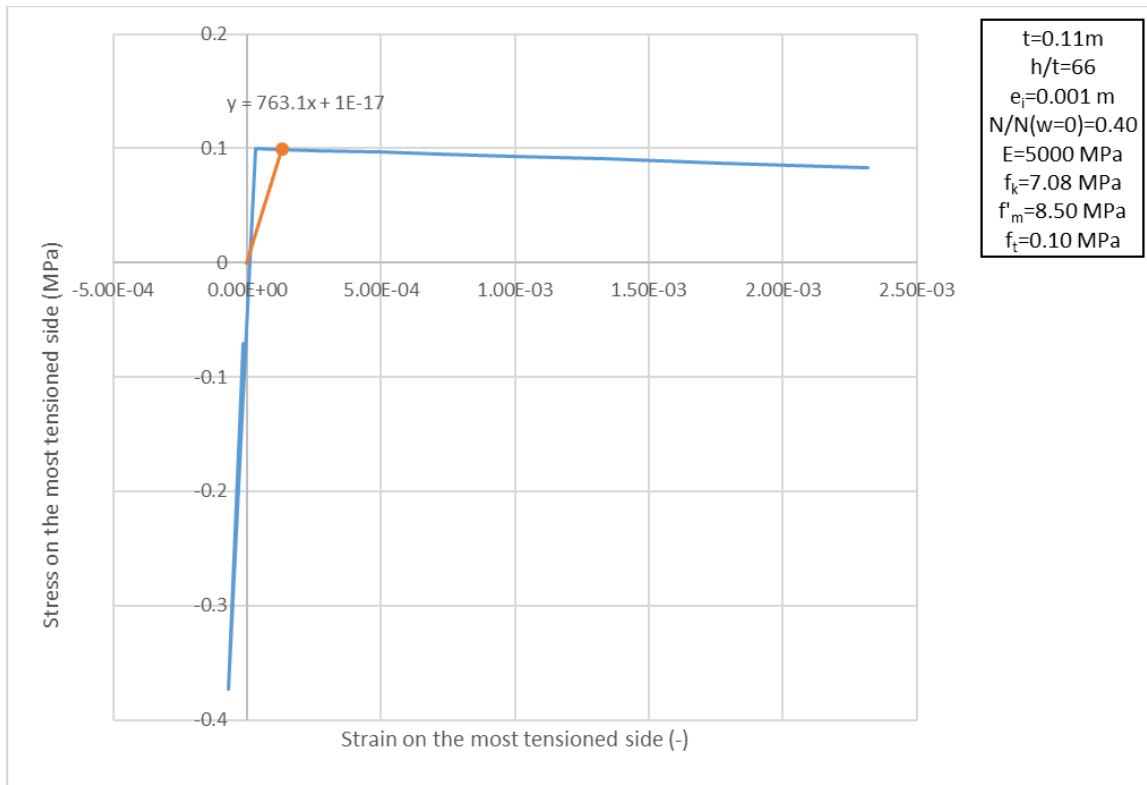
Fig. E. 4 Stress-Strain Evolution at the most tensioned side of the URM wall with h/t=66 – the dot represents the stress-strain state at the highlighted point on the respective curve in the graph in Fig. E. 1
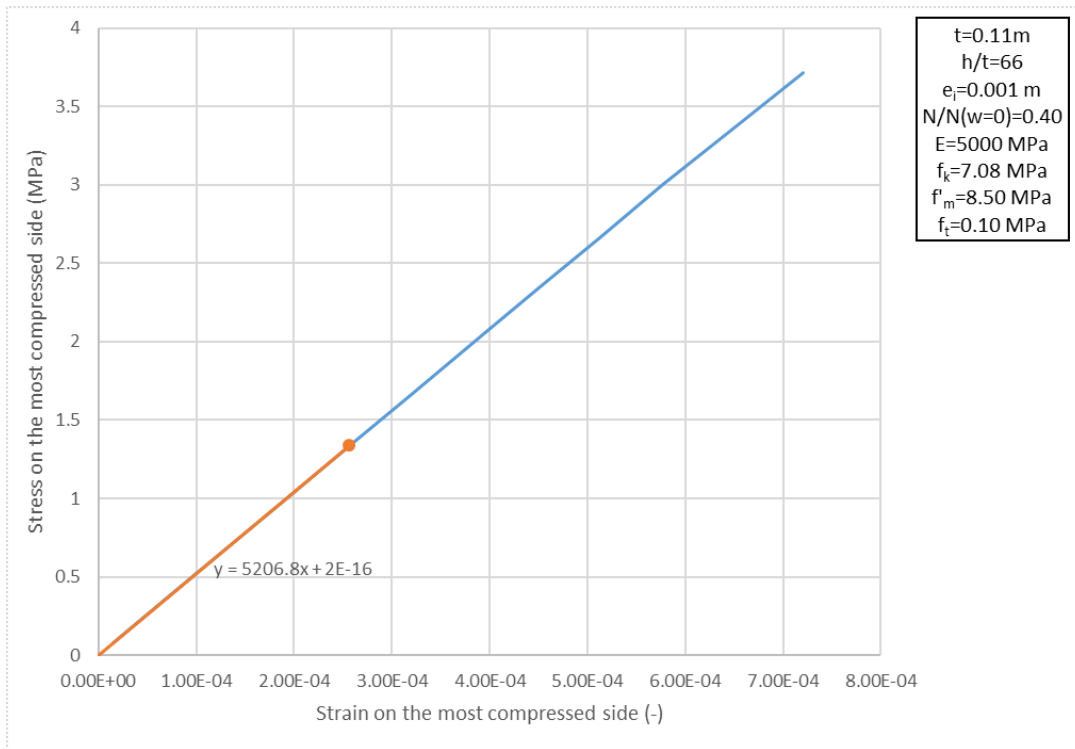
Fig. E. 5 Stress-Strain Evolution at the most compressed side of the URM wall with h/t=66 – the dot represents the stress-strain state at the highlighted point on the respective curve in the graph in Fig. E. 1
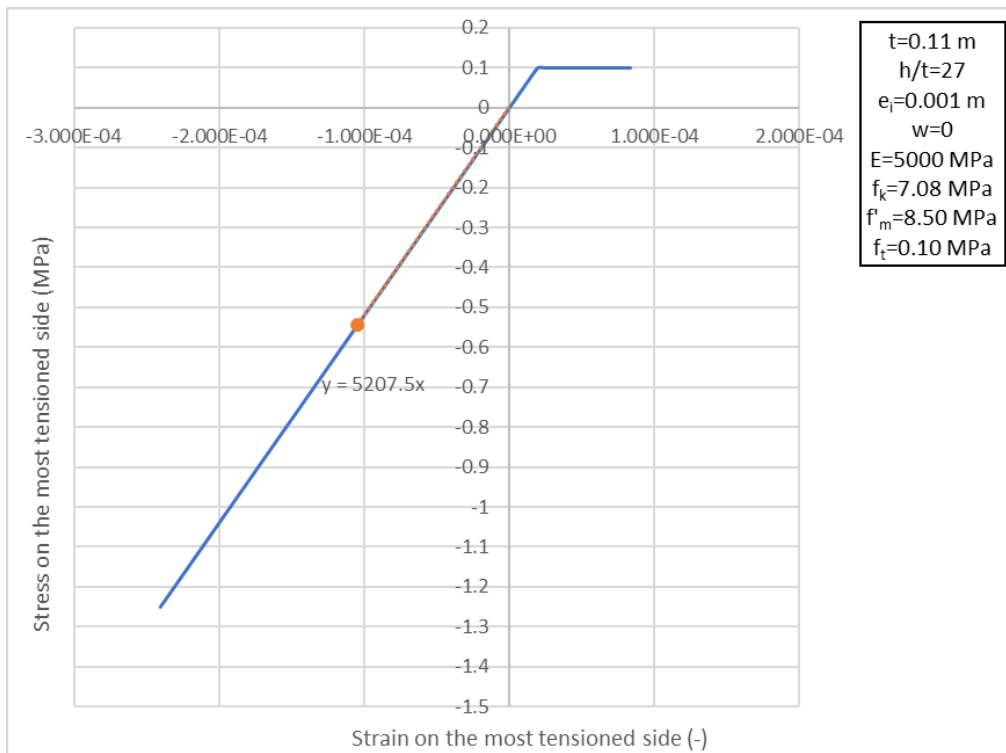
Fig. E. 6 Stress-Strain Evolution at the most tensioned side of the URM wall with h/t=27 – the dot represents the stress-strain state, when the maximum vertical load N(w=0) is attained
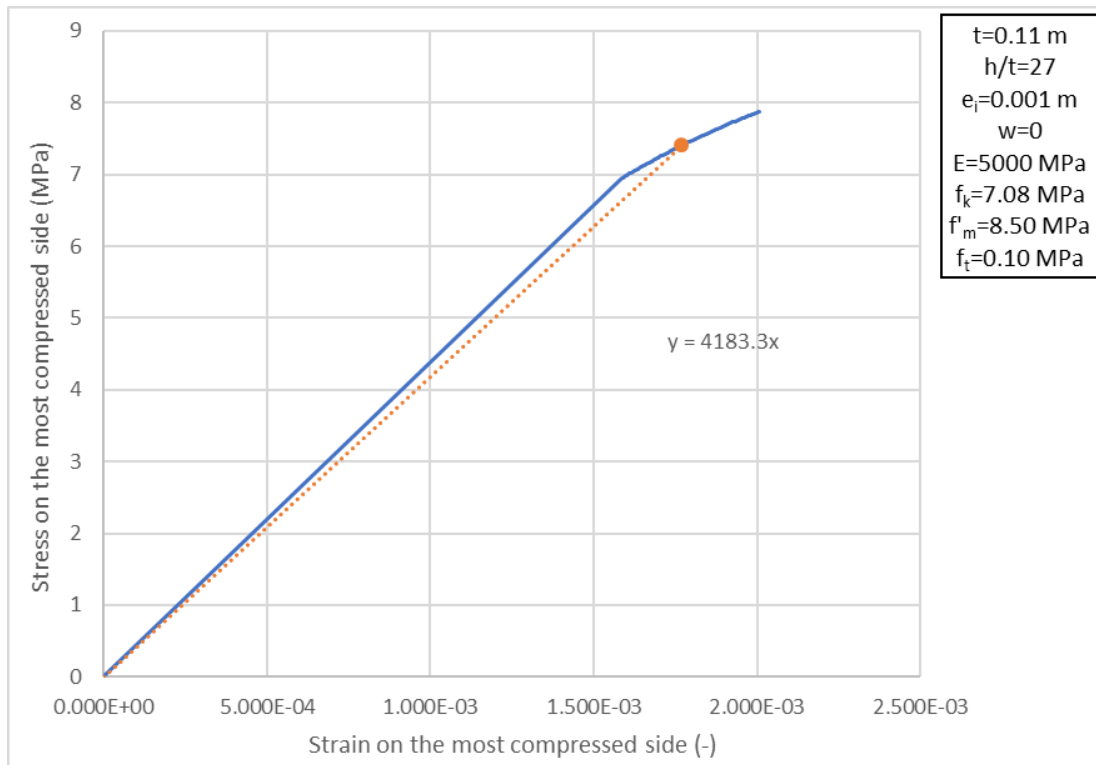
Fig. E. 7 Stress-Strain Evolution at the most compressed side of the URM wall with h/t=27 – the dot represents the stress-strain state, when the maximum vertical load N(w=0) is attained
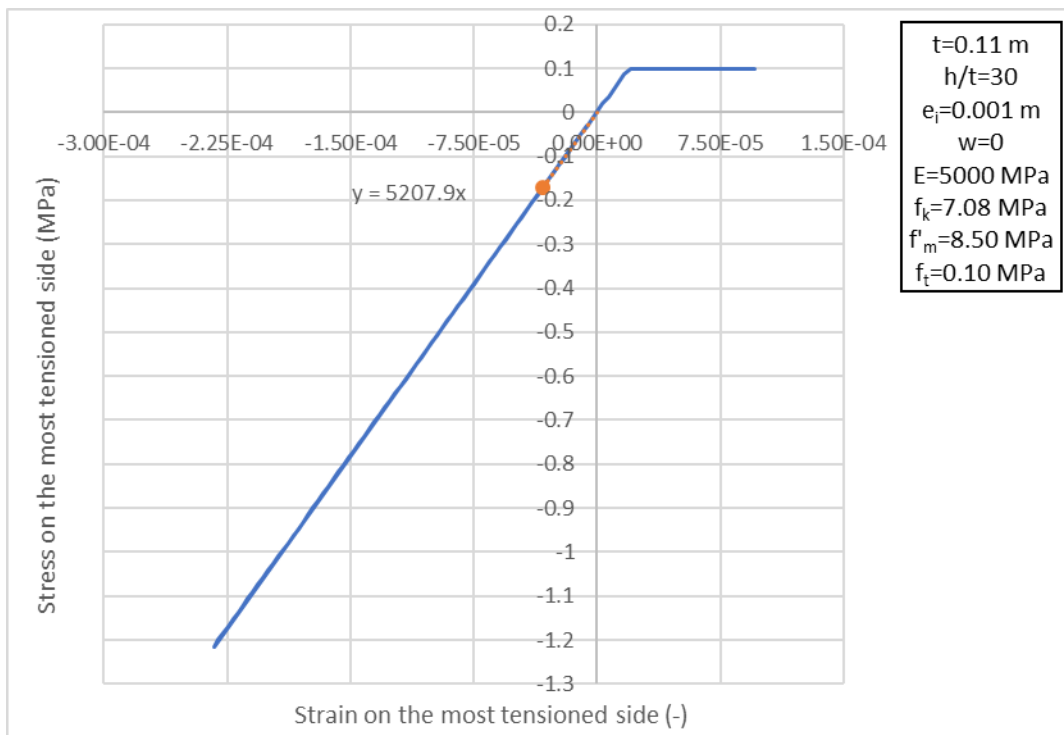
Fig. E. 8 Stress-Strain Evolution at the most tensioned side of the URM wall with h/t=30 – the dot represents the stress-strain state, when the maximum vertical load N(w=0) is attained
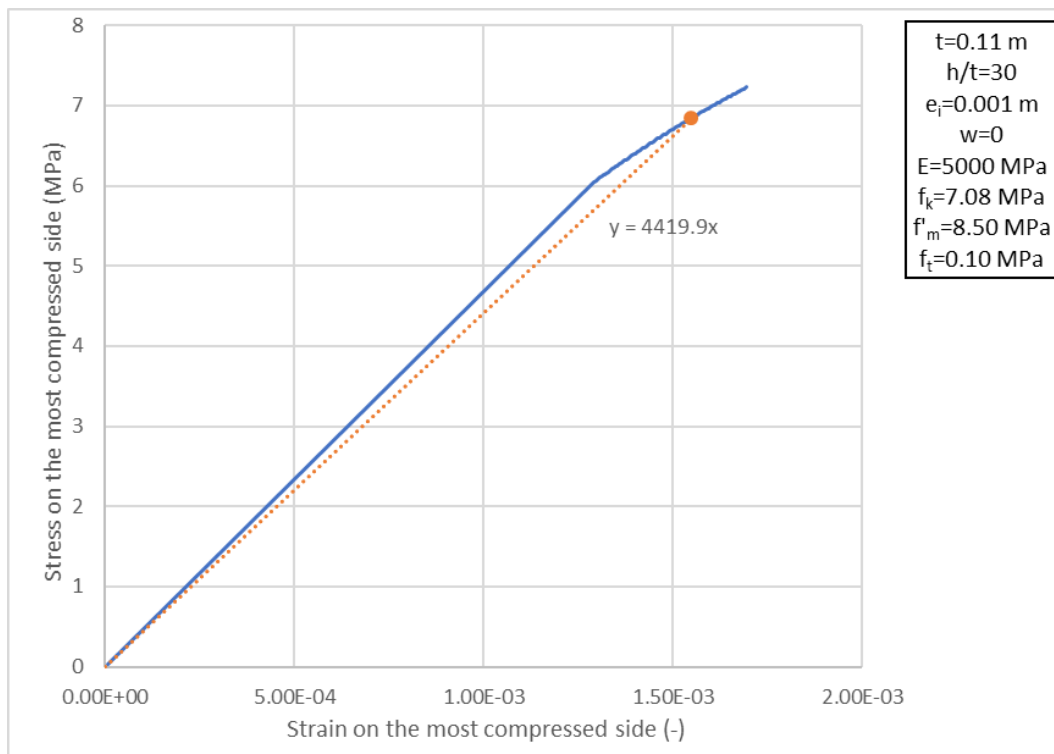
Fig. E. 9 Stress-Strain Evolution at the most compressed side of the URM wall with h/t=30 – the dot represents the stress-strain state, when the maximum vertical load N(w=0) is attained
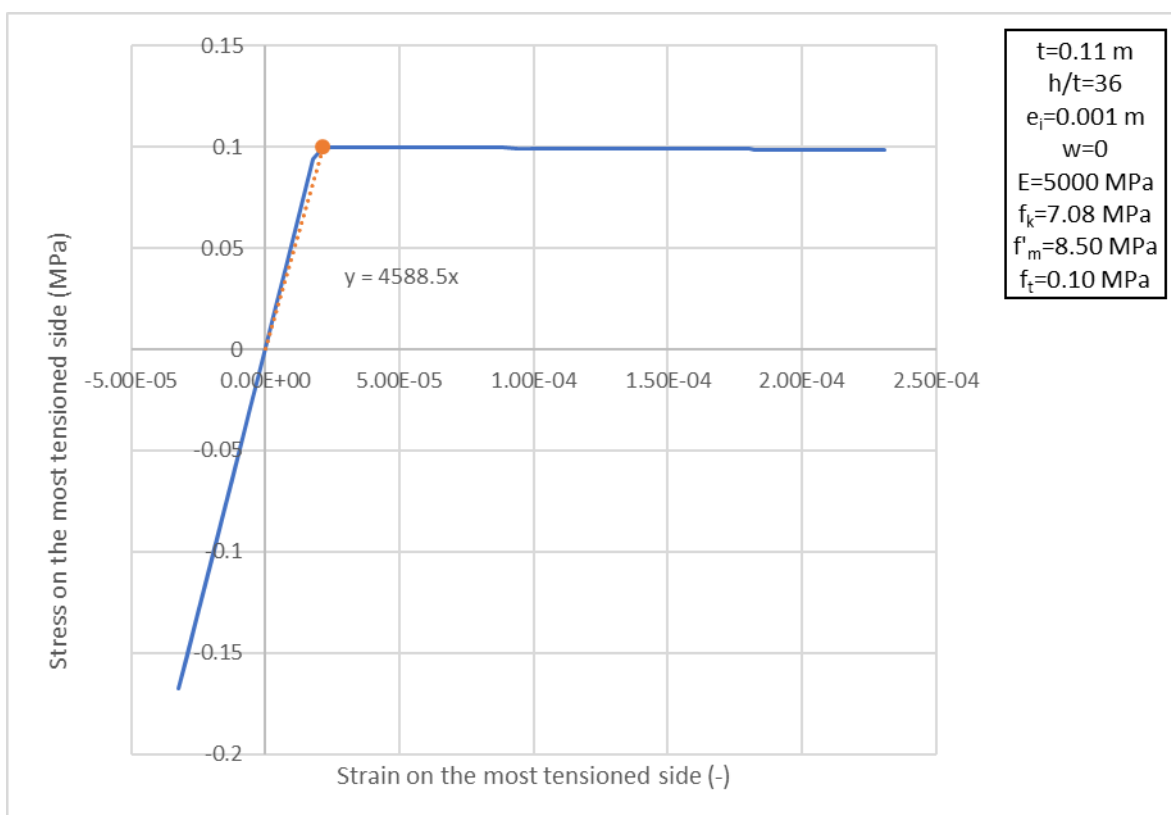
Fig. E. 10 Stress-Strain Evolution at the most tensioned side of the URM wall with h/t=36 – the dot represents the stress-strain state, when the maximum vertical load N(w=0) is attained
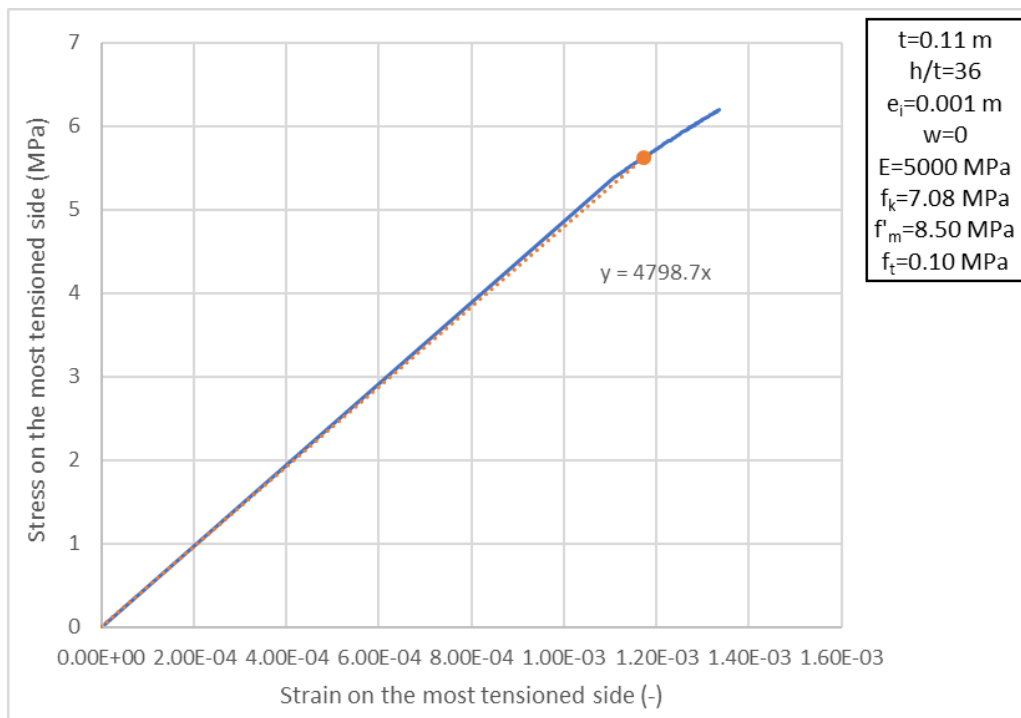
Fig. E. 11 Stress-Strain Evolution at the most compressed side of the URM wall with h/t=36 – the dot represents the stress-strain state, when the maximum vertical load N(w=0) is attained
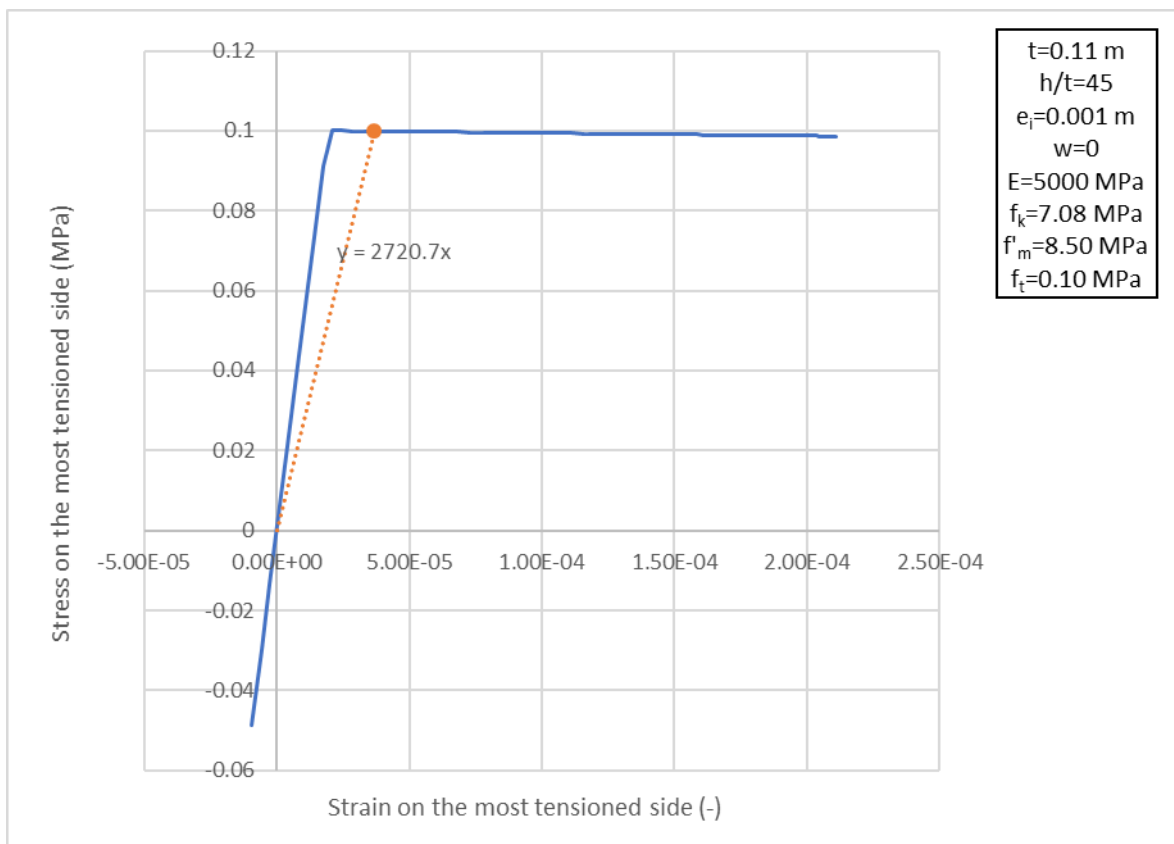
Fig. E. 12 Stress-Strain Evolution at the most tensioned side of the URM wall with h/t=45 – the dot represents the stress-strain state, when the maximum vertical load N(w=0) is attained
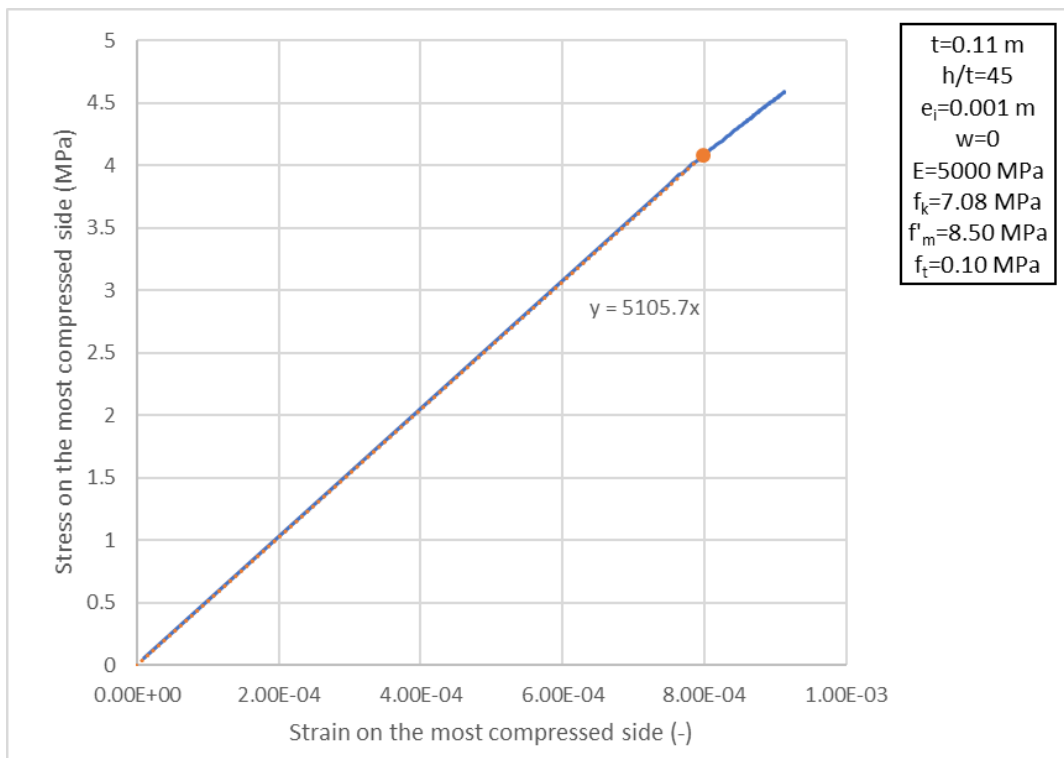
Fig. E. 13 Stress-Strain Evolution at the most compressed side of the URM wall with h/t=45 – the dot represents the stress-strain state, when the maximum vertical load N(w=0) is attained
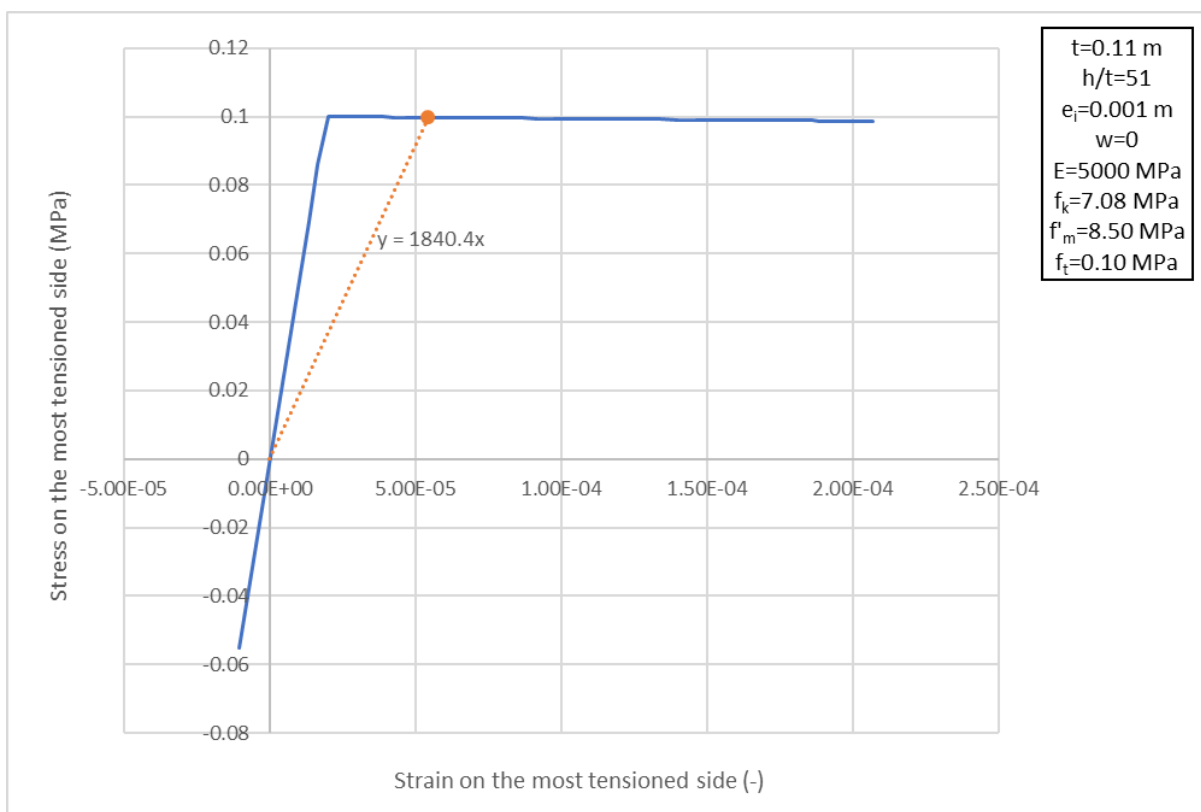
Fig. E. 14 Stress-Strain Evolution at the most tensioned side of the URM wall with h/t=51 – the dot represents the stress-strain state, when the maximum vertical load N(w=0) is attained

189
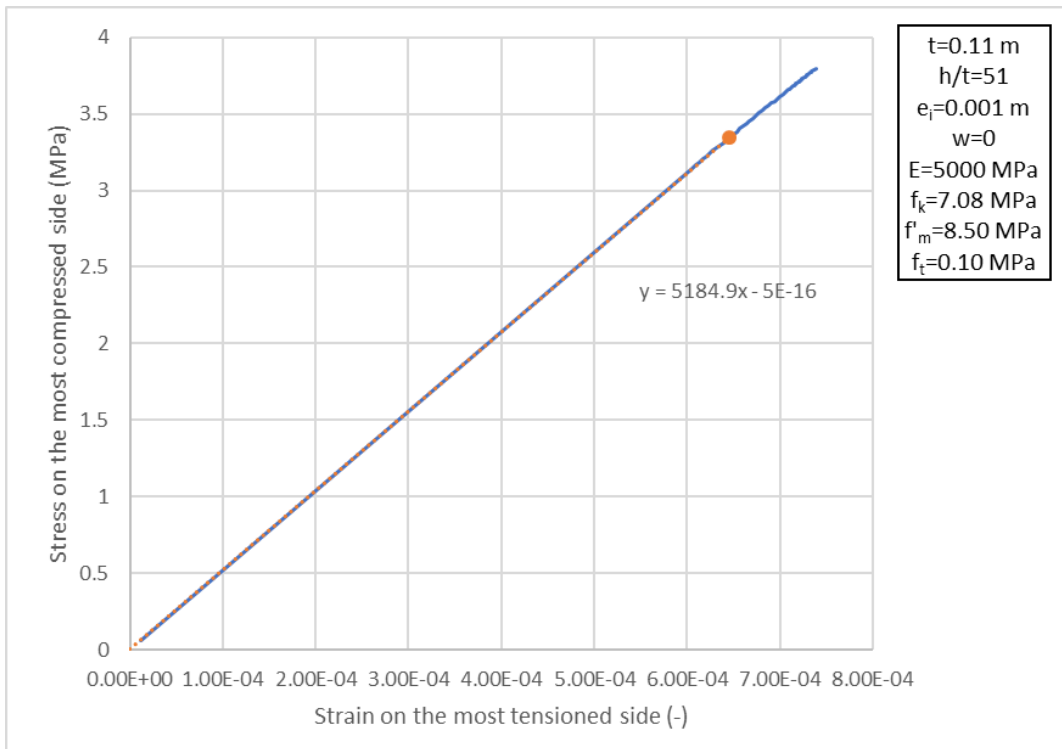
Fig. E. 15 Stress-Strain Evolution at the most compressed side of the URM wall with h/t=51 — the dot represents the stress-strain state, when the maximum vertical load N(w=0) is attained
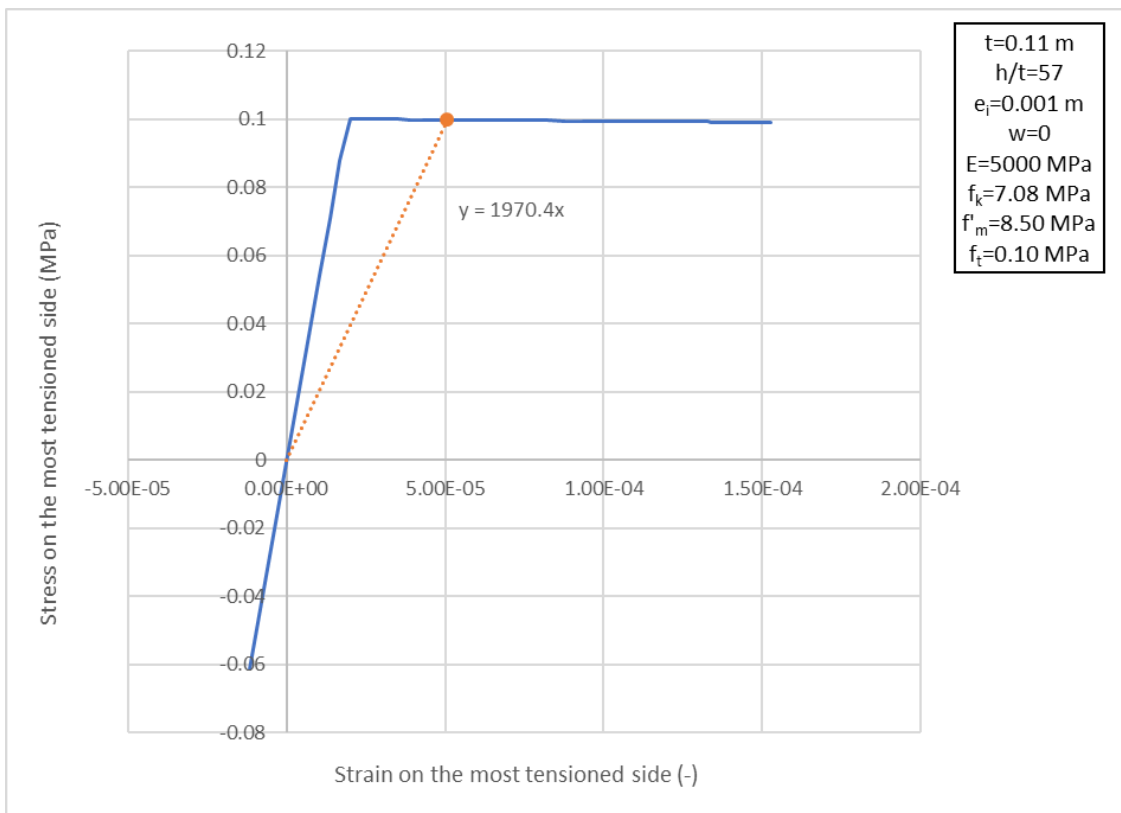
Fig. E. 16 Stress-Strain Evolution at the most tensioned side of the URM wall with h/t=57 — the dot represents the stress-strain state, when the maximum vertical load N(w=0) is attained
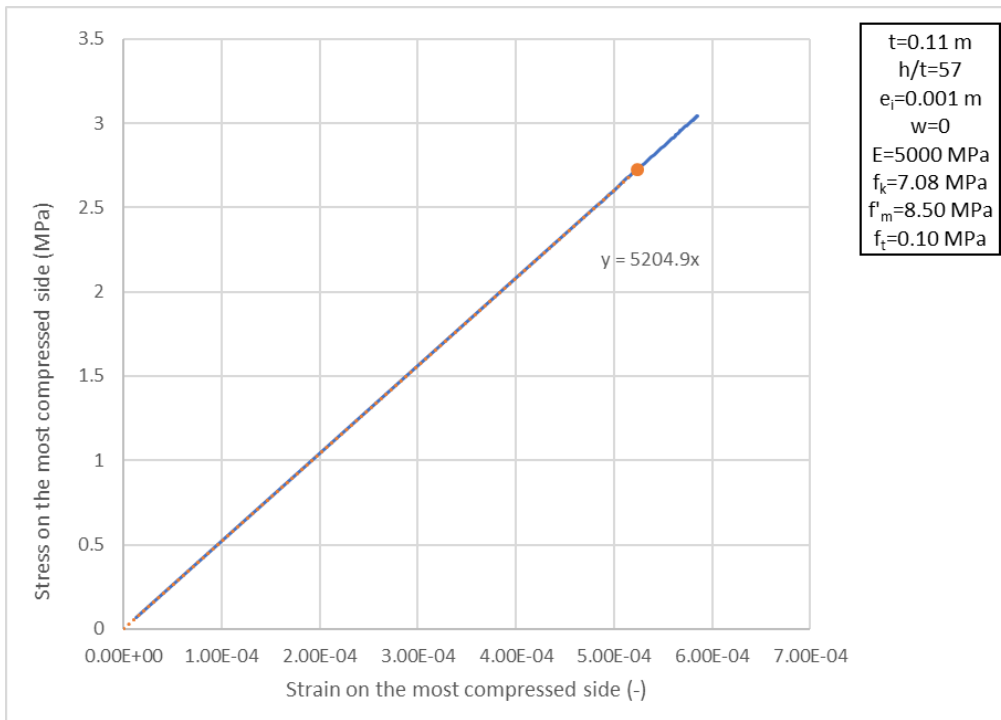
Fig. E. 17 Stress-Strain Evolution at the most compressed side of the URM wall with h/t=57 – the dot represents the stress-strain state, when the maximum vertical load N(w=0) is attained
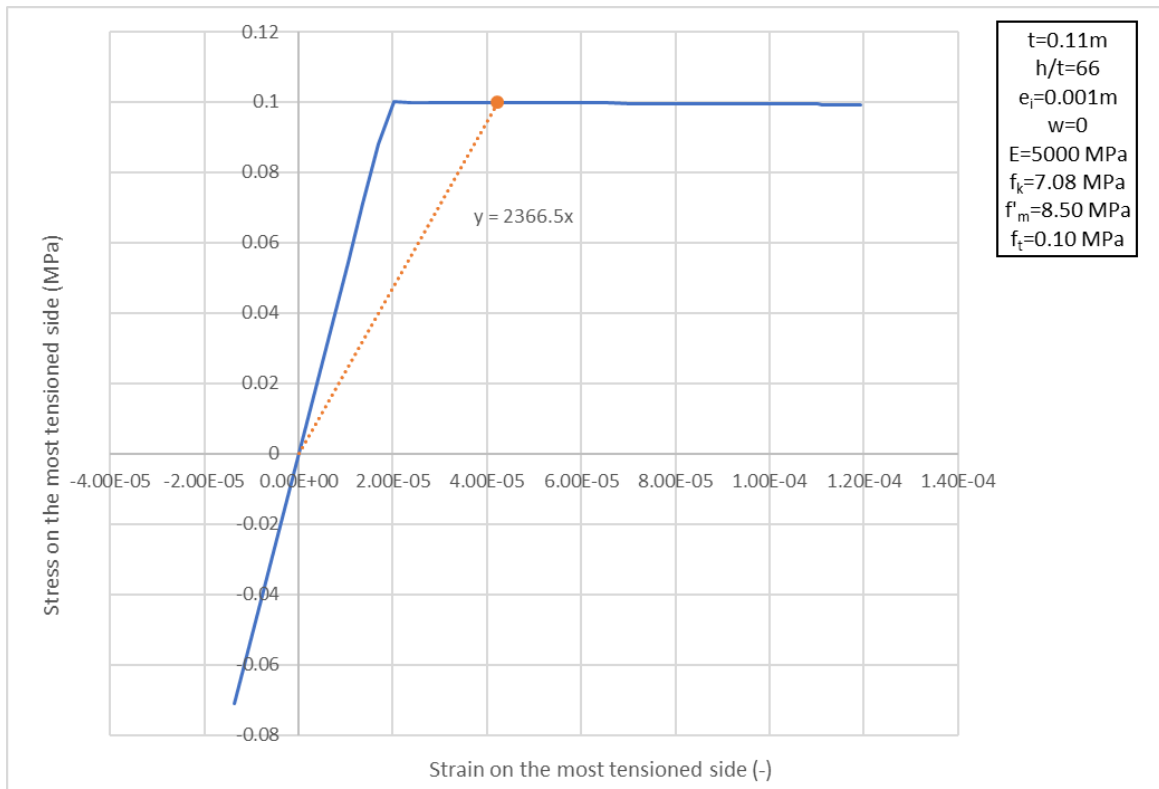
Fig. E. 18 Stress-Strain Evolution at the most tensioned side of the URM wall with h/t=66 – the dot represents the stress-strain state, when the maximum vertical load N(w=0) is attained
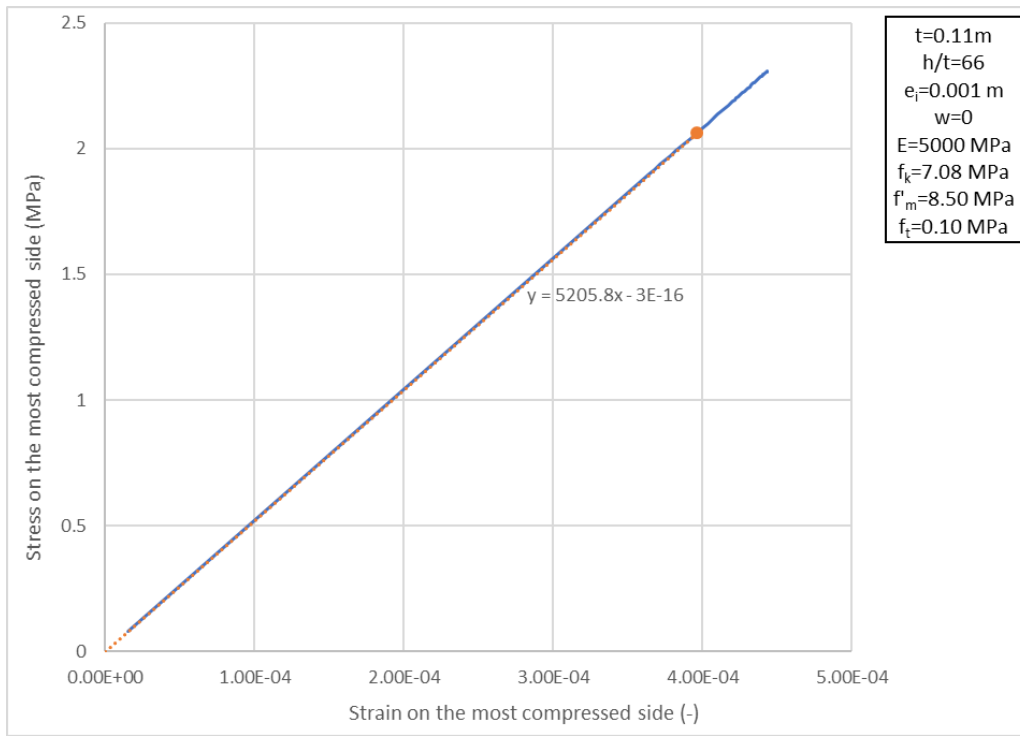
Fig. E. 19 Stress-Strain Evolution at the most compressed side of the URM wall with h/t=66 – the dot represents the stress-strain state, when the maximum vertical load N(w=0) is attained

Results from FE Analysis of URM walls with different values of Eccentricity at the Top or the Bottom
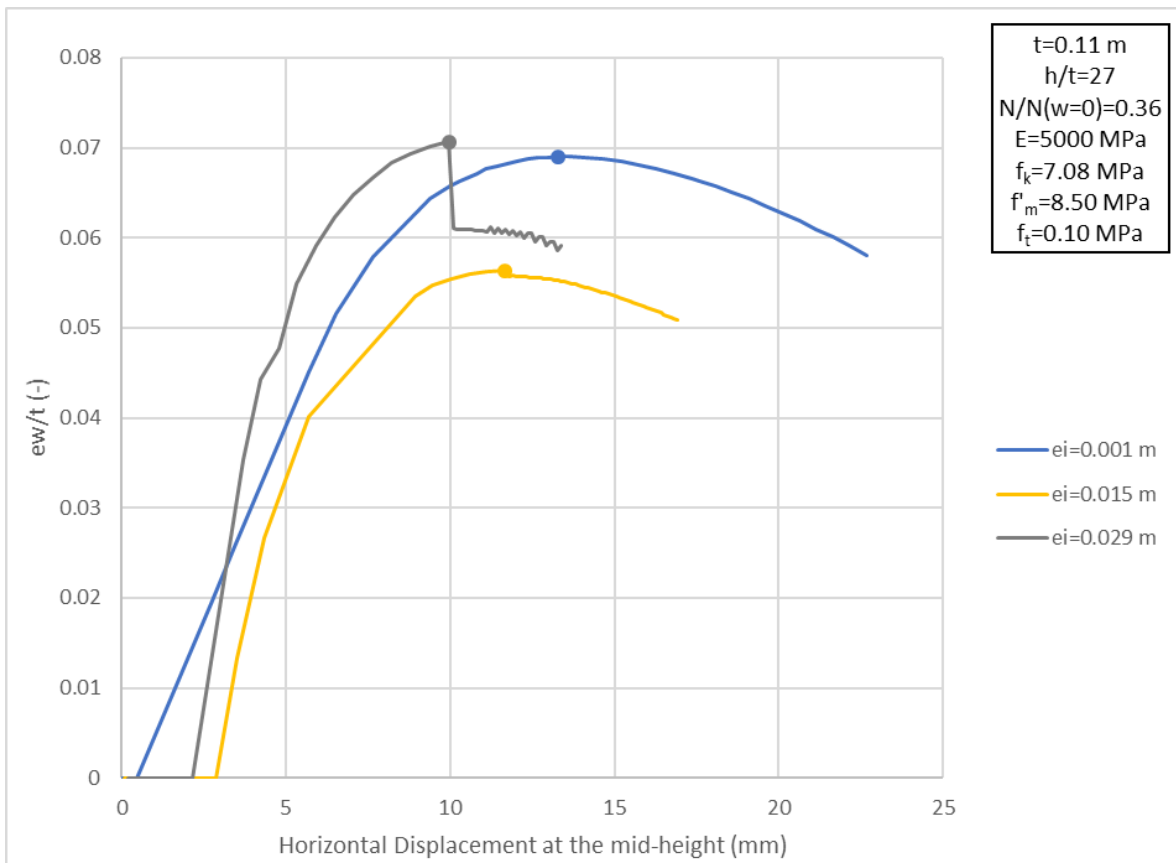
Fig. E. 20 Eccentricity due to wind load – Horizontal Displacement Curves for URM walls with different e_i

Appendix F
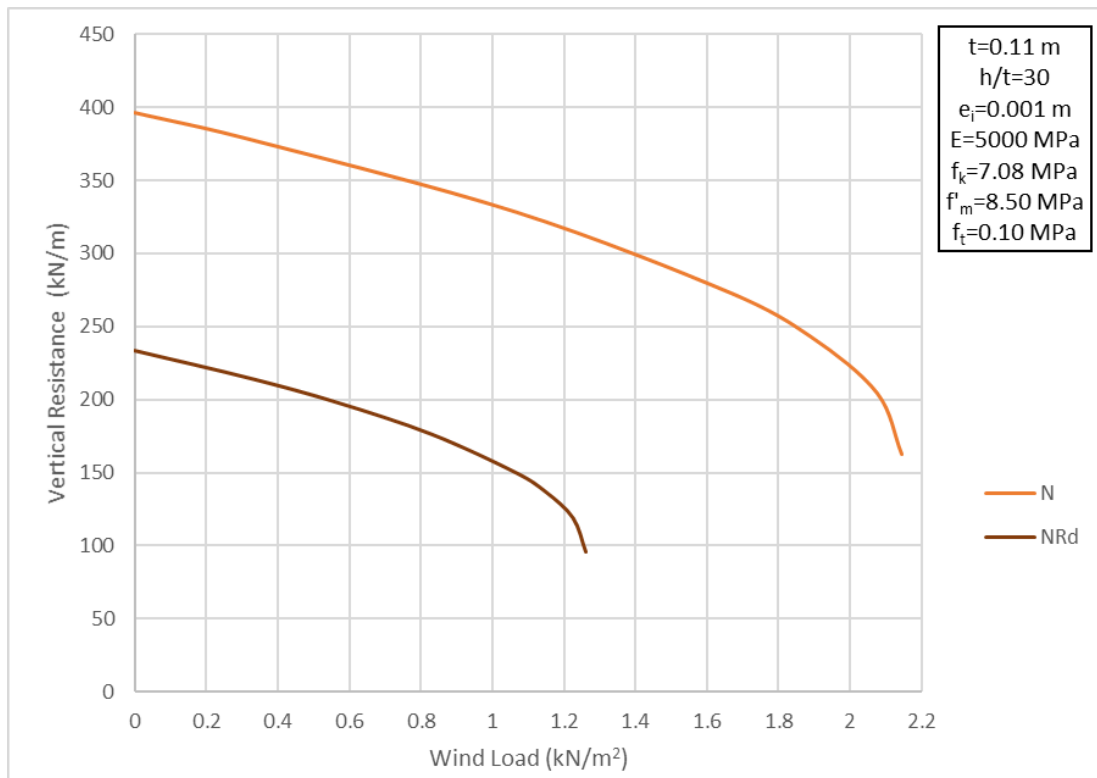
Fig. F. 1 Curves from formulas in Equation 67 & Equation 69 for a URM wall with h/t=30
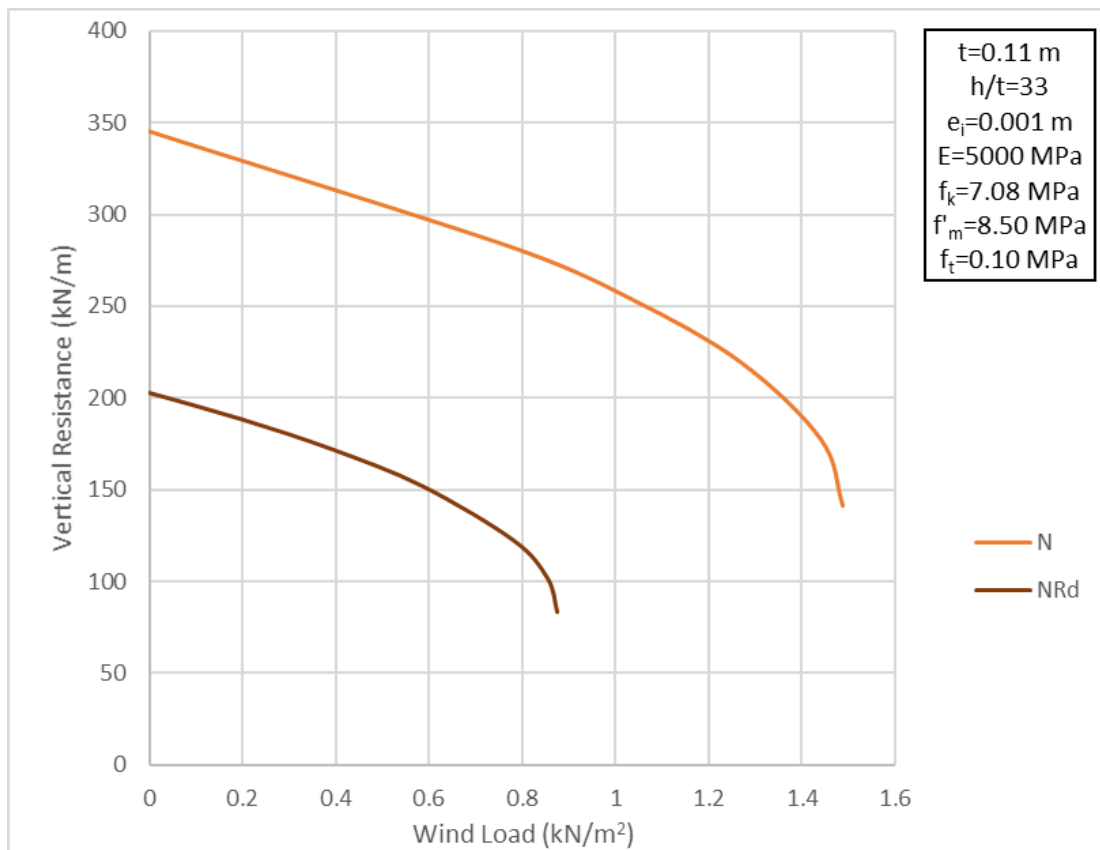
Fig. F. 2 Curves from formulas in Equation 67 & Equation 69 for a URM wall with h/t=33
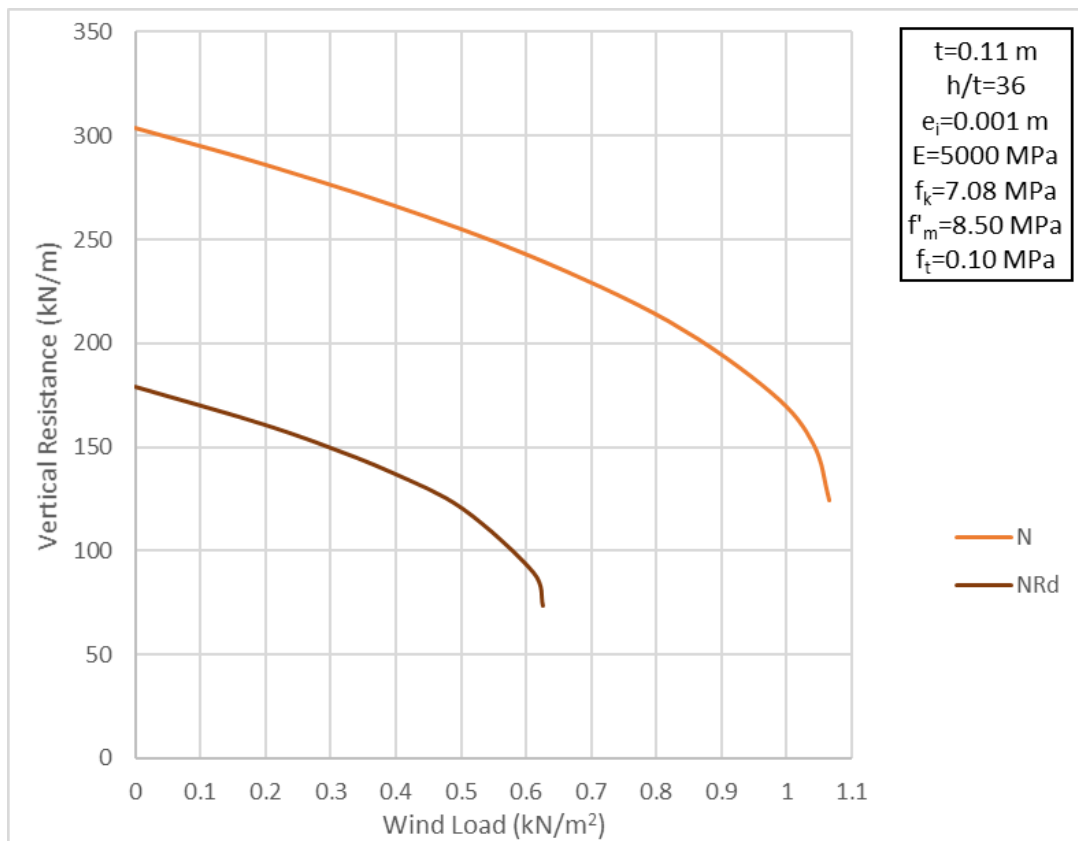
Fig. F. 3 Curves from formulas in Equation 67 & Equation 69 for a URM wall with h/t=36
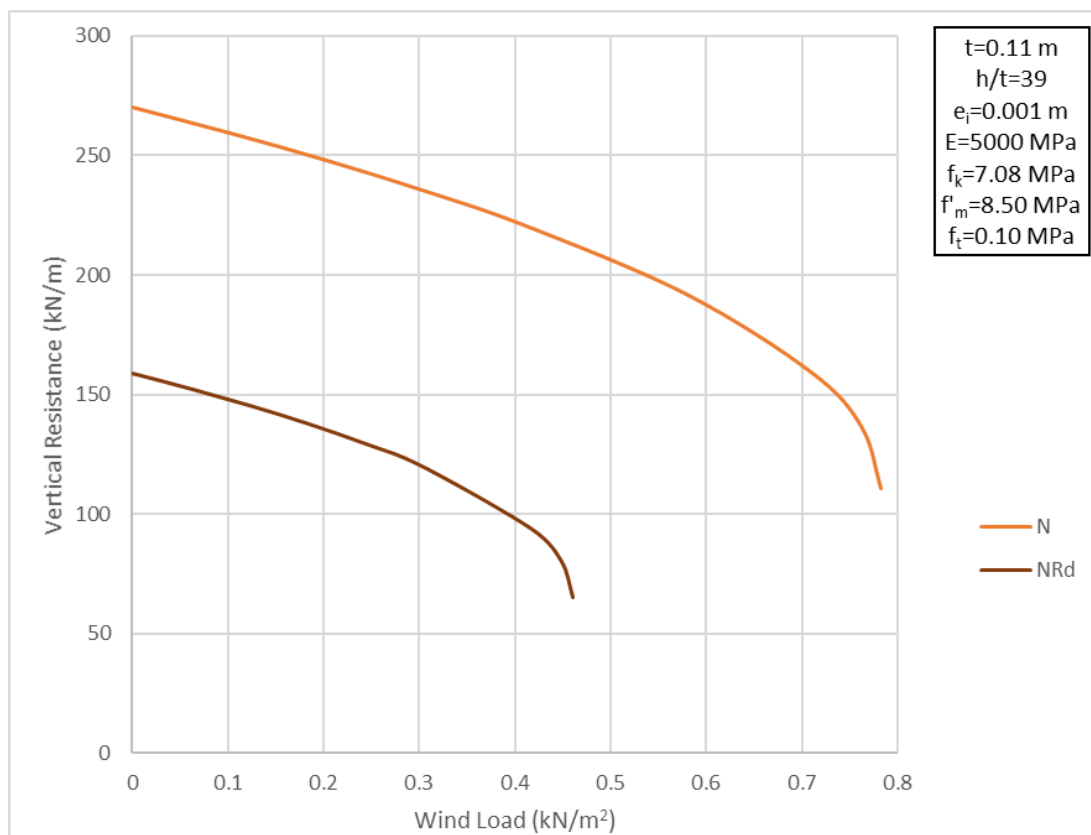
Fig. F. 4 Curves from formulas in Equation 67 & Equation 69 for a URM wall with h/t=39
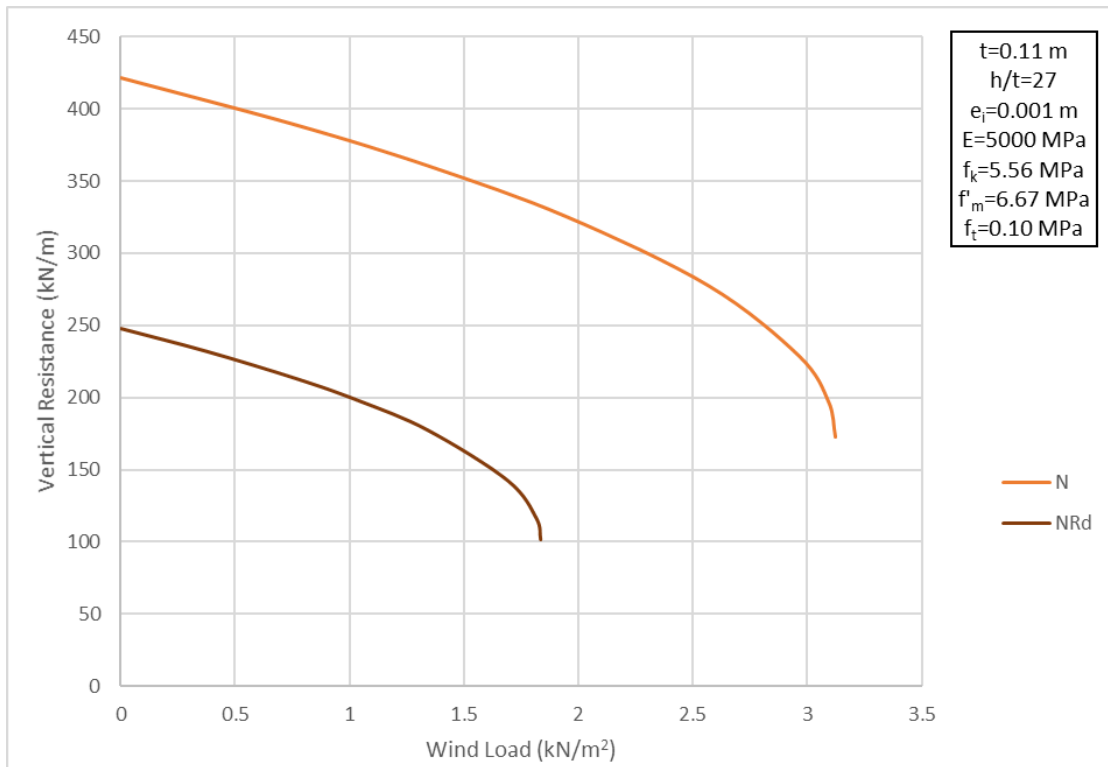
Fig. F. 5 Curves from formulas in Equation 67 & Equation 69 for a URM Wall with E=5000 MPa, f_k=5.56 MPa and h/t=27
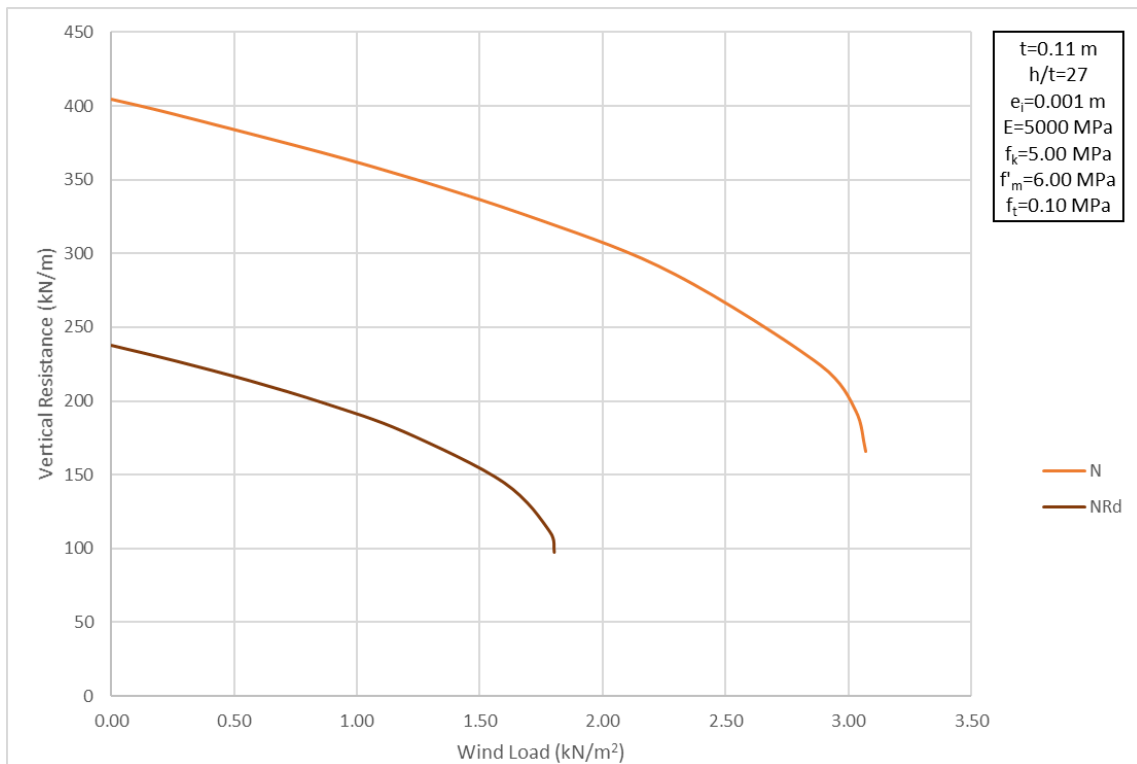
Fig. F. 6 Curves from formulas in Equation 67 & Equation 69 for a URM Wall with E=5000 MPa, f_k=5.00 MPa and h/t=27
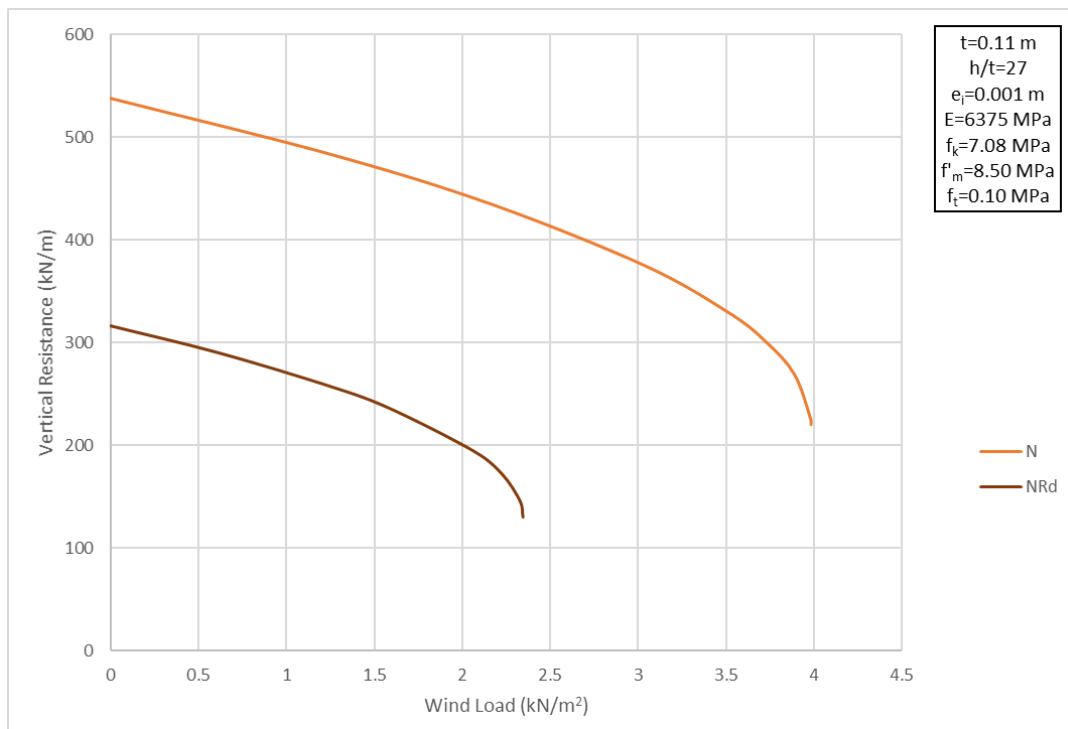
Fig. F. 7 Curves from formulas in Equation 67 & Equation 69 for a URM Wall with E=6375 MPa, f_k=7.08 MPa and h/t=27
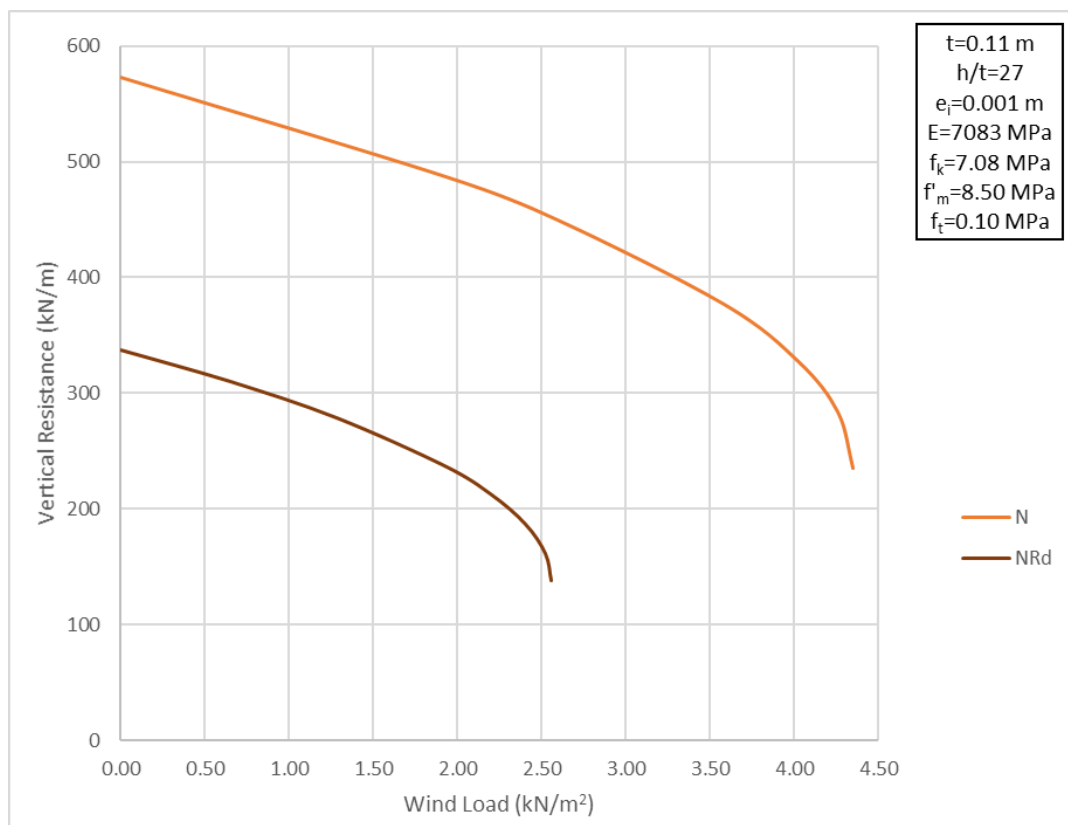
Fig. F. 8 Curves from formulas in Equation 67 & Equation 69 for a URM Wall with E=7083 MPa, f_k=7.08 MPa and h/t=27
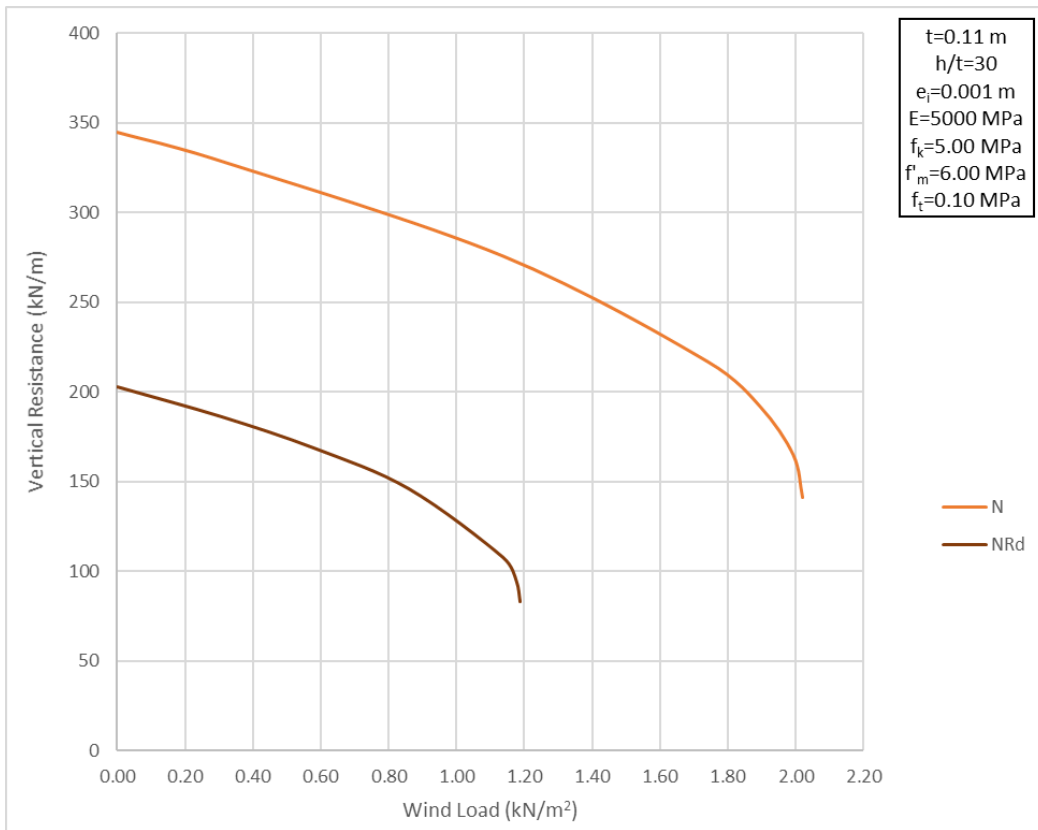
Fig. F. 9 Curves from formulas in Equation 67 & Equation 69 for a URM Wall with E=5000 MPa, f_k=5.00 MPa and h/t=30
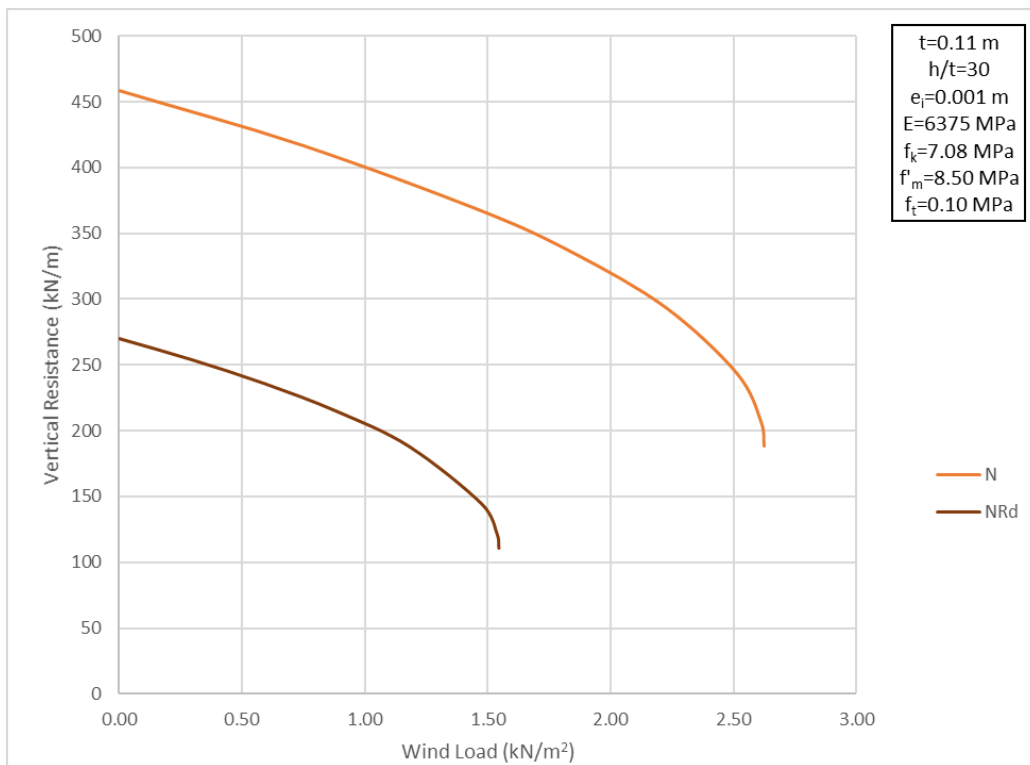
Fig. F. 10 Curves from formulas in Equation 67 & Equation 69 for a URM Wall with E=6375 MPa, f_k=7.08 MPa and h/t=30
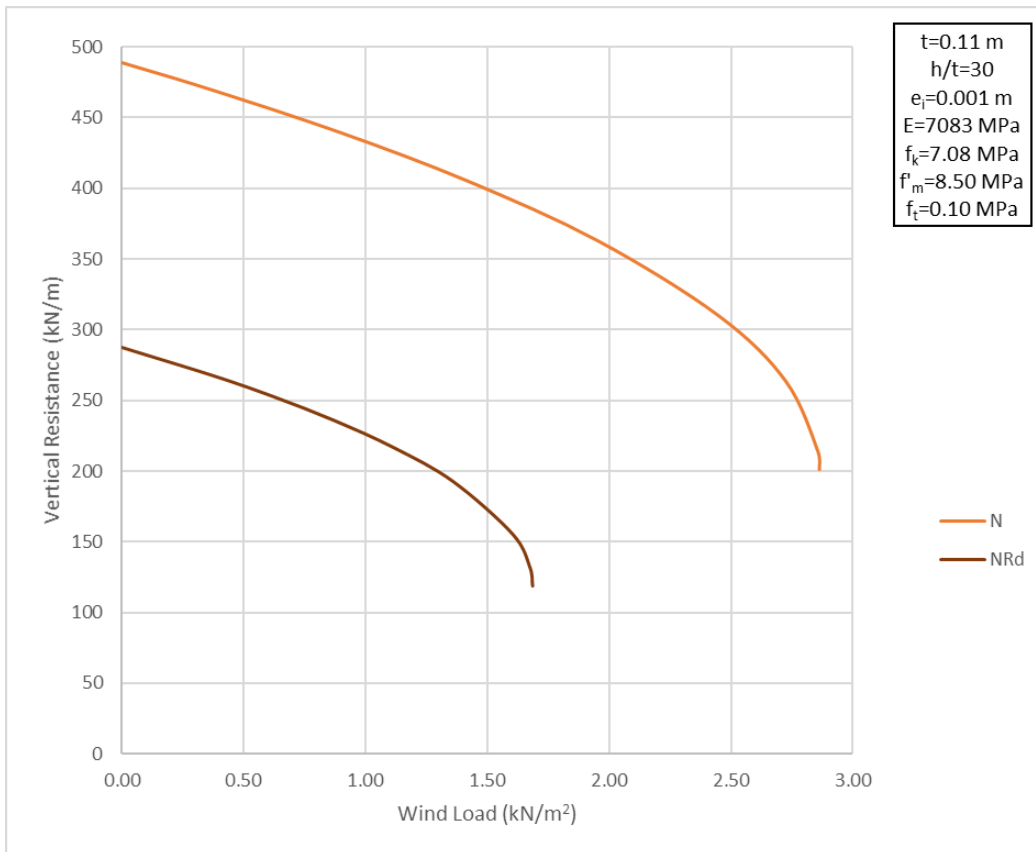
Fig. F. 11 Curves from formulas in Equation 67 & Equation 69 for a URM Wall with E=7083 MPa, f_k=7.08 MPa and h/t=30
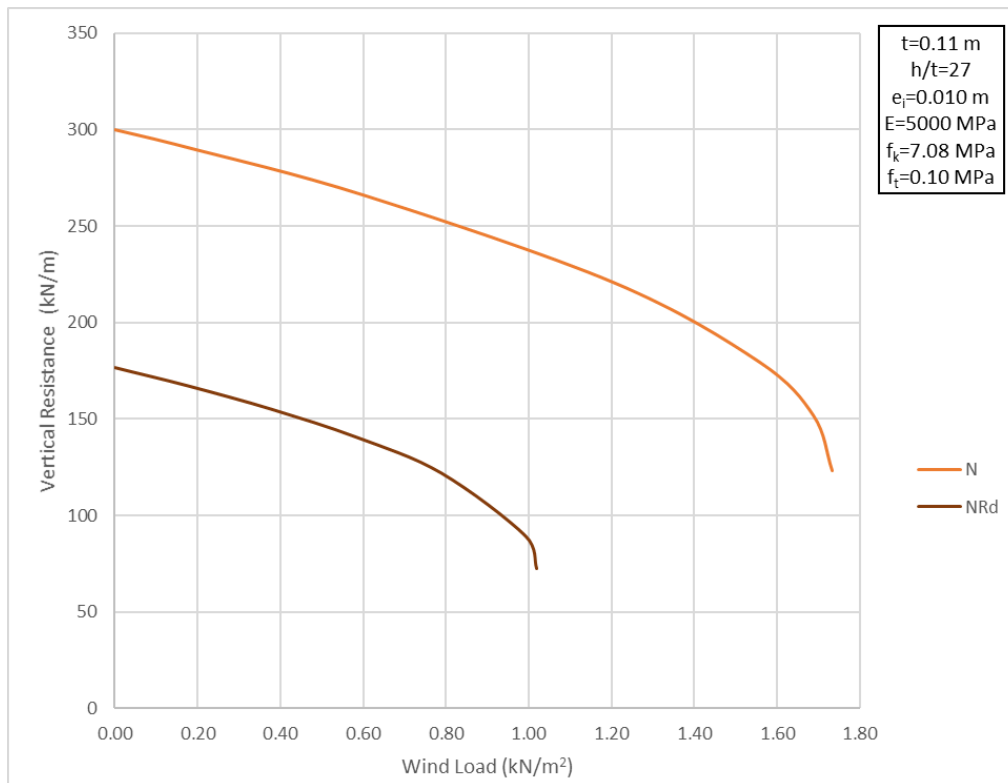
Fig. F. 12 Curves from formulas in Equation 67 & Equation 69 for a URM Wall with e_i=0.010 m
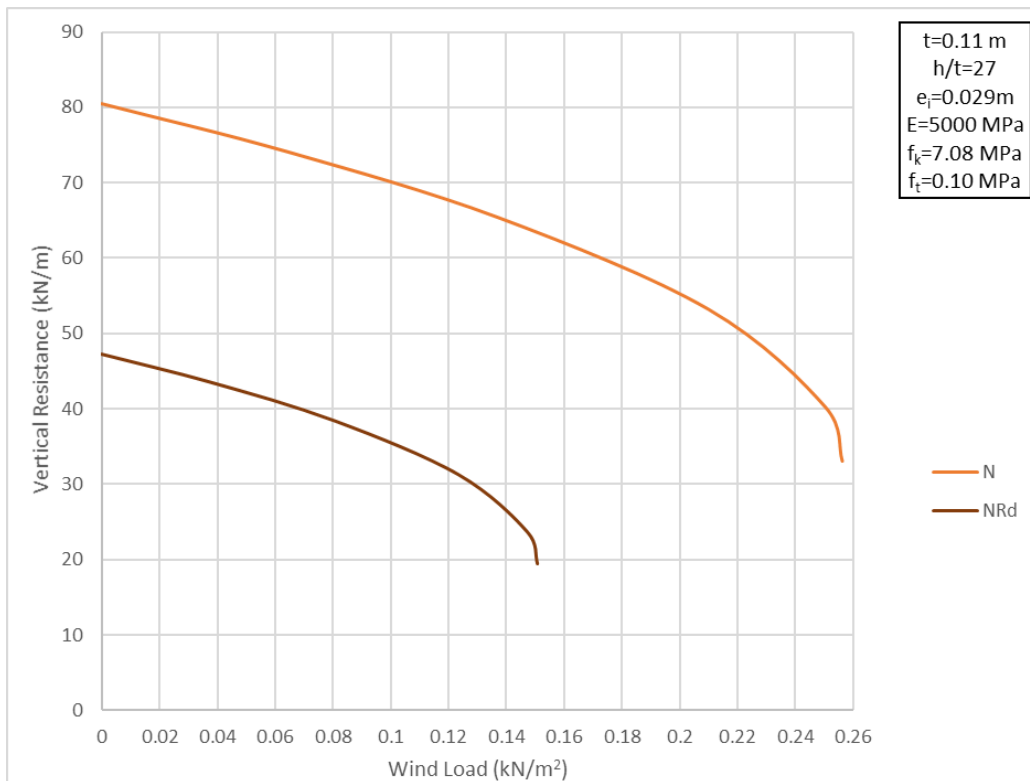
Fig. F. 13 Curves from formulas in Equation 67 & Equation 69 for a URM Wall with e_i=0.029 m

Fig. F. 14 Curves from formulas in Equation 67 & Equation 69 for a URM Wall with h/t=33 and e_i=0.010 m